# Doctoral Dissertation

# 博士論文

## Developments of

## d/π Electron–Proton-coupled Functionalities

## in Metal Dithiolene Complex Crystals

(金属ジチオレン錯体結晶における d/π電子−プロトン相関型

機能物性の開拓)

So Yokomori

横森　創

# Abstract

## Chapter 1 General introduction

Functionalities of molecular crystals have been explored based on designing the chemical structure of the constituent molecules and tuning intermolecular interactions, which is decisive to molecular arrangements. Hydrogen bond (H-bond) is one of the important intermolecular interactions to control the molecular arrangements because of its intermediate strength between covalent bonds and van der Waals interactions. In addition to the feature as a structural regulator, H-bond formation and/or proton dynamics act as an additional degree of freedom to significantly modulate the electronic structures of molecular crystals. Our group has recently found proton-(deuteron-) dynamics-coupled magnetism and electrical conductivity switching in the crystal consisting of catechol-fused tetrathiafulvalene: novel phenomena where $\pi$ electron is coupled with H-bonding.[1–4] Therefore, the proper introduction of H-bond into molecular crystals leads to developments of novel electronic functionalities and phenomena coupled to a proton in H-bonds; however, the number of such examples have been limited.

As the constituent molecules to widely explore such novel phenomena, the author focused on metal dithiolene complexes having d electrons in addition to $\pi$ electrons. Owing to d/$\pi$ electron conjugation, various choices of the central metals and the precisely designable dithiolene ligands, they show stable multi-redox abilities and rich electronic properties and functionalities in the solid state (e.g., optical properties, electrical conductivities, and magnetism), leading to the significant discoveries in chemistry and physics, such as two-dimensional d/$\pi$-conjugated nanosheets and the single-component molecular superconductor.[5,6] Therefore, material developments based on metal dithiolene complexes with H-bonding should enable us to explore the novel phenomena unique to a coupling of proton and d/$\pi$ electrons; however, such phenomena have not been discovered in solid state. Based on the background, this Ph. D. research aims to develop novel functional metal dithiolene complex crystals based on a coupling of proton and d/$\pi$ electrons.

## Chapter 2 Three-dimensional hydrogen-bonded frameworks based on metal dithiolene complex and a role of crystal solvent on the assembled structures

The author first focused on the metal catecholdithiolene complexes with four hydroxy groups, and aimed to develop the crystals with the H-bond network based on metal dithiolene complexes and to control the molecular arrangement. In this chapter, the first three-dimensional (3D) H-bonded frameworks based on metal dithiolene complex have been realized by using the gold catecholdithiolene complex.[7]
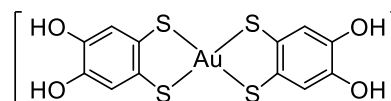


**Fig.1** Chemical structure of the gold dithiolene complex, [Au(catdt)$_2$].

New gold catecholdithiolene complex, [Au(catdt)$_2$]$^-$ (Fig.1, catdt = catechol-4,5-dithiolate), was synthesized. The complex was crystallized as 1:1 salts of Ph$_4$P$^+$ cation, and three kinds of the crystals containing different crystal solvents were obtained: (Ph$_4$P)[Au(catdt)$_2$]·0.5H$_2$O (**3-Au·0.5H$_2$O**), (Ph$_4$P)[Au(catdt)$_2$]·Et$_2$O (**3-Au·Et$_2$O**), and (Ph$_4$P)[Au(catdt)$_2$]·2THF (**3-Au·2THF**) (Fig.2a). In the crystals, the rigid and planar [Au(catdt)$_2$]$^-$ complex are connected by multiple intermolecular [O–H···O] H-bonds between the four hydroxy groups (Fig.2b). Interestingly, **3-Au·0.5H$_2$O** and **3-Au·Et$_2$O** have 3D H-bonded
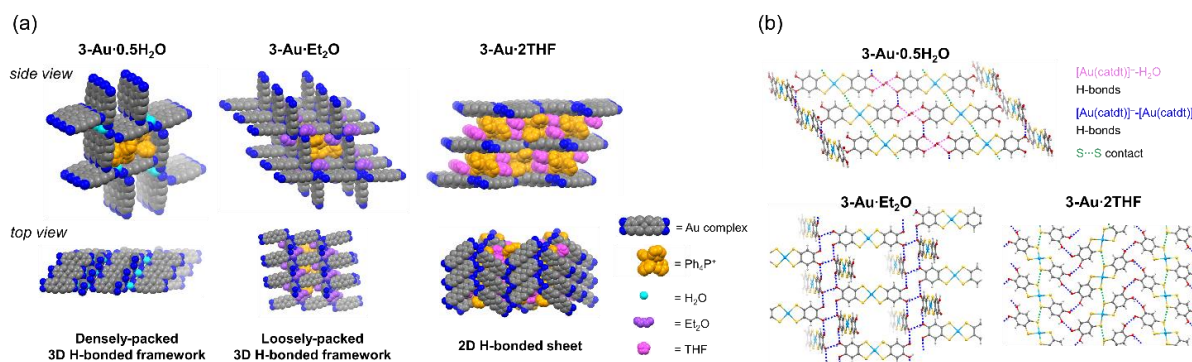
**Fig.2** (a) Assembled structures and (b) H-bonding structures based on [Au(catdt)$_2$]$^-$ complexes in each crystal.

frameworks, which are different structures from each other (Fig.2a left and middle). The counter cations, Ph$_4$P$^+$, are included in the framework with multiple cation-anion short contacts, which would stabilize these 3D frameworks. These are the first examples of 3D framework structures based on metal dithiolene complexes. On the other hand, **3-Au·2THF** formed a 2D H-bonded sheet structure (Fig.2a right). In order to explain the difference in assembled structures, the author focused on the H-bonding ability, size, and shape of the crystal solvents. The smallness and proton-accepting and -donating properties of the water facilitate the formation of the densely-packed 3D framework (Fig2a left). On the other hand, bulky Et$_2$O molecule prevents the gold complexes from approaching each other, resulting in the loosely-packed 3D framework (Fig.2a middle). In **3-Au·2THF**, due to the disk shape of the THF molecule, the THF molecules are positionally disordered, which leads to the formation of the THF-THF H-bonds. These H-bonds would interfere with the formation of the 3D structure. Therefore, in these crystals, the structure and dimensionality of the frameworks can be modulated by changing the crystal solvents, in which interactions between the solvent molecules play an important role.

The characteristic molecular assembly which had not been observed for the metal dithiolene complexes will lead to the peculiar functionalities derived from their framework structures. Therefore, these findings indicate that the metal catecholdithiolene complexes are a good building block for constructing H-bonded molecular frameworks with d/π-electrons, leading to the basis of the playground for electron–proton coupled functionalities in the crystal.

## Chapter 3 Magnetic property change with PCET of metal dithiolene complex and the effect of deprotonation on d/π-electronic states

Proton-coupled electron transfer (PCET) is an important phenomenon upon the development of novel functionalities combining protonic and electronic properties.[8] In this chapter, by exchanging the central metal of the metal catecholedithiolene complexes from gold to nickel (Fig.3), the author realized protonation/deprotonation-coupled



**Fig.3** Chemical structure of the nickel dithiolene complex, [Ni(catdt)$_2$].

magnetic property change of nickel dithiolene complex crystals via PCET in the solution process.

From the reported nickel complex salt, (Ph$_4$P)$_3$[Ni(catdt)$_2$]2Br, four kinds of new crystals were successfully obtained by recrystallization: (Ph$_4$P)[Ni-H$_4$(catdt)$_2$]·DMSO, **3-Ni-4H·DMSO**, (Ph$_4$P)[Ni-H$_3$(catdt)$_2$]·THF, **3-Ni-3H·0.5THF**, (Ph$_4$P)[Ni-H$_3$(catdt)$_2$]·0.5H$_2$O, **3-Ni-3H·0.5H$_2$O**, and (Ph$_4$P)$_2$[Ni-H$_2$(catdt)$_2$]·H$_2$O, **3-Ni-**

**Fig.4** (a) Assembled structures, (b) C–O bond lengths of the nickel complexes, and (c) change of the electronic states of the nickel complexes through PCET in solution processes in each crystal.
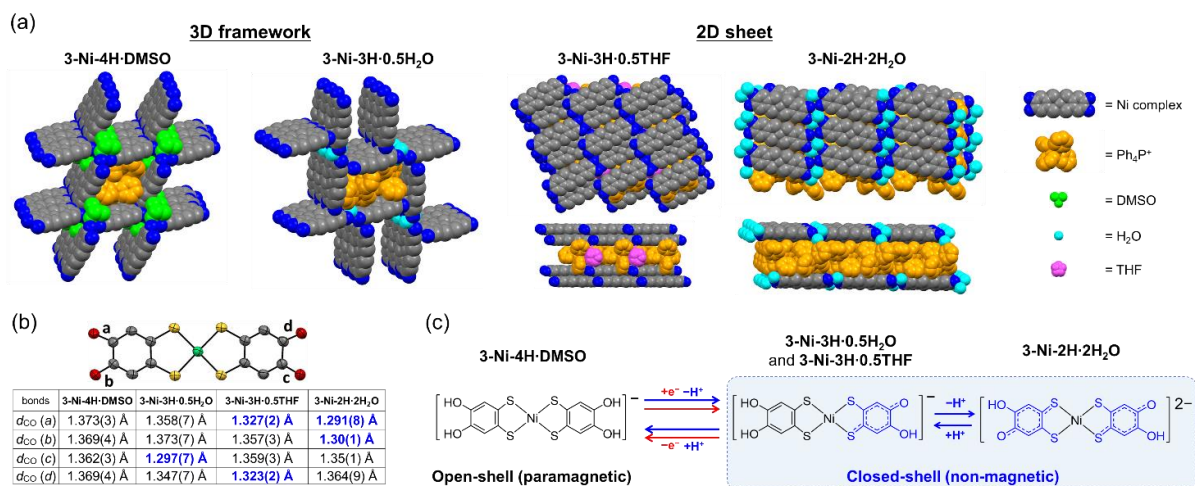
**2H·2H$_2$O**.

Firstly, focusing on the crystal structures, **3-Ni-4H·DMSO** and **3-Ni-3H·0.5H$_2$O** has a 3D framework structure based on the nickel complexes formed by [O–H⋯O] H-bonds between nickel complexes and those between nickel complex and crystal solvents (Fig.4a left). On the other hand, **3-Ni-3H·0.5THF** and **3-Ni-2H·2H$_2$O** had 2D sheet structures formed by [O–H⋯O] H-bonds based on nickel complexes (Fig.4a right). Interestingly, in **3-Ni-3H·0.5H$_2$O** and **3-Ni-3H·0.5THF**, the nickel complexes formed anionic [O–H⋯O]$^-$ H-bonds ($d_{O⋯O}$ = ~2.59 Å) with each other. Such low-barrier H-bonds have a potential for proton transfer between the O atoms with external-stimuli.[2] Furthermore, a detailed comparison of the bond lengths of the nickel complexes in each crystal revealed that the molecular structures and electronic states are significantly different (Fig.4b). The C–O bond lengths of the nickel complex in each crystal suggest that partial deprotonation of catechol moiety of the nickel complexes should occur in **3-Ni-3H·0.5H$_2$O**, **3-Ni-3H·0.5THF**, and **3-Ni-2H·2H$_2$O** (Fig. 4b). Considering that the nickel complexes in **3-Ni-3H·0.5H$_2$O** and **3-Ni-3H·0.5THF** are monoanionic states and that in **3-Ni-2H·2H$_2$O** is dianionic state, electronic states and properties should also be changed by oxidation.

In order to investigate the spin-states of the nickel complexes in each crystal, electron spin resonance (ESR) measurements were carried out. The ESR signal was observed for the non-deprotonated crystal, **3-Ni-4H·DMSO**; on the other hand, the deprotonated crystals, **3-Ni-3H·0.5H$_2$O**, **3-Ni-3H·0.5THF** and **3-Ni-2H·2H$_2$O**, showed no ESR signals. This result indicates that the nickel complexes of these crystals are singly or doubly deprotonated with one-electron oxidation, as shown in Fig.4c. Therefore, the magnetic properties in the crystals are changed from paramagnetic to non-magnetic through PCET in solution (Fig.4c). In addition, the DFT calculations based on the crystal structures reveal that the d/π electronic states were significantly modulated with the deprotonation. This result indicates that the complex is a good candidate for exploring novel functionalities and phenomena based on d/π electrons coupled to proton dynamics in solid state.

# Chapter 4 Vapochromism induced by intermolecular electron transfer coupled with hydrogen bond formation

Vapochromic materials, which respond with color changes when exposed to vapors, have attracted much attention as good candidates for chemical sensors because they can directly visualize external environmental changes.[9] In this chapter, the author successfully developed the novel vapochromic metal-dithiolene-based crystals



**Fig.5** Chemical structure of the zinc dithiolene complex, [Zn(4-mxbdt)$_2$].

and realized a new mechanism based on electron transfer coupled with H-bond formation.[10]

A zinc complex salt **4-Zn**, (Ph$_4$P)$_2$[Zn(4-mxbdt)$_2$] (4-mxbdt: 4-methoxybenzenedithiolate, Fig.5), was newly synthesized. The methanol-containing salt, **4-Zn·2MeOH**, was obtained by slow evaporation of methanol solution as yellow crystals. In this crystal, methanol molecules formed [S···H–O] H-bonds with S atoms on the [Zn(4-mxbdt)$_2$]$^{2-}$ complex (Fig.6a top). Interestingly, drying the crystals under vacuum resulted in the color change from yellow to orange, maintaining its single-crystalline state. From the structural analysis, the two methanol in **4-Zn·2MeOH** desorbed completely being converted to the orange crystal **4-Zn** with changes in molecular structure and arrangement. This process is reversible, and a similar color was also observed by the sorption of water vapor in the atmosphere. (**4-Zn·H$_2$O**; Fig.6a bottom).

To elucidate the mechanism of vapochromism in this crystal, the author firstly compared the crystal structures before and after vapor sorption. Both **4-Zn·H$_2$O** and **4-Zn·2MeOH** have [S···H–O] H-bonds between the [Zn(4-mxbdt)$_2$]$^{2-}$ complex and the absorbed vapor molecules (Fig.6a). On the other hand, significant changes in the molecular structure and arrangement of the [Zn(4-mxbdt)$_2$]$^{2-}$ complexes were observed only in the methanol sorption process. These results suggest that the vapochromism in this crystal is related to H-bond formation, rather than molecular and assembled structure changes which have been proposed for conventional vapochromic materials. Then, DFT calculations based on the experimentally observed crystal structures were carried out to reveal the effect of H-bond formation on the vapochromism. Calculated absorption spectra based on hypothetical crystal structures "**4-Zn·2MeOH** without 2MeOH", where only the structural changes of the zinc complexes are considered, was almost the same as that of **4-Zn**;



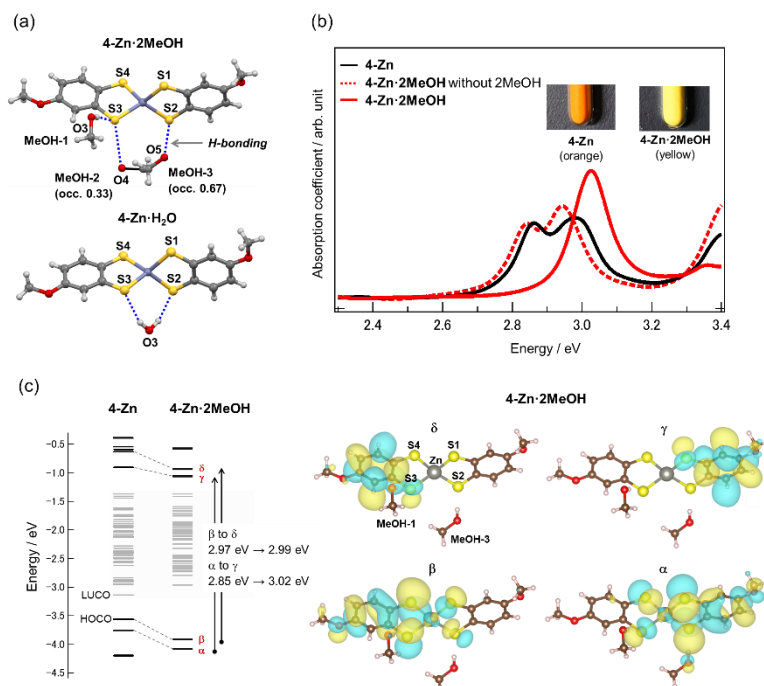**Fig.6** (a) H-bonding structures in **4-Zn·2MeOH** and **4-Zn·H$_2$O**. (b) The calculated absorption spectra of **4-Zn**, **4-Zn·2MeOH** and the hypothetical "**4-Zn·2MeOH** without 2MeOH" based on the experimentally observed crystal structures. The photograph of the crystalline materials. (c) (left) Crystal orbital energies of **4-Zn** and **4-Zn·2MeOH**, and (right) corresponding crystal orbitals in **4-Zn·2MeOH**.

on the other hand, calculated absorption spectra based on the real crystal structure "**4-Zn·2MeOH**" considering the interactions with the vapor molecules through H-bonds showed a blue shift (Fig.4b). These results indicate that the origin of the vapochromism in this crystal is the intermolecular H-bond formation. In addition, from Mulliken population analysis, significant electron transfer from the $[Zn(4\text{-mxbdt})_2]^{2-}$ complex to methanol or water molecules were observed. These results reveal that the H-bond formation causes electron transfer.

To elucidate the relationship between the blue shift and the electron transfer through H-bonds, the author focused on the energy and distribution of the crystal orbitals related to the visible-light absorption. The energy diagram shows that the blue shift is caused by stronger stabilization of the crystal orbitals $\alpha$ and $\beta$ compared with $\gamma$ and $\delta$ (Fig.6c left). This comparatively strong stabilization of $\alpha$ and $\beta$ is due to the large orbital weight on the H-bonding S atoms of $\alpha$ and $\beta$ (Fig.6c right). Therefore, a new vapochromism mechanism based on electron transfer through H-bond formation was successfully realized in this crystal. The findings here provide important insights to expand the scope of molecular designs for vapochromic as well as other stimuli-responsive materials. In this work, the author demonstrated the d/$\pi$ electronic state modulation coupled with H-bonding proton: electron–proton coupled optical functionality.

**Chapter 5 General conclusion**

In this Ph.D. study, the author demonstrated the first 3D H-bonded framework based on metal dithiolene complexes through the synthesis of gold catecholdithiolene complex crystals in Chapter 2, which can be the basis for novel electron–proton coupled functionalities unique to the framework structures. Then, based on this result, by exchanging the central metal from gold to nickel, the protonation/deprotonation-coupled magnetic property change (from paramagnetic to non-magnetic) through PCET in solution processes was realized in crystalline solid states in Chapter 3. Furthermore, in Chapter 4, d/$\pi$ electronic states modulation based on electron transfer coupled with H-bond formation was revealed in the novel zinc-dithiolene-based vapochromic crystal, leading to the optical functionalities. This is the first vapochromic behavior caused by only the H-bond formation. Therefore, the author achieved the development of the novel metal dithiolene complex crystals exhibiting peculiar functionalities based on a coupling of H-bonding protons and d/$\pi$ electrons in this Ph. D. study. These findings provide an important basis for realizing novel phenomena, where $\pi$ and d electrons are coupled with the electrostatic effect of H-bonding and proton dynamics in solid state.

**Reference**

[1] T. Isono et al., *Nat. Commun.* **2013**, *4*, 1344. [2] A. Ueda et al., *J. Am. Chem. Soc.* **2014**, *136,* 12184. [3] T. Isono et al. *Phys. Rev. Lett.* **2014**, *112*, 177201. [4] M. Shimozawa et al., *Nat. Commun.* **2017**, *8*, 1812. [5] T. Kambe et al., *J. Am. Chem. Soc.* **2013**, *135*, 2462. [6] H. Cui et al., *J. Am. Chem. Soc.* **2014**, *136*, 7619. [7] S. Yokomori et al., *CrystEngComm* **2019**, *21*. 2940. [8] D. R. Weinberg et al., *Chem. Rev.* **2014**, *112*, 4016. [9] E. Li et al., *Chem. Soc. Rev.* **2020**, *49*, 1517. [10] S. Yokomori et al., *J. Mater. Chem. C*, **2020**, *8*. 14939.

# Contents

# Chapter 1

## General Introduction

### 1.1 Functional molecular materials

In human history, developments of organic/inorganic materials always lead to the basis for elucidation of the principles of nature and many scientific innovations. Among them, the functional materials, which are used in our lives everywhere, are essential for our society, e.g., for a better quality of life and work productivity. Functional "molecular" materials have been actively developed and studied particularly in the last decades, owing to the expansion of synthesis techniques for organic molecules. Compared to typical inorganic materials composed of atoms as the basic components, molecular materials have almost infinite possibilities to pioneer and tune the functionalities owing to multiple degrees of freedom, such as diversity of chemical structure and combination of constituent molecules as well as a variety of molecular arrangements. In addition, physical flexibility and solution processability are helpful to applications for next-generation electronics, such as electronic devices and switching sensors. Such applications are based on functionalities of molecular materials, and, of course, the functionalities are originated from constituent molecules. For example, metal-organic frameworks (MOFs)[1], which are one of the most famous multi-functional molecular materials, show gas separation/storage abilities based on the porous framework structures[2] together with other many functionalities, such as magnetic[3,4], optical, electronic/ionic transport[5–7], and catalytic[8] properties. Here, the ligand molecules and metal ions have been designed and combined corresponding to the desired functionality. Other representative molecules or materials for various functionalities are described in Fig.1-1. To realize desired functionalities for further applications, developments of new functional molecular materials based on understanding detailed structure-property relationships are essential tasks.

Functionalities of molecular materials have been explored based on designing the chemical structure of the constituent molecules and tuning intermolecular interactions, which is decisive to molecular arrangements. Even the slight differences in the chemical structure can cause significant changes in the assembled structures, resulting in changes in their functionalities. For example, although many crystals of charge-transfer (CT) salts consisting of tetrathiafulvalene and inorganic anions ($(TTF)_2X$) showed the disappearance of metallic or semiconducting behavior at low temperature due to Peierls instability derived from the one-dimensional (1D) $\pi$-$\pi$ stacking structure,[9–12] a crystal of CT salts based on bis(ethylenedithio)-TTF (BEDT-TTF) demonstrated Q1D or 2D molecular arrangements, achieving the metallic conducting behavior down to low temperature (at least 2 K) and superconductivity.[13,14] This result is derived from the introduction of the ethylenedithio groups, where the sulfur-rich substituent deviated from the TTF plane helps the formation of multiple intermolecular S⋯S contacts and modulation of simple 1D stacking arrangement, leading to the construction of 2D $\pi$-$\pi$ interaction. As with this case, the electrical conductivity of organic conductors has been modulated and controlled by modification of the constituent molecules to tune intermolecular interaction and molecular arrangements.[13,15–18] Criteria for the structural modifications rely on the accumulated knowledge of detailed crystal structural analysis, electrical conductivity measurements, and band calculations. In this way, a single crystallinity (uniform and unambiguous composition and structure) is of significant advantage to reveal the structure-property relationships by such crystallographic and theoretical studies as well as proper evaluation of the intrinsic physical properties. Therefore, to understand the detailed structure-property relationships, it is important to synthesize new single-crystalline functional molecular materials and to elucidate the mechanism of the functionalities based on physical property measurements as well as crystallographic and theoretical studies.
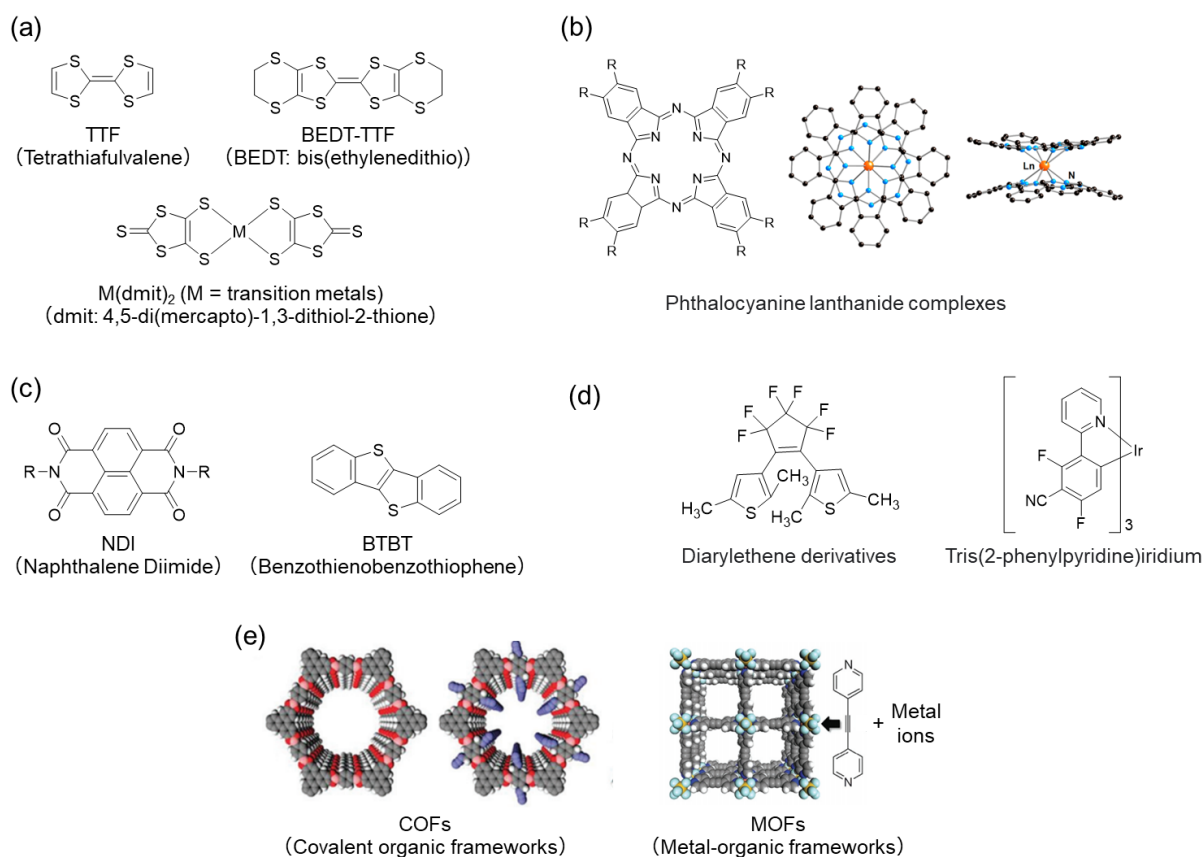
**Fig. 1-1** Various functional molecular materials and the representative molecules or materials. (a) molecular conductor,[15,19] (b) molecular magnets,[20] (c) molecular semiconductor for OFET,[21,22] (d) luminescent and chromic molecular materials,[23] and (e) gas separation/storage materials.[24,25]
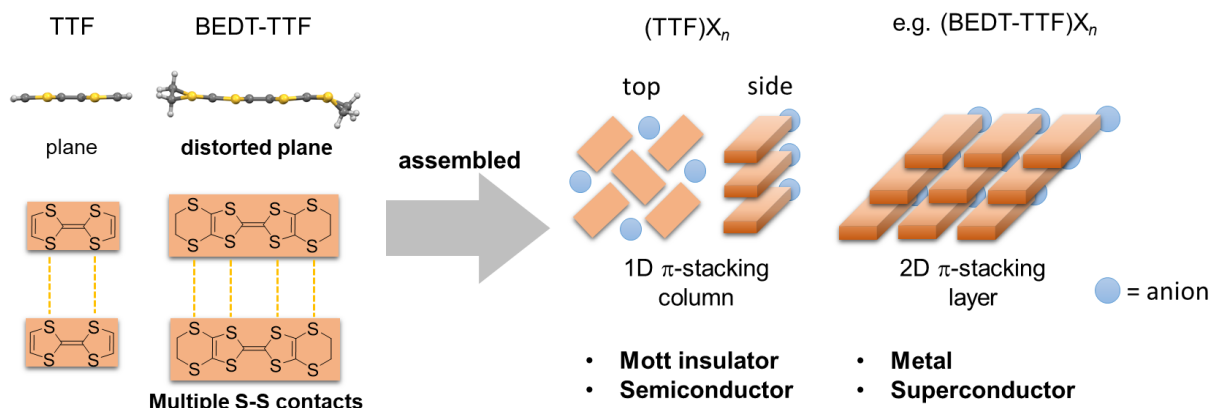


**Fig. 1-2** A strategy of the development of organic molecular conductors. The introduction of ethylenedithio group to the TTF molecule leads to distortion of the molecular structure and formation of multiple intermolecular S⋯S contacts, resulting in modulation of molecular arrangement and electrical conducting properties of the crystals.

## 1.2 Hydrogen bond in molecular crystals

Recently, Hydrogen-bond (H-bond) has attracted much attention as a dominant intermolecular interaction in molecular materials, which modulates the assembled structures and thus can drastically change the functionalities. H-bonds play a role in structural regulation everywhere in nature. As one of the most famous examples, it is a well-known fact that H-bond formation is used to construct the complementary helical structure in DNA.[26]

H-bond is an electrostatic non-covalent interaction between proton acceptor and proton donor. It was discovered by Moore and Winmill in 1912,[27] and then Pauling proposed that H-bond is one type of chemical bond described by [D–H···A] (D: proton donor, A: proton acceptor).[28] Generally, oxygen, nitrogen, sulfur, and halogen atoms can be the A and D. The high directionality and intermediate strength (4–40 kcal/mol, Table 1.1) between vdW and $\pi$-$\pi$ interactions (< ~10 kcal/mol), and coordination and covalent bonds (> ~80 kcal/mol) of the H-bond makes it useful for controlling the molecular structures and arrangements (Table 1.1). In addition, the variation of structure and interaction energy of H-bond often leads to a variety of molecular and crystal structures. Very strong H-bonds, such as $[O···H···O]^-$ and $[N···H···N]^+$, will be single-well or low-barrier H-bonds, although other common H-bonds have double-well-type potentials.[29] Proton or deuteron in these H-bonds can be reversibly delocalized or localized between the mother atoms (D and A) with external-stimuli (temperature change, pressure, and electric field) or isotope substitution (i.e., deuterium), leading to dielectric properties.[29,30] On the other hand, [C–H···O]-, [O–H···$\pi$]-, and [C–H···$\pi$]-type interactions are recently recognized as weak H-bonds (< 4 kcal/mol, Table 1.1).[31] By using the above-mentioned high directionality, intermediate strength, and variation of structure and interaction energy, H-bonded molecular materials have been actively studied from the viewpoint of crystal engineering and the development of functionalities based on structural regulations.

**Table 1-1** H-bonds with various strengths.[31]

| | Very strong | Strong | Weak |
|---|---|---|---|
| Bond energy (−kcal/mol) | 15–40 | 4–15 | <4 |
| Examples | $[F\cdots H\cdots F]^-$ | $O-H\cdots O=C$ | $C-H\cdots O$ |
| | $[N\cdots H\cdots N]^+$ | $N-H\cdots O=C$ | $O-H\cdots \pi$ |
| | $P-OH\cdots O=P$ | $O-H\cdots O-H$ | $Os-H\cdots O$ |
| IR $v_s$ relative shift | >25% | 5–25% | <5% |
| Bond lengths | $H-A \approx X-H$ | $H\cdots A > X-H$ | $H\cdots A \gg X-H$ |
| Lengthening of $X-H$ (Å) | 0.05–0.2 | 0.01–0.05 | ≤0.01 |
| $D(X\cdots A)$ range (Å) | 2.2–2.5 | 2.5–3.2 | 3.0–4.0 |
| $d(H\cdots A)$ range (Å) | 1.2–1.5 | 1.5–2.2 | 2.0–3.0 |
| Bonds shorter than vdW | 100% | Almost 100% | 30–80% |
| $\theta(X-H\cdots A)$ range (°) | 175–180 | 130–180 | 90–180 |
| $kT$ (at room temperature) | >25 | 7–25 | <7 |
| Effect on crystal packing | Strong | Distinctive | Variable |
| Utility in crystal engineering | Unknown | Useful | Partly useful |
| Covalency | Pronounced | Weak | Vanishing |
| Electrostatics | Significant | Dominant | Moderate |

By using intermolecular H-bonds as a structural regulator, unique assembled structures can be constructed: for example, H-bonded organic frameworks (HOFs) with porous structure.[32–44] HOFs have been actively studied for the development of functionalities, such as sensors, proton conductors, and gas absorption and storages.[32–44] In addition to the functionalities, HOFs have some advantages, such as high crystallinity and solution processability for recrystallization and purification, compared to other porous frameworks such as covalent organic frameworks (COFs)[45–47] and metal-organic frameworks (MOFs)[1,2,48]. These advantages enable us to obtain a high-quality crystal, which leads to an understanding of the intermolecular interactions and structure-property relationships in detail. Hisaki et al. have reported many porous HOFs consisting of π-conjugated organic molecules.[37,39,44,49–52] Carboxyphenyl-substituted trinaphthylene derivatives having six carboxy groups at the molecular terminal constructed H-bonded hexagonal networks to form HOFs showing significant thermal stability (Fig. 1-3a).[39,44,50] In particular, a HOF consisting of the trinaphthylene derivatives with acid-responsive moiety on the core unit exhibits reversible optical property changes (color and emission property changes) with exposure to acid vapor due to the accessibility to the acid-responsive

moiety derived from the porous structure.[44] On the other hand, X-type π-conjugated molecules having four carboxy groups at the molecular terminal (Fig. 1-3b) have formed rhombic network (RhomNet) sheet structures due to the high directionality of intermolecular H-bond formation between carboxy groups (Fig. 1-3b).[37] The X-ray structural analysis reveals that the stacking manners of the RhomNet sheets depend on the molecular conformation/symmetry and interlayer interactions. In these crystals, the high crystallinity of these three HOFs made it possible to reveal how the stacking manner changes with molecular structures and intermolecular interactions.
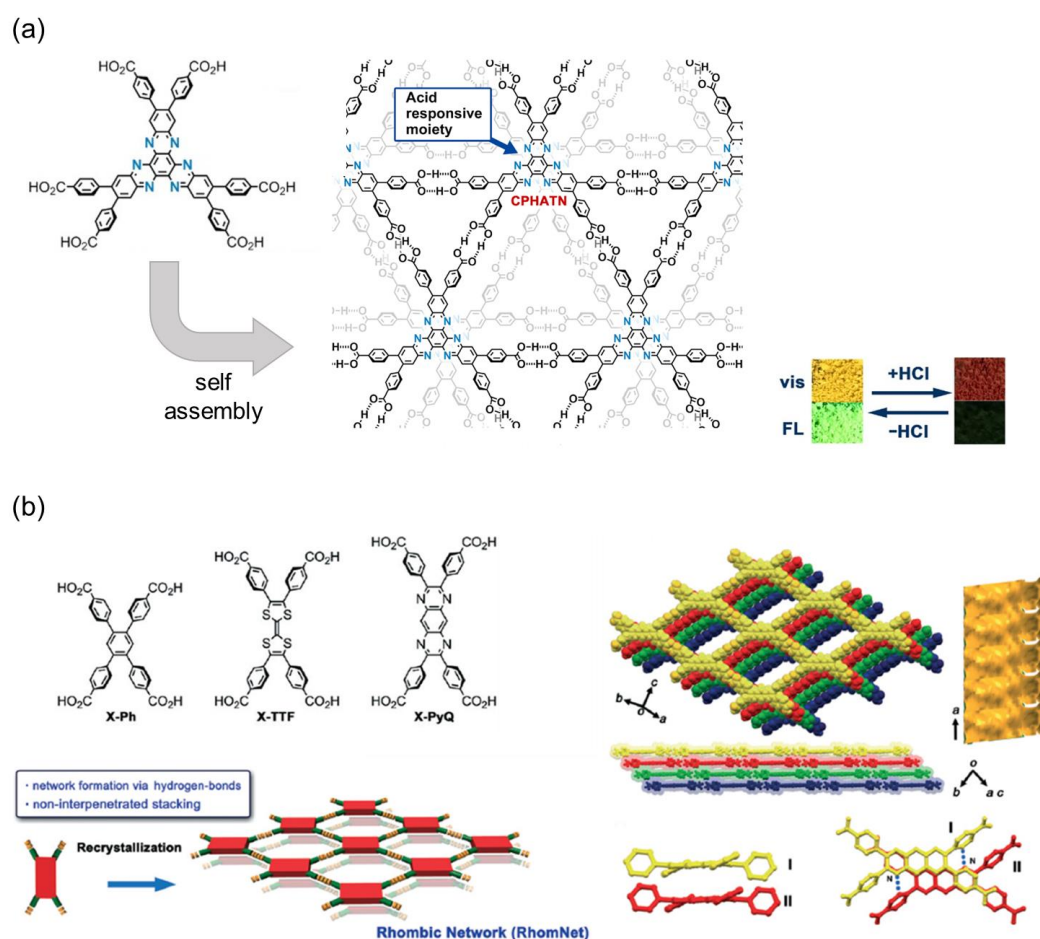


**Fig. 1-3** (a) Carboxyphenyl-substituted trinaphthylene derivatives, the 2D hexagonal HOF structure, and optical properties responsivity to acid vapor (HCl).[44] (b) X-type π-conjugated organic molecules with H-bonding ability, the RhomNet sheet structure and the stacking manner, and intermolecular interactions between the layers.[37]

Structural regulation utilizing H-bond has also been used for control of the electronic functionalities via control of the molecular assembly. A CT salt based on benzothienobenzothiophene (BTBT), $(BTBT)_2PF_6$, is a molecular conductor with metallic behavior at room temperature; however, it changes to an insulator at low temperature owing to the instability derived from the 1D conducting column structure (Fig. 1-4).[53] On the other hand, a CT complex based on the BTBT bearing hydroxy groups exhibits a construction of Q1D conducting layer originating from intermolecular H-bond formation, leading to a metallic behavior down to lower temperature. In another case, the intermediate strength and various manner of H-bond, as explained above, lead to a variety of assembled structures with changing the recrystallization conditions. The crystals constructed from bis(hydrazone)iron(II) complex and chloranilic acid display multiple H-bonded network structures (1, 2, and 3D) depending on the recrystallization solvents (Fig. 1-5).[54] This difference in the assembled structures would be related to the polarity and proton-donating/accepting abilities of recrystallization solvents. For the different assembled structures, only the crystal with 2D H-bonded sheet structures demonstrated gas absorption properties and vapochromism against various organic vapors (dichloromethane, methanol, and tetrahydrofuran etc.). As with these cases, electronic functionalities of most H-bonded molecular crystals have been developed and controlled by utilizing the H-bond as a structural regulator so far.
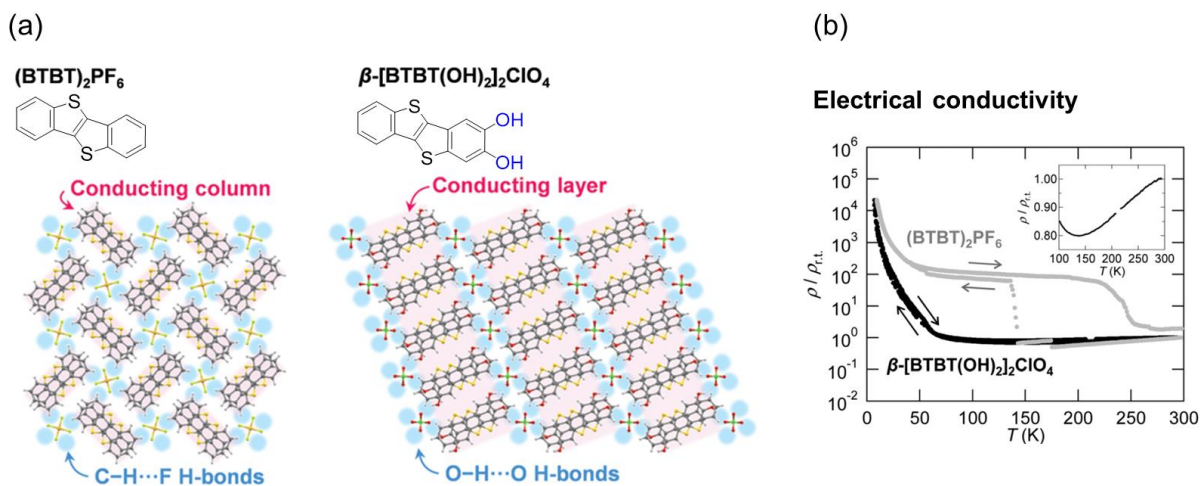
**Fig. 1-4** (a) Crystal structure of (BTBT)$_2$PF$_6$ (left) and β-[BTBT(OH)$_2$]$_2$ClO$_4$ (right). (b) Temperature dependence of the relative resistivity.[53]
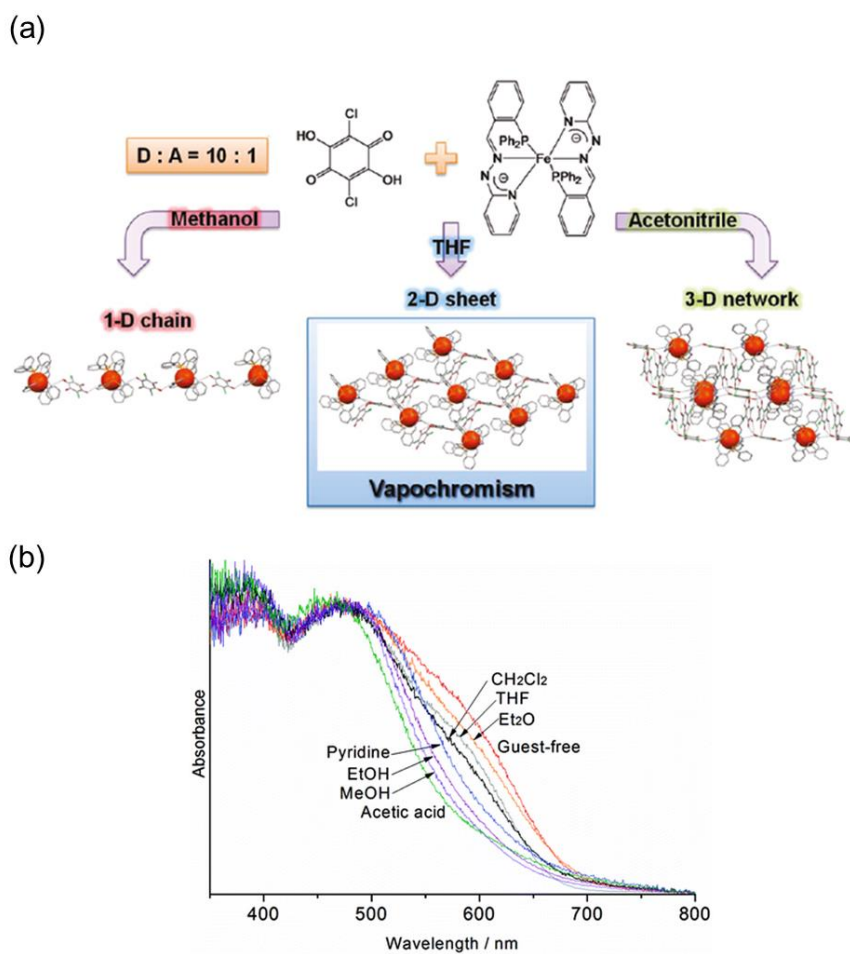


**Fig.1-5** (a) Various H-bonding network structures based on bis(hydrazone)iron(II) complex and (b) the UV-vis diffuse reflectance spectral change of the crystal with 2D sheet structure.[54]

## 1.3 Electron–proton coupled functionalities: electronic-states modulation coupled with a proton in hydrogen bonds

In addition to the above-mentioned feature as a structural regulator, recently, H-bond formation and/or proton dynamics act as an additional charge degree of freedom to directly modulate the electronic structures of the molecular crystals: electron–proton coupled phenomena. Several electron–proton coupled functionalities have been demonstrated.

### 1.3.1 Electrostatic effects by the hydrogen bond formation

H-bonding substituents (i.e., OH and NH groups) have large dipole moments derived from the large difference in electronegativities between O/N and H. Thus, the H-bond formation can modulate the electrostatic potentials affecting the electronic states of molecules or crystals. Nakasuji and Morita demonstrated π-electronic state modulation coupled with H-bond or proton in TTF-based molecular conductors.[55–61] They synthesized molecular conductors based on imidazole-substituted TTF (Im-TTF) and various acceptors (e.g., TCNQ and anilic acid) (Fig. 1-6a).[56] In the crystals, the Im-TTF formed intermolecular H-bonds with itself, acceptors, or solvent molecule, where the polarity of H-bonds tunes the redox potential of the Im-TTF and the acceptors (i.e., chloranilic acid) revealed by DFT calculations. This afforded different ionicity in complexes from those expected by the difference of redox potentials between the isolated imidazole-substituted TTF and the acceptors, which lead to the realization of the first metallic donor-acceptor CT complex crystal based on H-bond functionalized TTF (Fig. 1-6b). In addition to this compound, molecular conductor based on pyridyl-substituted TTF (Py-TTF) exhibits a unique electronic structure originating from a positive charge of H-bonding proton (Fig. 1-6c).[62] In this crystal, two Py-TTF were connected by one $[N–H \cdots N]^+$ H-bond, which induced the difference in the oxidation state of the Py-TTF (+0.3 and +0.7, Fig. 1-6c bottom and d).
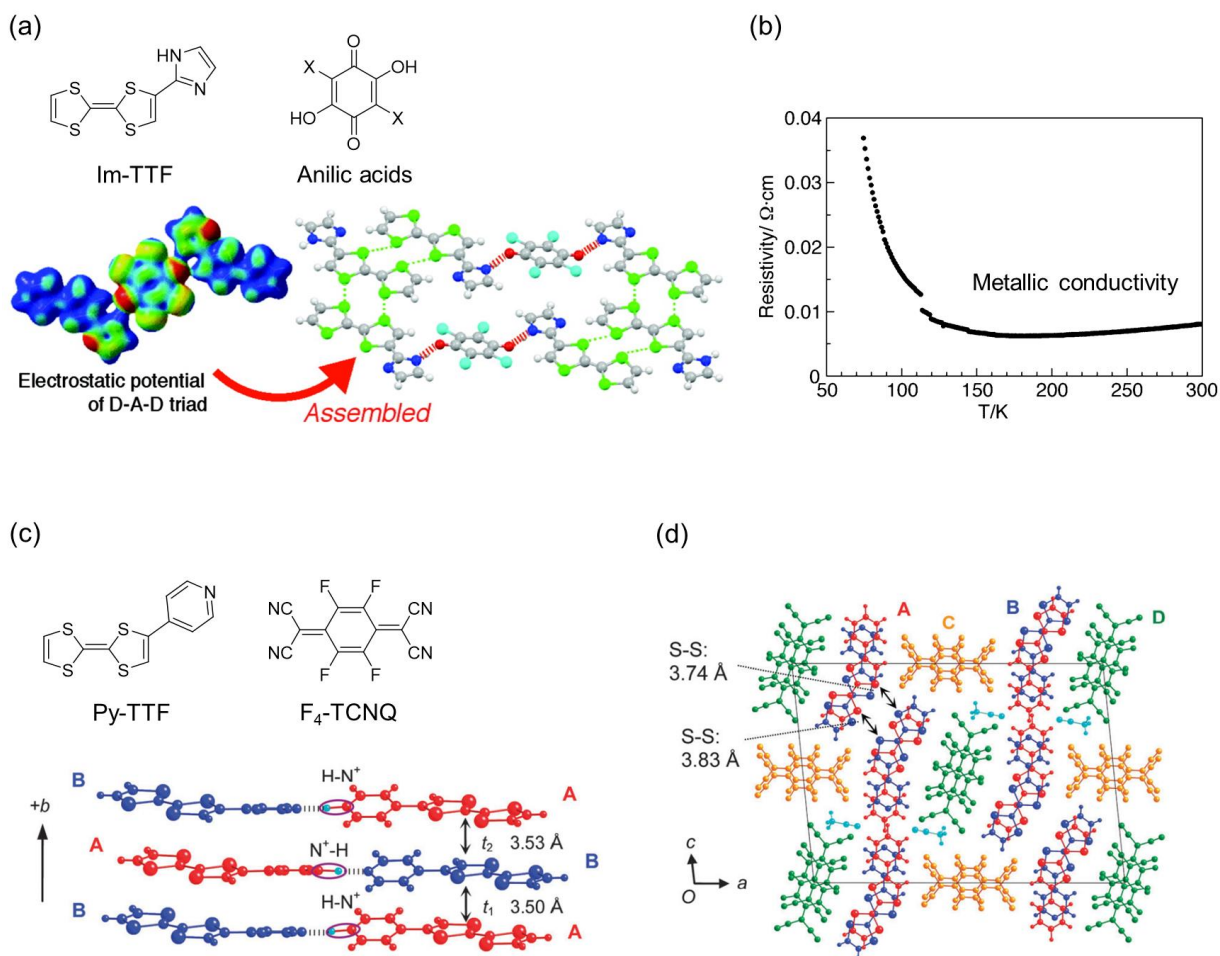
**Fig.1-6** (a) Chemical structures of Im-TTF and anilic acids and the assembled structures of the crystal and (b) the temperature dependence of resistivity.[56] (c) Chemical structures of Py-TTF and F$_4$-TCNQ and difference of the oxidation state in two Py-TTF connected by a [N–H···N]$^+$ H-bond and (d) the crystal structure of the CT complex.[62]

### 1.3.2 Proton-coupled electron transfer via solution states

In solution processes, the proton-coupled electronic properties have been studied using molecules with H-bonding protons, which are readily dissociated and mobile. Proton-coupled electron transfer (PCET)[63,64] is one of the most well-known phenomena using charge degree of freedom and dynamic properties of H-bonding proton; it is a type of chemical reaction with the transfer of protons and electrons from one molecule to another molecule. Because PCET involves the electronic-state modulation, it can be utilized to control the solid-state electronic functionalities via conversion (i.e., protonation/deprotonation with redox) of the constituent

molecules.

An H-bonded CT crystal based on the palladium complex with hydroethylenediaminoglyoxime and TCNQ, showing electronic functionalities related to the deprotonation ability, was reported by Nakasuji et al. and Yamashita et al (Fig. 1-7a).[65,66] These palladium complexes were partially deprotonated depending on pH conditions on the crystallization, leading to the partially reduced TCNQ (−0.3) as a counter anion. The partially oxidized/reduced states of constituent molecules lead to modulating band-filling, and thus the crystal displayed metallic conduction behavior at room temperature (Fig. 1-7b). Also, recently, Kobayashi et al. demonstrated metallic conduction with very high electrical conductivity ($\delta_{rt}$ = 2300 S cm$^{-1}$, $\delta_{2K}$ = 30000 S cm$^{-1}$) in a single-component molecular conductor composed of TTF-extended dicarboxylate (TED; Fig. 1-7c,d).[67,68] TED molecules are assembled by deprotonation of carboxy group and oxidation of TTF moiety as radical neutral molecules. This compound is one of the organic conductors with the highest electrical conductivity, including non-crystalline materials. These compounds are an example of tuning the electrical conductivity by PCET in a solution state.
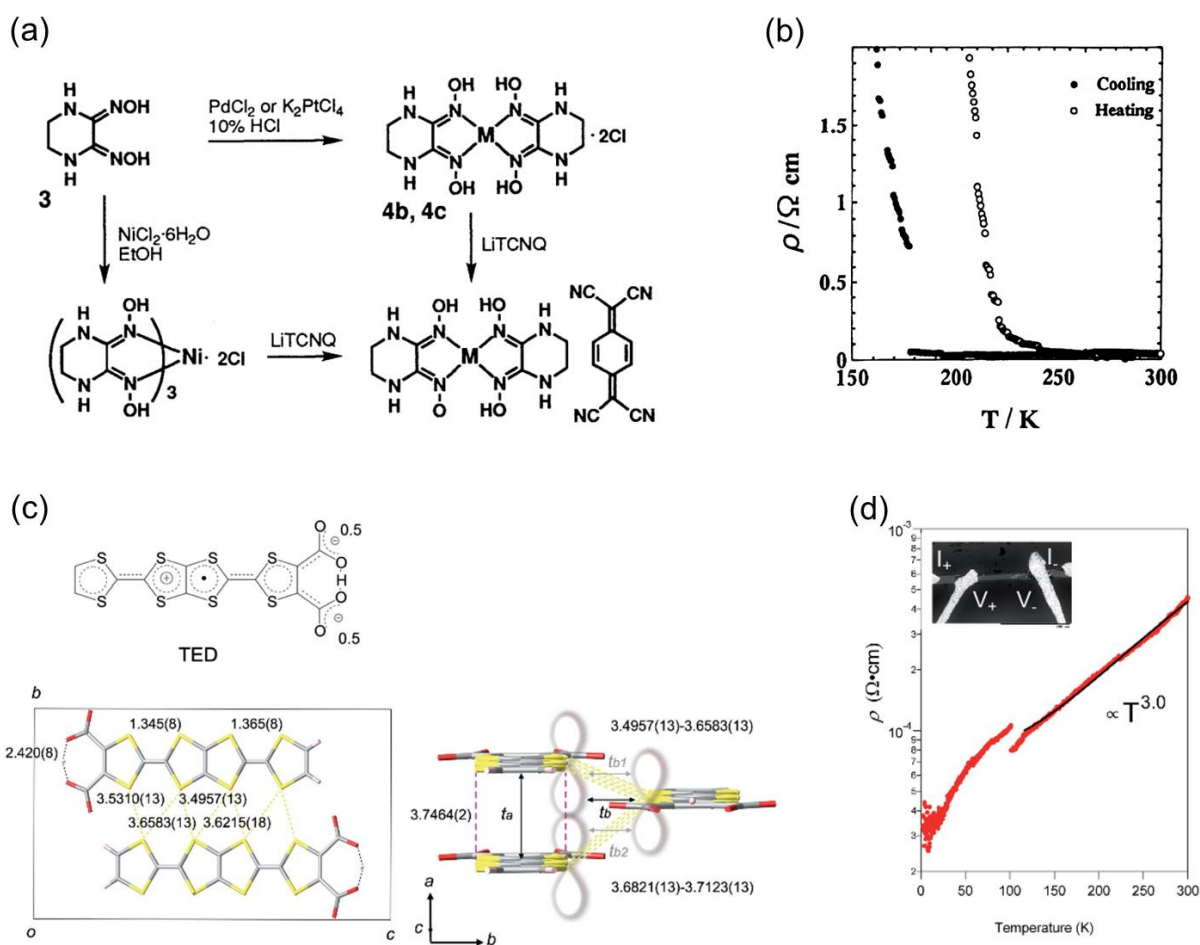
**Fig.1-7** (a) Synthetic scheme of the H-bonded CT crystal based on Pd complex with hydroethylenediaminoglyoxime and TCNQ and (b) the temperature dependence of resistivity. [64,65] (c) Chemical structure and assembled structure of TTF-extended dicarboxylate (TED) and (d) temperature dependence of the resistivity. [67,68]

### 1.3.3 Proton dynamics in crystalline solid states

Proton transfer (dynamics) can also occur in solid state. As explained in Section 1.2, very strong H-bonds (i.e., ionic H-bonds: $[O \cdots H \cdots O]^-$, $[N \cdots H \cdots N]^+$) have single-well or low-barrier double-well potential. [28] Thus, delocalization/localization of the proton in such H-bonds can be controlled by external stimuli and/or isotope substitution, leading to the electron–proton coupled functionalities in solid state. In 1988, proton-electron transfer in quinhydrone complex had been reported. [69,70] This material is constructed from *p*-benzoquinone with electron and proton accepting properties and *p*-hydroquinone with electron and proton donating properties,

where the molecules form π-stacking column structure and intermolecular [O–H···O] H-bond (Fig. 1-8a). The molecular arrangement makes π electrons and protons possible to transfer between the molecules. Actually, under high pressure, Raman and infrared spectral changes were observed, indicating the proton-electron transfer with the modulation of electronic states of the molecule.[70] However, the detailed crystal structure and physical properties have not been revealed due to the difficulty of the measurements under high-pressure conditions. In another case, such electron–proton coupling has been mentioned in ferroelectric molecular materials consisting of π-conjugated organic molecules.[71–76] In the crystal based on phenazine and anilic acid, Horiuchi et al. proposed based on DFT calculation result that the large dielectric constant is significantly related to modulation of π electron orbital with proton transfer (Fig. 1-8b).[72] Very recently, spin-crossover behavior, coupled with intramolecular proton transfer in crystalline states, has also been demonstrated, though the proton transfer was driven by modulation of the electronic configuration of the complex.[77,78]
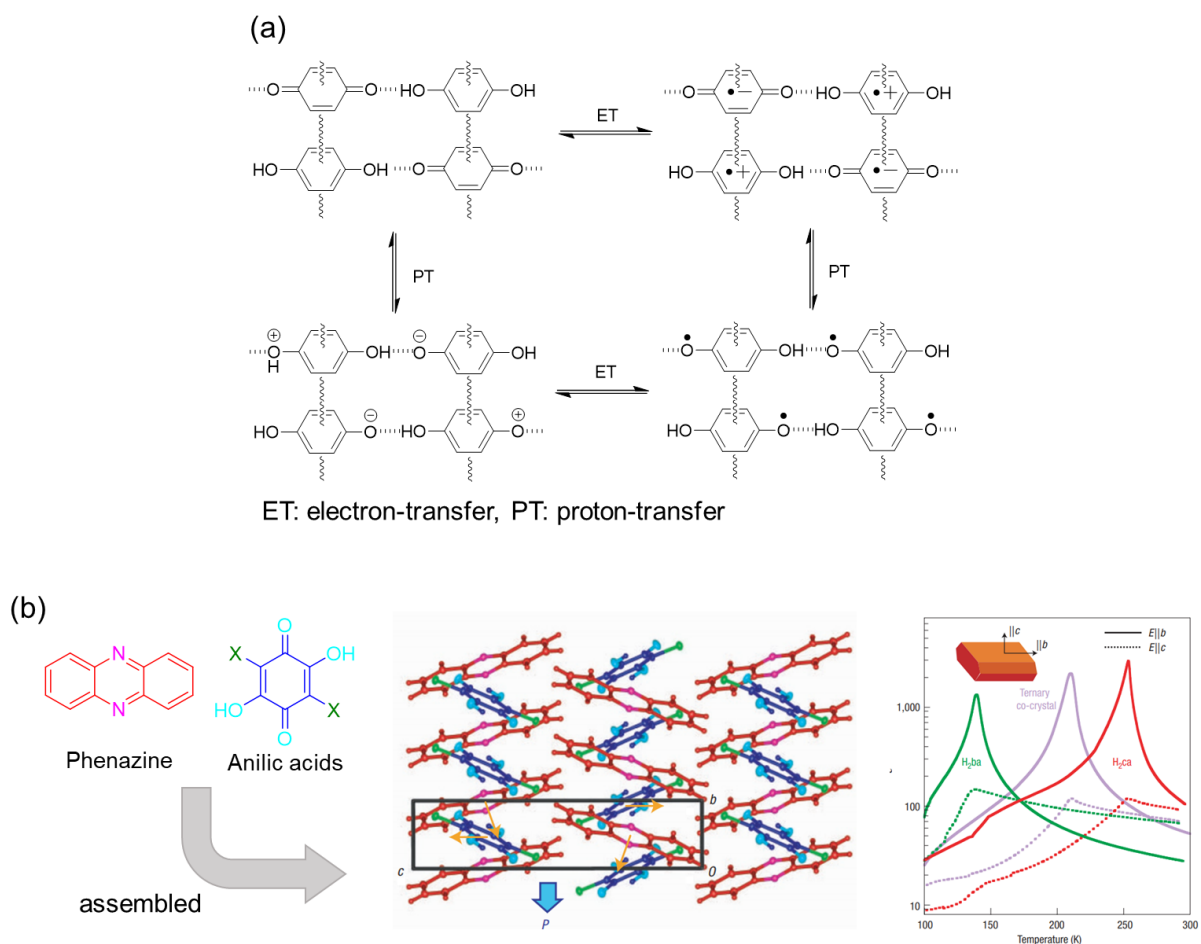
**Fig. 1-8** (a) PCET processes of quinhydrone complex crystal under pressure.[69,70] (b) chemical structures of phenazine and anilic acids (left), the assembled structure of their cocrystal (center), and the temperature dependence of dielectric constant (right).[72]

Mori and Ueda et al. has recently discovered deuteron dynamics-coupled switching of magnetism and electrical conductivity in the crystal consisting of catechol-fused TTF ($\kappa$-$D_3$(Cat-EDT-TTF)$_2$) (Fig. 1-9).[79–84] These crystals were formed by a molecular unit consisting of two Cat-TTF molecules connected by anionic [O···D···O]$^-$ type H-bond (Fig. 1-9a). The deuteron was located at the intermediate position between the oxygen atoms of the H-bonding part at room temperature, and the TTF moieties were uniformly oxidized to +0.5 state. As a result, the crystals exhibit electrical conductivity (Fig. 1-9c) and magnetism (paramagnetic semiconductor) at room temperature. Interestingly, in the deuterated crystal, the deuterons on

the anionic H-bond were localized near the oxygen atom on one side with decreasing temperature, leading to π electronic state modulation ((+0.5, +0.5) → (+0.06, +0.94), Fig. 1-9a and b).[80] This electronic-state modulation induced switching of the magnetism and the electronic conductivity from a paramagnetic semiconductor to a non-magnetic insulator. On the other hand, a proton-substituted crystal does not show any localization behavior of the protons down to very low temperature due to the quantum fluctuation of protons, leading to the proton-fluctuation-induced quantum spin liquid/ quantum paraelectric state.[81,82] In this proton-substituted crystal, the π electronic functionalities switching with proton transfer can be induced by physical pressure.[84] The mechanisms of these electron–proton coupling phenomena have been demonstrated based on detailed X-ray structural analysis, physical property measurement, and theoretical study.[85]
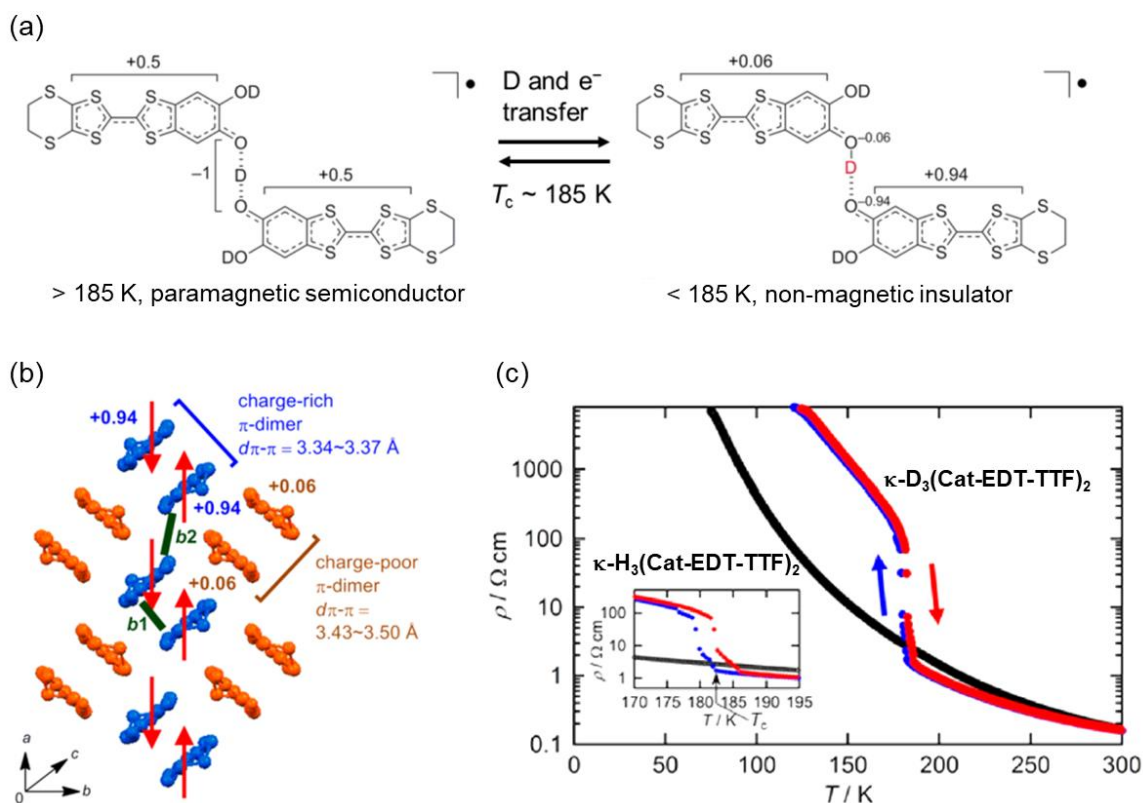


**Fig.1-9** (a) Chemical structures of $D_3$(Cat-EDT-TTF)$_2$ and electronic state modulation depending on temperature dependence. (b) Molecular arrangement and electronic structure of the low-temperature phase of κ-$D_3$(Cat-EDT-TTF)$_2$. (c) The temperature dependence of the resistivity of κ-$H_3$(Cat-EDT-TTF)$_2$ and κ-$D_3$(Cat-EDT-TTF)$_2$.[80]

Such electron–proton coupled functionalities and phenomena, as described above, are exciting from the perspective of pioneering novel physical properties in addition to basic science, such as electronic functionalities driven by electrostatic effect or dynamics of protons, and multiple functionalities originating from both electrons and protons. As seen in these compounds, intermolecular H-bond formation with π-conjugated parts can modulate the electronic states, leading promisingly to the electron–proton coupled functionalities. In particular, ionic H-bonds (single-well or low-barrier H-bonds), such as $[\text{O}\cdots\text{H}\cdots\text{O}]^-$ and $[\text{N}\cdots\text{H}\cdots\text{N}]^+$, are important to realize the electronic functionalities coupled with proton dynamics in solid states because localization/delocalization of proton in such H-bonds can be tuned by external-stimuli and/or isotopic substitution. In order to pioneer such electron–proton coupled phenomena and to apply the phenomena to a wide range of electronic functionalities, it is necessary to develop the material design criteria. However, the examples of such materials have been very limited, and the structure-property relationships and the detailed mechanism in crystals are not well-understood. Therefore, to establish the material design criteria, synthesis of the new molecular materials consisting of multi-functional molecules with ionic intermolecular H-bonds, which can show the electron–proton coupled phenomena, together with a well understanding of the mechanism, is crucial.

## 1.4 Metal dithiolene complexes for electron–proton coupled functional materials

### 1.4.1 Advantages as a component of functional materials

Metal dithiolene complexes have been firstly reported by G. N. Schrauzer and V. P. Mayweg in 1962 and actively studied the properties of the molecules and crystals.[86] Especially, metal bis(dithiolene) complexes (Fig. 1-10a) have attracted much attention as the constituent molecules to widely explore electronic functionalities in crystalline solid states. The complexes

are d/π electron-conjugated molecules consisting of central metal ions (e.g., Au, Cu, Ni, Pd, Pt, Zn, etc.) and dithiolene ligands, as shown in Fig. 1-10a.[87] The metal–sulfur bonds have a covalent character with strong hybridization, resulting in the peculiar orbitals delocalized to whole the molecule (Fig. 1-10b).[87] This strongly hybridized and delocalized d/π orbital character realizes their narrow HOMO-LUMO gaps compared to the π-conjugated molecules (HOMO: highest occupied molecular orbital, LUMO: lowest unoccupied molecular orbital) and significant intermolecular orbital hybridization between the complex molecules. Due to these features, the metal-dithiolene complexes exhibit rich electronic functionalities in solid states: magnetism[88–90], electrical conductivity[19,91–95], optical properties (visible-light absorption and photoluminescence)[96–101], and multiple redox activities[99,102] (Fig. 1-10c).[87] Furthermore, tunable d/π electronic states by modulation of the dithiolene ligand and exchange of the central metals have led to many studies to develop the electronic functionalities in sold states. As a result, a lot of significant discoveries in chemistry and physics have been found.
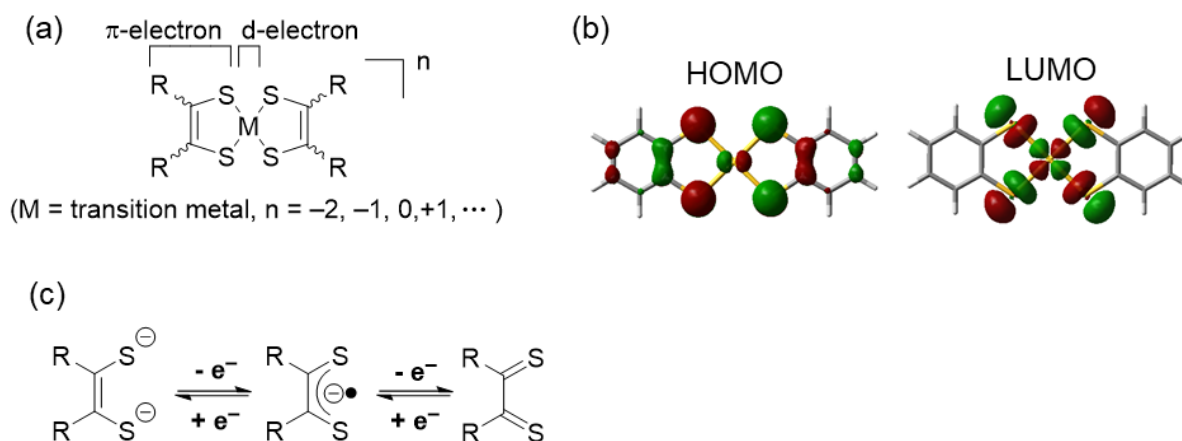


**Fig. 1-10** (a) Chemical structures of metal bis(dithioelene) complexes and (b) the typical HOMO and LUMO of metal bis(dithiolene) complex (i.e., metal benzenedithiolate complex monoanion). (c) The multiple redox processes of the dithiolene ligand.

The number of electrons and open or closed-shell states of metal dithiolene complexes can be tuned by the selection of central metal ions. The neutral gold dithiolene complexes become

open-shell states; thus, the many single-component molecular conductors based on gold dithiolene complexes have been found with ligand modification.[103–110] On the other hand, neutral nickel (or palladium and platinum) dithiolene complexes have a closed-shell state, to construct a band insulator in solid state as it is.[111] Due to the narrow HOMO-LUMO gap and $\pi$-stacking structure, it becomes a single-component field-effect transistor (n-type, p-type, and ambipolar).[112–115] Such electronic states and functionalities can also be modulated by modifying the dithiolene ligands. For example, by introducing the TTF moiety to the ligands, an open-shell state and high electrical conductivity were induced in nickel dithioelene complexes.[91,94,117–119] In such complex molecules, TTF moieties are partially oxidized with intramolecular charge transfer between the TTF parts and the dithioelene part. This leads to HOMO-LUMO band overlap derived from narrow HOMO-LUMO gap and significant interorbital interaction, to generate the charge carriers.[118] The first single-component molecular metal, Ni(tmbt)$_2$,[117] and the first single-component molecular superconductor, Ni(hfdt)$_2$,[94] have been realized by Kobayashi et al. (Fig. 1-11). In addition, in 2018, although there had been no single-component molecular metal without TTF moiety, Lorcy et al. demonstrated the first single-component molecular metal consisting of metal dithiolene complex without TTF moieties.[109] The key for the achievement was a 3D Fermi surface based on S⋯S contacts connecting the 2D $\pi$-$\pi$ stacking structures derived from the ligand design.
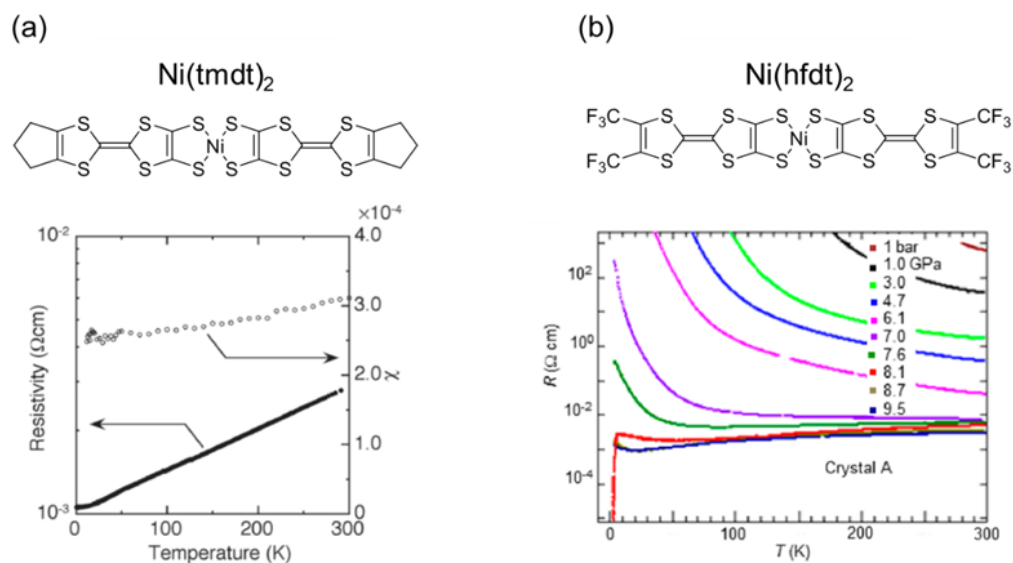
**Fig.1-11** (a) single-component molecular metal, Ni(tmbt)$_2$ and (b) single-component molecular surperconductor Ni(hfdt)$_2$.[94,117]

Also, crystalline 2D coordination polymers based on the dithiolene complex have been reported, which exhibit characteristic electronic functionalities. Nishihara et al. developed a coordination polymer consisting of nickel and benzenehexathiol having metal dithiolene unit in mixed-valence states, where the metal bis(dithiolene) unit took 0 or -1 oxidation states (Average charge of metal bis(dithiolene) unit is -3/4) (Fig. 1-12a and b).[102,120–122] This compound shows switchable d/π electronic states by chemical redox, leading to significant modulation of electrical conductivity (Fig. 1-12c). Furthermore, in the last five years, the dithiolene-based coordination polymers with high crystallinity have been reported to display metallic conductivity[123,124], superconductivity[125], and high-performance ambipolar transport properties.[126]

In addition to the electrical conductivity and carrier transport properties, many other interesting electronic functionalities have been explored in metal-dithiolene complexes. The family of dithiolene complexes bearing 1,2-dithiole-2-thione-4,5-dithiolate, M(dmit)$_2$,[93] have a half charge ($-0.5$) to form a dimer ($-1.0$) in crystalline solid states. Thanks to this feature, and

19

various electronic states and assembled structures by an exchange of counter cation and central metal, the crystals of the complex show a wide range of electronic properties, such as ferromagnetic interactions[88,127–129] and quantum spin liquid,[89,90] in addition to high conductivity (metallic and superconducting).[93] More recently, it was demonstrated that single-component molecular conductor, Pd(dddt)$_2$ (dddt: 5,6-dihydro-1,4-dithiin-2,3-dithiolate) becomes a Dirac electron system under high pressure.[130–132]
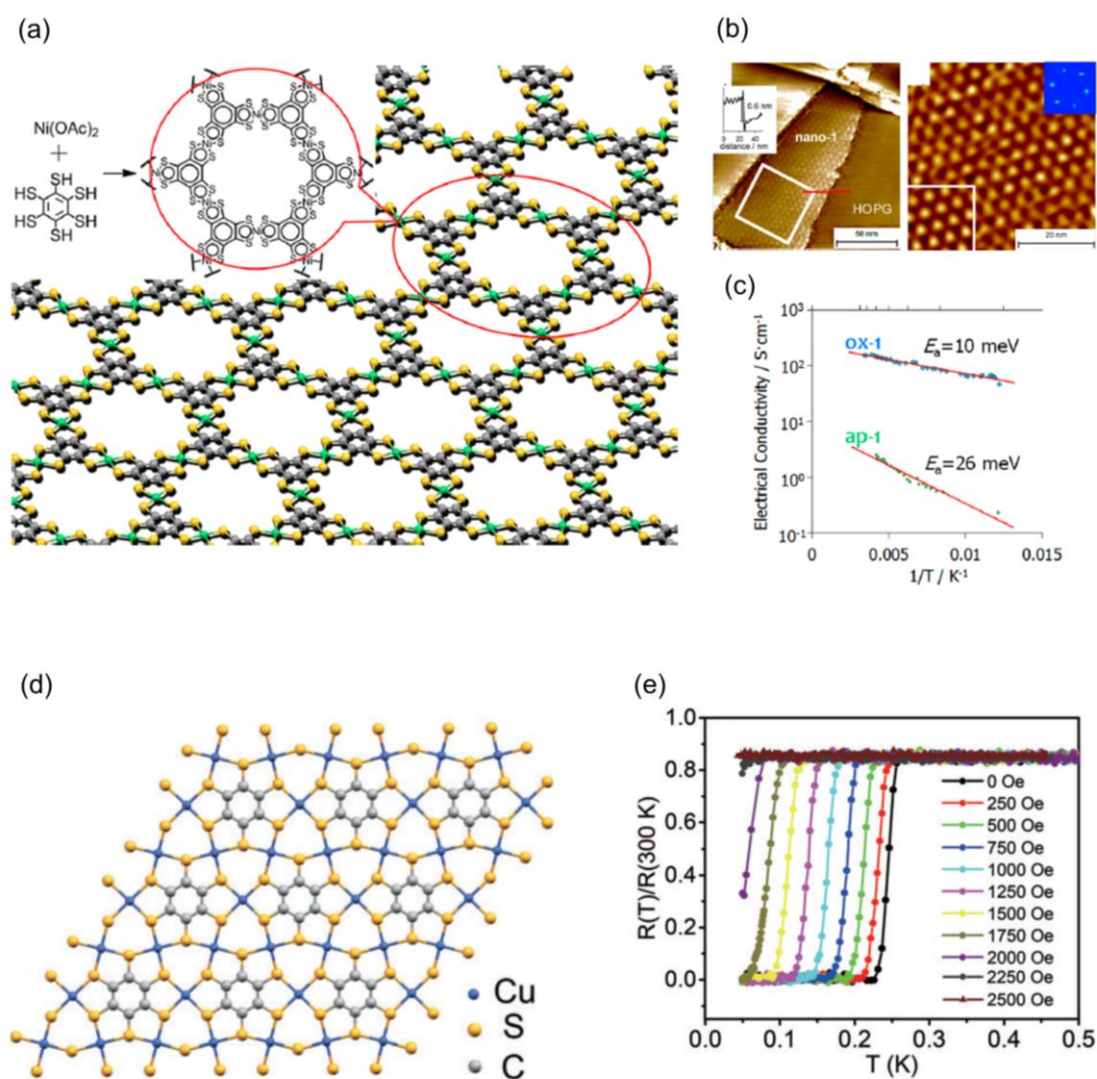


**Fig. 1-12** Structure of the π-conjugated nano-sheet consisting of nickel and benzenehexathiol, (b) the STM image of a single layer of the sheet, and (c) temperature dependence of the electrical conductivities of the nano-sheet with monoanionic and neutral states.[101,120] (d) Structure of the π-conjugated nano-sheet consisting of cupper and benzenehexathiol and (e) the temperature dependence of R(T)/R(300) (ratio of resistivity at arbitrary temperature and resistivity at 300 K) of the sheet near $T_c$ in constant applied magnetic fields up to 2500 Oe.[125]

As introduced above, such d/π electronic functionalities, not seen in π-conjugated molecular crystals, have been demonstrated based on a modification of the ligands and metals to modulate the intermolecular π-π interaction and intramolecular d-π interactions. Thus, material development based on metal dithiolene complexes using H-bonds leads to realizing the novel unique phenomena and functionalities related to d and π electrons and protons.

### 1.4.2 Hydrogen-bonding metal dithiolene complexes

Of course, some metal dithioelene complexes having H-boning parts have been reported so far.[107,110,133] However, in most crystals, H-bond is used to regulate the molecular arrangement to modulate the functionalities. Avarvari and Batail synthesized the nickel dithiolene complexes appended with imide or amide groups as H-bonding moieties (Fig. 1-13a).[133] The complexes form multiple intermolecular [O···H–N] H-bonds in the crystal to construct 2D H-bonded sheets (Fig. 1-13b). This 2D sheet strongly linked by intermolecular H-bonds interferes with the formation of the π-π stacking structure, resulting in the paramagnetic property. Also, Lorcy and Fourmigué reported a single-component molecular conductor based on a dithiolene complex having alkyl hydroxy groups, Au(EtOH-thiazdt)$_2$ and M(HOEtS-tzdt)$_2$ (M = Au and Ni) (Fig. 1-13c).[107,110] The former has intermolecular [O–H···S] H-bonds, and the latter has intermolecular [O–H···N] H-bonds. Particularly in the latter crystal, the H-bond plays an important role in the control of the assembled structures. The corresponding nickel counterpart is isostructural with the gold one due to the same style of the H-bond formation; this is a rare case in bis(dithiolene) chemistry, and thus indicates that the assembled structure is dominated by H-bond formation in this system (Fig. 1-13d). The gold complex crystallizes into uniform π-π stacks because of the formation of crystallographically equivalent H-bond between the complex molecules belonging to a different column, although much radical gold dithiolene complex has a strong tendency to dimerize in the crystal. As a result, the gold complex crystal

exhibit relatively high electrical conductivity ($6 \times 10^{-2}$ S cm$^{-1}$). The problems with these dithiolene complex having H-bonding substituents, that are difficult to be (de)protonated, are that (1) the electron–proton coupled phenomena (e.g., PCET) cannot be expected with the complexes, and/or (2) the frontier molecular orbitals are not distributed on the H-bonding parts. These make the electronic state of the complexes difficult to be modulated by electrostatic effect and dynamics of the H-bonding proton.
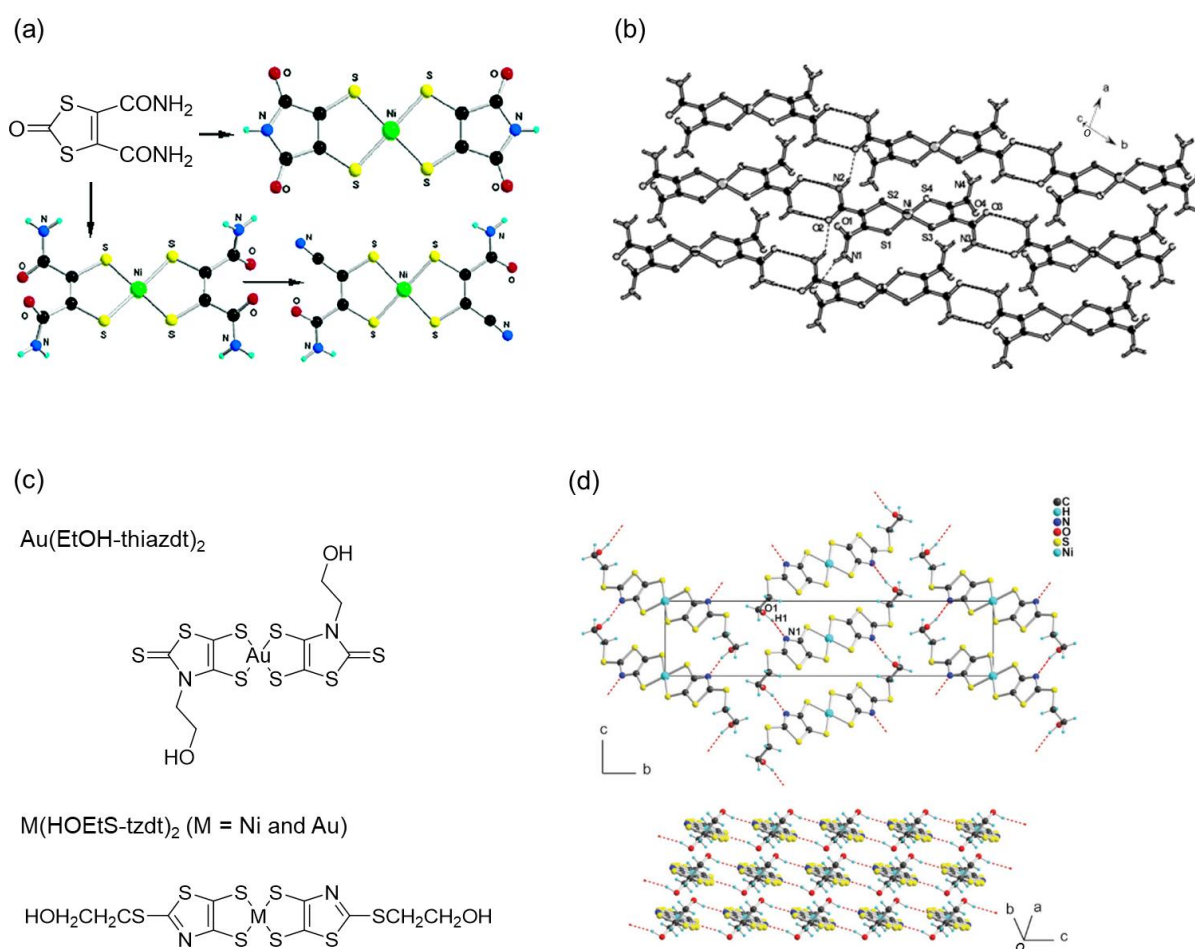


**Fig. 1-13** (a) Nickel dithiolene complexes appended with imide or amide groups and (b) intermolecular [O···H–N] H-bonds in the 2D sheet.[133] (c) H-bonding metal dithiolene complexes, Au(EtOH-thiazdt)$_2$ and M(HOEtS-tzdt)$_2$ and (d) H-bonding network (top) and uniform π-π stacking structure of the crystal of Ni(HOEtS-tzdt)$_2$.[107,110]

In contrast to the above H-bonding metal dithiolene complexes, the family of dithiolene complexes with pyrazine or pyridine moieties (Fig. 1-14a) are the only examples where the electronic functionalities have been studied based on H-bond and proton.[134–141] These complexes have multiple protonation ability and the H-bonding part with significant distribution of frontier molecular orbitals; thus, the PCET property in solution processes and the crystals composed of the protonated complex with intermolecular H-bonds, have been demonstrated (Fig. 1-14b). For example, the metal-substitution effect on the strongness of d/π hybridization and PCET ability of pyrazinedithiolane complexes was revealed from the theoretical and electrochemical studies.[142] Many other studies related to PCET in solution processes have been undertaken as well.

In addition to studies in a solution state, a lot of crystals consisting of the protonated and/or reduced species of the complexes have been synthesized. The dianionic nickel pyridinedithiolene complex was assembled with two-protonation as a crystal (Fig. 1-14c).[137] By using the complex, the CT complex with TCNQ was synthesized, resulting in a semiconductor with a room-temperature conductivity of $2.7 \times 10^{-2}$ S cm$^{-1}$. Also, Hayashi and Kitagawa et al. reported a single-component crystal by protonation of binuclear nickel complex (Fig. 1-14d).[139,140] In this crystal, the complexes construct a 2D H-bonded sheet structure with 1D channel-like spaces based on cationic $[N \cdots H-N]^+$ H-bond formation. The crystal exhibits an increase of electrical conductivity based on pressure-induced intramolecular charge transfer (from $1.1 \times 10^{-5}$ S cm$^{-1}$ at ambient to $1.6 \times 10^{-2}$ S cm$^{-1}$ at 8.8 GPa), which is related to the 1D stacking column of the donor-acceptor-donor complex stabilized by H-bonding formation. Furthermore, in the nickel pyrazinedithiolane complex with four cyano groups, the crystal composed of the protonated complex was synthesized, and the neutral radical complex was successfully obtained as an amorphous state due to a stabilization of the neutral radical state by the electron-withdrawing property of the introduced cyano groups.[141] Most recently, it was demonstrated that a crystal of closed-shell copper (I) pyrazinedithiolene complex with fully

protonated ligands change to open-shell copper (II) complex with dehydrogenation upon heating.[143]

Although many crystals of metal pyrazine/pyridinedithiolene complexes with intermolecular ionic $[N–H\cdots N]^+$ H-bonds were synthesized, electron–proton coupled functionalities based on proton dynamics in solid state have not been realized. This fact indicates the necessity to switch our focus from these pyrazine/pyridinedithiolene complexes to novel molecular designs for further developing electron–proton coupled functionalities. Furthermore, most crystals of the complexes are crystallized in only one of the several protonated states; the crystals of the complexes undergoing PCET in solution processes are rare. This also prevents the development of new electron–proton coupled functionalities based on the metal-dithiolene complexes. In addition to the issue of the property of the complex molecules, the limitation of the number of H-bonding metal dithiolene complex crystals is also a serious problem for exploring. Hence, based on synthesis and crystallization of the new H-bonding metal dithiolene complex, developments of a new basis stage to realize novel d/π electron–proton coupled functionalities are important.
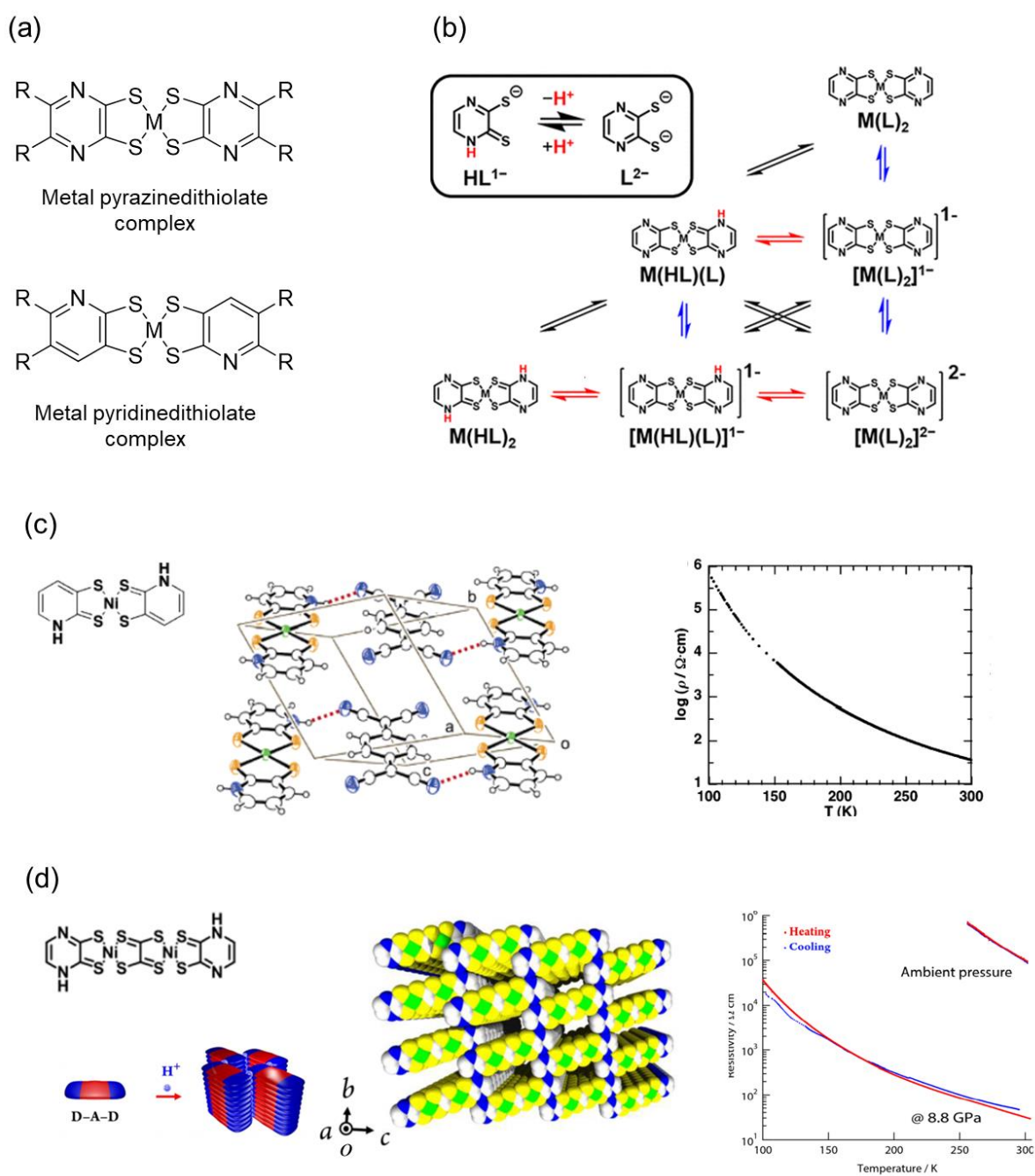
**Fig. 1-14** (a) Chemical structures of dithiolene complexes with pyrazine or pyridine moieties. (b) PCET scheme in solution processes of metal pyrazinedithiolene complex.[142] (c) Chemical structure of nickel pyridinedithiolene complex, the crystal structure of the CT complex with TCNQ, and the temperature dependence of the resistivity.[137] (d) Chemical structure of binuclear nickel pyridinedithiolene complex, the molecular arrangement of the single-component crystal, and the temperature dependence of the resistivity.[139,140]

## 1.5 Purpose and structure of this dissertation

The purpose of this dissertation is to realize the d/$\pi$ electron–proton coupled functionalities in metal dithiolene complex crystals (Fig. 1-15). Also, based on the elucidation of the origin and mechanism of the functionalities by crystallographic and theoretical studies, the author aims to develop a new playground to pioneer d/$\pi$ electron–proton coupled functionalities. In this dissertation, electron–proton coupled functionalities mean the functionalities realized based on direct modulation of electronic properties originating from electrostatic and charge properties of H-bonding proton, as described in Section 1.3. In light of the paucity of the H-bonding metal dithiolene complexes, which have great potential to pioneer novel electron–proton coupled functionalities, synthesis and crystallization of new metal dithiolene complexes are performed. Then, the single-crystal X-ray structural analyses of the obtained crystals reveal the molecular structure, molecular arrangement, and intermolecular interactions. Then, the electronic functionalities (i.e., magnetic properties and optical properties) are measured. The electronic structures of the complex molecules and the crystals are investigated by DFT calculations. Based on these results, the structure-property relationship and the d/$\pi$ electron–proton coupling on the functionalities are discussed in detail.

In Chapter 2, for construction of a novel structural basis to explore new d/$\pi$ electron–proton coupled functionalities, the author firstly aims to develop the crystals with the H-bond network based on metal dithiolene complexes and to control the molecular arrangement, i.e., the framework structures. To achieve this purpose, the author focused on the metal catecholdithiolene complex with four hydroxy groups in anticipation of the H-bond formation in the solid state. Here, three crystals consisting of a new gold catecholdithiolene complex were synthesized, and the first 3D H-bonded frameworks based on the complex are demonstrated. In these crystals, the gold complexes are three-dimensionally connected by multiple intermolecular H-bonds through the four hydroxy groups. Furthermore, a detailed comparison of the crystal structures and intermolecular interactions revealed that the structure and

dimensionality of the frameworks could be modulated by changing the crystal solvents, in which interactions between the solvent molecules play an important role.

In Chapter 3, by exchanging the metal center from gold to nickel, the author attempted the introduction of electronic functionalities based on electron spin to the H-bonded framework; namely, the author aimed to develop the H-bonded metal-dithiolene-based crystals with functionalities based on a coupling of d/$\pi$ electron and H-bonding proton. Four crystals consisting of non-deprotonated, one-deprotonated, or two-deprotonated nickel complexes were successfully synthesized. X-ray structural analyses demonstrated the one-deprotonated complexes form intermolecular anionic [O−H···O]$^-$ H-bonds with each other. Also, ESR measurements revealed that the magnetic properties of the complex crystals were changed from paramagnetic of non-deprotonated complex to non-magnetic of one- or two-deprotonated complexes through PCET in solution processes. Furthermore, the DFT calculations based on the crystal structures suggest that the significant d/$\pi$ electronic state modulation with deprotonation, which leads to the possibility of d/$\pi$ electronic functionality with proton dynamics in solid state.

In Chapter 4, through material developments using other metal dithiolene complex (i.e., zinc methoxybenzenedithiolene complex) to realize novel electron–proton coupled functionality, the author realized control of vapochromic behavior by direct modulation of d/$\pi$ electronic states through H-bonding in a novel crystal consisting of zinc methoxybenzenedithiolene complex. The crystal exhibits changes in both visible-light absorption and photoluminescence with single-crystal-to-single-crystal transformations upon methanol or water vapor sorption, involving H-bond formation between the zinc complex and vapor molecules. Based on the detailed X-ray structural analyses and first-principles calculations considering intermolecular interactions with the periodic structure model of the crystal, a new mechanism of vapochromism in this crystal, that is, not molecular structure and arrangement changes but electron transfer coupled with H-bond formation is revealed for the first time.

Chapter 5 is the conclusion of this dissertation, in which the results in each chapter are summarized and the perspective of this study is described.
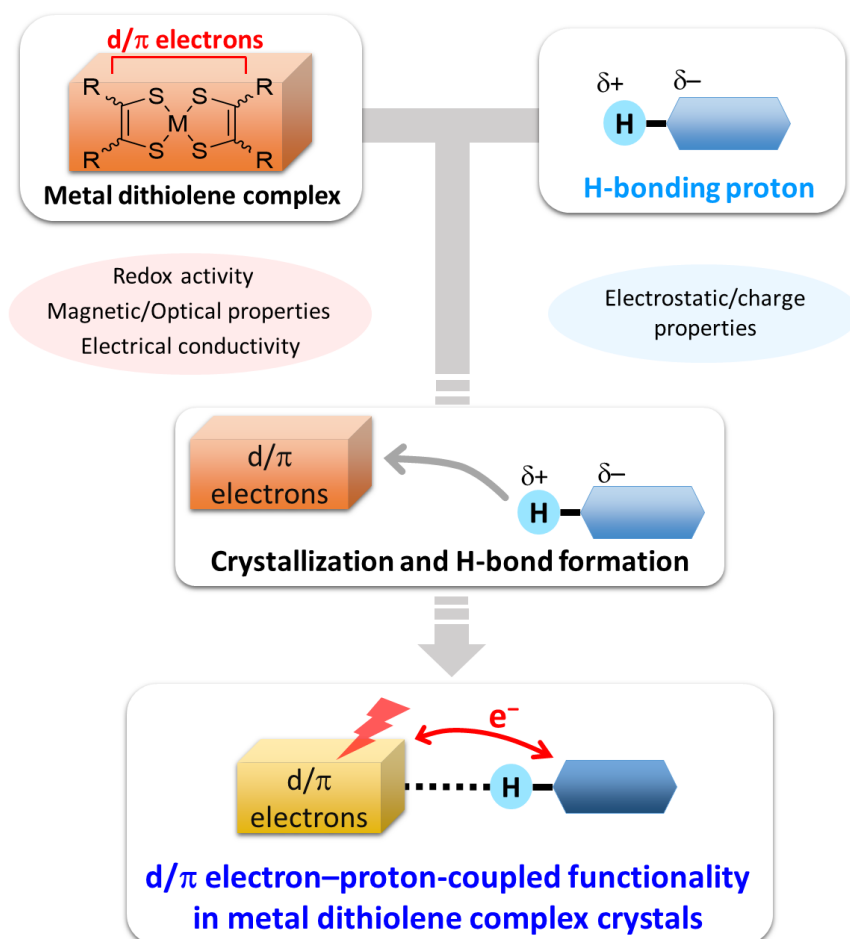


**Fig. 1-15** A scheme of the strategy to realize novel d/π-electron-proton-coupled functionalities as the research target of this dissertation.

## 1.6 References

1   Q.-L. Zhu and Q. Xu, *Chem. Soc. Rev.*, 2014, **43**, 5468.

2   N. Stock and S. Biswas, *Chem. Rev.*, 2012, **112**, 933.

3   M. Kurmoo, *Chem. Soc. Rev.*, 2009, **38**, 1353.

4   A. E. Thorarinsdottir and T. D. Harris, *Chem. Rev.*, 2020, **120**, 8716.

5   Y. Yoshida and H. Kitagawa, *ACS Sustainable Chem. Eng.*, 2019, **7**, 70.

6   D.-W. Lim and H. Kitagawa, *Chem. Rev.*, 2020, **120**, 8416.

7   L. S. Xie, G. Skorupskii and M. Dincă, *Chem. Rev.*, 2020, **120**, 8536.

8   A. Dhakshinamoorthy, Z. Li and H. Garcia, *Chem. Soc. Rev.*, 2018, **47**, 8134.

9   S. La and P. W. R. Corfie, *Solid State Commun.*, 1975, **17**, 635.

10  R. B. Somoano, A. Gupta, V. Hadek, M. Novotny, M. Jones, T. Datta, R. Deck and A. M. Hermann, *Phys. Rev. B*, 1977, **15**, 595.

11  B. A. Scott, S. J. La Placa, J. B. Torrance, B. D. Silverman and B. Welber, *J. Am. Chem. Soc.*, 1977, **99**, 6631.

12  R. Williams, C. Lowe Ma, S. Samson, S. K. Khanna and R. B. Somoano, *J. Chem. Phys.*, 1980, **72**, 3781.

13  R. P. Shibaeva and E. B. Yagubskii, *Chem. Rev.*, 2004, **104**, 5347.

14  N. Tajima, S. Sugawara, M. Tamura, Y. Nishio and K. Kajita, *J. Phys. Soc. Jpn.*, 2006, **75**, 051010.

15  D. Jérome, *Chem. Rev.*, 2004, **104**, 5565.

16  C. Rovira, *Chem. Rev.*, 2004, **104**, 5289.

17  A. Gorgues, P. Hudhomme and M. Sallé, *Chem. Rev.*, 2004, **104**, 5151.

18  P. Frère and P. J. Skabara, *Chem. Soc. Rev.*, 2005, **34**, 69.

19  R. Kato, *Chem. Rev.*, 2004, **104**, 5319.

20  D. N. Woodruff, R. E. P. Winpenny and R. A. Layfield, *Chem. Rev.*, 2013, **113**, 5110.

21  H. Minemawari, T. Yamada, H. Matsui, J. Tsutsumi, S. Haas, R. Chiba, R. Kumai and T.

Hasegawa, *Nature*, 2011, **475**, 364.

22  M. Al Kobaisi, S. V. Bhosale, K. Latham, A. M. Raynor and S. V. Bhosale, *Chem. Rev.*, 2016, **116**, 11685.

23  M. Irie, T. Fukaminato, K. Matsuda and S. Kobatake, *Chem. Rev.*, 2014, **114**, 12174.

24  X. Zhao, Y. Wang, D.-S. Li, X. Bu and P. Feng, *Adv. Mater.*, 2018, **30**, 1705189.

25  S. Yuan, X. Li, J. Zhu, G. Zhang, P. Van Puyvelde and B. Van der Bruggen, *Chem. Soc. Rev.*, 2019, **48**, 2665.

26  M. Bansal, *Curr. Sci.*, 2003, **85**, 8.

27 T. S. Moore, T. F. Winmill, *J. Chem. Soc., Trans.* **1912**, *101*, 1635.

28  Linus. Pauling, *J. Am. Chem. Soc.*, 1931, **53**, 1367.

29  T. Steiner, *Angew. Chem. Int. Ed.*, 2002, 48.

30  T. Akutagawa, S. Takeda, T. Hasegawa and T. Nakamura, *J. Am. Chem. Soc.*, 2004, **126**, 291.

31  G. R Desiraju, T. Steiner, *The Weak Hydrogen Bond*; Oxford University Press: New York, 1999.

32  P. Li, Y. He, J. Guang, L. Weng, J. C.-G. Zhao, S. Xiang and B. Chen, *J. Am. Chem. Soc.*, 2014, **136**, 547.

33  P. Li, Y. He, Y. Zhao, L. Weng, H. Wang, R. Krishna, H. Wu, W. Zhou, M. O'Keeffe, Y. Han and B. Chen, *Angew. Chem. Int. Ed.*, 2015, **54**, 574.

34  W. Yang, B. Li, H. Wang, O. Alduhaish, K. Alfooty, M. A. Zayed, P. Li, H. D. Arman and B. Chen, *Cryst. Growth Des.*, 2015, **15**, 2000.

35  A. Karmakar, R. Illathvalappil, B. Anothumakkool, A. Sen, P. Samanta, A. V. Desai, S. Kurungot and S. K. Ghosh, *Angew. Chem.*, 2016, **128**, 10825.

36  W. Yang, J. Wang, H. Wang, Z. Bao, J. C.-G. Zhao and B. Chen, *Cryst. Growth Des.*, 2017, **17**, 6132.

37  I. Hisaki, N. Q. Emilya Affendy and N. Tohnai, *CrystEngComm*, 2017, **19**, 4892.

38  Y.-F. Han, Y.-X. Yuan and H.-B. Wang, *Molecules*, 2017, **22**, 266.

39  I. Hisaki, N. Ikenaka, E. Gomez, B. Cohen, N. Tohnai and A. Douhal, *Chem. Eur. J.*, 2017, **23**, 11611.

40  F. Hu, C. Liu, M. Wu, J. Pang, F. Jiang, D. Yuan and M. Hong, *Angew. Chem.*, 2017, **129**, 2133.

41  H. Wang, Z. Bao, H. Wu, R.-B. Lin, W. Zhou, T.-L. Hu, B. Li, J. C.-G. Zhao and B. Chen, *Chem. Commun.*, 2017, **53**, 11150.

42  H. Wahl, D. A. Haynes and T. le Roex, *Cryst. Growth Des.*, 2017, **17**, 4377.

43  S. Cai, H. Shi, Z. Zhang, X. Wang, H. Ma, N. Gan, Q. Wu, Z. Cheng, K. Ling, M. Gu, C. Ma, L. Gu, Z. An and W. Huang, *Angew. Chem. Int. Ed.*, 2018, **57**, 4005.

44  I. Hisaki, Y. Suzuki, E. Gomez, Q. Ji, N. Tohnai, T. Nakamura and A. Douhal, *J. Am. Chem. Soc.*, 2019, **141**, 2111.

45  X. Feng, X. Ding and D. Jiang, *Chem. Soc. Rev.*, 2012, **41**, 6010.

46  S.-Y. Ding and W. Wang, *Chem. Soc. Rev.*, 2013, **42**, 548.

47  F. Beuerle and B. Gole, *Angew. Chem. Int. Ed.*, 2018, **57**, 4850.

48  A. E. Baumann, D. A. Burns, B. Liu and V. S. Thoi, *Commun Chem*, 2019, **2**, 86.

49  I. Hisaki, S. Nakagawa, N. Tohnai and M. Miyata, *Angew. Chem. Int. Ed.*, 2015, **54**, 3008.

50  I. Hisaki, H. Toda, H. Sato, N. Tohnai and H. Sakurai, *Angew. Chem. Int. Ed.*, 2017, **56**, 15294.

51  I. Hisaki, S. Nakagawa, N. Ikenaka, Y. Imamura, M. Katouda, M. Tashiro, H. Tsuchida, T. Ogoshi, H. Sato, N. Tohnai and M. Miyata, *J. Am. Chem. Soc.*, 2016, **138**, 6617.

52  I. Hisaki, S. Nakagawa, H. Sato and N. Tohnai, *Chem. Commun.*, 2016, **52**, 9781.

53  T. Higashino, A. Ueda, J. Yoshida and H. Mori, *Chem. Commun.*, 2017, **53**, 3426.

54  M. Chang, A. Kobayashi, K. Nakajima, H.-C. Chang and M. Kato, *Inorg. Chem.*, 2011, **50**, 8308.

55  T. Murata, Y. Morita, K. Fukui, K. Sato, D. Shiomi, T. Takui, M. Maesato, H. Yamochi, G. Saito and K. Nakasuji, *Angew. Chem. Int. Ed.*, 2004, **43**, 6343.

56  T. Murata, Y. Morita, Y. Yakiyama, K. Fukui, H. Yamochi, G. Saito and K. Nakasuji, *J. Am. Chem. Soc.*, 2007, **129**, 10837.

57  T. Murata, S. Maki, M. Ohmoto, E. Miyazaki, Y. Umemoto, K. Nakasuji and Y. Morita, *CrystEngComm*, 2011, **13**, 6880.

58  T. Murata, Y. Yakiyama, K. Nakasuji and Y. Morita, *CrystEngComm*, 2011, **13**, 3689.

59  T. Murata, Y. Umemoto, E. Miyazaki, K. Nakasuji and Y. Morita, *CrystEngComm*, 2012, **14**, 6881.

60  T. Murata, E. Miyazaki, K. Nakasuji and Y. Morita, *Cryst. Growth Des.*, 2012, **12**, 5815.

61  Y. Morita, T. Murata and K. Nakasuji, *Bull. Chem. Soc. Jpn.*, 2013, **86**, 183.

62  S. C. Lee, A. Ueda, H. Kamo, K. Takahashi, M. Uruichi, K. Yamamoto, K. Yakushi, A. Nakao, R. Kumai, K. Kobayashi, H. Nakao, Y. Murakami and H. Mori, *Chem. Commun.*, 2012, **48**, 8673.

63  M. H. V. Huynh and T. J. Meyer, *Chem. Rev.*, 2007, **107**, 5004.

64  D. R. Weinberg, C. J. Gagliardi, J. F. Hull, C. F. Murphy, C. A. Kent, B. C. Westlake, A. Paul, D. H. Ess, D. G. McCafferty and T. J. Meyer, *Chem. Rev.*, 2012, **112**, 4016.

65  H. Kitagawa, H. Okamoto, T. Mitani and M. Yamashita, *Mol. Cryst. Liq. Cryst.*, 1993, **228**, 155.

66  T. Itoh, K.-I. Iijima, J. Toyoda and K. Nakasuji, *Mol. Cryst. Liq. Cryst.*, 1996, **285**, 287–294.

67  Y. Kobayashi, T. Terauchi, S. Sumi and Y. Matsushita, *Nat. Mater.*, 2017, **16**, 109.

68  Y. Kobayashi, K. Hirata, S. N. Hood, H. Yang, A. Walsh, Y. Matsushita and K. Ishioka, *Chem. Sci.*, 2020, **11**, 11699.

69  T. Mitani, G. Saito and H. Urayama, *Phys. Rev. Lett.*, 1988, **60**, 2299.

70  M. Kubinyi and G. Keresztury, *Spectrochim. Acta A: Mol. Spectrosc.*, 1989, **45**, 421.

71  S. Horiuchi, F. Ishii, R. Kumai, Y. Okimoto, H. Tachibana, N. Nagaosa and Y. Tokura, *Nat. Mater*, 2005, **4**, 163.

72  S. Horiuchi, R. Kumai and Y. Tokura, *J. Am. Chem. Soc.*, 2005, **127**, 5010.

73  R. Kumai, S. Horiuchi, Y. Okimoto and Y. Tokura, *J. Chem. Phys.*, 2006, **125**, 084715.

74  S. Horiuchi, Y. Tokunaga, G. Giovannetti, S. Picozzi, H. Itoh, R. Shimano, R. Kumai and Y. Tokura, *Nature*, 2010, **463**, 789.

75  T. Akutagawa, H. Koshinaka, D. Sato, S. Takeda, S.-I. Noro, H. Takahashi, R. Kumai, Y. Tokura and T. Nakamura, *Nat. Mater*, 2009, **8**, 342.

76  Z.-S. Yao, K. Yamamoto, H.-L. Cai, K. Takahashi and O. Sato, *J. Am. Chem. Soc.*, 2016, **138**, 12005.

77  T. Nakanishi, Y. Hori, H. Sato, S.-Q. Wu, A. Okazawa, N. Kojima, T. Yamamoto, Y. Einaga, S. Hayami, Y. Horie, H. Okajima, A. Sakamoto, Y. Shiota, K. Yoshizawa and O. Sato, *J. Am. Chem. Soc.*, 2019, **141**, 14384.

78  V. Jornet-Mollá, C. Giménez-Saiz, L. Cañadillas-Delgado, D. S. Yufit, J. A. K. Howard and F. M. Romero, *Chem. Sci.*, 2021, DOI: 10.1039.D0SC04918B.

79  T. Isono, H. Kamo, A. Ueda, K. Takahashi, A. Nakao, R. Kumai, H. Nakao, K. Kobayashi, Y. Murakami and H. Mori, *Nat. Commun*, 2013, **4**, 1344.

80  A. Ueda, S. Yamada, T. Isono, H. Kamo, A. Nakao, R. Kumai, H. Nakao, Y. Murakami, K. Yamamoto, Y. Nishio and H. Mori, *J. Am. Chem. Soc.*, 2014, **136**, 12184.

81  T. Isono, H. Kamo, A. Ueda, K. Takahashi, M. Kimata, H. Tajima, S. Tsuchiya, T. Terashima, S. Uji and H. Mori, *Phys. Rev. Lett.*, 2014, **112**, 177201.

82  M. Shimozawa, K. Hashimoto, A. Ueda, Y. Suzuki, K. Sugii, S. Yamada, Y. Imai, R. Kobayashi, K. Itoh, S. Iguchi, M. Naka, S. Ishihara, H. Mori, T. Sasaki and M. Yamashita, *Nat. Commun*, 2017, **8**, 1821.

83  A. Ueda, *BCSJ*, 2017, **90**, 1181.

84  A. Ueda, K. Kishimoto, T. Isono, S. Yamada, H. Kamo, K. Kobayashi, R. Kumai, Y. Murakami, J. Gouchi, Y. Uwatoko, Y. Nishio and H. Mori, *RSC Adv.*, 2019, **9**, 18353.

85  T. Tsumuraya, H. Seo, R. Kato and T. Miyazaki, *Phys. Rev. B*, 2015, **92**, 035102.

86  G. N. Schrauzer and V. Mayweg, *J. Am. Chem. Soc.*, 1962, **84**, 3221.

87  E. I. Stiefel and K. D. Karlin: Progress in Inorganic Chemistry, Dithiolene Chemistry: Synthesis, Properties, and Applications, Wiley-Interscience, New York (2003).

88  T. Kusamoto, H. M. Yamamoto, N. Tajima, Y. Oshima, S. Yamashita and R. Kato, *Inorg. Chem.*, 2013, **52**, 4759.

89  T. Itou, A. Oyamada, S. Maegawa, M. Tamura and R. Kato, *Phys. Rev. B*, 2008, **77**, 104413.

90  M. Yamashita, N. Nakata, Y. Senshu, M. Nagata, H. M. Yamamoto, R. Kato, T. Shibauchi and Y. Matsuda, *Science*, 2010, **328**, 1246.

91  A. Kobayashi, E. Fujiwara and H. Kobayashi, *Chem. Rev.*, 2004, **104**, 5243.

92  D. Lorcy, N. Bellec, M. Fourmigué and N. Avarvari, *Coord. Chem. Rev.*, 2009, **253**, 1398.

93  R. Kato, *Bull. Chem. Soc. Jpn.*, 2014, **87**, 355.

94  H. Cui, H. Kobayashi, S. Ishibashi, M. Sasa, F. Iwase, R. Kato and A. Kobayashi, *J. Am. Chem. Soc.*, 2014, **136**, 7619.

95  F. Pop and N. Avarvari, *Coord. Chem. Rev*, 2017, **346**, 20.

96  V. Madhu and S. K. Das, *Inorg. Chem.*, 2006, **45**, 10037.

97  T. Naito, T. Karasudani, S. Mori, K. Ohara, K. Konishi, T. Takano, Y. Takahashi, T. Inabe, S. Nishihara and K. Inoue, *J. Am. Chem. Soc.*, 2012, **134**, 18656.

98  K. Mebrouk, S. Debnath, M. Fourmigué and F. Camerel, *Langmuir*, 2014, **30**, 8592.

99  D. Espa, L. Pilia, L. Marchiò, M. L. Mercuri, A. Serpe, A. Barsella, A. Fort, S. J. Dalgleish, N. Robertson and P. Deplano, *Inorg. Chem.*, 2011, **50**, 2058.

100 S. Attar, D. Espa, F. Artizzu, M. L. Mercuri, A. Serpe, E. Sessini, G. Concas, F. Congiu, L. Marchiò and P. Deplano, *Inorg. Chem.*, 2016, **55**, 5118.

101 I. A. Wright, C. Wilson, S. J. Coles and P. J. Skabara, *Dalton Trans.*, 2019, **48**, 107.

102 T. Kambe, R. Sakamoto, T. Kusamoto, T. Pal, N. Fukui, K. Hoshiko, T. Shimojima, Z. Wang, T. Hirahara, K. Ishizaka, S. Hasegawa, F. Liu and H. Nishihara, *J. Am. Chem. Soc.*, 2014, **136**, 14357.

103 O. J. Dautel, M. Fourmigué, E. Canadell and P. Auban-Senzier, *Adv. Funct. Mater.*, 2002, **12**, 693.

104 W. Suzuki, E. Fujiwara, A. Kobayashi, Y. Fujishiro, E. Nishibori, M. Takata, M. Sakata, H. Fujiwara and H. Kobayashi, *J. Am. Chem. Soc.*, 2003, **125**, 1486.

105 N. Tenn, N. Bellec, O. Jeannin, L. Piekara-Sady, P. Auban-Senzier, J. Íñiguez, E. Canadell and D. Lorcy, *J. Am. Chem. Soc.*, 2009, **131**, 16961.

106 G. Yzambart, N. Bellec, G. Nasser, O. Jeannin, T. Roisnel, M. Fourmigué, P. Auban-Senzier, J. Íñiguez, E. Canadell and D. Lorcy, *J. Am. Chem. Soc.*, 2012, **134**, 17138.

107 Y. Le Gal, T. Roisnel, P. Auban-Senzier, T. Guizouarn and D. Lorcy, *Inorg. Chem.*, 2014, **53**, 8755.

108 T. Higashino, O. Jeannin, T. Kawamoto, D. Lorcy, T. Mori and M. Fourmigué, *Inorg. Chem.*, 2015, **54**, 9908.

109 Y. Le Gal, T. Roisnel, P. Auban-Senzier, N. Bellec, J. Íñiguez, E. Canadell and D. Lorcy, *J. Am. Chem. Soc.*, 2018, **140**, 6998.

110 H. Hachem, N. Bellec, M. Fourmigué and D. Lorcy, *Dalton Trans.*, 2020, **49**, 6056.

111 B. Garreau-de Bonneval, K. I. Moineau-Chane Ching, F. Alary, T.-T. Bui and L. Valade, *Coord. Chem. Rev.*, 2010, **254**, 1457.

112 T. D. Anthopoulos, S. Setayesh, E. Smits, M. Cölle, E. Cantatore, B. de Boer, P. W. M. Blom and D. M. de Leeuw, *Adv. Mater.*, 2006, **18**, 1900.

113 T. Taguchi, H. Wada, T. Kambayashi, B. Noda, M. Goto, T. Mori, K. Ishikawa and H. Takezoe, *Chem. Phys. Let.*, 2006, **421**, 395.

114 T. D. Anthopoulos, G. C. Anyfantis, G. C. Papavassiliou and D. M. de Leeuw, *Appl. Phys. Lett.*, 2007, **90**, 122105.

115 H. Wada, T. Taguchi, B. Noda, T. Kambayashi, T. Mori, K. Ishikawa and H. Takezoe, *Org. Electronics*, 2007, **8**, 759.

116 L. Qu, Y. Guo, H. Luo, C. Zhong, G. Yu, Y. Liu and J. Qin, *Chem. Commun.*, 2012, **48**,

9965.

117 H. Tanaka, Y. Okano, H. Kobayashi, W. Suzuki and A. Kobayashi, *Science*, 2001, **291**, 285.

118 A. Kobayashi, H. Tanaka and H. Kobayashi, *J. Mater. Chem.*, 2001, **11**, 2078.

119 H. Cui, J. S. Brooks, A. Kobayashi and H. Kobayashi, *J. Am. Chem. Soc.*, 2009, **131**, 6358.

120 T. Kambe, R. Sakamoto, K. Hoshiko, K. Takada, M. Miyachi, J.-H. Ryu, S. Sasaki, J. Kim, K. Nakazato, M. Takata and H. Nishihara, *J. Am. Chem. Soc.*, 2013, **135**, 2462.

121 R. Sakamoto, K. Takada, X. Sun, T. Pal, T. Tsukamoto, E. J. H. Phua, A. Rapakousiou, K. Hoshiko and H. Nishihara, *Coord. Chem. Rev.*, 2016, **320–321**, 118.

122 R. Sakamoto, K. Takada, T. Pal, H. Maeda, T. Kambe and H. Nishihara, *Chem. Commun.*, 2017, **53**, 5781.

123 A. J. Clough, J. M. Skelton, C. A. Downes, A. A. de la Rosa, J. W. Yoo, A. Walsh, B. C. Melot and S. C. Marinescu, *J. Am. Chem. Soc.*, 2017, **139**, 10863.

124 A. J. Clough, N. M. Orchanian, J. M. Skelton, A. J. Neer, S. A. Howard, C. A. Downes, L. F. J. Piper, A. Walsh, B. C. Melot and S. C. Marinescu, *J. Am. Chem. Soc.*, 2019, **141**, 16323.

125 X. Huang, S. Zhang, L. Liu, L. Yu, G. Chen, W. Xu and D. Zhu, *Angew. Chem. Int. Ed.*, 2018, **57**, 146.

126 X. Huang, P. Sheng, Z. Tu, F. Zhang, J. Wang, H. Geng, Y. Zou, C. Di, Y. Yi, Y. Sun, W. Xu and D. Zhu, *Nat. Commun*, 2015, **6**, 7408.

127 O. Jeannin, R. Clérac, T. Cauchy and M. Fourmigué, *Inorg. Chem.*, 2008, **47**, 10656.

128 T. Kusamoto, H. M. Yamamoto, N. Tajima, Y. Oshima, S. Yamashita and R. Kato, *Inorg. Chem.*, 2012, **51**, 11645.

129 R. Dong, Z. Zhang, D. C. Tranca, S. Zhou, M. Wang, P. Adler, Z. Liao, F. Liu, Y. Sun, W. Shi, Z. Zhang, E. Zschech, S. C. B. Mannsfeld, C. Felser and X. Feng, *Nat. Commun*, 2018, **9**, 2637.

130 R. Kato, H. Cui, T. Tsumuraya, T. Miyazaki and Y. Suzumura, *J. Am. Chem. Soc.*, 2017, **139**, 1770.

131 R. Kato and Y. Suzumura, *J. Phys. Soc. Jpn.*, 2017, **86**, 064705.

132 R. Kato, H. Cui, T. Minamidate, H. H.-M. Yeung and Y. Suzumura, *J. Phys. Soc. Jpn.*, 2020, **89**, 124706.

133 S. A. Baudron, N. Avarvari and P. Batail, *Inorg. Chem.*, 2005, **44**, 3380.

134 T. Kubo, M. Ohashi, K. Miyazaki, A. Ichimura and K. Nakasuji, *Inorg. Chem.*, 2004, **43**, 7301.

135 X. Ribas, J. C. Dias, J. Morgado, K. Wurst, E. Molins, E. Ruiz, M. Almeida, J. Veciana and C. Rovira, *Chem. Eur. J.*, 2004, **10**, 1691.

136 T. Kubo, M. Ohashi, H. Kitagawa and K. Nakasuji, *Polyhedron*, 2005, **24**, 2528.

137 S. Shibahara, H. Kitagawa, Y. Ozawa, K. Toriumi, T. Kubo and K. Nakasuji, *Inorg. Chem.*, 2007, **46**, 1162.

138 A. C. Cerdeira, D. Belo, S. Rabaça, L. C. J. Pereira, J. T. Coutinho, D. Simão, R. T. Henriques, O. Jeannin, M. Fourmigué and M. Almeida, *Eur. J. Inorg. Chem.*, 2013, 4612.

139 M. Hayashi, K. Otsubo, T. Kato, K. Sugimoto, A. Fujiwara and H. Kitagawa, *Chem. Commun.*, 2015, **51**, 15796.

140 M. Hayashi, K. Otsubo, M. Maesato, T. Komatsu, K. Sugimoto, A. Fujiwara and H. Kitagawa, *Inorg. Chem.*, 2016, **55**, 13027.

141 Y. Kimura, M. Hayashi, Y. Yoshida and H. Kitagawa, *Inorg. Chem.*, 2019, **58**, 3875.

142 M. Hayashi, Y. Takahashi, Y. Yoshida, K. Sugimoto and H. Kitagawa, *J. Am. Chem. Soc.*, 2019, **141**, 11686.

143 S. Henfling, R. Kempt, J. Klose, A. Kuc, B. Kersting and H. Krautscheid, *Inorg. Chem.*, 2020, **59**, 16441.

# Chapter 2

# Three-dimensional hydrogen-bonded framework based on metal dithiolene complex and a role of crystal solvent on the assembled structures

## 2.1 Introduction

Metal-organic frameworks (MOFs)[1] and covalent organic frameworks (COFs)[2–4] are classes of crystalline materials with highly ordered structures, which are constructed through coordination or covalent bonds. Extensive synthetic studies of these materials have been carried out because of their characteristic, even porous in many cases, framework structures and the resultant functionalities, such as gas storage/separation, catalytic, and sensing abilities and ion transport property together with guest-inclusion ability.[5–15] Hydrogen-bonded (H-bonded) organic frameworks (HOFs)[16] have recently emerged as a new class of such crystalline materials. As mentioned in Section 1.2, H-bonds have intermediate bond strength, which is weaker than the coordination/covalent bonds yet strong enough for facile crystallization. By utilizing H-bonds instead of coordination or covalent bonds, HOFs generally have better crystallinity, solution processability, and flexibility than MOFs and COFs, allowing further development of the material properties and functionalities.[17–20] However, the examples of HOFs based on functional molecules have been limited compared to that of MOFs and COFs. Thus, developments of new HOF materials are important from the viewpoint of crystal engineering and the exploration of new functionalities in H-bonded materials.

As one approach to explore electron–proton coupled metal dithiolene complexes, the author focused on the metal dithiolene complexes with H-bonding moiety, which are also the constituent molecules of HOF. The characteristic framework structures of HOF are beneficial

for the novel functionality based on H-bonds. Besides, because the metal-dithiolene complexes exhibit rich electronic functionalities in solid state[21–26], as introduced in Chapter 1, the introduction of the metal-dithiolene complexes into HOFs as the constituents will also lead to the developments of a new series of functional HOFs; however, there have been no metal-dithiolene-based crystals having 3D H-bonded frameworks.

Based on this background, in this chapter, the author aims to develop the crystals with the H-bond network based on metal dithiolene complexes and to control the molecular arrangement, i.e., the framework structures. To achieve this purpose, the author focused on the metal catecholdithiolene complex with four hydroxy groups in anticipation of the H-bond formation in the solid state. Despite its high potential to form intermolecular H-bonds with each other, there has been only one crystal of the complex reported previously, where the intermolecular H-bonds between the complexes exist.[27] In this chapter, novel three-dimensional (3D) molecular frameworks based on a new anionic gold dithiolene complex, $[Au(catdt)_2]^-$ complex (Fig. 2-1, catdt = catechol-4,5-dithiolate), are demonstrated. Interestingly, the rigid, planar molecular skeletons of $[Au(catdt)_2]^-$ complex are three-dimensionally connected by multiple intermolecular H-bonds through the terminal four hydroxy groups. A large number of anionic metal-dithiolene complexes have been synthesized to date[24]; however, to our best knowledge, no example of 3D framework structures based on metal dithiolene complexes are reported and such examples are very rare.[25–26] Furthermore, the author found that the structure and dimensionality of the frameworks can be modulated by changing the crystal solvents, in which interactions between the solvent molecules play an important role.
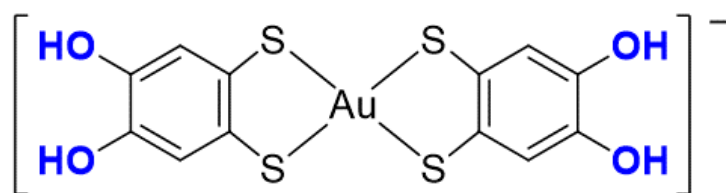


**Fig. 2-1** Chemical structure of gold catecholdithiolene complex, $[Au(catdt)_2]^-$.

## 2.2 Experimental

**Materials and methods**

Commercially available chemicals were used without further purification. The chemicals used here are listed below. Tetrahydrofuran, *N,N*-dimethylformamide, and acetone (Guaranteed reagent, FUJIFILM Wako Pure Chemical lndustries Co., Ltd.); hexane, diethyl ether, and methanol (super dehydrated grade, FUJIFILM Wako Pure Chemical lndustries CO., Ltd.); tetraphenylphosphonium bromide (Tokyo Chemical Industries Ltd.); Na(AuCl$_4$)·2H$_2$O (Guaranteed reagent, Kanto Chemical Co., inc.).

$^1$H NMR (300 MHz) spectra measurements were carried out with a JEOL JNM-AL300 spectrometer with DMSO-$d_6$ as a solvent and Me$_4$Si as the internal standard.

UV-vis spectra were recorded on a Hitachi UV-3010 UV-vis spectrometer using *N,N*-dimethylformamide (DMF) solutions. Infrared spectra of KBr pellet samples were recorded on a Horiba FT-730 spectrometer. The decomposition point was measured with a hot-stage system.

Cyclic Voltammetry (CV) measurements were carried out with an ALS 610DB electrochemical analyzer in DMF solutions containing 0.1 M Bu$_4$NClO$_4$ (working electrode: glassy carbon, counter electrode: platinum wire, reference electrode: saturated calomel electrode (SCE), scan rate: 0.100 V s$^{-1}$).

Density functional theory (DFT) calculations were performed by using Gaussian09 program (revision E.01) at the CAM-B3LYP/6-311G++(d,p) level of theory for geometry optimization of the complexes.[28] Note that SDD was applied only to the Au atom as the basis.

**Synthesis and crystal preparations**

According to the literature[27], the ligand precursor, H$_2$catdt·2Ph$_4$PBr·H$_2$O (Ph$_4$P$^+$ = tetraphenylphosphonium; catdt = catechol-4,5-dithiolate), **1**, were prepared. A mixture of **1** (412 mg, 0.40 mmol) and NaAuCl$_4$·2H$_2$O (80 mg, 0.20 mmol) in DMF (12 mL) was stirred at room temperature for 10 min under argon atmosphere. By complexation of the ligand and

NaAuCl$_4$·2H$_2$O in *N,N*-dimethylformamide, new gold dithiolene complex, [Au(catdt)$_2$] was synthesized. The reaction mixture was filtered to remove the insoluble materials, and diethyl ether was slowly layered with the reaction solution, to give crystal **2-Au**, (Ph$_4$P)$_3$[Au(catdt)$_2$]Br$_{2x}$Cl$_{2(1-x)}$ (This compound has Br$^-$ and Cl$^-$ derived from those reactants, compound **1** and NaAuCl$_4$·2H$_2$O. From single-crystal X-ray structural analysis, the ratio of Br:Cl is estimated to be 0.87:0.13 (i.e., n = 1.74)), as yellow plate crystals (210 mg, 0.12 mmol, 61%). mp 230 °C (decomp.); $^1$H NMR (300 MHz, DMSO-$d_6$): 6.43 (s, 4H), 7.71–8.00 (m, 60H), 8.43 (br, 4H); UV/Vis (DMF): $\lambda_{max}$ ($\varepsilon$, M$^{-1}$ cm$^{-1}$) = 692 nm (171), 442 nm (458), 337 nm (17600); IR(cm$^{-1}$): 3429(m), 3271(s), 1585(m), 1485(s), 1439(s), 1398(s), 1338(m), 1313(m), 1261(s), 1167(m), 1109(s), 997(s), 862(m).

Then, the compound **2-Au** (61 mg, 0.036 mmol) was suspended in a mixture of MeOH (4 mL) and H$_2$O (20 mL) and stirred at room temperature for one day under an argon atmosphere. The resulting off-yellow suspension was filtered and washed with water, to give the brownish-yellow powder (19 mg). $^1$H NMR analysis indicates that this powder contain Ph$_4$P$^+$ and [Au(catdt)$_2$]$^-$ in 1:1 ratio by removal of 2Ph$_4$PBr ($^1$H NMR (300 MHz, DMSO-$d_6$): 6.43 (s, 4H), 7.71–8.00 (m, 20H), 8.41 (s, 4H)). This powder (2 mg) was then recrystallized from acetone/hexane (ca. 1:2) at room temperature under air for five days to give (Ph$_4$P)[Au(catdt)$_2$]·0.5H$_2$O, **3-Au·0.5H$_2$O** as yellowish-brown needle-like crystals suitable for X-ray analysis with a lot of amorphous solid. Also, (Ph$_4$P)[Au(catdt)$_2$]·Et$_2$O·n(solv) (solv = acetone and/or diethyl ether), **3-Au·Et$_2$O** and (Ph$_4$P)[Au(catdt)$_2$]·2THF (THF = tetrahydrofuran), **3-Au·2THF** were obtained by recrystallization from acetone/Et$_2$O and THF/hexane at room temperature under air as yellow plate-like crystal and green plate-like crystal, respectively.
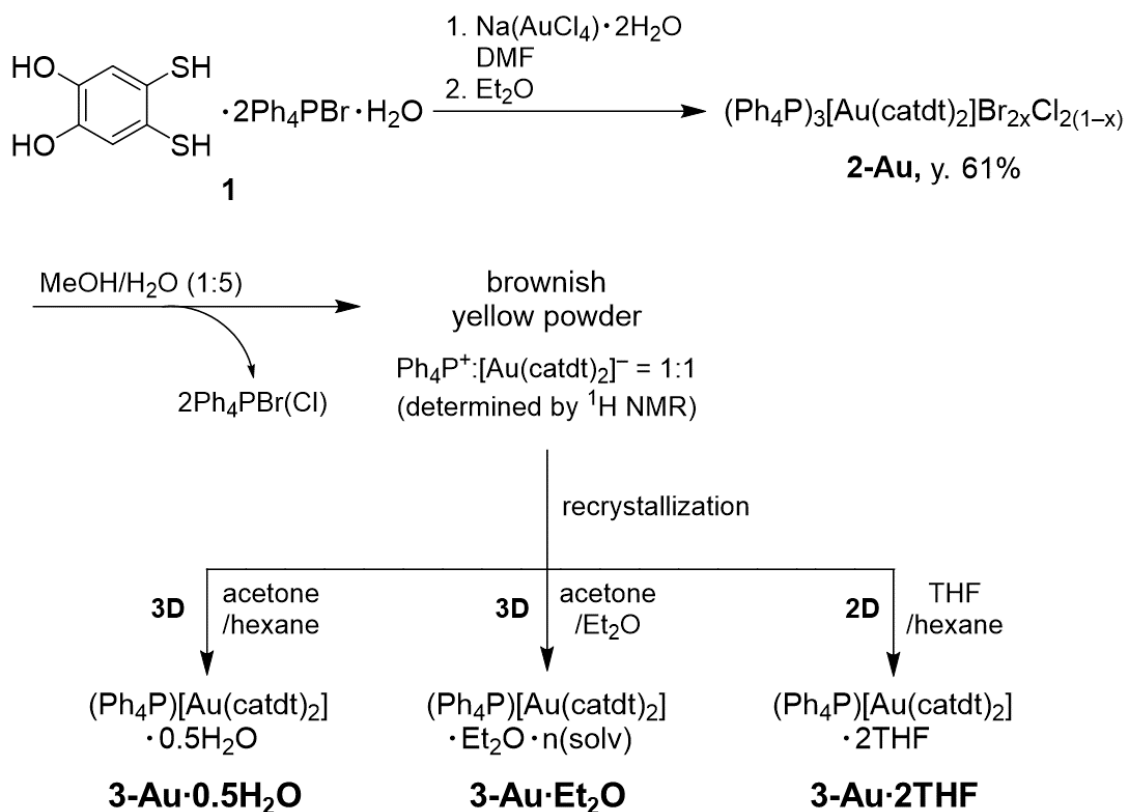
Scheme 2-1 Synthesis of $(Ph_4P)[Au(catdt)_2]\cdot 0.5H_2O$, **3-Au·0.5H₂O**, $(Ph_4P)[Au(catdt)_2]\cdot Et_2O\cdot n(solv)$ (solv = acetone and/or $Et_2O$), **3-Au·Et₂O**, and $(Ph_4P)[Au(catdt)_2]\cdot 2THF$, **3-Au·2THF**, through $(Ph_4P)_3[Au(catdt)_2]Br_nCl_{2-n}$.


**Single crystal X-ray structure analysis**

X-ray diffraction measurements for **2-Au**, **3-Au·0.5H₂O**, and **3-Au·Et₂O** were carried out on a Rigaku MercuryII CCD X-ray diffractometer (MoKα, $\lambda = 0.71073$ Å) and those for **3-Au·2THF** were performed on a Rigaku imaging plate system (synchrotron, $\lambda = 0.68889$ Å) at the BL-8A in the Photon Factory (PF), the High Energy Accelerator Research Organization (KEK), Japan. The initial structures were solved by direct methods (SHELXT) and refined with a full-matrix least-squares technique (SHELXL) using CrystalStructure 4.3.2 (Rigaku Corporation). Anisotropic thermal parameters were applied to all non-hydrogen atoms. The position of hydrogen atoms on hydroxy groups was refined, and the other hydrogen atoms were

generated geometrically (C–H = 0.950 Å). The SQUEEZE equipped in the PLATON program[28–30] was used to remove disordered molecules in the void spaces of **3-Au·Et₂O**.

**Processing of the CSD**

Processing of the Cambridge Structure Database (v 5.40) using the ConQuest module (v 2.0.0) was performed to judge whether 3D molecular frameworks based on H-bonded metal dithiolene complexes is the first report or not. In the search, crystal structural data without errors and $R$1-factor below 0.1 were considered. Also, focusing on the metal dithiolene skeleton and H-bond ($X_1$–H···$X_2$; $X_1$ = N, O, and S; $X_2$ = N, O, S, and halogen atoms), two searches were carried out with the following parameters. The H-bond distances $d_1$ ($X_1$···$X_2$) or $d_2$ (H···$X_2$) are separately used for the parameters, and the distances were restricted by the sum of van der Waals radii.[32]As a result, 214 (with the restriction on $d_1$) and 312 (with the restriction on $d_2$) kinds of crystal data appeared, respectively. However, there is no "3D molecular framework based on H-bonded metal dithiolene complexes". Therefore, the author concluded that our crystals **3-Au·0.5H₂O** and **3-Au·Et₂O** are the first examples of such materials.

## 2.3 Optical and electrochemical properties and DFT calculation

Firstly, to investigate the optical and electrochemical properties of the new gold-dithiolene complex, the DMF solution of **2-Au** was investigated by CV and UV-vis absorption measurements. DMF solution of compound **2-Au** was used for optical and electrochemical properties of the gold catecholdithiolene complex in solution (Fig. 2-2 and 2-3). The cyclic voltammogram shows two redox processes at $-0.843$ V and $+0.303$ V vs. SCE. The first wave corresponds to one-electron reduction from the monoanionic species, $[Au(catdt)_2]^-$ to dianion species, $[Au(catdt)_2]^{2-}$ and the second wave corresponds to one-electron oxidation from the monoanion, $[Au(catdt)_2]^-$ to neutral radical species, $[Au(catdt)_2]$ (Fig. 2-2)$\cdot$. The oxidation potential from monoanion ($+0.303$ V) is lower than the corresponding value of $[Au(bdt)_2]^-$ (bdt = benzene-4,5-dithiolate, $+0.865$ V vs. SCE). This fact indicates that the electron-donating ability of the complex is significantly enhanced by the attachment of four hydroxy groups.

The UV-vis spectrum of **2-Au** in solution exhibits a weak broad absorption at 692 nm (Fig. 2-3) and a similar absorption was observed in the benzo-analogue, $[Au(bdt)_2]^-$ (637 nm).[33] The absorption band is attributed to the transition between HOMO and LUMO in the previous study[30,33], and thus this absorption at 692 nm is also assigned as the HOMO-LUMO transition. Furthermore, due to destabilization and more delocalized distribution of HOMO by attaching four hydroxy groups to the benzodithiolene ligand, the HOMO-LUMO gap is expected to be reduced. Actually, the redshift of the absorption of $[Au(catdt)_2]^-$ complex compared with that of $[Au(bdt)_2]^-$ complex was observed.
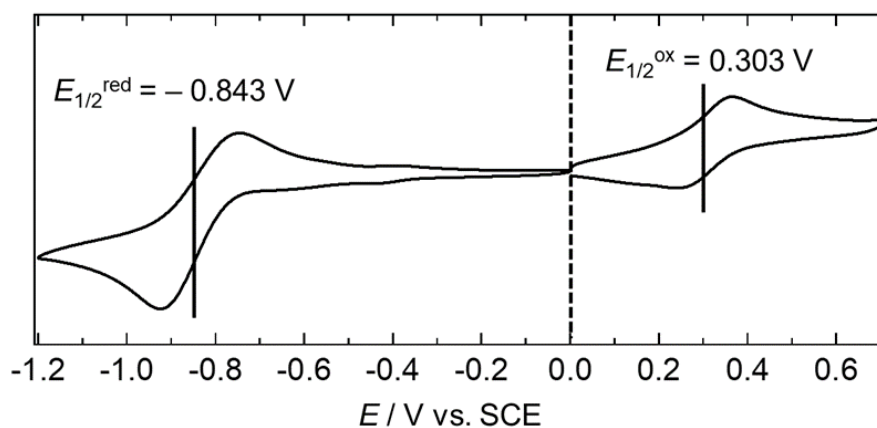
**Fig. 2-2** Cyclic voltammogram of $[Au(catdt)^2]^-$ complex in a DMF solution of compound **2-Au** with 0.1 M Bu$_4$NClO$_4$ (vs. SCE).
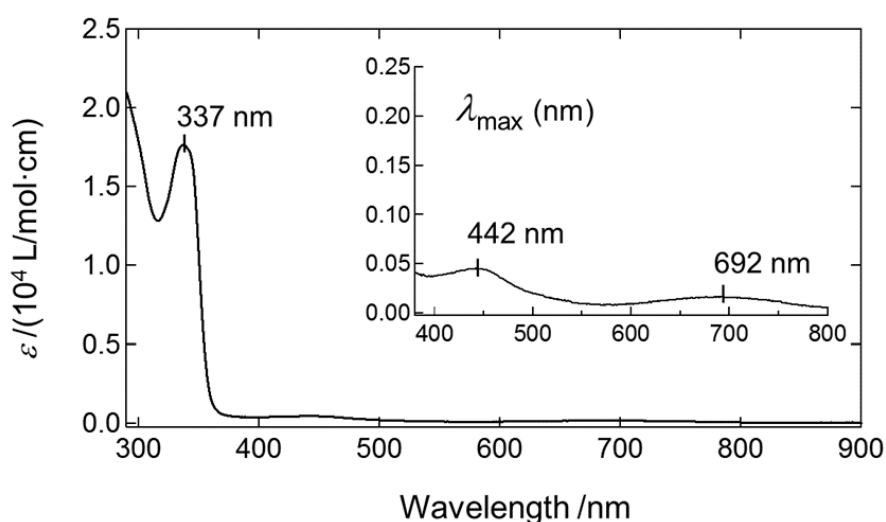


**Fig. 2-3** UV-vis absorption spectrum of $[Au(catdt)_2]^-$ complex in a DMF solution of compound **2-Au** ($1.11 \times 10^{-4}$ M ).

The density functional theory (DFT) calculations supported the results of CV and UV-vis absorption measurements. The calculated HOMO energy of the $[Au(catdt)_2]^-$ complex ($-3.23$ eV) was higher than that of $[Au(bdt)_2]^-$ complex ($-3.34$ eV). This result is consistent with the result of CV measurement. The HOMO-LUMO energy gap of $[Au(catdt)_2]^-$ complex (4.71 eV)

was also smaller than that of [Au(bdt)$_2$]$^-$ complex (4.89 eV), which is similar to a tendency observed in the UV-vis measurement. Notably, the HOMO of [Au(catdt)$_2$]$^-$ complex is widely delocalized on the whole molecule, including the four hydroxy groups on the terminal, which would contribute to decreasing the HOMO-LUMO energy gap.
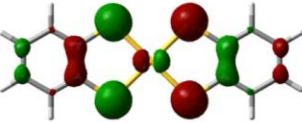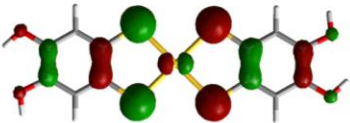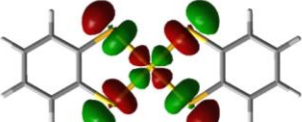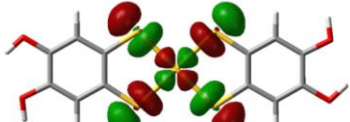
| complex | [Au(bdt)$_2$]$^-$ | [Au(catdt)$_2$]$^-$ |
|---|---|---|
| HOMO |  |  |
| LUMO |  |  |
| $E^{ox}_{1/2}$ (V) | +0.865 [ref.11] | +0.303 |
| HOMO energy (eV) (from DFT calc.) | −3.34 | −3.23 |
| LUMO energy (eV) (from DFT calc.) | +1.55 | +1.48 |
| HOMO energy (eV) (= −$E^{ox}_{1/2}$ − 4.44) | −5.31 | −4.74 |

**Fig. 2-4** Comparison of the electronic states of gold dithiolene complex, [Au(bdt)$_2$]$^{-}$[33,34] and [Au(catdt)$_2$]$^-$. The distributions of HOMO and LUMO were obtained from DFT calculations (CAM-B3LYP/6-311++G(d,p) (SDD for Au)).[31] Each structure was optimized based on the X-ray crystal structure data[35] and energies were estimated by DFT calculation. The experimental HOMO energies estimated from CV measurement using the equation, E$^{HOMO}$ = −$E^{ox}_{1/2}$ − 4.44,[36,37] are also shown.

## 2.4 Crystal structures

As described in Section 2.2, new crystals of **2-Au**, **3-Au·0.5H₂O**, **3-Au·Et₂O**, and **3-Au·2THF** were successfully obtained from the compound **2-Au**. The crystal of compound **2-Au** has Br⁻ and Cl⁻ ions originated from those reactants, the ligand precursor and NaAuCl₄·2H₂O. From single-crystal X-ray structural analysis, the ratio of Br: Cl is estimated to be 0.87:0.13 (i.e., n = 1.74). The crystallographic data for all crystals of **2-Au**, **3-Au·0.5H₂O**, **3-Au·Et₂O**, and **3-Au·2THF** is shown in Table 2-1.

**Table 2-1** The crystallographic data for crystals of **2-Au**, **3-Au·0.5H₂O**, **3-Au·Et₂O**, and **3-Au·2THF**.

| crystals | 2-Au | 3-Au·0.5H$_2$O | 3-Au·Et$_2$O [b] | 3-Au·2THF |
|---|---|---|---|---|
| formula | C$_{84}$H$_{68}$AuBr$_n$Cl$_{2-n}$O$_4$P$_3$S$_4$[a] | C$_{36}$H$_{29}$AuO$_{4.5}$PS$_4$ | C$_{40}$H$_{38}$AuO$_5$PS$_4$[b] | C$_{44}$H$_{44}$AuO$_6$PS$_4$ |
| formula weight | 1707.84 [a] | 889.80 | 954.92[b] | 1025.01 |
| crystal system | monoclinic | monoclinic | monoclinic | monoclinic |
| space group | $P2_1/c$ | $P2_1/c$ | $P\bar{1}$ | $C2/c$ |
| $a$ (Å) | 18.636(3) | 7.4715(17) | 10.783(3) | 24.0138(4) |
| $b$ (Å) | 14.5547(19) | 16.423(4) | 14.172(4) | 7.3818(4) |
| $c$ (Å) | 27.872(4) | 27.825(7) | 13.481(5) | 25.0096(7) |
| $\alpha$ (deg) | 90 | 90 | 65.051(8) | 90 |
| $\beta$ (deg) | 92.464(2) | 90.076(3) | 80.380(13) | 110.8721(7) |
| $\gamma$ (deg) | 90 | 90 | 79.305(14) | 90 |
| $V$ (Å$^3$) | 7553.0(17) | 3414.3(14) | 2232.8(11) | 4142.4(3) |
| $Z$ | 4 | 4 | 2 | 4 |
| $T$ (K) | 293 | 293 | 293 | 100 |
| $D_{calc}$ (g· cm$^{-3}$) | 1.502 | 1.731 | 1.420[b] | 1.643 |
| $\lambda$ (Å) | 0.71073 | 0.71073 | 0.71073 | 0.68889 |
| $R_{int}$ | 0.0440 | 0.0372 | 0.0321 | 0.0350 |
| $R_1$ ($I$>2.00σ($I$)) | 0.0553 | 0.0462 | 0.0431 | 0.0289 |
| $wR_2$ (All reflections) | 0.1467 | 0.1177 | 0.1154 | 0.0895 |
| GOF | 1.067 | 1.117 | 0.994 | 0.950 |
| CCDC | 1897712 | 1897713 | 1897714 | 1897715 |

[a] The ratio of Br and Cl cannot be accurately determined due to disorder in the same position. The formula weight was calculated by using the value (n = 1.74) obtained from the single-crystal X-ray structural analysis. [b] Due to the presence of disordered crystals solvents in large voids in the unit cell, PLATON/SQUEEZE software[28–30] was used during the structural refinement. Therefore, the formula and parameters were determined without considering the disordered crystal solvents.

**Table 2-2** The C–S and C–O bond lengths (in Å) of the anionic metal dithiolene complex in **2-Au**, **3-Au·0.5H₂O**, **3-Au·Et₂O**, and **3-Au·2THF**.

| crystals | C–S | C–S | C–O | C–O |
|---|---|---|---|---|
| **2-Au** | 1.763(5) | 1.761(5) | 1.385(7) | 1.364(7) |
| | 1.770(6) | 1.761(6) | 1.362(7) | 1.366(7) |
| **3-Au·0.5H₂O** | 1.769(5) | 1.758(5) | 1.384(7) | 1.383(7) |
| | 1.762(5) | 1.764(5) | 1.367(7) | 1.379(7) |
| **3-Au·Et₂O** | 1.748(6) | 1.777(5) | 1.385(5) | 1.350(7) |
| | 1.774(6) | 1.765(5) | 1.373(7) | 1.382(6) |
| **3-Au·2THF** | 1.761(3) | 1.771(3) | 1.363(5) | 1.360(4) |

## 2.4.1 (Ph₄P)[Au(catdt)₂]·0.5H₂O: 3D framework structure

First, the crystal structure of the water-containing salt **3-Au·0.5H₂O** was shown in Fig. 2-5, 2-6, 2-7, and 2-8, Table 2-1. The asymmetric unit consists of one $Ph_4P^+$ cation, one gold dithiolene complex, and half a water molecule. Thus, the gold dithiolene complex is deduced to be the monoanionic species, $[Au(catdt)_2]^-$ complex, with a closed-shell electronic structure due to the Au(III) state. As displayed in Fig. 2-5, the $[Au(catdt)_2]^-$ complex has a planar structure, typical for gold dithiolene complexes.[33,35] The C–S distances ($d_{C-S}$) in this $[Au(catdt)_2]^-$ complex are 1.769(5), 1.758(5), 1.762(5), and 1.764(5) Å (Table 2-2), supporting the monoanionic state of this complex.[35] Also, the C–O bond lengths (1.384(7), 1.383(7), 1.367(7), and 1.379(7) Å; Table 2-2) are similar to those in non-deprotonated catechol derivatives.[30] These results prove the non-deprotonated monoanionic state of this gold dithiolene complex.
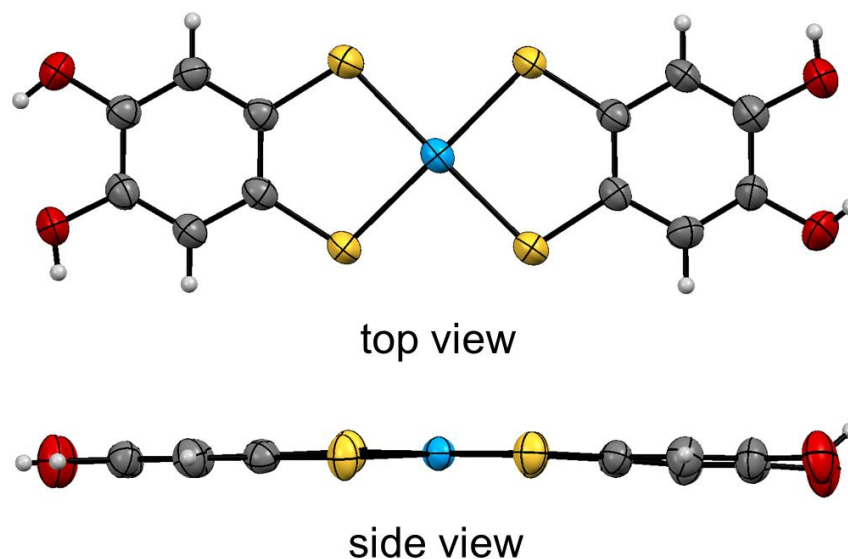
**top view**

**side view**

**Fig. 2-5** ORTEP drawings of the [Au(catdt)₂]⁻ complex in the crystal of **3-Au·0.5H₂O**; top view (top), side view (bottom). Light blue = Au, yellow = S, gray = C, red = O, white = H.

In the crystal, the rigid, planar [Au(catdt)₂]⁻ complexes are connected by multiple intermolecular H-bonds through the terminal four hydroxy groups and the water molecules (blue ellipses in Fig. 2-6a), to give a 3D framework structure with tubular channels (Fig. 2-6a, b). The counter cations, Ph₄P⁺, are included in the channels with multiple cation-anion short contacts (Fig. 2-7c), which should stabilize this 3D framework structure. To our knowledge, this is the first 3D molecular framework based on H-bonded metal dithiolene complexes (see "Processing of the CSD" in Section 2.2).
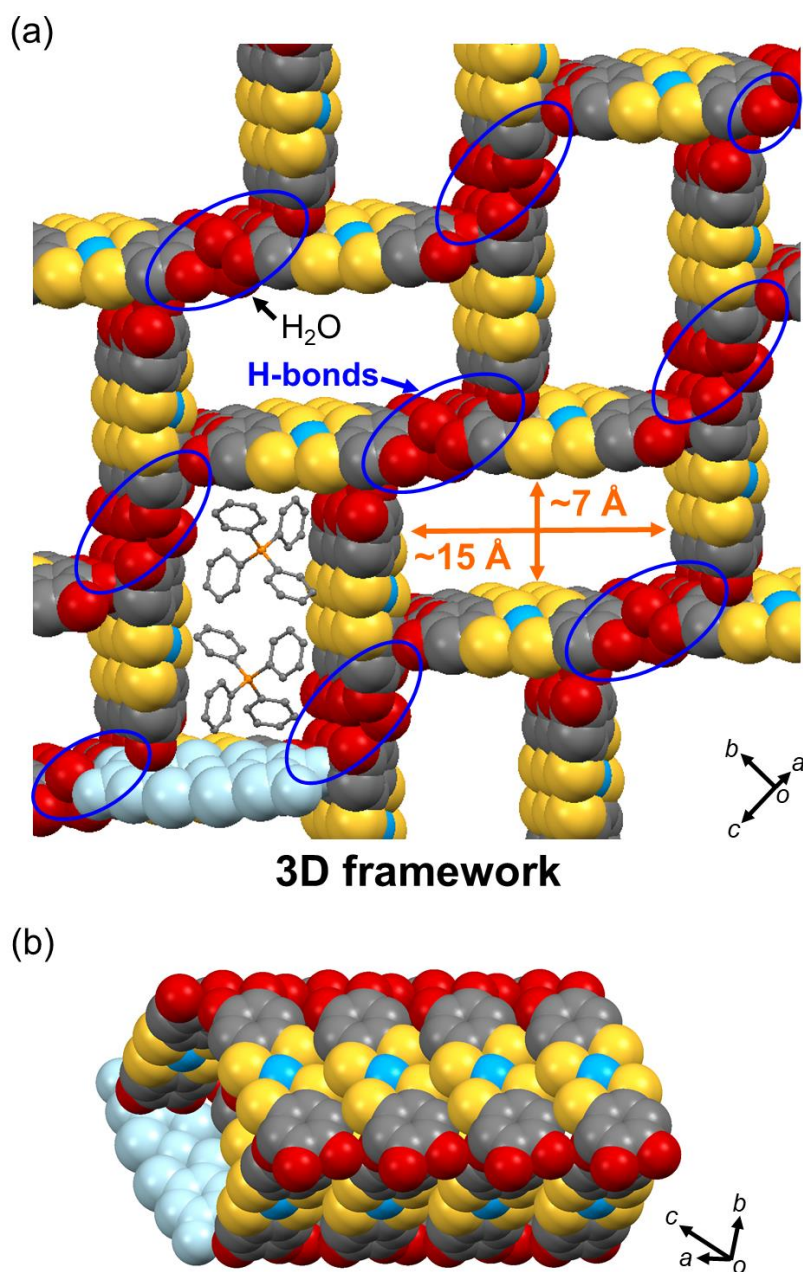
**Fig. 2-6** Crystal structure of the anion salt **3-Au·0.5H₂O**. (a) Overview of the 3D framework structure, (b) the tubular channel structure in the 3D framework. For clarify, all hydrogen atoms are omitted in (a) and (b). The light blue molecule shows that at the same position in (a) and (b).
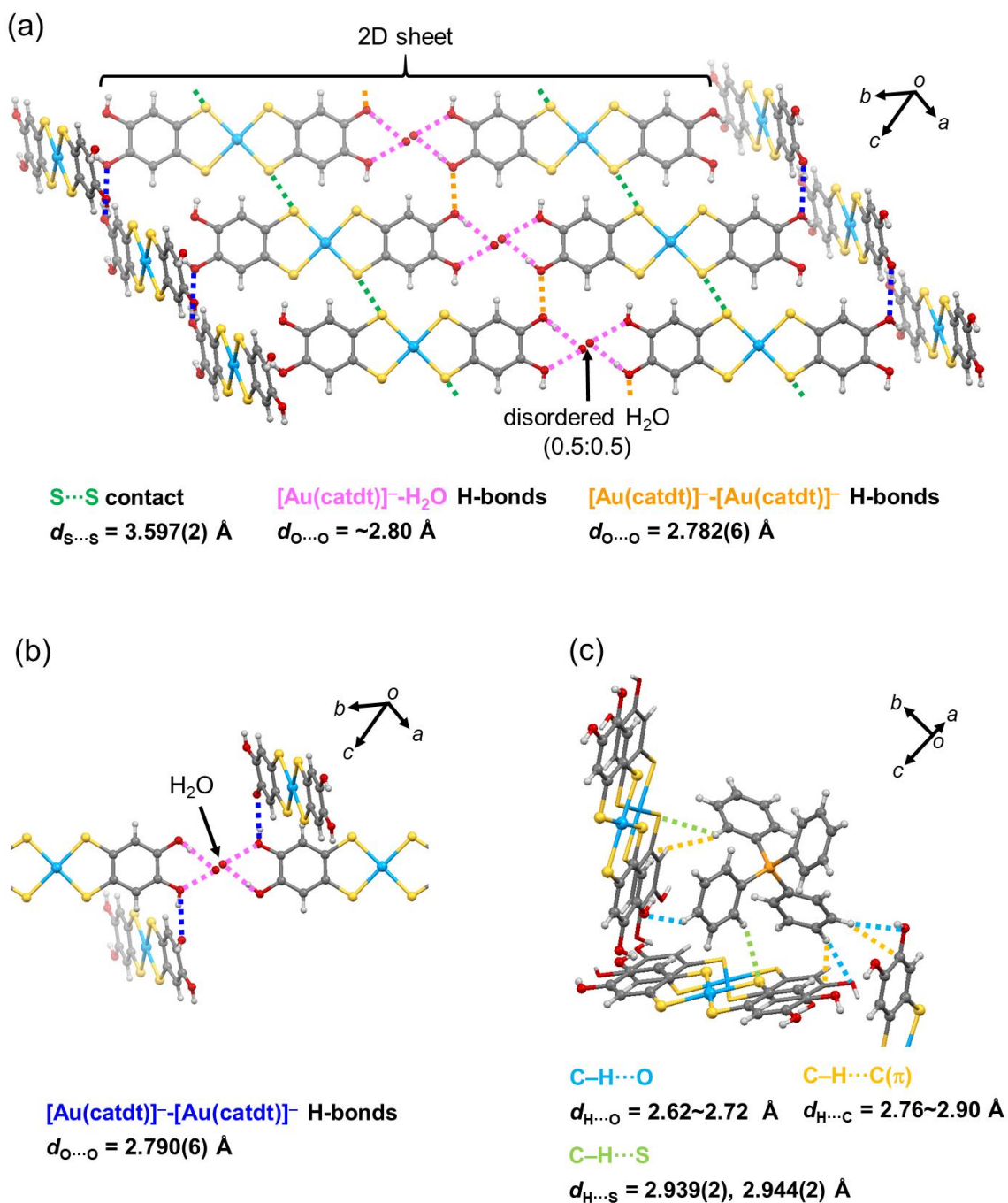
**Fig. 2-7** Intermolecular interactions in the anion salt **3-Au·0.5H₂O**. (a) Intermolecular interactions in the 2D sheet structure of the framework, (b) H-bonds in the node part of the 3D framework, and (c) the intermolecular short contacts between [Au(catdt)₂]⁻ complex and Ph₄P⁺.

Here, we describe the details of the molecular arrangement and intermolecular interactions in this 3D structure in Fig. 2-6 and 2-7. The framework itself is constructed based on a 2D sheet structure shown in Fig. 2-7a, where $[Au(catdt)_2]^-$ complex and water molecules are densely packed through $[O–H\cdots O]$ H-bonds (orange dashed lines, $d_{O\cdots O} = 2.782(6)$ Å; pink dashed lines, $d_{O\cdots O} = {\sim}2.80$ Å) and $S\cdots S$ contacts (green dashed lines, $d_{S\cdots S} = 3.597(2)$ Å) (the water molecules are positionally disordered in a ratio of 0.5:0.5; for details, see Fig. 2-8a). As shown in Fig. 2-7a and b, the 2D sheets are connected to each other by $[O–H\cdots O]$ H-bonds between $[Au(catdt)_2]^-$ complexes (blue dashed lines, $d_{O\cdots O} = 2.790(6)$ Å), to give the 3D framework. Furthermore, there are multiple short atomic contacts between the $[Au(catdt)_2]^-$ complexes and $Ph_4P^+$ molecules (Fig. 2-7c; $C–H\cdots O$ ($d_{H\cdots O} = 2.62 \sim 2.72$ Å), $C–H\cdots C(\pi)$ ($d_{H\cdots C} = 2.76 \sim 2.90$ Å), and $C–H\cdots S$ ($d_{H\cdots S} = 2.939(2), 2.944(2)$ Å)), suggesting the existence of effective electrostatic interactions between these anion and cation species to stabilize the 3D framework. Therefore, the combination of H-bonds and other intermolecular interactions, such as $S\cdots S$ and cation-anion contacts, seems to allow the construction of this 3D framework based on metal dithiolene complexes.
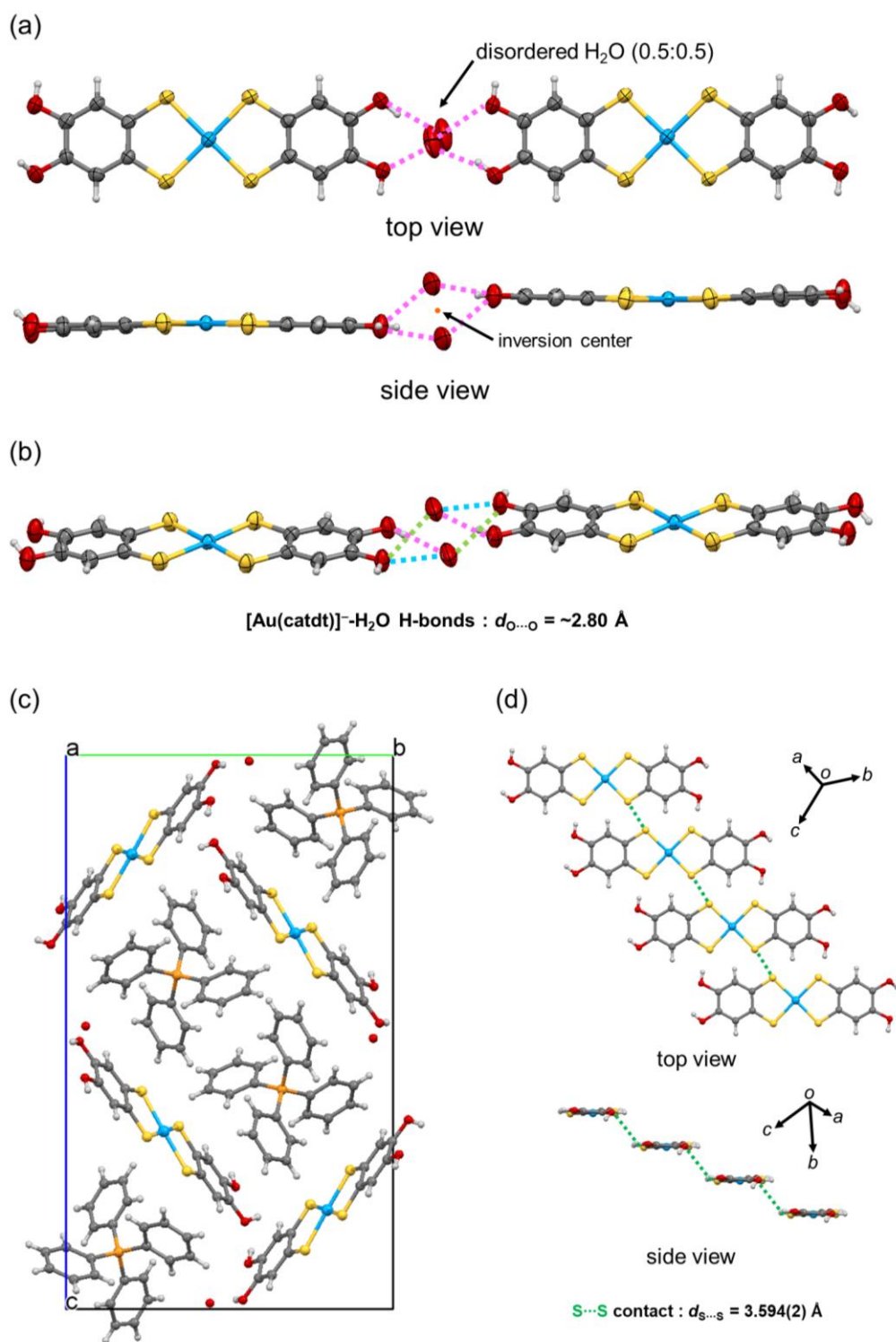
**Fig. 2-8** H-bonded motif with positionally disordered $H_2O$ molecules (0.5:0.5) and H-bonds between [Au(catdt)$_2$]$^−$ complex and water molecules in **3-Au·0.5H$_2$O**. (a) Top view (top), side view (bottom) and (b) diagonal view. The thermal ellipsoids are scaled to the 50% probability level. Crystallographically equivalent H-bonds are shown in the same color dashed line in (b). (c) Molecular arrangements in the unit cell of **3-Au·0.5H$_2$O**, viewed along the *a*-axis. (d) Top view (top) and side view (side) of [Au(catdt)$_2$]$^−$ complexes in 2D sheet on 3D framework.

### 2.4.2 (Ph₄P)[Au(catdt)₂]·Et₂O·n(solv): 3D framework structure

The title salt **3-Au·Et₂O** also has a 3D anionic framework based on [Au(catdt)₂]⁻ complexes (Fig. 2-9, 2-10, and 2-11 Table 2-1). The molecular structure and bond lengths of [Au(catdt)₂]⁻ complex in **3-Au·Et₂O** are similar to those in **3-Au·0.5H₂O** (Table 2-2 and Fig. 2-10a), and the channel size of these frameworks is roughly the same (ca. 9 Å × 12 Å (**3-Au·Et₂O**)), ca. 7 Å × 15 Å (**3-Au·0.5H₂O**)); thus, both of the frameworks take Ph₄P⁺ molecules in their tubular channels. On the other hand, there is a difference in the components of their frameworks; namely, although the framework in **3-Au·0.5H₂O** is composed of [Au(catdt)₂]⁻ complex and water molecules (Fig. 2-7), that in **3-Au·Et₂O** is composed only of [Au(catdt)₂]⁻ complex (Fig. 2-9 and 10b), which are directly connected each other by H-bonds (blue dashed lines in Fig. 2-10b, $d_{O\cdots O}$ = 2.748(5), 2.762(5) and 2.972(5) Å). This difference should cause differences in the molecular arrangement in the framework; actually, in this salt **3-Au·Et₂O**, lateral S···S contacts between the [Au(catdt)₂]⁻ complexes, seen in **3-Au·0.5H₂O**, are not present (Fig. 2-9b and 2-10b), which results in the formation of small voids on the framework walls. This means that such S···S contacts are not necessary for obtaining 3D frameworks in this type of salts. On the other hand, short atomic contacts between the [Au(catdt)₂]⁻ and Ph₄P⁺ molecules are observed not only in **3-Au·0.5H₂O** (Fig. 2-7c) but also in **3-Au·Et₂O** (Fig. 2-11), suggesting that the inclusion of such a large cation is the key to construct these 3D anionic molecular frameworks. In addition, there are Et₂O molecules at corners of the channels (Fig. 2-9a and 2-11b), forming H-bonds with [Au(catdt)₂]⁻ complexes in the framework. Interestingly, phenyl groups of the Ph₄P⁺ molecules and methyl groups of the Et₂O molecules partially penetrate into the small voids on the framework walls (Fig. 2-9b). Such penetration of molecules into the framework walls is not observed in **3-Au·0.5H₂O**, because of its densely packed wall structure without accessible voids (Fig. 2-6b and 2-7a). These results indicate that the crystal solvent molecules greatly affect the H-bonds and molecular arrangement of [Au(catdt)₂]⁻ complex, which leads to structural variations in this new type of anionic molecular framework.

**(a)**

H-bonds

~9 Å

~12 Å

Et₂O

**3D framework**

**(b)**

Ph₄P⁺   Et₂O   [Au(catdt)₂]⁻
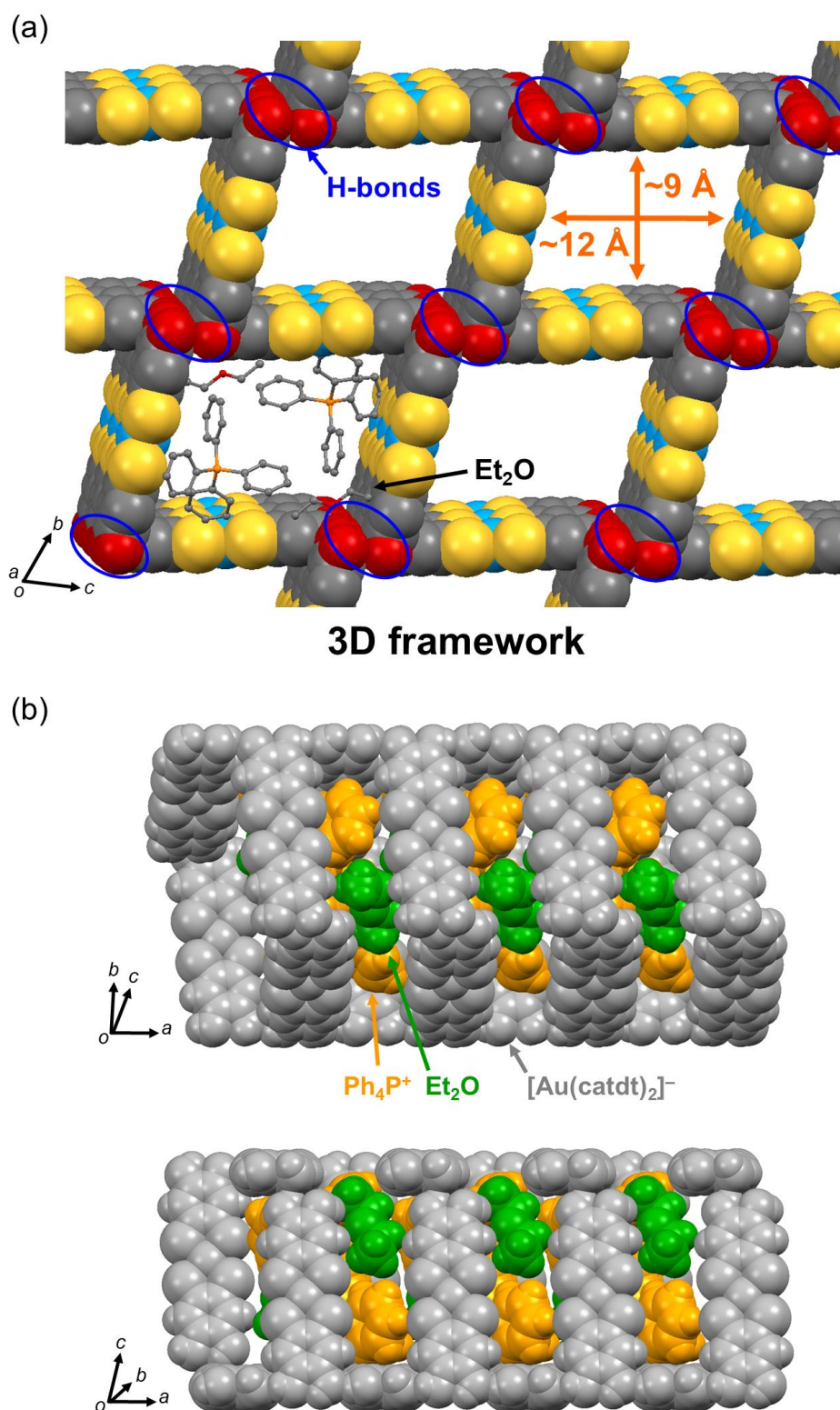
**Fig. 2-9** Crystal structure of the anion salt **3-Au·Et₂O**. (a) Overview of the 3D framework structure, (b) diagonal view (top) and side view (bottom) of the tubular channel structure in 3D framework. For clarify, all hydrogen atoms are omitted in (a). Ph₄P⁺ (orange) and Et₂O (green) molecules partially penetrate in void between [Au(catdt)₂]⁻ complexes (grey) in (b). The disordered phenyl group is omitted for clarity.

**(a)**

[Au(catdt)$_2$]$^-$ molecule A    [Au(catdt)$_2$]$^-$ molecule B

top view    top view

side view    side view

**(b)**

**[Au(catdt)]$^-$-[Au(catdt)]$^-$ H-bonds**
$d_{O \cdots O}$ = 2.744(5), 2.761(5) and 2.974(5) Å
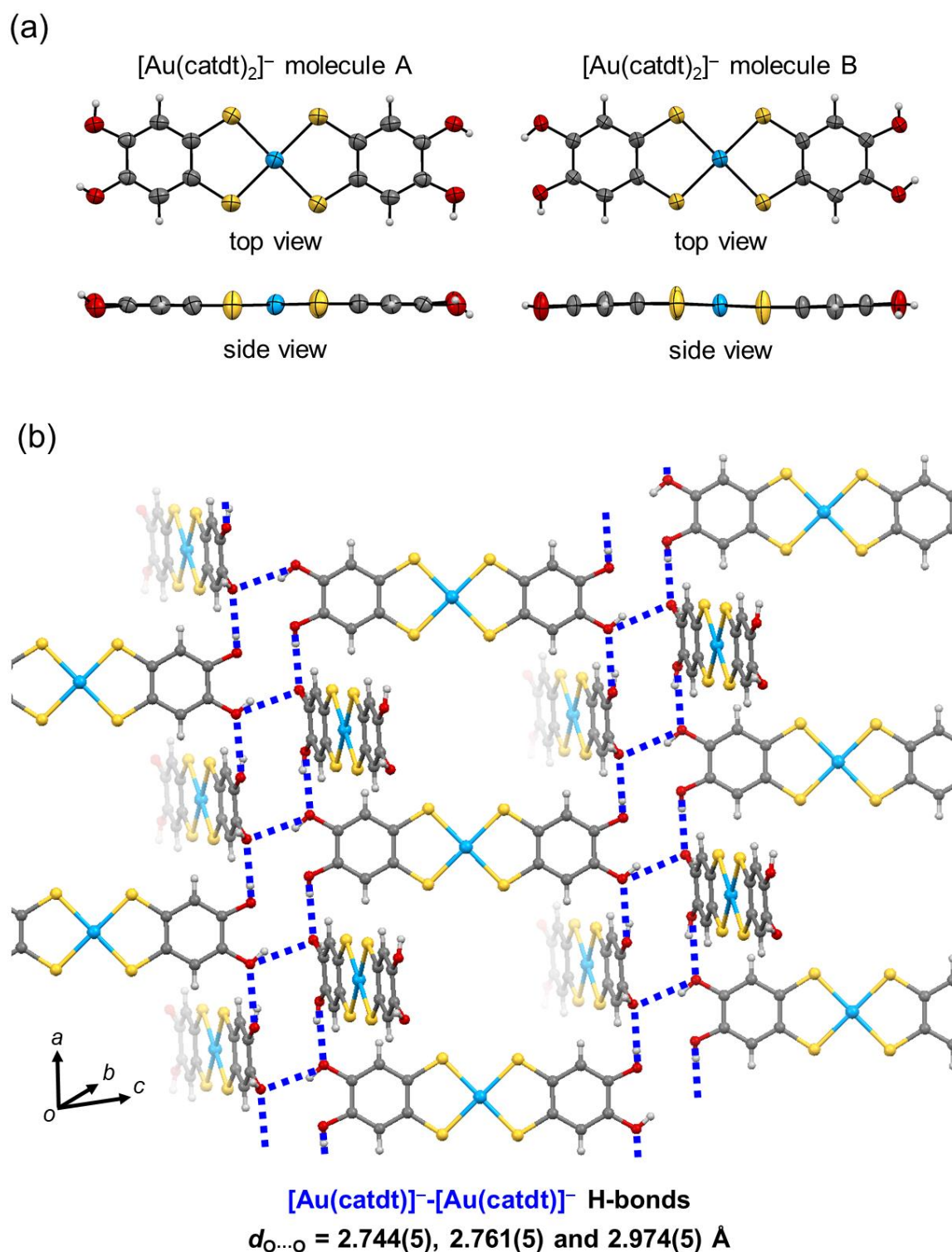
**Fig. 2-10** (a) ORTEP drawings of two kinds of [Au(catdt)$_2$]$^-$ complexes in **3-Au·Et₂O**; top view (top), side view (bottom). The thermal ellipsoids are scaled to the 50% probability level. (b) Intermolecular interactions of the anion salt **3-Au·Et₂O**. H-bonds between [Au(catdt)$_2$]$^-$ complexes in the 3D framework are illustrated by blue-dashed lines.

(a)

o → a
↘ b
↓ c

large void
(ca. 372 Å³)

tubular channel

(b)

Et₂O

Et₂O

b
↘ a
o → c

[Au(catdt)]⁻-Et₂O H-bonds: $d_{O⋯O}$ = 2.695(5) Å

(c)

b
a
o → c

C–H⋯C(π): $d_{H⋯C}$ = 2.70~2.90 Å

C–H⋯S: $d_{H⋯S}$ = 2.81~2.96 Å
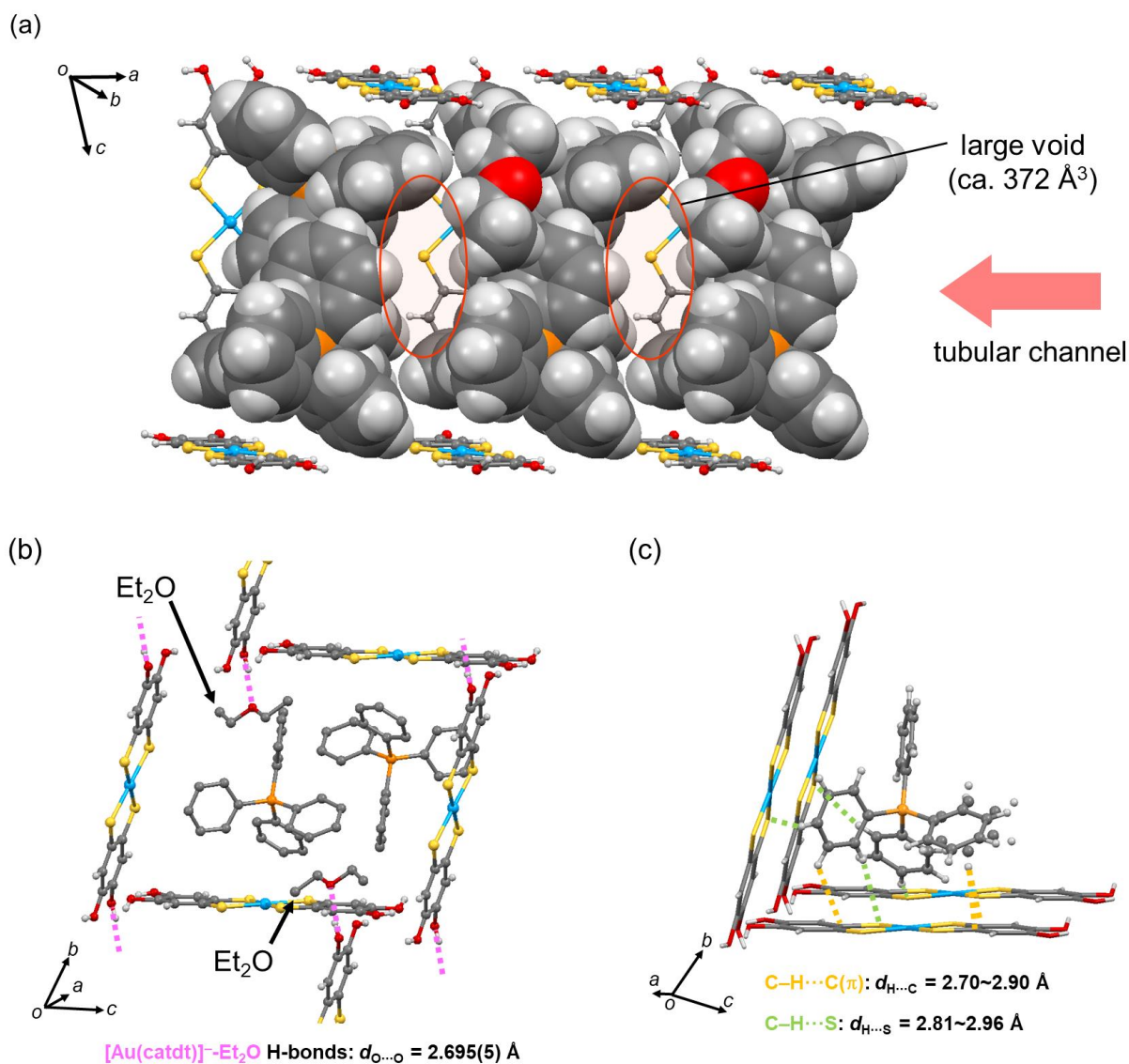
**Fig. 2-11** (a) Voids formed between $Ph_4P^+$ and $Et_2O$ molecules in the 1D channel. The volume of each void was calculated to be about 370 Å³ by the Platon/SQUEEZE program[28–30]. According to the crystal structure data, there should be solvent molecules in these voids; however, they are highly disordered and not to be determined. Thus their electron densities were removed by the Platon/SQUEEZE program. (b) Intermolecular H-bonds between $[Au(catdt)_2]^-$ complex and $Et_2O$ in the tubular channel of the framework. Hydrogen atoms on $Ph_4P^+$ and $Et_2O$ molecules are omitted in (b) and a disordered phenyl group is omitted in (a) and (b) for clarify. (c) Intermolecular short contacts between $[Au(catdt)_2]^-$ complexes (framework-bone) and $Ph_4P^+$.

### 2.4.3 (Ph4P)[Au(catdt)2]·2THF: 2D layer structure

In contrast to **3-Au·0.5H2O** (Fig. 2-6 and 2-7) and **3-Au·Et2O** (Fig. 2-9 and 2-10), the THF-containing salt **3-Au·2THF** has a layered structure based on 2D layers composed of $[Au(catdt)_2]^-$ complexes (Fig. 2-12 and 2-13, Table 2-1). In the 2D layer (Fig. 2-12 and 2-13a), the $[Au(catdt)_2]^-$ complexes are connected by intermolecular O–H···O H-bonds (blue dashed lines in Fig. 2-13a, $d_{O···O} = 2.707(4)$ Å) and lateral S···S contacts (green dashed lines in Fig. 2-13a, $d_{S···S} = 3.407(1)$ Å). The $Ph_4P^+$ cations and THF molecules are sandwiched by the 2D layers (Fig. 2-12), where cation-anion ($Ph_4P^+$-$[Au(catdt)_2]^-$) short contacts (Fig. 2-14), solvent-anion (THF-$[Au(catdt)_2]^-$) H-bonds (Fig. 2-13b, c, $d_{O···O} = 2.842(6)$ Å), and solvent-solvent (THF-THF) H-bonds (light blue dashed lines in Fig. 2-13b, c, $d_{H···O} = 2.46, 2.47$ Å) are formed. The former two kinds of interactions are found in **3-Au·0.5H2O** (Fig. 2-6 and 2-7) and **3-Au·Et2O** (Fig. 2-9 and 2-10). However, the latter one is only seen in this salt **3-Au·2THF**, which actually leads to the layered structure. The THF-THF H-bonds are combined with the THF-$[Au(catdt)_2]^-$ H-bonds, resulting in the connection of the catechol OH groups of $[Au(catdt)_2]^-$ complexes in neighboring 2D layers through two THF molecules (Fig. 2-13b, c). Here, as shown in Fig. 2-13c, the THF-THF H-bonds are caused by a positional disorder of the THF molecules (site occupancy factors of 0.62:0.38); namely, due to the disorder, the THF molecules can form a head-to-tail arrangement with the intermolecular C–H···O H-bonds. Those THF-mediated H-bonds prevent the formation of direct H-bonds between $[Au(catdt)_2]^-$ complexes, and consequently the formation of a 3D framework based on $[Au(catdt)_2]^-$ complexes. Thus, the author finally compares the structures of these three kinds of salts and discusses the role and effect of the crystal solvent molecules on forming these 3D and 2D molecular architectures based on $[Au(catdt)_2]^-$ complexes.
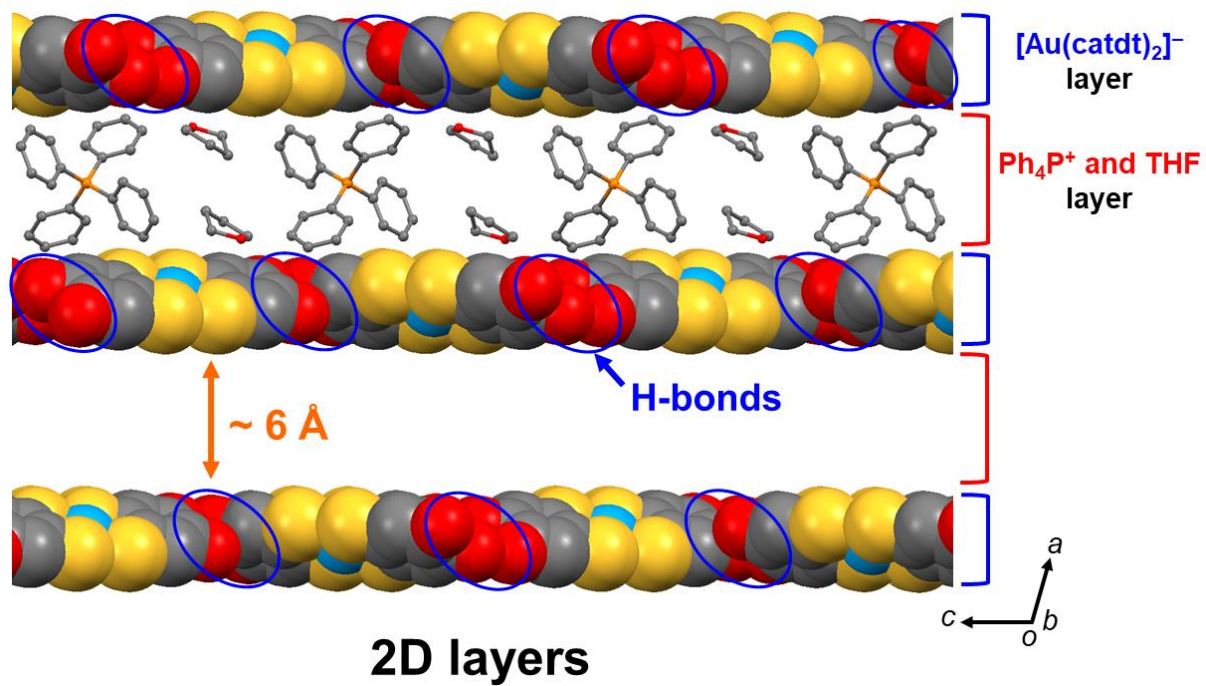
**Fig. 2-12** Overview of the layered structure of the anion salt **3-Au·2THF**. Blue circles show H-bonded parts.

(a)

b
a    c
O

**S···S contact**
$d_{S···S}$ = 3.407(1) Å

**[Au(catdt)]⁻-[Au(catdt)]⁻ H-bonds**
$d_{O···O}$ = 2.707(4) Å

(b)

**Ph₄P⁺ and THF layer**

**[Au(catdt)₂]⁻ layer**

b
a    O
c

THF

**THF-THF H-bonds (C–H···O)**

**[Au(catdt)]⁻-THF H-bonds**
$d_{O···O}$ = 2.842(6) Å

(c)

**major (62%)**

**THF-THF H-bonds (C–H···O)**
$d_{H···O}$ = 2.46, 2.47 Å

**minor (38%)**

b    c
a
O
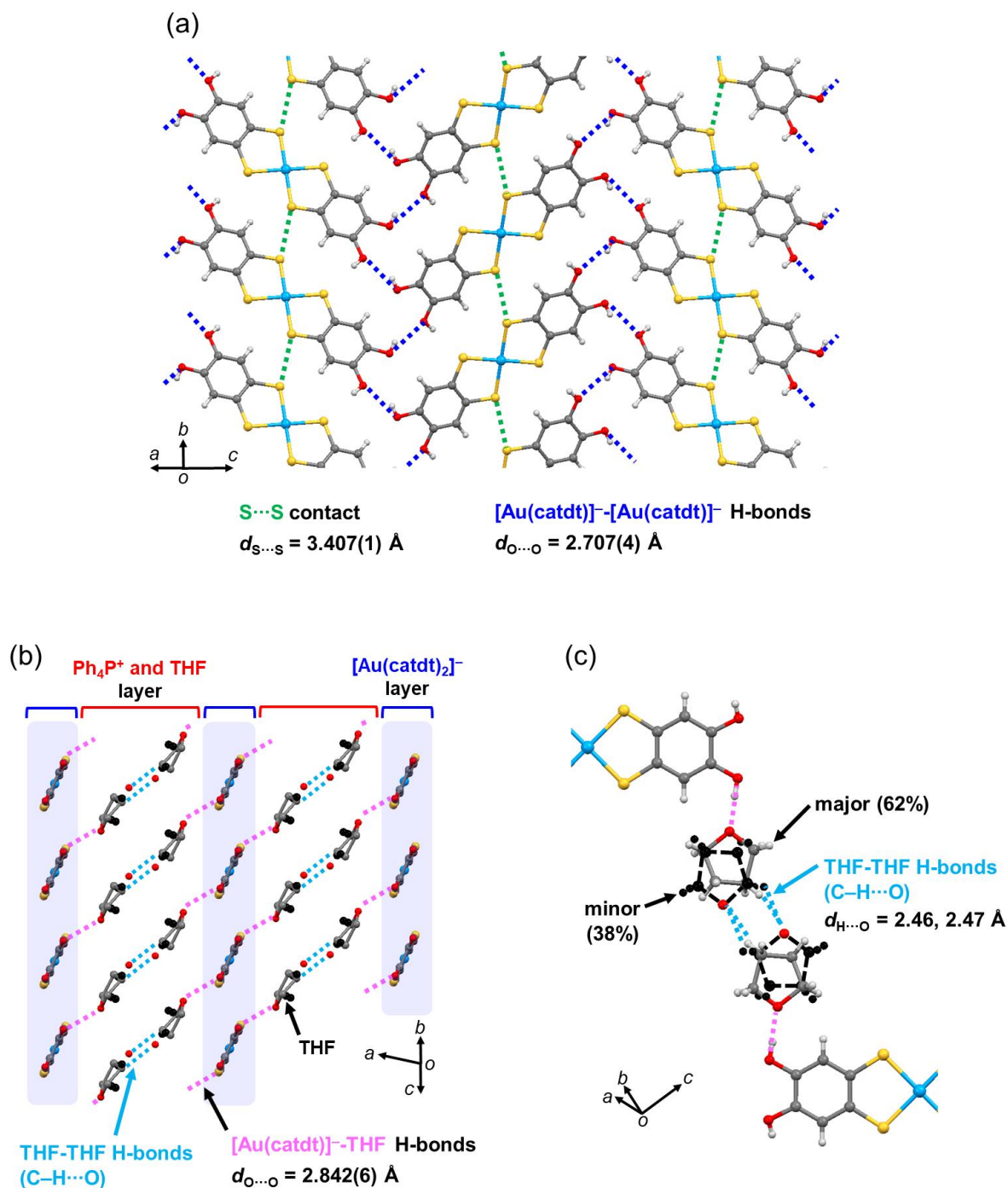
**Fig. 2-13** Crystal structure and intermolecular interactions of the anion salt **3-Au·2THF**. (a) 2D layer structure composed of [Au(catdt)₂]⁻ complexes, (b) 2D layers bridged by solvent-solvent (THF-THF) H-bonds and (c) intermolecular interactions between the THF molecules having a positional disorder in two positions with site occupancy factors of 0.62:0.38 (atoms of the minor THF molecule without oxygen atoms are described in black). Hydrogen atoms are omitted in (b) for clarify.
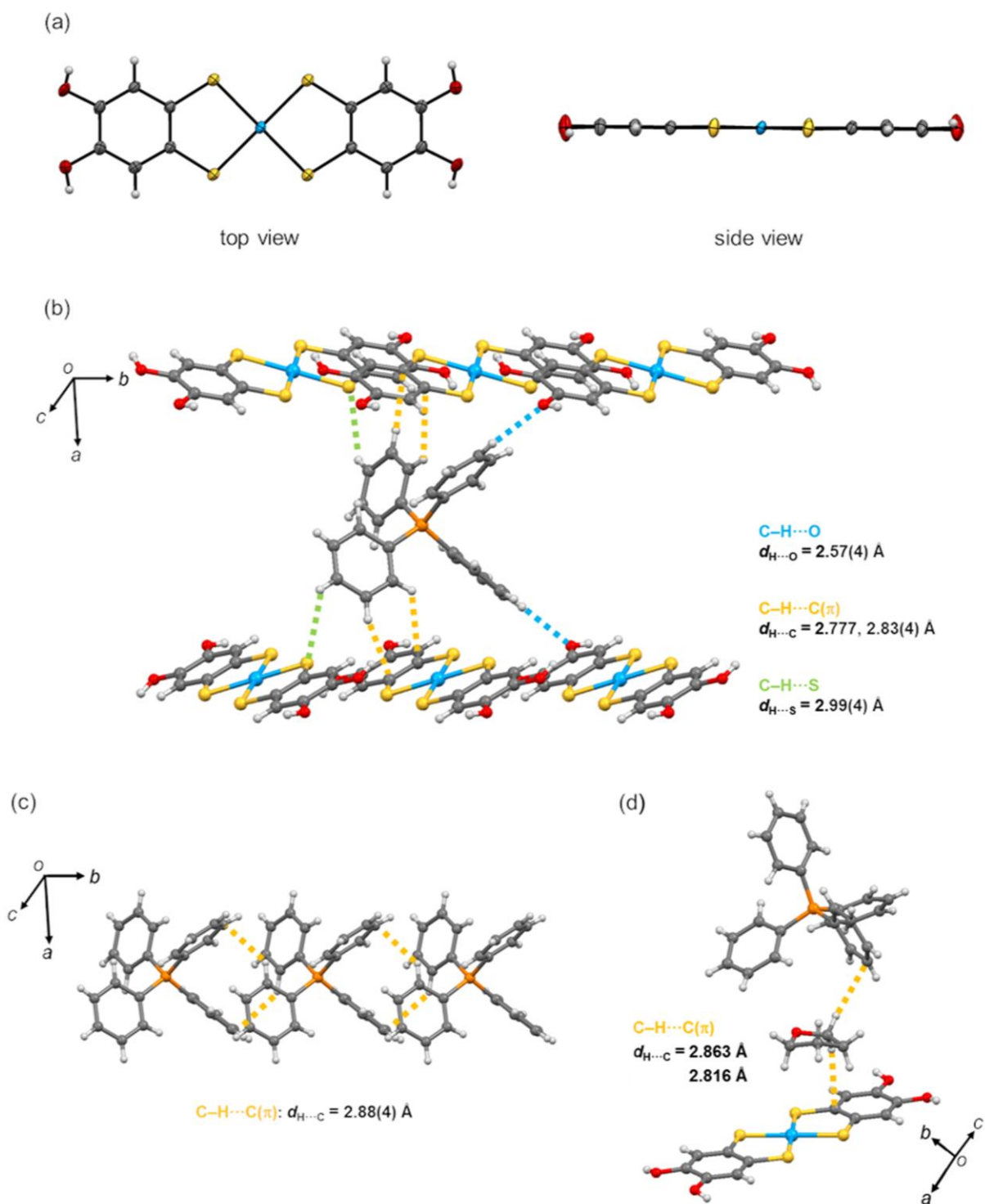
**Fig. 2-14** (a) ORTEP drawings of [Au(catdt)$_2$]$^-$ complex in **3-Au·2THF**; top view (left), side view (right). The thermal ellipsoids are scaled to the 50% probability level. (b) Intermolecular short contacts between [Au(catdt)$_2$]$^-$ complex and Ph$_4$P$^+$ molecules. (c) Intermolecular short contacts between Ph$_4$P$^+$ cations. (d) Intermolecular short contacts between THF and [Au(catdt)$_2$]$^-$ complex and between THF and Ph$_4$P$^+$ molecules.

## 2.5 Role of the crystal solvents on intermolecular interactions and crystal structures

In this section, the author first compares the structures of three kinds of new $[Au(catdt)_2]^-$-based salts, $(Ph_4P)[Au(catdt)_2] \cdot 0.5H_2O$, **3-Au·0.5H₂O**, $(Ph_4P)[Au(catdt)_2] \cdot Et_2O \cdot n(solv)$ (solv = acetone and/or $Et_2O$), **3-Au·Et₂O**, and $(Ph_4P)[Au(catdt)_2] \cdot 2THF$, **3-Au·2THF**. All of them are 1:1 salts of $Ph_4P^+$ and $[Au(catdt)_2]^-$; however, their crystal structures are dramatically different from each other, depending on the solvent molecules included in the crystal. The most notable difference is the dimensionality of the assembled structures of $[Au(catdt)_2]^-$ complexes; namely, in the water- and ether-containing salts **3-Au·0.5H₂O** and **3-Au·Et₂O**, this planar anionic complex forms a 3D assembled structure (i.e., 3D framework, Fig. 2-6 and 2-9). In contrast, in the THF-containing salt **3-Au·2THF**, it forms not a 3D but a 2D structure (i.e., 2D layers, Fig. 2-12). Furthermore, although both the 3D framework structures in **3-Au·0.5H₂O** and **3-Au·Et₂O** have tubular channels with a similar size, their walls' structures are significantly different from each other. The walls in **3-Au·0.5H₂O** are densely packed with $[Au(catdt)_2]^-$ complex, whereas those in **3-Au·Et₂O** are loosely packed to form voids, into which the cation and $Et_2O$ molecules partially penetrate (Fig. 2-9b). These differences should be caused by changing the intermolecular interactions between the component molecules upon the crystal solvent change.

Therefore, the author finally discusses how the crystal solvent makes differences in the intermolecular interactions and assembled structures. Here, the author focuses on the H-bonding ability, size, and shape of the crystal solvents. $Et_2O$, included in the 3D system **3-Au·Et₂O**, and THF, included in the 2D system **3-Au·2THF**, have a proton-accepting ability due to the ether oxygen atom, which allows them to form the H-bonds with the catechol O–H protons of $[Au(catdt)_2]^-$ complexes (Fig. 2-13b and c (pink lines)). On the other hand, the overall shapes of these solvent molecules are significantly different from each other (rod-shaped ($Et_2O$) *vs*. disk-shaped (THF)), which should contribute to the tremendous structural difference

64

in **3-Au·Et₂O** and **3-Au·2THF** (i.e., 3D *vs.* 2D; Fig. 2-9a and 2-12). Namely, due to the disk shape, the THF molecules are positionally disordered, which leads to the formation of the THF-THF H-bonds (Fig. 2-13c (light blue lines)) and consequently the 2D layered structure (Fig. 2-12 and 2-13b). In contrast, the rod-shaped Et₂O molecules have no such structural disorder and additional intermolecular interactions, and thus they seem to occupy the space between the large $Ph_4P^+$ molecule and $[Au(catdt)_2]^-$ complexes without interrupting the intermolecular interactions between the $Ph_4P^+$ molecule and $[Au(catdt)_2]^-$ complex for constructing the 3D framework (Fig. 2-9a, b). Meanwhile, due to the steric bulkiness of the ethyl groups in Et₂O, the walls of the 3D framework have voids (Fig. 2-9b and 2-10). In contrast, the water-containing 3D system **3-Au·0.5H₂O** has no such voids, and thus the wall is densely packed with the lateral S⋯S interactions between $[Au(catdt)_2]^-$ complexes (Fig. 2-6b and 2-7a). This is probably because the solvent water molecules are involved in the wall structure (Fig. 2-7a, b), which should eliminate the above-mentioned steric hindrance effect from the solvent molecules. Here, the water molecule has both proton-donating and –accepting abilities, in contrast to Et₂O and THF having the only proton-accepting ability. In addition, the size of the water molecule is much smaller than that of the others. These features should allow the water molecules to exist between the catechol moieties of $[Au(catdt)_2]^-$ complexes and participate in the densely packed wall structure of the 3D framework. Therefore, the author has successfully illustrated the role and effect of the crystal solvent molecules on constructing these new 3D anionic molecular frameworks based on $[Au(catdt)_2]^-$ complexes in terms of the molecular size and shape and H-bonding abilities.

## 2.6 Conclusion

In conclusion, on the basis of the synthesis of an anionic gold dithiolene complex $[Au(catdt)_2]^-$ with four hydroxy groups, the author has successfully constructed the first 3D molecular frameworks based on H-bonded metal dithiolene complexes. The key for constructing the 3D frameworks (observed in anion salts **3-Au·0.5H₂O** and **3-Au·Et₂O**) are (i) connecting the planar $[Au(catdt)_2]^-$ complexes with 3D intermolecular H-bonds and (ii) introducing large $Ph_4P^+$ cations into the channels. Interestingly, the former is highly influenced by the solvent molecules included in the crystals (especially, the molecular size and shape and H-bonding abilities), which leads to variations in the assembled structure of the $[Au(catdt)_2]^-$ complexes: namely, a 3D framework with densely packed walls in water-containing **3-Au·0.5H₂O**, a 3D framework with loosely packed walls in ether-containing **3-Au·Et₂O**, and a 2D layered structure in THF-containing **3-Au·2THF**. The variety of the characteristic framework realized in this study, and insight into the role of the crystal solvent on the H-bonding structure are important for developing electronic functionalities related closely to the molecular arrangements.[38]

In this chapter, the author realized peculiar 3D H-bonded molecular assemblies composed of metal dithiolene complex based on the modulation of [O–H···O] H-bonds with hydroxy groups and crystal solvent molecules. These findings indicate that the metal catecholdithiolene complexes are a good building block for constructing H-bonded molecular frameworks with d/π-electrons, leading to the basis for the playground for electron–proton coupled functionalities in the crystal.
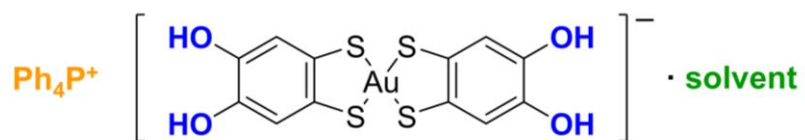
metal dithiolene complex
with hydrogen-bonding ability
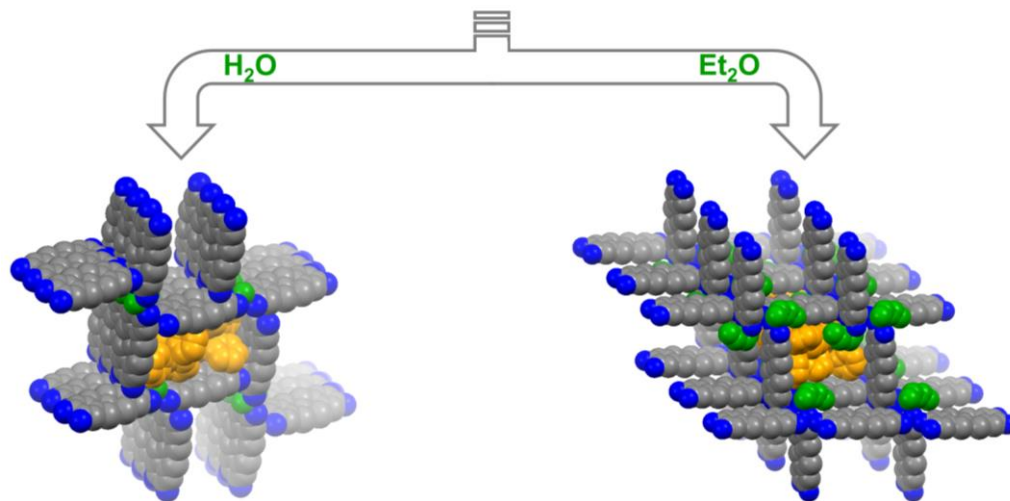
3D anionic frameworks based on H-bonds

## 2.7 Reference

1  L. R. MacGillivray, C. M. Lukehart, Metal-Organic Framework Materials; John Wiley & Sons, New York, 2014.

2  X. Feng, X. Ding and D. Jiang, *Chem. Soc. Rev.* 2012, **41**, 6010.

3  S.-Y. Ding and W. Wang, *Chem. Soc. Rev.* 2013, **42**, 548.

4  C. S. Diercks and O. M. Yaghi, *Science*, 2017, **355**, 923.

5  J.Y. Lee, O. K. Farha, J. Roberts, K. A. Scheidt, S.B. T. Nguyen and J. T. Hupp, *Chem. Soc. Rev.*, 2009, **38**, 1450.

6  J.-R. Li, R. J. Kuppler and H.-C. Zhou, *Chem. Soc. Rev.*, 2009, **38**, 1477.

7  S. Horike, S. Shimomura and S. Kitagawa, *Nat. Chem.*, 2009, **1**, 695.

8  S. S. Park, E. R. Hontz, L. Sun, C. H. Hendon, A. Walsh, T. V. Voorhis and M. Dincă, *J. Am. Chem. Soc.*, 2015, **137**, 1774.

9  J.-Z. Gu, X.-X. Liang, Y.-H. Cui, J. Wu, Z.-F. Shi and A. M. Kirillov, *CrystEngComm*, 2017, **19**, 2570.

10 H. Jiang, X.-C. Liu, Y. Wu, Y. Shu, X. Gong, F.-S. Ke and H. Deng, *Angew. Chem. Int. Ed.*, 2018, **57**, 3916.

11 N. Huang, X. Chen, R. Krishna and D. Jiang, *Angew. Chem. Int. Ed.*, 2015, **54**, 2986.

12 Z. Li, Y. Zhang, H. Xia, Y. Mu and X. Liu, *Chem. Commun.*, 2016, **52**, 6613.

13 N. Huang, L. Zhai, D. E. Coupry, M. A. Addicoat, K. Okushita, K. Nishimura, T. Heine and D. Liang, *Nat. Commun.*, 2016, **7**, 12325.

14 S. Lu, Y. Hu, S. Wan, R. McCaffrey, Y. Jin, H. Gu and W. Zhang, *J. Am .Chem. Soc.*, 2017, **139**, 17082.

15 H. S. Sasmal, H. B. Aiyappa, S. N. Bhange, S. Karak, A. Halder S. Kurungot and R. Banerjee, *Angew. Chem. Int. Ed.*, 2018, **57**, 10894.

16 Y.-F. Han, Y.-X. Yuan and H.-B. Wang, *Molecuels*, 2017, **22**, 266.

17  H. Wang, B. Li, H. Wu, T.-L. Hu, Z. Yao, W. Zhou, S. Xiang and B. Chen, *J. Am. Chem. Soc.*, 2015, **137**, 9963.

18  A. Karmakar, R. Illathvalappil, B. Anoyhumakkool, A. Sen, P. Samanta, A. V. Desai, S. Kurungot and S. K. Ghosh, *Angew. Chem. Int. Ed.*, 2016, **55**, 10667.

19  I. Hisaki, N. Q. Emilya Affendy and N. Tohnai, *CrystEngComm*, 2017, **19**, 4892.

20  D. V. Horváth, T. Holczbauer, L. Bereczki, R. Palkó, N. V. May, T. Soós and P. Bombicz, *CrystEngComm*, 2018, **20**, 1779.

21  N. Malek, T. Maris, M. Simard and J. D. Wuest, *J. Am. Chem. Soc.*, 2005, **127**, 5910.

22  A. Karmakar, A. V. Desai and S. K. Ghosh, *Coord. Chem. Rev.*, 2016, **307**, 313.

23  H. Chen, H. Tu, C. Hu, Y. Liu, D. Dong, Y. Sun, Y. Dai, S. Wang, H. Qian, Z. Lin and L. Chen, *J. Am. Chem. Soc.*, 2018, **140**, 896.

24  E. I. Stiefel and K. D. Karlin, *Progress in Inorganic Chemistry, Dithiolene Chemistry: Synthesis, Properties, and Applications*, Wiley-Interscience, New York, 2003.

25  S. Takaishi, M. Hosada, T. Kajiwara, H. Miyasaka, M. Yamashita, Y. Nakanishi, Y. Kitagawa, K. Yamaguchi, A. Kobayashi and H. Kitagawa, *Inorg. Chem.*, 2009, **48**, 9048.

26  Y. Kobayashi, B. Jacobs, M. D. Allendorf and J. R. Long, *Chem. Mater.*, 2010, **22**, 4120.

27  D. Coucouvanis, A. R. Paital, Q. Zhang, N. Lehnert, R. Ahlrichs, K. Fink, D. Fenske, A. K. Powell and Y. Lan, *Inorg. Chem.*, 2009, **48**, 8830.

28  P. v. d. Sluis and A. L. Spek, Acta Crystallogr., Sect. A: Found. Crystallogr., 1990, **46**, 194.

29  A. L. Spek, Acta Crystallogr., Sect. D: Biol. Crystallogr., 2009, **65**, 148

30  A. L. Spek, Acta Crystallogr. Sect. C, 2015, **71**, 9.

31  Gaussian 09, revision C.01, M. J. Frisch, et al. Gaussian, Inc., Wallingford, CT, **2010**.

32  A. Bondi, *J. Phys. Chem.,* 1964, **68**, 441.

33  N. C. Schiødt, P. Sommer-Larsen, T. Bjørnholm, M. F. Nielsen, J. Larsen and K. Bechgaard, *Inorg. Chem.*, 1995, **34**, 3688.

34 M. Murata, S. Kaji, H. Nishimura, A. Wakamiya and Y. Murata, *Eur. J. Inorg. Chem.*, 2016, 3228.

35 The C–S distances ($d_{C-S}$) are sensitive to the valence of this type of metal-dithiolene complexes. For example, the monoanionic [Au(bdt)$_2$]$^-$ species has the $d_{C-S}$ values of 1.76~1.77 Å, although the neutral [Au(bdt)$_2$] species has those of 1.73~1.74 Å, see: K. Ray, T. Weyhermuller, A. Goossens, M. W. J. Crajé and K. Wieghardt, *Inorg. Chem.*, 2003, **42**, 4082.

36 D. M. de Leew, M. M. J. Simenon, A. R. Brown and R. E. F. Einerhand, *Synth. Met.*, 1997, **87**, 53.

37 H. Meng, J. Zheng, A. J. Lovinger, B.-C. Wang, P. G. V. Patten and Z. Bao, *Chem. Mater.*, 2003, **15**, 1778.

38 S. Yokomori, A. Ueda, T. Higashino, R. Kumai, Y.Murakami, and H. Mori, *CrystEngComm*, 2019, **21**, 2940.

# Chapter 3

# Magnetic property change with PCET of metal dithiolene complex and the effect of deprotonation on d/π-electronic states

## 3.1 Introduction

Electrostatic and dynamic properties of protons with a positive charge can modulate the electronic states of molecular crystals through inter-molecular H-bonds. Proton-coupled electron transfer (PCET) is one of the important electron–proton coupled phenomena for the realization of novel electronic functionalities as introduced in Section 1.3 .[1] Generally, PCET is observed in solution states; however, observation of PCET in solid states is rare, which, in the limited cases, leads to switching of electronic functionalities.[2–9] For example, in single-component organic conductors based on catechol-fused tetrathiafulvalene (Cat-TTF) having anionic $[O \cdots H(D) \cdots O]^-$ H-bond, unique electronic functionalities and phenomena coupled with proton or deuteron dynamics have been realized, such as quantum spin liquid state associated with a quantum fluctuation of protons[10] and switching of magnetism and electrical conductivity[6]. In this crystal, the formation of such "anionic H-bonds" (i.e., single-well or low-barrier H-bonds) between functional molecules is the key to realize the electron–proton coupled functionalities in solid state. As seen in the above example, the electronic functionality switching driven by proton transfer is so attractive from the viewpoint of the development of novel functionalities and basic science; however, the materials showing such functionalities in solid state have been very limited.

As introduced in Chapter 1, the metal dithiolene complexes exhibit many electronic functionalities in solid states (magnetic/optical properties and electrical conductivity)[11–16]. In

particular, their multiple redox activity is advantageous for modulation of their electronic state with proton transfer. However, the metal dithiolene complexes studied about PCET have been limited to a few examples even in solution states[17–22], and not reported in solid states. Thus, there should be much room for the developments of unique physical properties and novel phenomena coupled with d/π electrons and proton, i.e., based on PCET.

In this chapter, by taking the advantages of metal catecholdithiolene complexes revealed in Chapter 2 (intermolecular H-bond formation and variety of assembled structures) and exchanging the metal center from gold to nickel,[23,24] the author aimed to develop the H-bonded metal-dithiolene-based crystals with functionalities based on d/π electron and proton. The previous reports have shown the existence of PCET of the nickel complex in solution states; however, the resultant crystals have no intermolecular H-bonds between the complexes due to extra Ph$_4$PBr or complete deprotonation of the catechol moieties (i.e., *o*-benzoquinondithiolene complex).[23] Here, the author successfully synthesized new crystals consisting of the nickel complexes having anionic [O–H⋯O] H-bonds, which are suggested to be low-barrier H-bonds, by deprotonation of the hydroxy group. Importantly, electron spin resonance (ESR) measurements indicated that the magnetic properties were changed from paramagnetic to non-magnetic with the oxidation of the nickel complexes through PCET in the solution processes. Furthermore, from the DFT calculation, the d/π electronic states of the nickel complex in each crystal are significantly modulated by the deprotonation and oxidation.
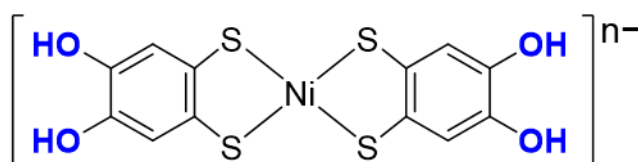


**Fig. 3-1** Chemical structure of the nickel catecholdothiolate complex, [Ni(catdt)$_2$]$^{n-}$.

## 3.2 Experimental

**Materials and methods**

Commercially available chemicals were used without further purification. The chemicals used here are listed below. Tetrahydrofuran and *N,N*-dimethylformamide (Guaranteed reagent, FUJIFILM Wako Pure Chemical lndustries Ltd.); hexane, diethyl ether, acetic acid, and methanol (super dehydrated grade, FUJIFILM Wako Pure Chemical Co., Ltd.); tetraphenylphosphonium bromide (Tokyo Chemical Industry Co., Ltd.); $Ni(OAc)_2 \cdot 4H_2O$ (Guaranteed reagent, Kanto Chemical Co., inc.).

$^1$H NMR (300 MHz) spectra measurements were carried out with a JEOL JNM-AL300 spectrometer with DMSO-$d_6$ as a solvent and $Me_4Si$ as the internal standard.

**Synthesis and crystal preparation**

The crystals of nickel catecholdithiolene complex, $(Ph_4P)_3[Ni-H_4(catdt)_2]Br_2$, **2-Ni**, was synthesized according to the literature,[23] as blown plate crystals. Then, the compound **2-Ni** was stirred at room temperature overnight under an argon atmosphere in a mixture of MeOH (4 mL) and $H_2O$ (20 mL). The resulting green powder was filtered and washed with $H_2O$. This powder was recrystallized from DMSO/$H_2O$ under argon atmosphere for several days to obtain green crystals of a DMSO-containing crystal and two $H_2O$-containing crystals with a large portion of amorphous solid: $(Ph_4P)[Ni-H_4(catdt)_2] \cdot DMSO$, **3-Ni-4H·DMSO** (dark green block), $(Ph_4P)[Ni-H_3(catdt)_2] \cdot 0.5H_2O$, **3-Ni-3H·0.5H₂O** (dark green needle), and $(Ph_4P)_2[Ni-H_2(catdt)_2] \cdot 2H_2O$, **3-Ni-2H·H₂O** (brown plate). The crystals of **3-Ni-4H·DMSO** were also obtained by recrystallization of the compound **2-Ni** from DMSO/$H_2O$ without a lot of amorphous. These **3-Ni-4H·DMSO** crystals were used for the magnetic susceptibility measurements. On the other hand, recrystallization of the green powder from THF/AcOH/hexane (ca. 10:1:30, AcOH = acetic acid) under argon atmosphere for several days gives THF-containing crystal, $(Ph_4P)[Ni-H_3(catdt)_2] \cdot 0.5THF$, **3-Ni-3H·0.5THF**, as dark green

block crystal without a lot of amorphous. All the obtained materials contained good single crystals suitable for X-ray analysis, and only **3-Ni-4H·DMSO** was obtained in mg order.
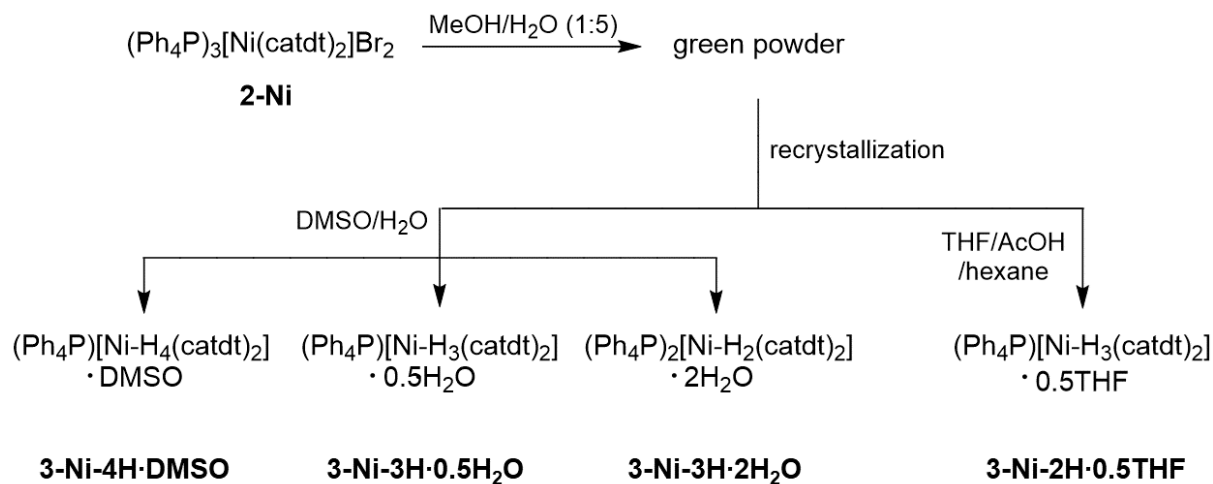


**Scheme. 3-1** Synthesis of $(Ph_4P)[Ni-H_4(catdt)_2]\cdot DMSO$, **3-Ni-4H·DMSO**, $(Ph_4P)[Ni-H_3(catdt)_2]\cdot 0.5H_2O$, **3-Ni-3H·0.5H$_2$O**, $(Ph_4P)_2[Ni-H_2(catdt)_2]\cdot 2H_2O$, **3-Ni-2H·2H$_2$O**, and $(Ph_4P)[Ni-H_3(catdt)_2]\cdot 0.5THF$, **3-Ni-3H·0.5THF**, through $(Ph_4P)_3[Ni-H_4(catdt)_2]Br_2$.

**Single crystal X-ray structure analysis**

X-ray diffraction (XRD) measurements for **3-Ni-4H·DMSO** and **3-Ni-3H·0.5H$_2$O** were performed on a Rigaku MercuryII CCD X-ray diffractometer (Mo $K\alpha$, $\lambda = 0.71073$ Å), and those for **3-Ni-2H·H$_2$O** were carried out on a Rigaku imaging plate system (synchrotron, $\lambda = 0.99968$ Å) at the BL-8A in the Photon Factory (PF), the High Energy Accelerator Research Organization (KEK), Japan. The initial structures were solved by direct methods (SHELXT version 2018/2) and refined with a full-matrix least-squares technique (SHELXL version 2018/3) using Olex2-1.3 (OlexSys).[25] Anisotropic thermal parameters were applied to all atoms without hydrogen atoms. The position of hydrogen atoms on hydroxy groups was refined, and the other hydrogen atoms were generated geometrically (C–H = 0.950 Å).

## Magnetic susceptibility measurements

The magnetic susceptibility measurement of a polycrystalline **3-Ni-4H·DMSO** was performed on a Quantum Design SQUID magnetometer MPMS-XL in the temperature range of 2−300 K at the static magnetic field of 10000 Oe. The magnetic susceptibility was corrected with the blank data of the aluminum foil obtained separately. According to the literature, the diamagnetic contribution of the compound was estimated to be $-4.75 \times 10^{-4}$ emu/mol from Pascal constants.[26] The magnetic susceptibility of the compound was estimated from the difference between that of the compound without the blank and the temperature-independent diamagnetic contribution. The temperature dependence of the susceptibility was fitted by using the Curie-Weiss law, where the $\chi$, $C$, $T$, and $T_c$ are magnetic susceptibility, Curie constant, absolute temperature, and Curie temperature, respectively.

$$\chi = \frac{C}{T - T_c}$$

Also, the $g$ value was calculated from the result of the fitting by using the Curie constant.

## Electron spin resonance (ESR) measurements

The X-band continuous wave ESR measurements were carried out using a Bruker EMXmicro spectrometer (9.435300–9.435596 GHz) at room temperature under air. Single crystals of **3-Ni-4H·DMSO**, **3-Ni-3H·0.5THF**, **3-Ni-3H·0.5H₂O**, and **3-Ni-2H·2H₂O** attached to Teflon® tube in a quartz glass were used for the measurements. For **3-Ni-4H·DMSO**, the ESR signals were collected by rotating the crystal around the $a$-axis of the crystal (0°: magnetic field perpendicular to the $c$-axis, 90°:perpendicular to the $b$-axis). The ESR data were fitted by a differentiated Lorentz function, and the $g$ value was estimated based on the fitting according to the following formula, where $I_m$, $\Delta B_{pp}$, and $B_0$ show maximum intensity, peak-to-peak width, and resonance center, respectively.

$$I(B) = \frac{16I'\,_m(B_0-B)/(\Delta B_{pp}/2)}{\left[3+\left\{(B_0-B)/(\Delta B_{pp}/2)\right\}^2\right]^2}$$

**First-principles calculations**

All the DFT calculations were performed by the OpenMX software (Ver. 3.9) based on optimized localized basis functions and pseudopotentials (PPs). The basis functions used are H6.0-s2p1, C6.0-s2p2d1, O6.0-s2p2d1, S7.0-s2p2d1f1, and Ni6.0H-s3p2d1 for hydrogen, carbon, oxygen, sulfur, and nickel, respectively, wherein the abbreviation of basis functions such as C6.0-s2p2d1, C stands for the atomic symbol, 6.0 the cutoff radius (Bohr) in the generation by the confinement scheme, and s2p2d1 means the employment of two, two, and one optimized radial functions for the s-, p-, and d-orbitals, respectively. The radial functions were optimized by a variational optimization method.[27,28] As valence electrons in the PPs, the author included 1s for hydrogen, 2s and 2p for carbon and oxygen, 3s and 3p for sulfur, 3s, 3p, 3d, and 4s for Ni, respectively. All the PPs and pseudo-atomic orbitals the author used in this study were taken from the database (2019) in the OpenMX website, which was benchmarked by the delta gauge method.[29] Realspace grid techniques are used for the numerical integrations and the solution of the Poisson equation using FFT with the energy cutoff of 220 Ryd.[30] the author used a generalized gradient approximation (GGA) proposed by Perdew, Burke, and Ernzerhof to the exchange-correlation functional.[31] An electronic temperature of 300 K is used to count the number of electrons by the Fermi-Dirac function for all the systems the author considered. For the k-point sampling, the author used a regular mesh of 1×1×1.

Calculations of crystal orbitals were carried out based on the crystal structure obtained by single-crystal XRD measurements. In this calculation, the occupancy of disordered hydrogen atoms was assumed to be 1.00. For the calculations, totally three periodic hypothetical structures of **3-Ni-4H·DMSO**, **3-Ni-3H·0.5THF** and **3-Ni-2H·2H₂O** were used for these calculations, where both $Ph_4P^+$ cations and crystal solvents were removed for **3-Ni-4H·DMSO**

and **3-Ni-3H·0.5THF**, or only the Ph$_4$P$^+$ cations were removed for **3-Ni-2H·2H₂O**. Structural optimization was applied only H atoms on O atoms of below-mentioned anionic H-bond with short O···O distance in **3-Ni-3H·0.5THF**, and on O atoms of water molecules in **3-Ni-2H·2H₂O** because the positions of the H atoms could not be determined by X-ray structural analysis.

## 3.3 Crystal and molecular structures

The compositions and structures of the four crystals were determined by single-crystal X-ray structural analysis. The crystallographic data for all crystals of **3-Ni-4H·DMSO**, **3-Ni-3H ·0.5THF**, **3-Ni-3H·0.5H₂O** and **3-Ni-2H·2H₂O** is shown in Table 3-1.

**Table 3-1** The crystallographic data for the crystals of **3-Ni-4H·DMSO**, **3-Ni-3H·0.5THF**, **3-Ni-3H·0.5H₂O**, and **3-Ni-2H·2H₂O**.

| crystals | 3-Ni-4H· DMSO | 3-Ni-3H· 0.5H$_2$O | 3-Ni-3H· 0.5THF | 3-Ni-2H· 2H$_2$O |
|---|---|---|---|---|
| formula | C$_{38}$H$_{34}$NiO$_5$PS$_5$ | C$_{36}$H$_{29}$NiO$_5$PS$_4$ | C$_{38}$H$_{31}$NiO$_{4.5}$PS$_4$ | C$_{60}$H$_{46}$NiO$_6$P$_2$S$_4$ |
| formula weight | 820.66 | 759.51 | 777.55 | 1111.86 |
| crystal system | triclinic | monoclinic | triclinic | triclinic |
| space group | $P\overline{1}$ | $P2_1/c$ | $P\overline{1}$ | $P\overline{1}$ |
| $a$ (Å) | 10.188(2) | 7.1612(5) | 11.3377(2) | 13.9446(3) |
| $b$ (Å) | 13.333(3) | 16.3222(8) | 12.8849(2) | 12.5782(3) |
| $c$ (Å) | 13.7783) | 28.1125(15) | 13.4427(7) | 17.5902(7) |
| $\alpha$ (deg) | 92.947(3) | 90 | 80.666(1) | 70.3620(10) |
| $\beta$ (deg) | 99.616(4) | 90.563(5) | 69.189(1) | 76.0230(10) |
| $\gamma$ (deg) | 94.177(4) | 90 | 69.799(1) | 104.3310(10) |
| $V$ (Å$^3$) | 1836.5(8) | 3285.8(3) | 1720.99(10) | 2631.12(14) |
| $Z$ | 2 | 4 | 2 | 2 |
| $T$ (K) | 293 | 293 | 293 | 293 |
| $D_{calc}$ (g· cm$^{-3}$) | 1.484 | 1.535 | 1.502 | 1.403 |
| $\lambda$ (Å) | 0.71073 | 0.71073 | 0.71073 | 0.99968 |
| $R_{int}$ | 0.0218 | 0.0878 | 0.0163 | 0.0307 |
| $R_1$ ($I$>2.00σ($I$)) | 0.0478 | 0.0890 | 0.0368 | 0.0386 |
| $wR_2$ (All reflections) | 0.1361 | 0.1475 | 0.0981 | 0.1074 |
| GOF | 1.065 | 1.108 | 1.032 | 0.740 |

### 3.3.1 Non-deprotonated Ni complex crystal: 3-Ni-4H·DMSO

The crystal structure of the DMSO-containing crystal **3-Ni-4H·DMSO** is shown in Fig. 3-2. The asymmetric unit consisted of one $Ph_4P^+$ cation, two half nickel complex, and one molecule of DMSO (formula:$(Ph_4P)[Ni-H_4(catdt)_2]\cdot DMSO$); the nickel complex is deduced to be monoanionic. In this crystal, three-dimensional (3D) framework structure (Fig. 3-2b) based on the nickel complexes was constructed by 1D H-bonded zig-zag chains formed by multiple [O–H···O] H-bonds between the nickel complexes, and between the nickel complex and DMSO molecule (Fig. 3-3a and b). The nickel complexes in neighboring 1D H-bonded zig-zag chains form [O–H···C] and [O–H···O] weak H-bonds with the nickel complex and DMSO molecule, respectively, and also O···O short contacts between the hydroxy groups of the nickel complexes (Fig. 3-3b and c). The bulky counter cations, $Ph_4P^+$, are included in the voids around the skeleton of the 3D framework, which is considered to stabilize this framework structure with multiple short atomic contacts similar to the $[Au(catdt)_2]^-$ complex crystals shown in Chapter 2.[24] Due to the construction of the 3D framework encapsulating the bulky cations, there are no significant π-π interactions (SOMO-SOMO interaction) between the nickel complexes. As mentioned in Chapter 2, the construction of such 3D framework based on metal dithiolene complex have been limited to a few examples of the crystals consisting of gold complex analogue, $[Au(catdt)_2]^-$,[24] or metal iodothiazoledithiolene complexes, $[M(I\text{-}tzdt)_2]$ (M = Au and Ni)[32], and thus it is rare.

Focusing on the details of molecular structures of the nickel complex in this crystal, as mentioned above, the composition indicates that the nickel complex is monoanionic species. The C–O and C–S bond lengths are almost the same as those of the $[Au(catdt)_2]^-$ complex in Chapter 2 (Fig. 3-3d Table 2-2 and 3-2). Therefore, hydroxy groups of the nickel complex are not deprotonated. Judging from this fact and monoanionic state of the nickel complex, the complex in this crystal is in a paramagnetic state ($S = 1/2$).
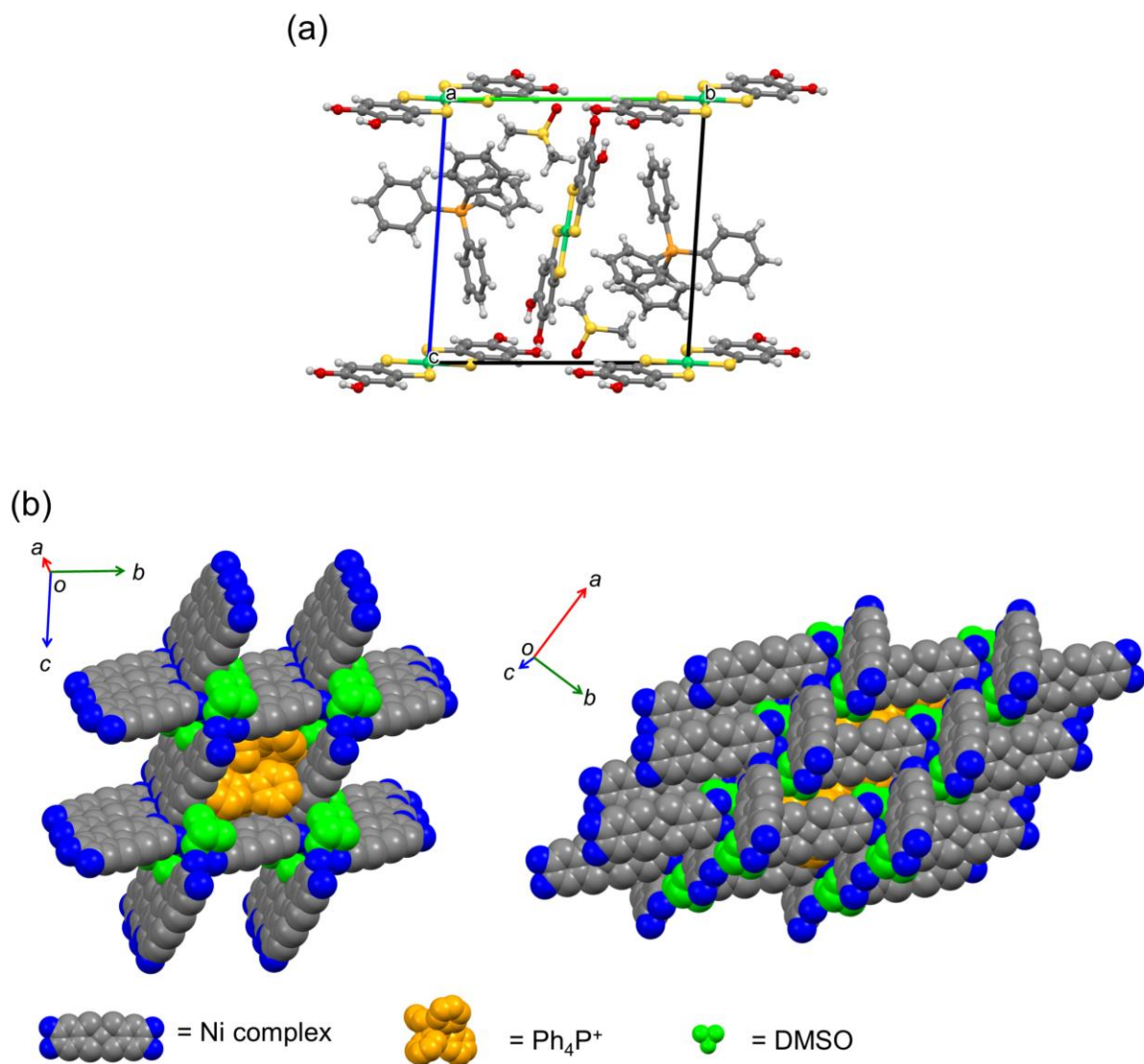
**Fig. 3-2** Structure of the DMSO-containing crystal **3-Ni-4H·DMSO**. (a) Unit cell and (b) overview of the 3D framework structure (left), and the top view of the framework (right). Light green = Ni, yellow = S, orange = P, gray = C, red = O, and white = H.
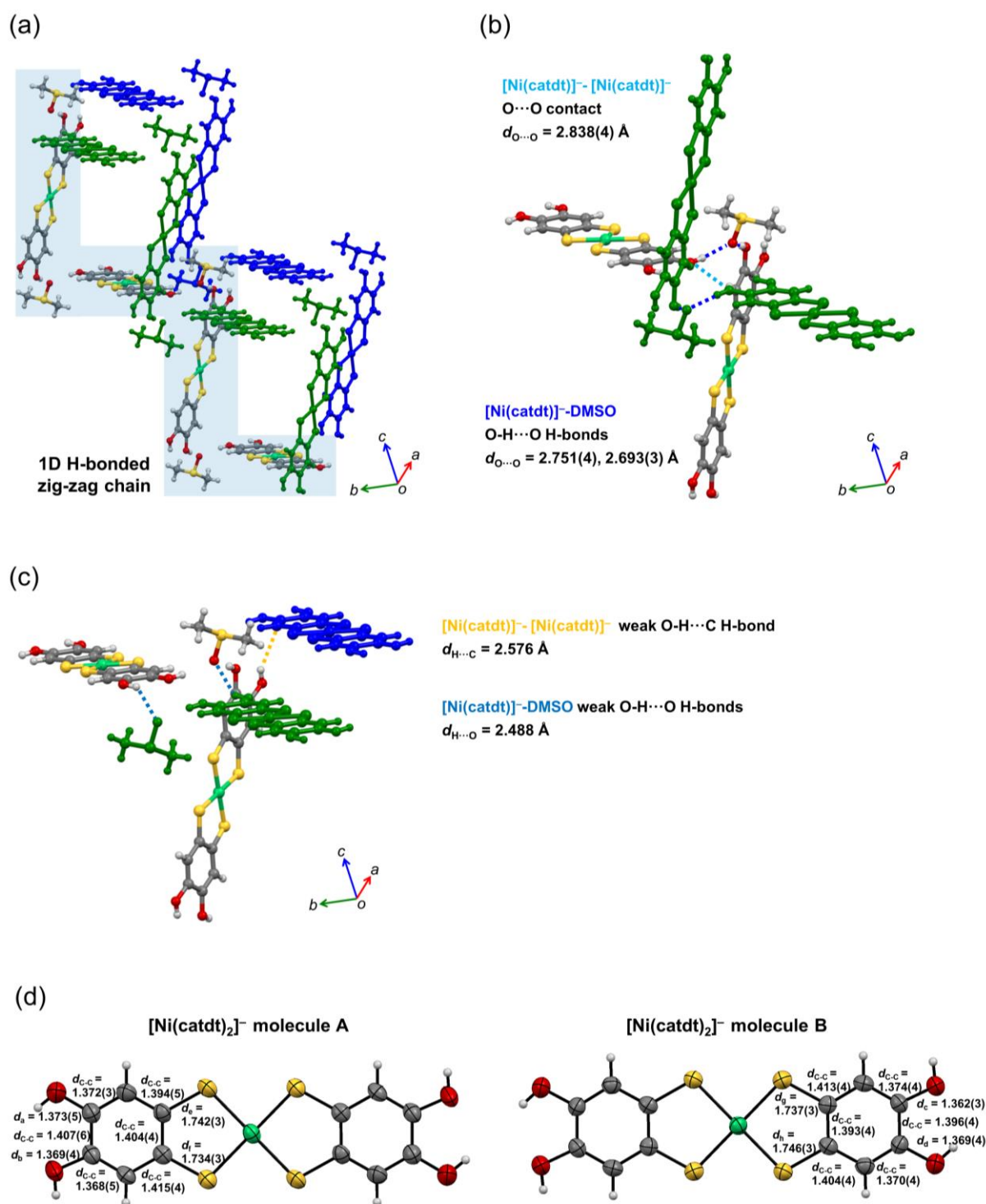
**Fig. 3-3** Details of the H-bonded structure and molecular structure in **3-Ni-4H·DMSO**. (a) The 1D H-bonded zig-zag chains in the 3D framework structure. Blue and green molecules belong to different 1D chains, respectively. (b) Intermolecular H-bond and O···O short contacts and (c) weak intermolecular H-bonds on a node of the framework structure. (d) The molecular structures and bond lengths of crystallographically half-independent nickel complexes.

**Table 3-2** The C–S and C–O bond lengths (in Å) of the nickel dithiolene complex of **3-Ni-4H·DMSO**, **3-Ni-3H·0.5H₂O**, **3-Ni-3H·0.5THF**, and **3-Ni-2H·2H₂O**.

| 3-Ni-4H·DMSO | | | | |
|---|---|---|---|---|
| C–O bonds | $d_a$ = 1.373(5) | $d_b$ = 1.369(4) | $d_c$ = 1.362(3) | $d_d$ = 1.369(4) |
| C–S bonds | $d_e$ = 1.742(3) | $d_f$ = 1.734(3) | $d_g$ = 1.737(3) | $d_h$ = 1.746(3) |

| 3-Ni-3H·0.5H₂O | | | | |
|---|---|---|---|---|
| C–O bonds | $d_a$ = 1.358(7) | $d_b$ = 1.373(7) | $d_c$ = 1.297(7) | $d_d$ = 1.347(7) |
| C–S bonds | $d_e$ = 1.732(5) | $d_f$ = 1.740(6) | $d_g$ = 1.725(6) | $d_h$ = 1.708(5) |

| 3-Ni-3H·0.5THF | | | | |
|---|---|---|---|---|
| C–O bonds | $d_a$ = 1.327(2) | $d_b$ = 1.357(3) | $d_c$ = 1.359(3) | $d_d$ = 1.323(2) |
| C–S bonds | $d_e$ = 1.736(2) | $d_f$ = 1.714(2) | $d_g$ = 1.727(2) | $d_h$ = 1.721(2) |

| 3-Ni-2H·2H₂O | | | | |
|---|---|---|---|---|
| C–O bonds | $d_a$ = 1.291(8) | $d_b$ = 1.30(1) | $d_c$ = 1.35(1) | $d_d$ = 1.364(9) |
| C–S bonds | $d_e$ = 1.763(7) | $d_f$ = 1.688(8) | $d_g$ = 1.781(7) | $d_h$ = 1.674(8) |

### 3.3.2 One-deprotonated Ni complex crystals: 3-Ni-3H·0.5H₂O and 3-Ni-3H·0.5THF

The crystal structure of **3-Ni-3H·0.5H₂O** was almost the same as that of the reported gold analog complex crystal, "**3-Au·0.5H₂O**" in Chapter 2;[24] the asymmetric unit consisted of one Ph₄P⁺ cation, one nickel complex, and a half water molecule (Fig. 3-4, formula: (Ph₄P)[Ni-H₃(catdt)₂]·0.5H₂O). Namely, the nickel complexes were three-dimensionally connected by multiple [O–H···O] H-bonds with the help of water molecules, to form a 3D framework (Fig. 3-5). However, the existence of the S···S short contacts and the molecular structure of the metal complexes were different from those in **3-Au·0.5H₂O** (Fig. 3-5a). The S···S short contacts were formed between the gold complexes in **3-Au·0.5H₂O**, whereas there is no S···S short contacts between the nickel complexes in **3-Ni-3H·0.5H₂O** (Fig. 3-5a). This loss of the short contact

would be because the dithiolene skeleton of the nickel complex is smaller than the benzene skeleton due to a decrease of the atomic radius from gold to nickel, as shown in Fig. 3-5b. On the other hand, although all the four C–O bond lengths of the gold complex in **3-Au·0.5H₂O** were almost the same, the C–O bond length of one hydroxy group of the nickel complex in **3-Ni-3H·0.5H₂O** was significantly short (Table 3-2 and Fig. 3-5d). Comparing the C–O bond lengths of the nickel complexes in non-deprotonated **3-Ni-4H·DMSO** with that of the nickel *o*-benzoquinonedithiolene complex,[23] and this crystal, one of four bond length (C–O bond $d_c$, in Fig. 3-5d) is the intermediate length between single-bonding C–O (~1.37 Å) and double-bonding C=O (~1.23 Å). This indicates that the hydroxy group of the nickel complex in this crystal is deprotonated, and the C–O bond has a double-bond character: semiquinone-like structure (Fig. 3-5d bottom). In addition, significantly short H-bonds (2.587(5) Å, C–O bond $d_c$, in Fig. 3-5c) and no proton acceptor around these hydroxy groups without itself strongly suggest the formation of anionic [O–H···O]⁻ H-bond between these hydroxy groups (Fig. 3-5c). Therefore, one-deprotonation occurs per one nickel complex in this crystal.

In general, anionic [O–H···O]⁻ H-bond is known to be a low-barrier H-bond, and thus it can be expected to transfer the protons with external stimuli, such as temperature changes. Hence, it may be possible to modulate electronic functionalities by proton dynamics in the H-bond with external-stimuli, like molecular crystals based on catechol-fused TTF.[6,8,9] On the other hand, considering the composition (monoanionic state) and the deprotonation, the nickel complex in this crystal should have been oxidized in solution processes (Section 3-2), suggesting that the nickel complex in this crystal was changed from a paramagnetic state ($S = 1/2$) to a non-magnetic state ($S = 0$). The electronic states of the nickel complex are discussed in Section 3.4 in detail.
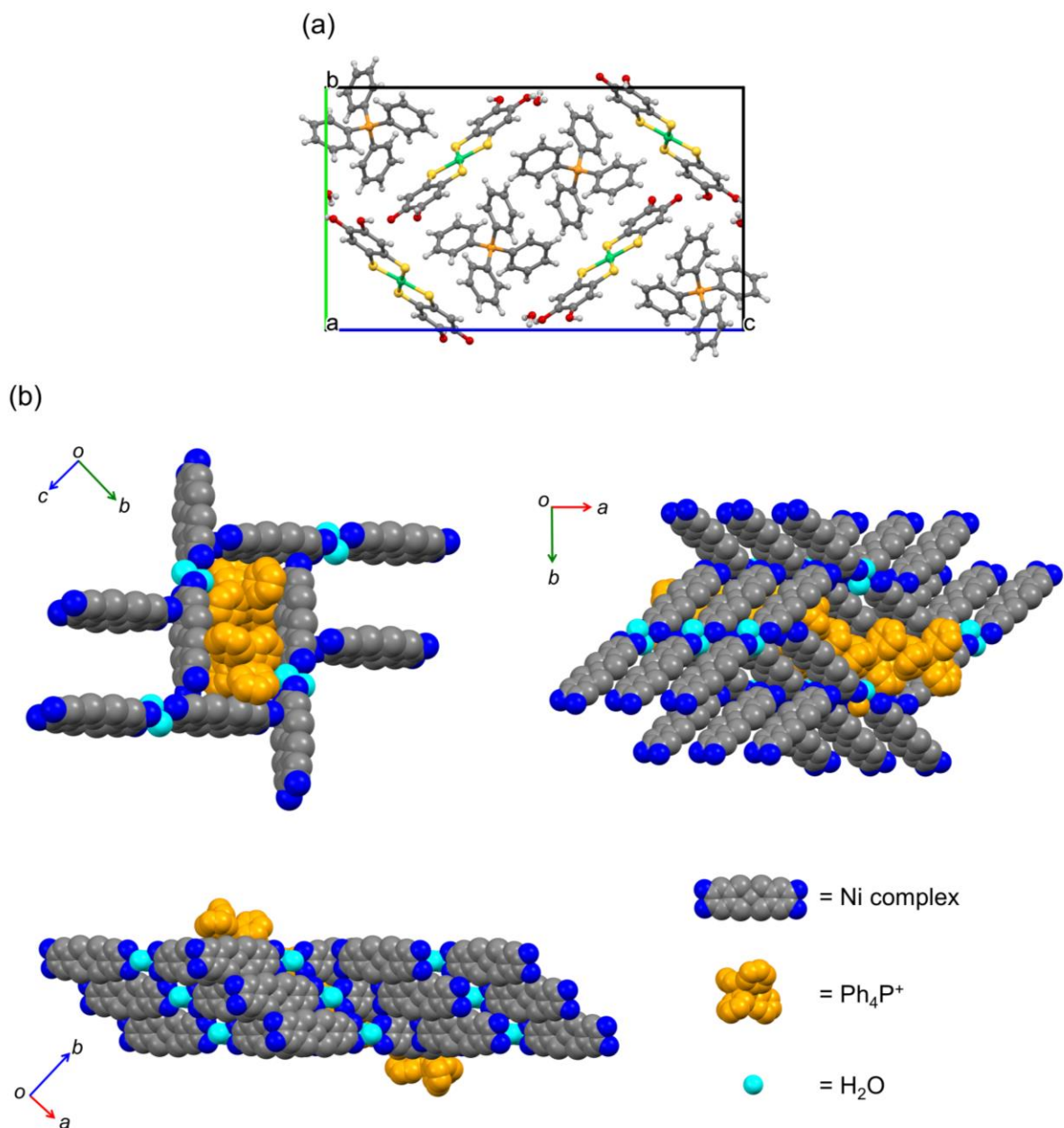
**Fig. 3-4** Structure of the $H_2O$-containing crystal **3-Ni-3H·0.5H₂O**. (a) Unit cell and (b) overview of the 3D framework structure from viewing along each axis. Light green = Ni, yellow = S, orange = P, gray = C, red = O, and white = H.
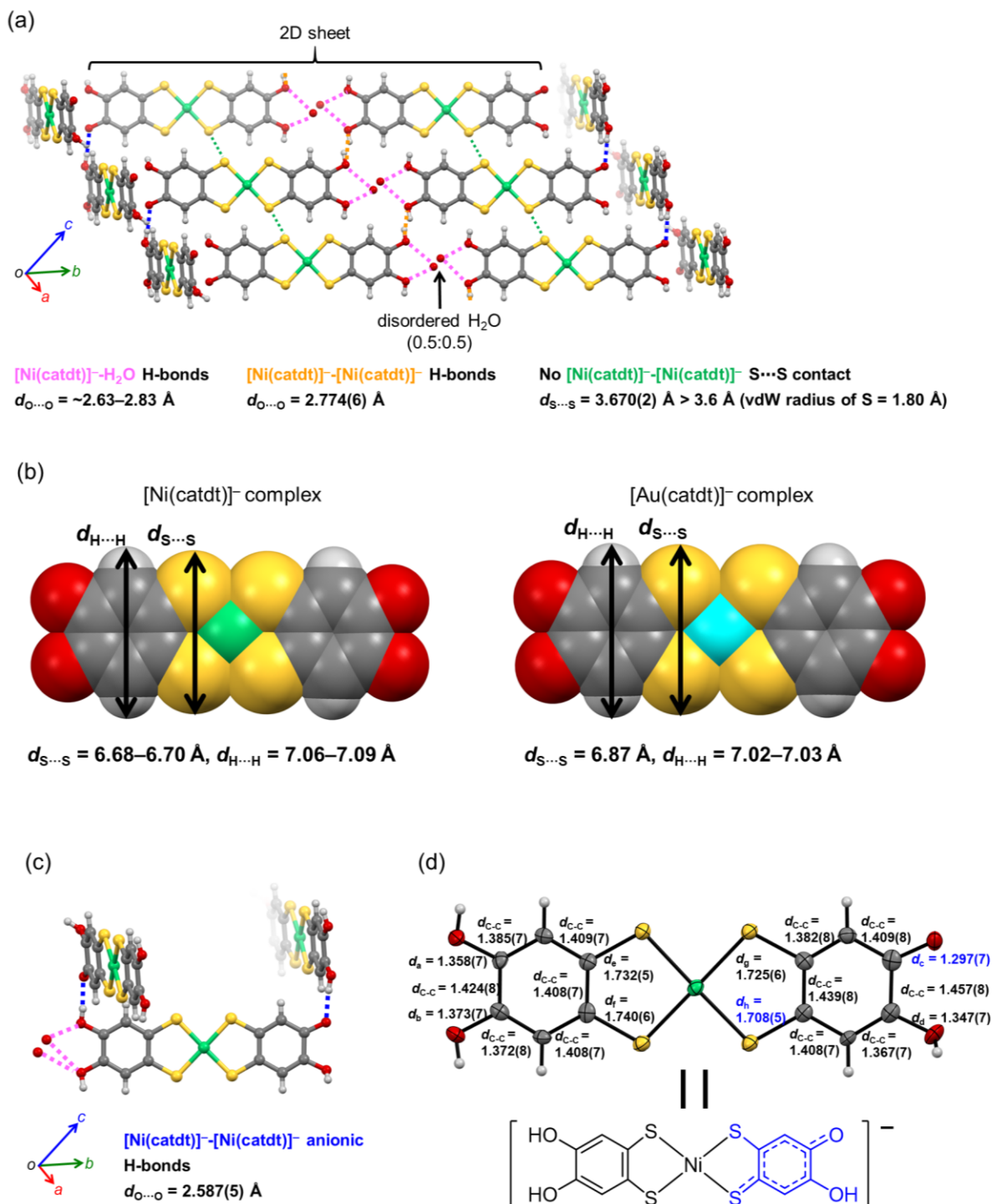
**Fig. 3-5** (a) 3D H-bonded framework structure consisting of the nickel complexes and water molecules in **3-Ni-3H·0.5H₂O** and (b) anionic [O–H···O] H-bond between the nickel complexes. (c) Molecular structure and bond distances (Å) and the possible chemical structure of the nickel complex. (d) Difference in molecular skeleton of the [Ni(catdt)₂]⁻ complex in **3-Ni-3H·0.5H₂O** and [Au(catdt)₂]⁻ complex in **3-Au·0.5H₂O**.

The crystal structure of **3-Ni-3H·0.5THF** was shown in Fig. 3-6. As with the **3-Ni-3H·0.5H$_2$O**, the X-ray structural analysis revealed that it consisted of one Ph$_4$P$^+$ cation, one nickel complex, and a half THF molecules, indicating the nickel complex is in the monoanionic state (formula: (Ph$_4$P)[Ni-H$_3$(catdt)$_2$]·0.5THF). In this crystal, the nickel complexes formed a 2D sheet structure, and Ph$_4$P$^+$ and THF molecules were sandwiched between the 2D sheets (Fig. 3-6b). The sheet was constructed from 1D H-bonded chains formed by multiple [O–H···O] H-bonds between hydroxy groups of the nickel complexes ($d_{O···O}$ = 2.788(2) Å and 2.590(3) Å, Fig. 3-7a and b). The neighboring H-bonded chains were connected by π-π interaction (multiple C–C contacts) between the nickel complexes, as shown in Fig. 3-7c, and thus the thickness of the sheet corresponded to approximately two nickel complexes (Fig. 3-6b). This π-π interaction is probably due to the high planarity and delocalized HOMO distribution of the nickel complex. In contrast to **3-Ni-4H·DMSO** and **3-Ni-3H·0.5H$_2$O**, the crystal solvent molecule, THF, have no H-bond with the nickel complex. Notably, one of the H-bonds has a significantly short distance ($d_{O–O}$ = 2.590(3) Å; Fig. 3-7b) similar to the anionic H-bond in **3-Ni-3H·0.5H$_2$O** (Fig. 3-5c).

The molecular structure of the nickel complex in this crystal was similar to that of **3-Ni-3H·0.5H$_2$O**; there are hydroxy groups having relatively short C–O bond length. In the case of this crystal, the C–O bond length of two hydroxy groups was shorter than the general C–O distance of catechol moiety ($d_{C–O}$ = 1.323(2) Å and 1.327(2) Å, C–O bond $d_a$ and $d_d$; Table 3-2 and Fig. 3-8b), where two hydroxy groups formed the above-mentioned H-bond with short length ($d_{O–O}$ = 2.590(3) Å; Fig. 3-7b). These features are similar to single-well [O···H···O] H-bond, and thus the proton could be located in the center of the H-bond. Note that the proton position on the two hydroxy groups cannot be determined by the X-ray structural analysis because of the shortness of both C–O bond lengths related to the anionic H-bond at this point. Thus, in order to investigate the position of the proton in the anionic H-bond, differential Fourier maps based on the XRD measurements were described in Fig. 3-8a. The very high crystallinity

of the single crystal made it possible to estimate the position of the proton from the differential Fourier maps. As shown in Fig. 3-8a, the electron density between the anionic H-bond is roughly distributed in the middle of the oxygen atoms. However, the shape appears to be divided into two positions (Fig. 3-8a right). Considering the moderately short C–O length of the two hydroxy groups and the shape of the electron density, the protons are disordered at two positions rather than in the middle (0.5:0.5, Fig. 3-8c). This result suggests that the nickel complex structure based on the X-ray structural analysis is an averaged structure, and the electronic configuration would be similar to that in **Ni-3H·0.5THF** (Fig. 3-8b). In addition, the position of the proton was not changed by temperature variation from 130 K to 293 K.
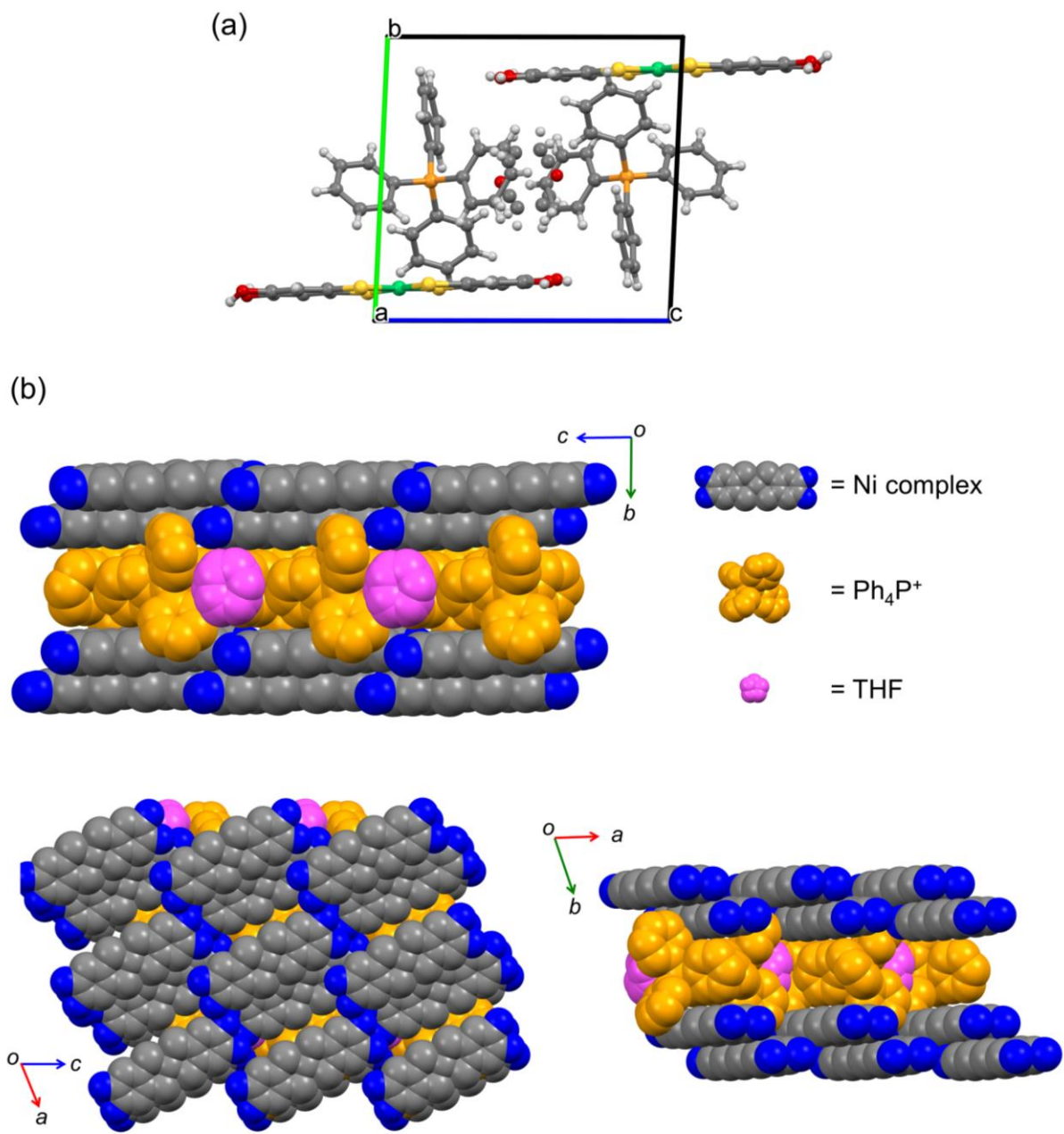
**Fig. 3-6** Structure of the THF-containing crystal, **3-Ni-3H·0.5THF**. (a) Unit cell and (b) overview of the 2D sheet structure viewed along each axis.
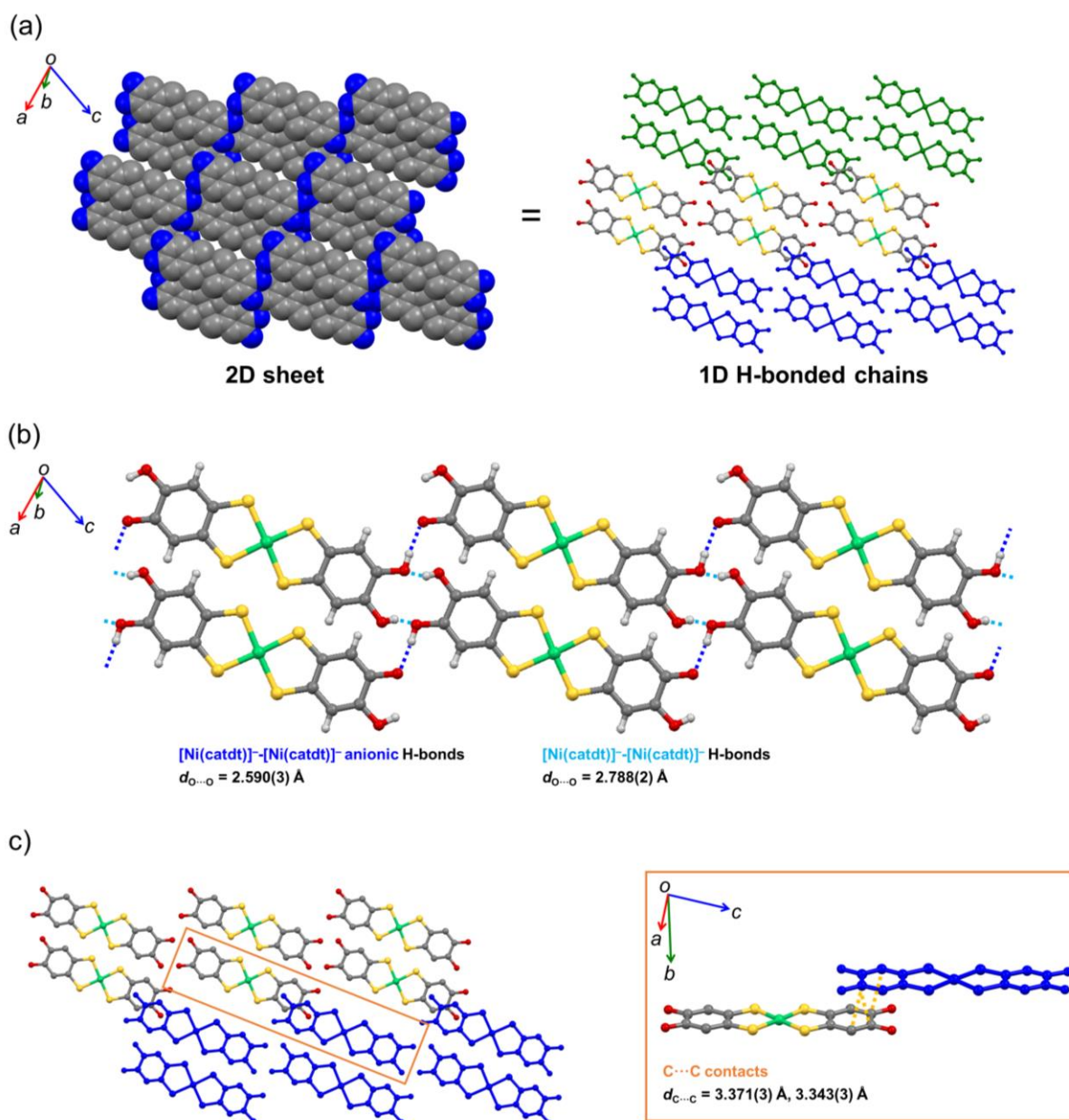
**Fig. 3-7** (a) Correspondance between the 2D sheet structure and 1D H-bonded chains. (b) 1D H-bonded chain in the 2D sheet structure of **3-Ni-3H·0.5THF**. (c) Neighboring 1D H-bonded chains. Colored nickel complexes belong to the same 1D H-bonded chain (left) and π-π interactions (C···C contacts) between nickel complexes belonging to each chain (right). The orange box focuses on the two nickel complexes belonging to different 1D H-bonded chains.
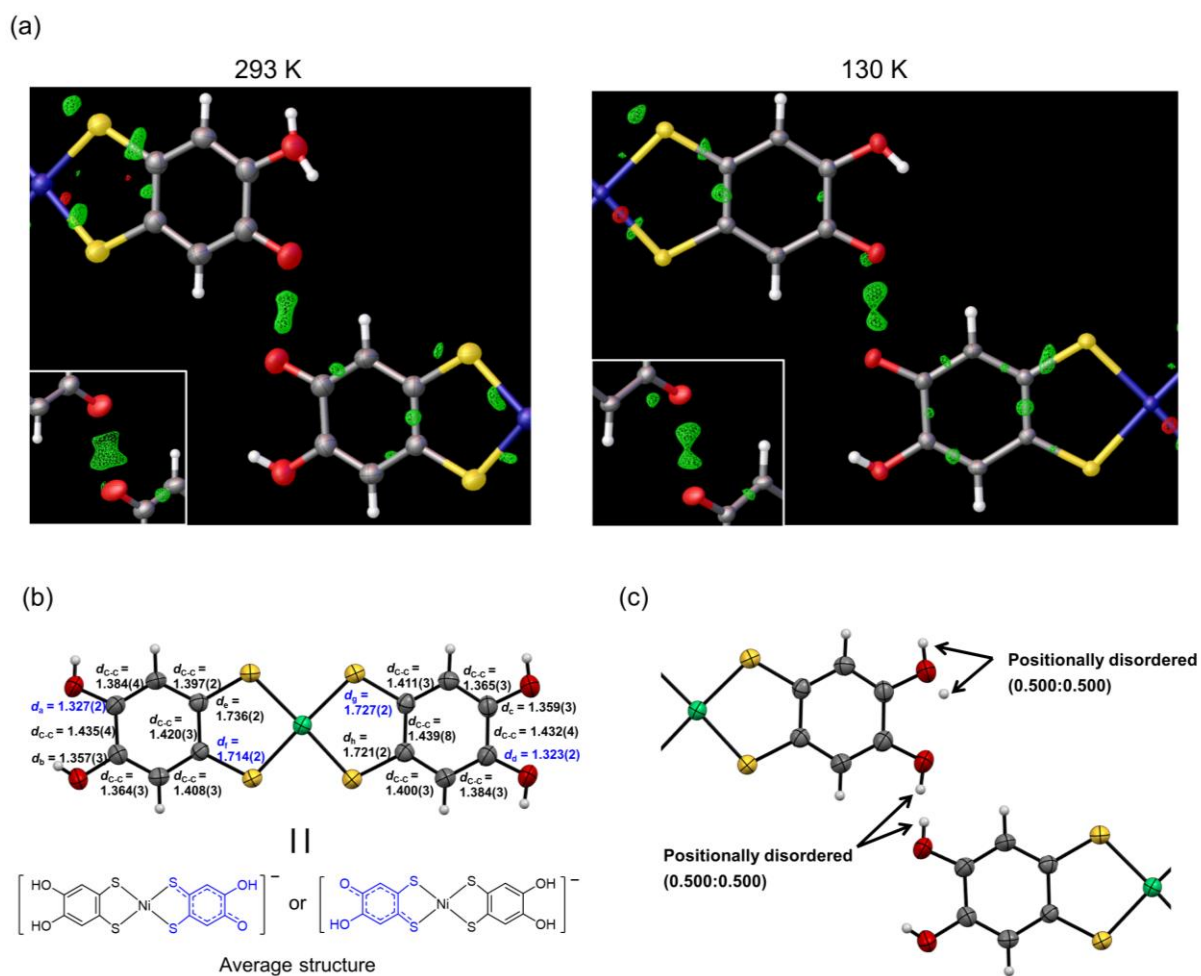
**Fig. 3-8** (a) Differential Fourier map on anionic H-bond part between hydroxy groups of nickel complex calculated from single-crystal XRD measurement. The threshold value of the differential Fourier surface is 0.300 electron/Å$^3$ a 293 K or 0.400 electron/Å$^3$ at 130 K. These figures were visualized by the Olex2 software.[25] (b) The crystal structural analysis of anionic H-bond part. (c) Molecular structure with bond lengths (Å) (top) and the possible chemical structure of the nickel complex (bottom).

### 3.3.3 Two-deprotonated Ni complex crystal: 3-Ni-2H·2H₂O

The crystal of **3-Ni-2H·2H₂O** was obtained together with **3-Ni-4H·DMSO** and **3-Ni-3H·0.5H₂O** crystals in the same recrystallization condition. Interestingly, although nickel complexes in the other three crystals discussed in Section 3.3.1 and 3.3.2 are monoanionic, this crystal contains $Ph_4P^+$ cation and nickel complex in the ratio of 2:1 (formula: $(Ph_4P)_2[Ni-H_2(catdt)_2]\cdot2H_2O$, Fig. 3-9a) from the X-ray structural analysis; the nickel complex is dianion. This crystal has a 2D H-bonded sheet structure based on the nickel complex similar to that of **3-Ni-3H·0.5THF** (Fig. 3-9b). In contrast to **3-Ni-3H·0.5THF**, the 2D sheet in this crystal consisted of the nickel complexes and water molecules with multiple [O–H···O] H-bonds ($d_{O···O}$ = 2.68–2.97 Å, Fig. 3-10a); the complexes in the 2D sheet were thoroughly constructed by the H-bonds. Although this crystal has two equivalent bulky cation molecules, the 2D H-bonded sheet structure was constructed. This construction would be due to a small water molecule having proton-accepting and -donating abilities that help to form multiple [O–H···O] H-bonds, connecting the nickel complexes. The inclusion of water molecules into the crystal would improve the dimensionality of the H-bonding network, as also shown in **3-Ni-3H·0.5H₂O**. On the other hand, the thickness of the 2D sheet corresponded to approximately two complexes in **3-Ni-3H·0.5THF**, while it was approximately one complex in **3-Ni-2H·2H₂O** (Fig. 3-6b and 3-9b). This difference in the thickness would be derived from the dianion state of the nickel complex in this crystal. In other words, the dianion state increases Coulomb repulsion between the complexes, preventing the nickel complexes from approaching each other. In addition, the increase of equivalence of counter cation ($Ph_4P^+$) from 1:1 to 2:1 also relates to this difference.
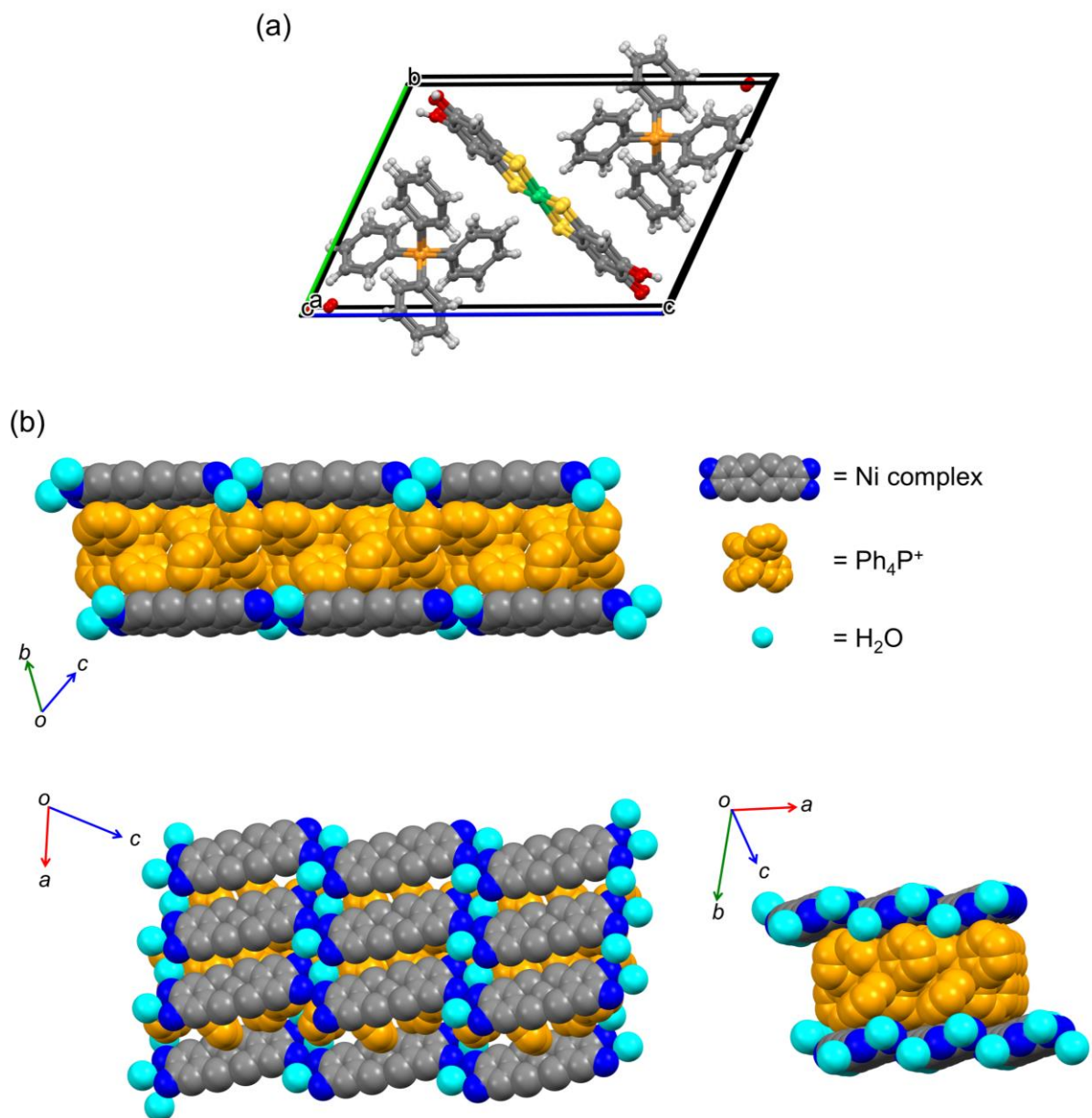
**Fig. 3-9** Structure of the water-containing crystal, **3-Ni-2H·2H₂O**. (a) Unit cell and (b) the 2D H-bonded sheet structure viewed along each axis.
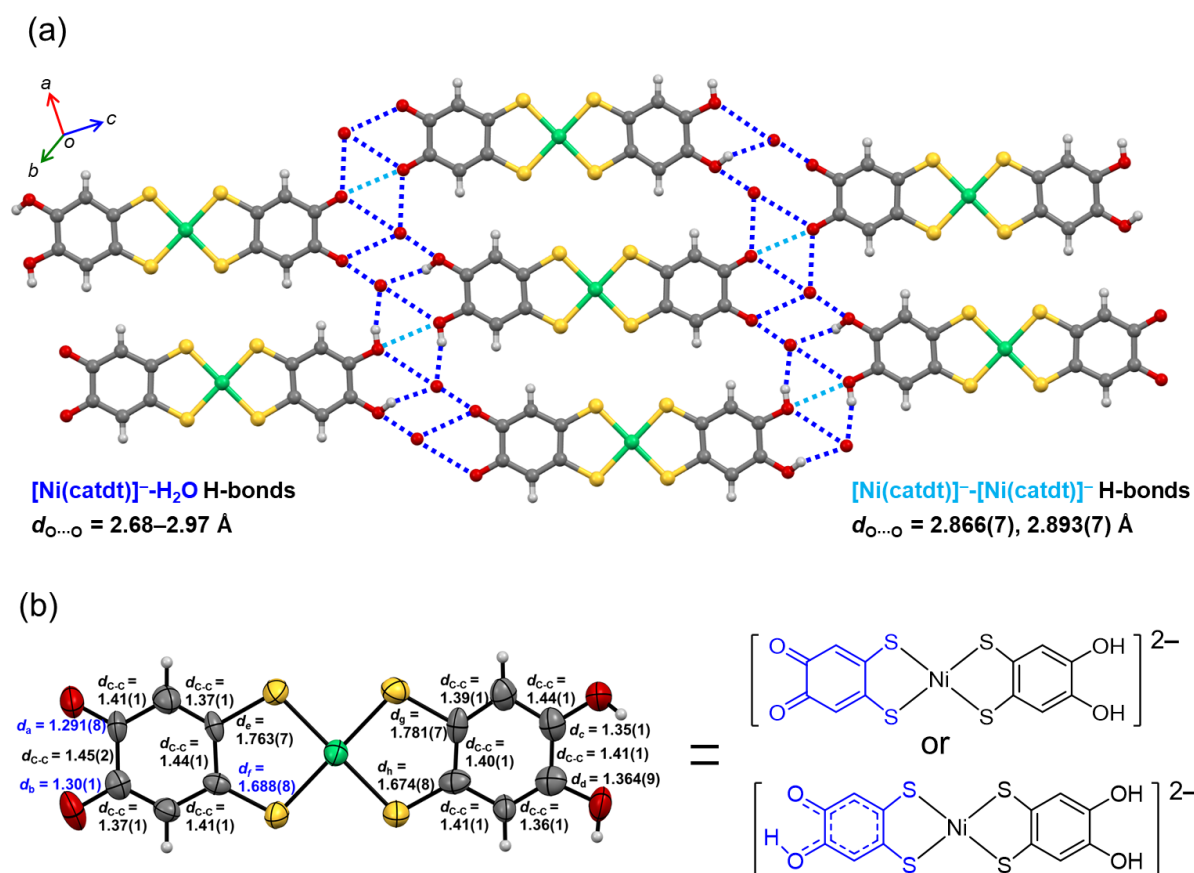
**Fig. 3-10** (a) H-bond structure in the 2D H-bonded sheet of **3-Ni-2H·2H₂O**. (b) Molecular structure and bond length (Å) and the possible chemical structure of the nickel complex.

Interestingly, the C–O bond lengths of the nickel complex also show different features from that of **3-Ni-3H·0.5H₂O** and **3-Ni-3H·0.5THF** (Table 3-2 and Fig. 3-10b). In this nickel complex, the C–O or C=O bond lengths of two hydroxy groups belonging to the same ligand ($d_a$ and $d_b$, Fig. 3-10b) were meaningfully short. This fact indicates that deprotonation occurs in one or two hydroxy groups. Nevertheless, this crystal has no [O–H···O] H-bonds with significantly short O···O distance between nickel complexes in contrast to **3-Ni-3H·0.5H₂O** and **3-Ni-3H·0.5THF**. This is probably because the nickel complexes are surrounded by water molecules, to prevent intermolecular H-bond formation between the nickel complexes. Namely, such short H-bond can be formed only between the equivalent molecules having the same electronic configuration.[4,6,10,33]

Here, from only the X-ray structural analysis, the number of deprotonated hydroxy groups can no longer be determined owing to the insufficient quality of the crystal. Considering the dianion state of the nickel complex, one- or two-deprotonation should result in non-oxidation or one-electron oxidation, respectively. Thus, the one- or two-deprotonated nickel complexes show paramagnetic or non-magnetic properties, respectively. As discussed in the next section, the number of deprotonated hydroxy groups is indirectly determined by the magnetic property measurements.

## 3.4 Magnetic properties and electronic states

Generally, the monoanionic nickel dithiolene complex is an open-shell state ($S = 1/2$), and the assembly has magnetic properties.[11] Thus, **3-Ni-4H·DMSO** should exhibit ESR signal and temperature dependence of magnetic susceptibility. On the other hand, in the deprotonated nickel complex crystals **3-Ni-3H·0.5H$_2$O**, **3-Ni-3H·0.5THF**, and **3-Ni-2H·2H$_2$O**, the electronic states of the nickel complexes will change through PCET in solution processes. The nickel complexes in the two one-deprotonated crystals (**3-Ni-3H·0.5H$_2$O** and **3-Ni-3H·0.5THF**) are in the monoanionic state, and the one-deprotonation will result in one-electron oxidation. When one-electron oxidation occurs, the nickel complex becomes a closed-shell state ($S = 0$). On the other hand, in the two-deprotonated crystal **3-Ni-2H·2H$_2$O**, the nickel complex is in the dianion state. Thus, one out of two deprotonation processes does not involve oxidation; the nickel complex becomes a closed-shell state ($S = 0$).

To investigate the electronic (oxidation) states of the nickel complexes and magnetic properties in each crystal, ESR measurements for all crystals and the magnetic susceptibility measurement for **3-Ni-4H·DMSO** were performed. As expected, the non-deprotonated complex crystal, **3-Ni-4H·DMSO**, showed an ESR signal at approximately 3200–3300 G, depending on the crystal orientation. The $g$ value is estimated to be 2.04–2.07 from fitting

analysis (Fig. 3-11). This value is consistent with those of reported nickel dithiolene complexes,[23] and thus this ESR signal is attributed to the nickel complex. Furthermore, the temperature dependence of the magnetic susceptibility obeys Curie–Weiss law with very weak antiferromagnetic interactions (Curie temperature $T_c$ = −0.149 K, Fig. 3-12). This result is consistent with the absence of significant π-π interactions between the nickel complexes in the 3D framework structure. Also, the Curie constant obtained by the fitting (0.382 emu K mol$^{-1}$) gives the g value to be 2.016 in the case of $S$ = 1/2. This value is similar to that obtained from ESR measurement, rather than that of organic radicals (2.003).
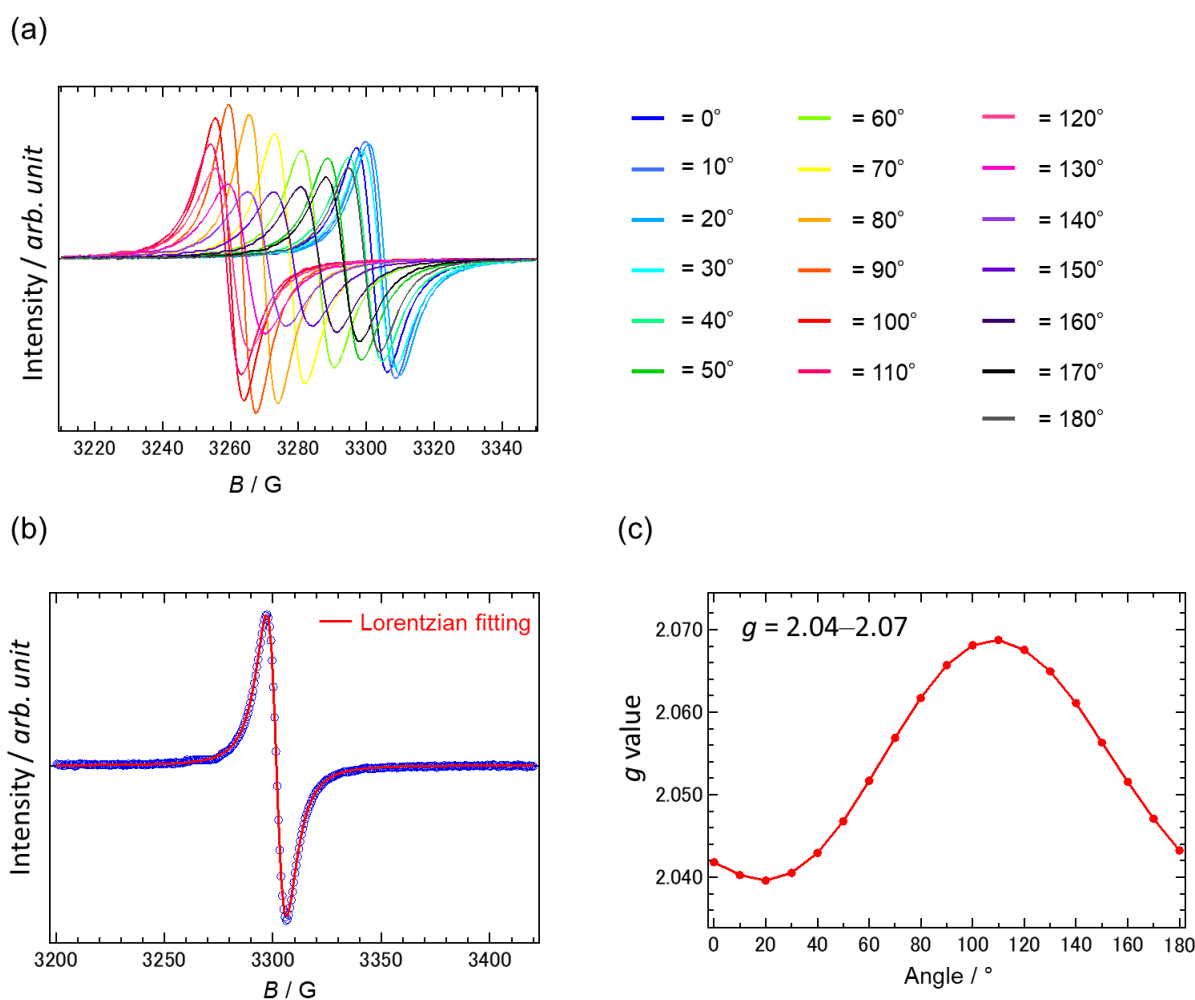


**Fig. 3-11** (a) ESR signals measured around the *a* axis of **3-Ni-4H·DMSO** single crystal. (b) Lorentzian fitting of the ESR signal at 0 degrees in (a). (c) Angle dependence of the *g* value estimated from the Lorentzian fitting for the measurements.
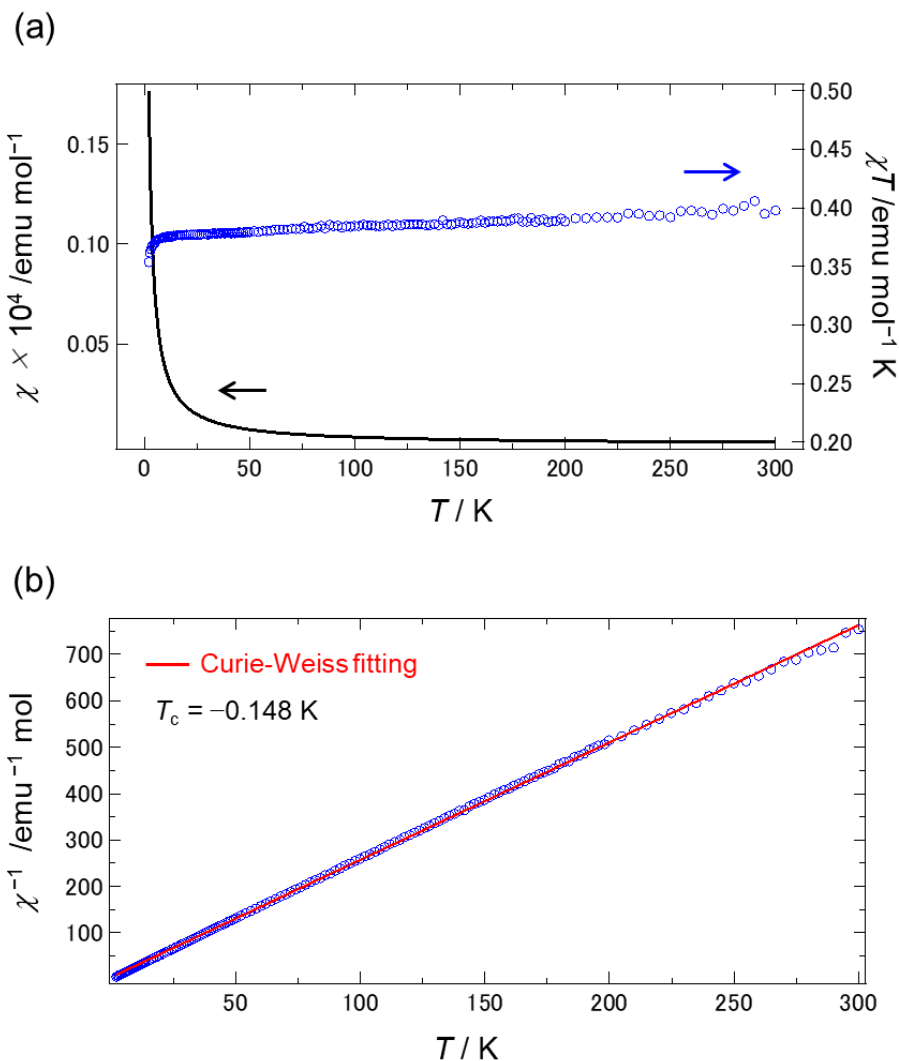
**Fig. 3-12.** Temperature dependences on the magnetic susceptibility of **3-Ni-4H·DMSO** polycrystals. (a) $\chi$–$T$ plot (black solid line) and $\chi T$–$T$ plot (blue circles). (b) $\chi^{-1}$–$T$ plot (blue circles) and Curie-Weiss fitting (red solid line).

On the other hand, interestingly, other deprotonated complex crystals (**3-Ni-3H·0.5H₂O**, **3-Ni-3H·0.5THF**, and **3-Ni-2H·2H₂O**) showed no ESR signal indicating that the nickel complexes in these crystals are in closed-shell states (Fig. 3-13). Therefore, the magnetic properties of these crystals were changed from paramagnetic to non-magnetic through PCET in solution processes, as described in Fig. 3-14; these crystals exhibited electron–proton coupled functionality via solution processes. Here, new electron–proton coupled functionalities will be

expected with the constituent molecules having PCET activity when the proton transfer occurs in solid state. However, considering that the anionic [O–H⋯O] H-bonds in **3-Ni-3H·0.5H₂O** and **3-Ni-3H·0.5THF** is probably not single-well H-bond at 293 K, proton transfer in the anionic H-bond with, at least, decreasing temperature would not be expected. Actually, X-ray structural analysis at a low-temperature of **3-Ni-3H·0.5THF** showed no signs of the proton transfer in the anionic H-bond in the range of 130 K to 293 K. In addition, unfortunately, because the deprotonated complex crystals have the periodic structure with the anionic H-bond and non-magnetic property, coherent local proton transfer on the H-bond would not induce macro magnetic property changing, as shown in Fig. 3-15.
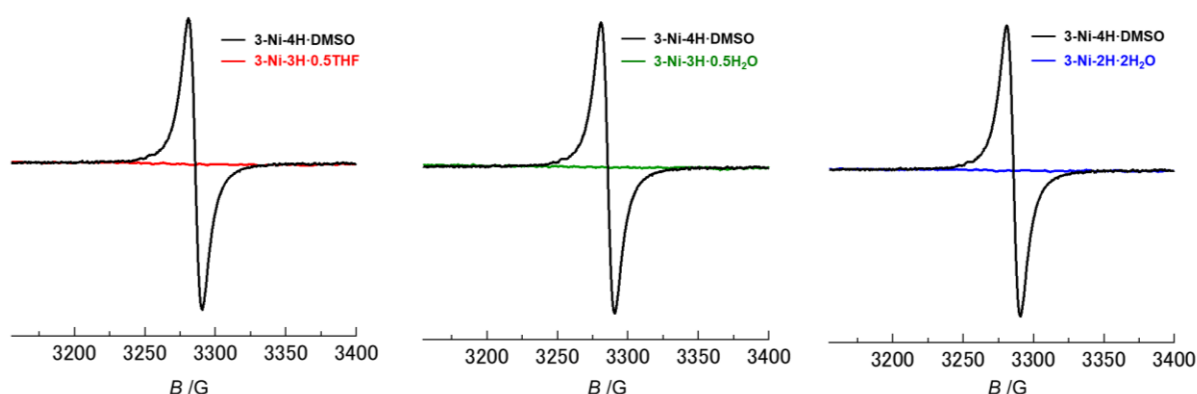


**Fig. 3-13** ESR signals of **3-Ni-4H·DMSO**, **3-Ni-3H·0.5H₂O**, **3-Ni-3H·0.5THF**, and **3-Ni-2H·2H₂O**. The ESR signals derived from an electron spin are not obtained in the three crystals except for **3-Ni-4H·DMSO**.
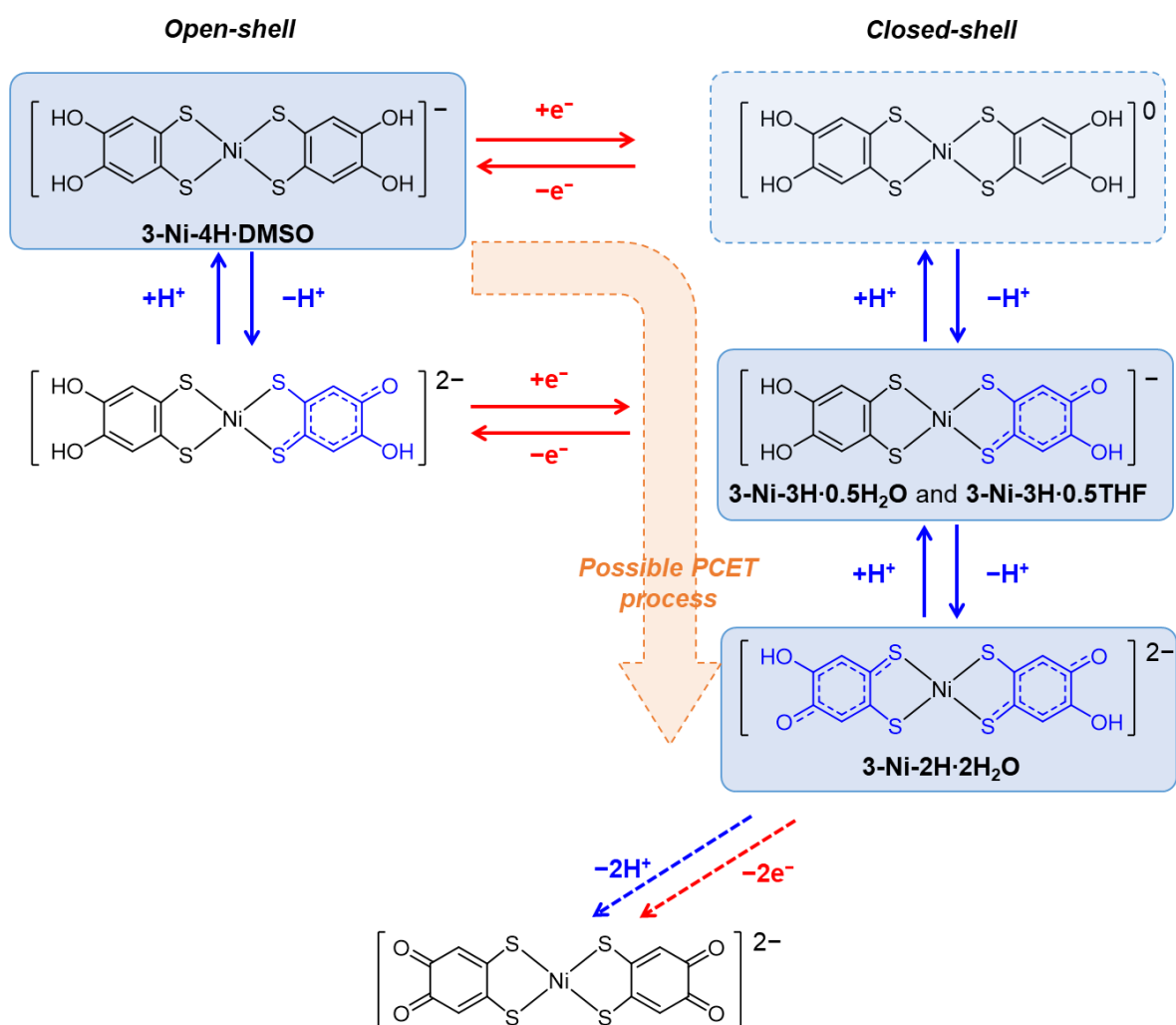
**Fig. 3-14** Possible PCET process and chemical structures of the nickel complexes in each state. Blue and red arrows show redox and protonation/deprotonation processes, respectively. The blue boxes with a solid line show obtained species of the nickel complex as crystals in this Chapter. Also, the blue box with a dashed line shows a species of the nickel complex as crystals with poor reproducibility presented in Appendix section.
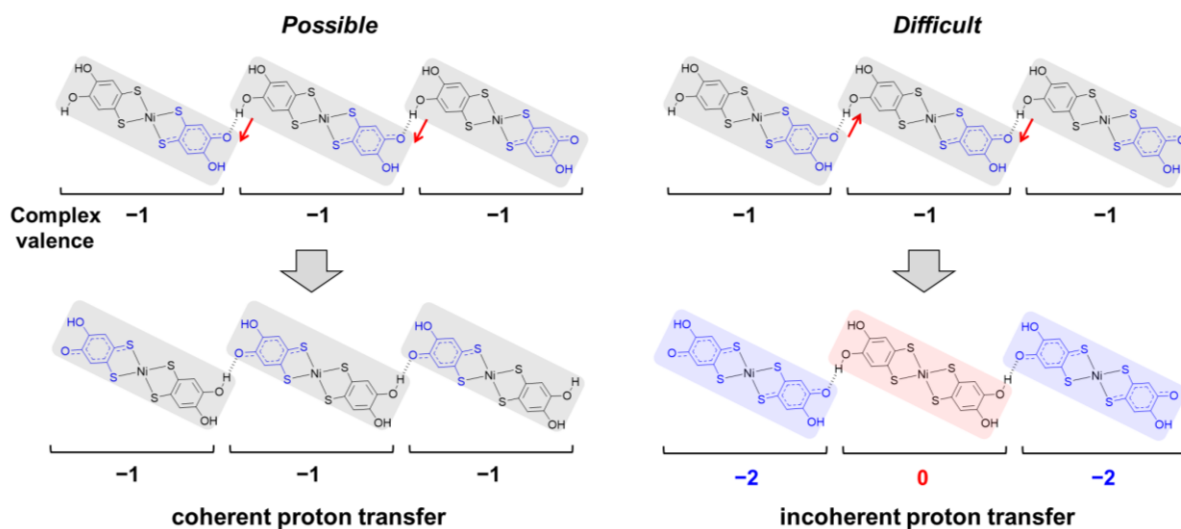
**Fig. 3-15** Possible proton transfer regime in the anionic H-bonds of **3-Ni-3H·0.5THF**.

Also, the results of ESR measurement indicate that the nickel complex is singly deprotonated in **3-Ni-3H·0.5H₂O** and **3-Ni-3H·0.5THF** and is doubly deprotonated in **3-Ni-2H·2H₂O**. Therefore, the three species of the nickel complex with PCET were obtained in the crystals. In addition to this, although reproducibility is not confirmed well, the crystals including neutral nickel complex without deprotonation, [Ni-H$_4$(catdt)$_2$], are also obtained by similar recrystallization method (DMF/Et$_2$O or acetone/AcOH/Hexane, the formula and crystal structure were shown in Appendix section). Considering these facts, the author proposes that the possible PCET process is thought to be oxidation followed by one- or two-deprotonation, as shown in Fig. 3-14.

Here, modulation of the electronic state in these crystals with proton transfer would be difficult because coherent proton transfer is most likely to occur (Fig. 3-15 left). However, the constituent nickel complex has the potential to exhibit novel electron–proton coupled functionalities. Therefore, to investigate the influence of the oxidation and deprotonation on the d/π electronic states of the nickel complexes, DFT calculations based on the structures of a non-deprotonated complex crystal (**3-Ni-4H·DMSO**) and deprotonated complex crystals (**3-Ni-**

**3H·0.5THF** and **3-Ni-2H·2H₂O**) were carried out. SOCOs (singly-occupied crystal orbitals) and LUCO (lowest unoccupied crystal orbital) of **3-Ni-4H·DMSO** were similar to HOMO and LUMO of typical monoanionic metal dithiolene complexes and monoanionic gold catecholdithiolene complex (Chapter 2).[24] On the other hand, the HOCOs (highest occupied crystal orbitals) and LUCOs of deprotonated crystals were significantly different, and the LUCOs were largely distributed on the whole nickel complex compared with the LUCO of **3-Ni-4H·DMSO**. This difference is due to a change of frontier crystal orbitals with one-electron oxidation: HOCO (next SOCO)→HOCO, SOCO→LUCO, and LUCO→next LUCO (Fig. 3-16). Actually, the next LUCOs of the deprotonated crystals are almost the same as the LUCO of the **3-Ni-4H·DMSO**. Then, comparing LUCO of **3-Ni-3H·0.5THF** and **3-Ni-2H·2H₂O** with SOCO of **3-Ni-4H·DMSO** to reveal the influence of the deprotonation on the orbital distributions, the crystal orbital weight on the deprotonated ligand is changed. The weight of the LUCOs on the deprotonated ligand of **3-Ni-3H·0.5THF** and **3-Ni-2H·2H₂O** significantly increase because of enhancements of the electron-accepting ability derived from the (semi)quinoid structure. Furthermore, the distribution of the HOCOs of the deprotonated crystals is quite different and more delocalized compared with that of the HOCO of **3-Ni-4H·DMSO**. This result indicates that the deprotonation efficiently modulates the orbitals of the nickel complexes in crystalline solids. This feature would work in favor of the d/π-electronic state modulation with proton dynamics. Although magnetic properties of **3-Ni-3H·0.5THF** and **3-Ni-2H·2H₂O** were the same (non-magnetic), a comparison between the frontier orbitals of **3-Ni-3H·0.5THF** and **3-Ni-2H·2H₂O** demonstrates significant modulation of the electronic state on metal dithiolene skeleton. These results indicate that the d/π electronic states of the nickel complex in deprotonated crystals were significantly changed with the deprotonation and oxidation states.
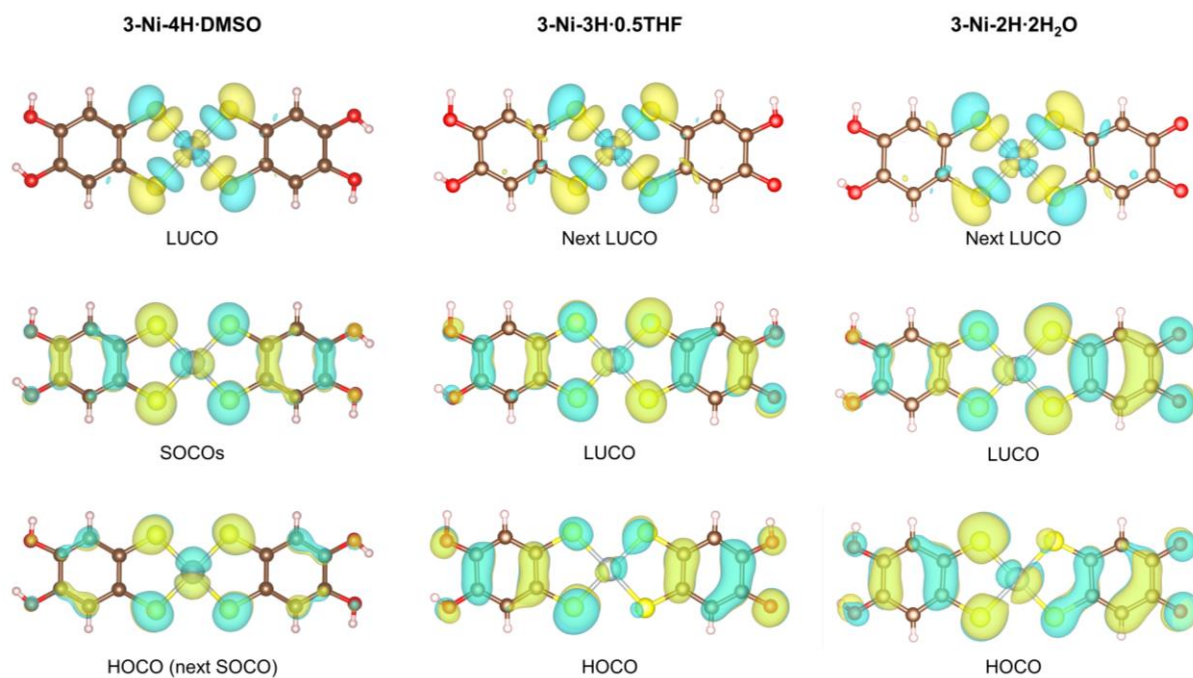
**Fig. 3-16** Distribution of the frontier orbitals of **3-Ni-4H·DMSO**, **3-Ni-3H·0.5THF**, and **3-Ni-2H·2H₂O**. For clarity, this figure shows the orbital distribution on the nickel complexes extracted from the calculated crystal orbitals. These figures were visualized by the VESTA.[34] Note that the SOCOs of **3-Ni-4H·DMSO** shows two degenerate crystal orbitals near the Fermi level. The shapes of these two orbitals are almost the same with each other.

## 3.5 Conclusion

In conclusion, four new crystals having intermolecular H-bonds based on the nickel catecholdithiolene complex were successfully synthesized. In the crystals, the nickel complexes constructed various assembled structures (3D framework and 2D sheet) and H-bonding network structures (2D framework and sheet, and 1D chain structures) similar to the crystals consisting of the gold catecholdithiolene complex (Chapter 2). Importantly, in **3-Ni-3H·0.5THF** and **3-Ni-3H·0.5H₂O**, the formation of anionic [O–H···O] H-bonds ($d_{O···O}$ = ~2.59 Å) having a potential of proton transfer between the O atoms with external-stimuli was observed. Furthermore, the comparison of C–O bond lengths suggests that the nickel complexes in the crystals except for **3-Ni-4H·DMSO** are deprotonated, which leads to a modulation of the d/π

electronic state of the nickel complex with deprotonation-coupled oxidation in solution process. ESR measurements of the deprotonated complex crystals realized that the deprotonation-coupled oxidation caused magnetic property changes from paramagnetic to non-magnetic: the d/π electronic functionality change based on PCET in solution processes. The DFT calculations based on the periodic structures suggest that the d/π electronic states are significantly different in each crystal derived from the deprotonation states. The fact indicates that the electronic functionalities can be changed by the modulation of d/π-electronic states with proton dynamics in the solid states. This finding provides significant insights for exploring novel physical properties and phenomena, where d/π electrons are coupled with proton transfer in solid states.

In this chapter, the author achieved the modulation of d/π electronic functionalities of crystalline solids induced by PCET in the solution processes, and provided a stage to realize the novel electron–proton coupled phenomena, switching of the d/π electronic functionalities by proton dynamics in solid states, for this Ph. D research.
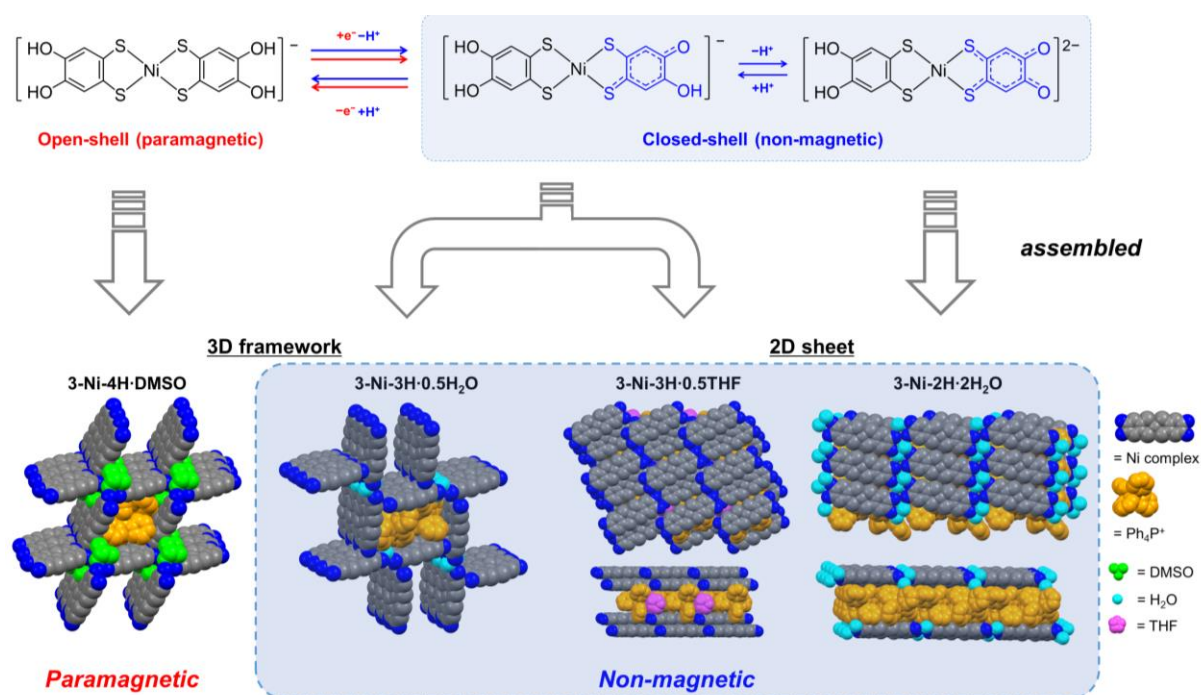
## 3.6 References

1    D. R. Weinberg, C. J. Gagliardi, J. F. Hull, C. F. Murphy, C. A. Kent, B. C. Westlake, A. Paul, D. H. Ess, D. G. McCafferty and T. J. Meyer, *Chem. Rev.*, 2012, **112**, 4016.

2    T. Mitani, G. Saito and H. Urayama, *Phys. Rev. Lett.*, 1988, **60**, 2299.

3    K. Nakasuji, K. Sugiura, T. Kitagawa, J. Toyoda, H. Okamoto, K. Okaniwa, T. Mitani, H. Yamamoto and I. Murata, *J. Am. Chem. Soc.*, 1991, **113**, 1862.

4    S. Horiuchi, Y. Tokunaga, G. Giovannetti, S. Picozzi, H. Itoh, R. Shimano, R. Kumai and Y. Tokura, *Nature*, 2010, **463**, 789.

5    S. Horiuchi, R. Kumai and Y. Tokura, *J. Am. Chem. Soc.*, 2013, **135**, 4492.

6    A. Ueda, S. Yamada, T. Isono, H. Kamo, A. Nakao, R. Kumai, H. Nakao, Y. Murakami, K. Yamamoto, Y. Nishio and H. Mori, *J. Am. Chem. Soc.*, 2014, **136**, 12184.

7    A. Ueda, *BCSJ*, 2017, **90**, 1181.

8    A. Ueda, K. Kishimoto, Y. Sunairi, J. Yoshida, H. Yamakawa, T. Miyamoto, T. Terashige, H. Okamoto and H. Mori, *J. Phys. Soc. Jpn.*, 2019, **88**, 034710.

9    A. Ueda, K. Kishimoto, T. Isono, S. Yamada, H. Kamo, K. Kobayashi, R. Kumai, Y. Murakami, J. Gouchi, Y. Uwatoko, Y. Nishio and H. Mori, *RSC Adv.*, 2019, **9**, 18353.

10   T. Isono, H. Kamo, A. Ueda, K. Takahashi, A. Nakao, R. Kumai, H. Nakao, K. Kobayashi, Y. Murakami and H. Mori, *Nat Commun*, 2013, **4**, 1344.

11   E. I. Stiefel and K. D. Karlin, *Progress in Inorganic Chemistry, Dithiolene Chemistry: Synthesis, Properties, and Applications*, Wiley-Interscience, New York, 2003.

12   R. Kato, *Chem. Rev.*, 2004, **104**, 5319.

13   A. Kobayashi, E. Fujiwara and H. Kobayashi, *Chem. Rev.*, 2004, **104**, 5243.

14   W.-Y. Guo, Z.-H. Peng, C.-G. Wang and Y.-H. Zhou, *J. Coord. Chem.*, 2006, **59**, 1213.

15   R. Kato, *Bull. Chem. Soc. Jpn.*, 2014, **87**, 355.

16   F. Pop and N. Avarvari, *Coord. Chem. Rev.*, 2017, **346**, 20.

17   T. Kubo, M. Ohashi, K. Miyazaki, A. Ichimura and K. Nakasuji, *Inorg. Chem.*, 2004, **43**,

7301.

18  S. Shibahara, H. Kitagawa, Y. Ozawa, K. Toriumi, T. Kubo and K. Nakasuji, *Inorg. Chem.*, 2007, **46**, 1162.

19  M. Hayashi, K. Otsubo, T. Kato, K. Sugimoto, A. Fujiwara and H. Kitagawa, *Chem. Commun.*, 2015, **51**, 15796.

20  S. R. Kennedy, P. Goyal, M. N. Kozar, H. P. Yennawar, S. Hammes-Schiffer, and B. J. Lear, *Inorg. Chem.*, 2016, **55**, 1433.

21  S. R. Kennedy, M. N. Kozar, H. P. Yennawar, and B. J. Lear, *Inorg. Chem.*, 2016, **55**, 8459.

22  M. Hayashi, Y. Takahashi, Y. Yoshida, K. Sugimoto and H. Kitagawa, *J. Am. Chem. Soc.*, 2019, **141**, 11686.

23  D. Coucouvanis, A. R. Paital, Q. Zhang, N. Lehnert, R. Ahlrichs, K. Fink, D. Fenske, A. K. Powell and Y. Lan, *Inorg. Chem.*, 2009, **48**, 8830.

24  S. Yokomori, A. Ueda, T. Higashino, R. Kumai, Y. Murakami and H. Mori, *CrystEngComm*, 2019, **21**, 2940.

25  O. V. Dolomanov, L. J. Bourhis, R. J. Gildea, J. A. K. Howard and H. Puschmann, *J. Appl. Crystallogr.*, 2009, **42**, 339.

26  G. A. Bain and J. F. Berry, *J. Chem. Educ.*, 2008, **85**, 532.

27  T. Ozaki, *Phys. Rev. B*, 2003, **67**, 155108.

28  T. Ozaki and H. Kino, *Phys. Rev. B*, 2004, **69**, 195113.

29  K. Lejaeghere, G. Bihlmayer, T. Bjorkman, P. Blaha, S. Blugel, V. Blum, D. Caliste, I. E. Castelli, S. J. Clark, A. Dal Corso, S. de Gironcoli, T. Deutsch, J. K. Dewhurst, I. Di Marco, C. Draxl, M. Du ak, O. Eriksson, J. A. Flores-Livas, K. F. Garrity, L. Genovese, P. Giannozzi, M. Giantomassi, S. Goedecker, X. Gonze, O. Granas, E. K. U. Gross, A. Gulans, F. Gygi, D. R. Hamann, P. J. Hasnip, N. A. W. Holzwarth, D. Iu an, D. B. Jochym, F. Jollet, D. Jones, G. Kresse, K. Koepernik, E. Kucukbenli, Y. O. Kvashnin, I. L. M. Locht, S. Lubeck, M. Marsman, N. Marzari, U. Nitzsche, L. Nordstrom, T. Ozaki, L. Paulatto, C. J.

Pickard, W. Poelmans, M. I. J. Probert, K. Refson, M. Richter, G.-M. Rignanese, S. Saha, M. Scheffler, M. Schlipf, K. Schwarz, S. Sharma, F. Tavazza, P. Thunstrom, A. Tkatchenko, M. Torrent, D. Vanderbilt, M. J. van Setten, V. Van Speybroeck, J. M. Wills, J. R. Yates, G.-X. Zhang and S. Cottenier, *Science*, 2016, **351**, aad3000.

30  T. Ozaki and H. Kino, *Phys. Rev. B*, 2005, **72**, 045121.

31  J. P. Perdew, K. Burke and M. Ernzerhof, *Phys. Rev. Lett.*, 1996, **77**, 3865.

32  H. Hachem, O. Jeannin, M. Fourmigué, F. Barrière and D. Lorcy, *CrystEngComm*, 2020, **22**, 3579.

33  J. Yoshida, A. Ueda, A. Nakao, R. Kumai, H. Nakao, Y. Murakami and H. Mori, *Chem. Commun.*, 2014, **50**, 15557.

34  K. Momma and F. Izumi, *J. Appl. Crystallogr.*, 2011, **44**, 1272.

# Chapter 4

# Vapochromism induced by intermolecular electron transfer coupled with hydrogen bond formation

## 4.1 Introduction

Reversible control of electronic functionalities of molecular materials using external stimuli and perturbations is important not only for applications to next-generation switching devices and sensors but also from the viewpoint of basic science to elucidate the mechanism and to establish the material design criteria.[1–10] As mentioned in Chapter1, H-bonds have charge degrees of freedom owing to the electrostatic property and proton dynamics, which enable us to directly modulate the electronic states.[11–19] In previous works, the electron–proton coupling phenomenon in H-bonded π-conjugated molecular crystals was demonstrated, in which magnetism and electrical conductivity were switched by proton (deuteron) dynamics in an intermolecular H-bond.[15–19] If control of the functionalities other than magnetism and electrical conductivity, such as optical properties, by modulating the electronic states through H-bond is well established, it will impact various research fields and greatly expand the design criteria of functional materials.

As one of the functional molecular materials with optical properties responsive to external stimuli, vapochromic materials, which respond with color changes when exposed to solvent vapors, have been actively studied as good candidates for their use as chemical sensors because they can directly visualize external environmental changes.[20–22] The vapochromism in previous research has been understood based on molecular structure and/or arrangement changes caused by vapor sorption.[23–32] Although several vapochromic materials involving H-bonds have been reported so far, the number of examples has been limited.[33–44] Furthermore, they have been explained based on molecular structure and/or arrangement changes similar to conventional

mechanisms, and have only been discussed with the electronic states of a hypothetical isolated molecule ignoring the intermolecular interactions. Therefore, the mechanism has poorly been elucidated, and the intrinsic effects of H-bonding on the electronic states have not been clarified.

In this chapter, the author realizes the control of vapochromic behavior by direct modulation of electronic states through H-bonding in a novel crystal consisting of zinc methoxybenzenedithiolene complex (compound **4-Zn** in Fig. 4-1; Ph$_4$P: tetraphenyl phosphonium, 4-mxbdt: 4-methoxybenzene-1,2-dithiolate). The compound **4-Zn** is a novel vapochromic crystal, which exhibits changes in both visible-light absorption and photoluminescence with single-crystal-to-single-crystal (SCSC) transformations upon methanol or water vapor sorption, involving H-bond formation between zinc complex and vapor molecules. Based on the detailed single-crystal structure analyses and first-principles calculations considering intermolecular interactions using the periodic structure model of the crystal, a new mechanism of vapochromism in **4-Zn**, that is, not molecular structure and arrangement changes but electron transfer coupled with H-bond formation is revealed for the first time.
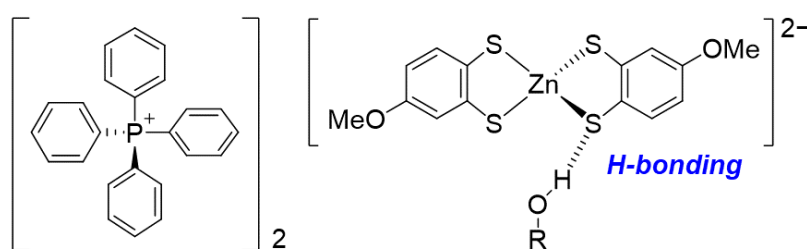


**Fig. 4-1** Chemical structure of (Ph$_4$P)$_2$[Zn(4-mxbdt)$_2$], **4-Zn** with H-bond formation.

## 4.2 Experimental

**Materials**

Commercially available chemicals, zinc chloride (II) (CAS: 7646-85-7, Sigma-Aldrich), tetraphenylphosphonium bromide (CAS: 2751-90-8, Tokyo Chemical Industry Co., Ltd.), sodium methoxide (5M in methanol) (CAS: 14-42-4, Tokyo Chemical Industry Co., Ltd.), methanol (CAS: 67-56-1, super dehydrated grade, FUJIFILM Wako Pure Chemical Industries Co., Ltd.), and liquid paraffin (CAS: 8042-47-5, FUJIFILM Wako Pure Chemical Industries Co., Ltd.) were used without further purification.

**Synthesis and crystallization of 4-Zn·2MeOH**

To a mixture of tetraphenylphosphonium bromide (1.89 g, 4.50 mmol), 1,2-bis(2'-cyanoethylthio)-4-methoxybenzene[45] (835 mg, 3.00 mmol), and methanol (30 mL) was added a solution of sodium methoxide (6.0 mL, 5 M in methanol, 30.0 mmol) and zinc chloride (204 mg, 1.50 mmol) at room temperature under argon atmosphere. After the mixture was stirred for two hours, a precipitated yellow solid was collected by filtration and rinsed subsequently with water (20 mL) and diethyl ether (20 mL) to give yellow polycrystals of $(Ph_4P)_2[Zn(4-mxbdt)_2]\cdot n$(solvent) (4-mxbdt: 4-methoxybenzene-1,2-dithiolate). After drying the polycrystals in vacuo for a few hours, the orange polycrystals were obtained; the amount of these crystals was estimated as 1.34 mmol (1.45 g, 84%). ^{1}H NMR (300 MHz) and ^{13}C NMR (75 MHz) spectra were recorded on a JEOL JNM-AL300 spectrometer with DMSO-$d_6$ as a solvent and $Me_4Si$ as an internal standard. The structure of **4-Zn** was confirmed by NMR analysis: ^{1}H NMR (300 MHz, DMSO-$d_6$; $Me_4Si$) δ 3.54 (s, 6H), 6.01 (dd, $J$ = 2.6, 8.3 Hz, 2H), 6.80 (d, $J$ = 2.6 Hz, 2H), 7.01 (d, $J$ = 8.3 Hz, 2H), 7.70–8.00 (m, 40H); ^{13}C NMR (75 MHz, DMSO-$d_6$; $Me_4Si$) δ 54.7, 106.1, 114.4, 117.0, 118.3, 128.7, 130.4, 130.5, 134.4, 134.6, 135.3, 135.4, 139.8, 149.7, 153.1.

On the other hand, from the remaining filtrate after removing polycrystals of $(Ph_4P)_2[Zn(4-$

mxbdt)$_2$]·$n$(solvent) by filtration, a single crystal of **4-Zn·2MeOH** was grown by the slow evaporation of the filtrate at room temperature. The single-crystal X-ray diffraction (XRD) measurement confirmed the compositional formula as (Ph$_4$P)$_2$[Zn(4-mxbdt)$_2$]·2CH$_3$OH (**4-Zn·2MeOH**).

**SCSC transformation of 4-Zn with vapor sorption**

Vapor-desorbed crystals **4-Zn** were prepared by drying **4-Zn·2MeOH** crystal under vacuum for four days. The crystal structure of **4-Zn** was determined by single-crystal XRD measurement, where the crystal was coated with Apiezon® N-type grease to prevent the absorption of moisture in the air during the single-crystal XRD measurement. After the measurement, Apiezon grease around the crystal was removed by washing with hexane, and the recovered crystal **4-Zn** was subsequently used for the preparation of methanol-absorbed crystal **4-Zn·2MeOH**; **4-Zn** was placed under methanol vapor/nitrogen atmosphere for two days to obtain single crystals of **4-Zn·2MeOH** that is subjected to the single-crystal XRD measurement. Therefore, the reversibility of the SCSC transformation with methanol sorption was confirmed. Also, for water-absorbed crystal **4-Zn·H$_2$O**, the crystal **4-Zn** was placed under the atmosphere for two days to obtain single crystals of **4-Zn·H$_2$O** that is subjected to the single-crystal XRD measurement. Then, this crystal was again dried in vacuo for four days. Complete desorption of water out of the crystal and **4-Zn·H$_2$O** was confirmed by single-crystal XRD measurements; the structure after drying was confirmed to be identical to **4-Zn**. Therefore, the reversibility of the SCSC transformation with water sorption was also confirmed.

**Single-crystal X-ray diffraction (XRD) measurements**

Single-crystal XRD measurements were performed using a Rigaku MercuryII CCD X-ray diffractometer (Mo $K\alpha$, $\lambda = 0.71073$ Å). The structures of **4-Zn·2MeOH**, **4-Zn**, and **4-Zn·H$_2$O** were solved by direct methods (SHELXT version 2018/2) and refined with full-matrix least-

squares technique (SHELXL version 2018/3) using Olex2-1.2[46] (OlexSys) and CrystalStructure 4.3.2 (Rigaku Corporation) software. Anisotropic thermal parameters were applied to all non-hydrogen atoms. The hydrogen atoms on oxygen atoms were refined under the restrictions on the bond angle and length (C–O–H angle = 109.5°, O–H = 0.840 Å), and the other hydrogen atoms were generated geometrically (C–H = 0.950 Å).

For **4-Zn·2MeOH**, because of the severely disordered MeOH molecules, the H atom in the O–H group of the disordered MeOH molecules did not reside in a reasonable position in the refined structure. Therefore, the author analyzed the crystal **4-Zn·2MeOH** without the H atoms on analysis.

## Powder X-ray diffraction measurement (PXRD)

PXRD measurements of polycrystals of **4-Zn·2MeOH** and **4-Zn·H₂O** were performed at room temperature by a Rigaku SmartLab 3KW diffractometer (Cu $K\alpha$, $\lambda$ = 1.5405 Å). The samples were prepared by exposing the polycrystalline powder of **4-Zn** to air or methanol vapor for two days.

## UV-Vis absorption spectra measurements

The polycrystalline powders of **4-Zn·2MeOH**, **4-Zn**, and **4-Zn·H₂O** were diluted with KBr powder and then compressed into KBr pellets ($\phi$ = 10 mm). The KBr pellets were covered with liquid paraffin to prevent moisture absorption or desorption of the solvent molecules. Solid-state UV-vis-NIR spectra were recorded on a JASCO UV/vis-NIR spectrophotometer V-570 equipped with a JASCO integrating sphere attachment ISN-470, in a range of wavelength 250–900 nm with an increment of 1.00 nm.

## Photoluminescence spectra measurements

Polycrystalline powder of **4-Zn** was sealed in a quartz glass tube ($\phi$ = 5 mm) under vacuum.

Polycrystalline powder of **4-Zn·2MeOH** and **4-Zn·H₂O** were sealed in the individual separate tubes under methanol or water vapor atmosphere. Solid-state photoluminescence spectra were recorded on a Horiba Spex Fluorolog-NIR spectrofluorometer, with an excitation wavelength of 410 nm, the measurement range of 450–900 nm, the increment of 1.00 nm, slit width of 5.00 nm, and the integration time of 0.100 sec.

**First-principles calculations**

All the DFT calculations were performed by the OpenMX software (Ver. 3.9) based on optimized localized basis functions and pseudopotentials (PPs). The basis functions used are H6.0-s2p1, C6.0-s2p2d1, O6.0-s2p2d1, P7.0-s2p2d1f1, S7.0-s2p2d1f1, and Zn6.0-s3p2d1 for hydrogen, carbon, oxygen, phosphorous, sulfur, and zinc, respectively, wherein the abbreviation of basis functions such as C6.0-s2p2d1, C stands for the atomic symbol, 6.0 the cutoff radius (Bohr) in the generation by the confinement scheme, and s2p2d1 means the employment of two, two, and one optimized radial functions for the s-, p-, and d-orbitals, respectively. The radial functions were optimized by a variational optimization method.[47,48] As valence electrons in the PPs, the author included 1s for hydrogen, 2s and 2p for carbon and oxygen, 3s and 3p for phosphorous and sulfur, 3s, 3p, 3d, and 4s for Zn, respectively. All the PPs and pseudo-atomic orbitals the author used in this study were taken from the database (2019) in the OpenMX website,[49] which were benchmarked by the delta gauge method.[50] Realspace grid techniques are used for the numerical integrations and the solution of the Poisson equation using FFT with the energy cutoff of 220 Ryd.[51] The author used a generalized gradient approximation (GGA) proposed by Perdew, Burke, and Ernzerhof to the exchange-correlation functional[52] An electronic temperature of 300 K is used to count the number of electrons by the Fermi-Dirac function for all the systems the author considered. For the k-point sampling, the author used a regular mesh of 3×3×3. The absorption spectra were calculated by the Kubo-Greenwood formula within a linear response theory.[53]

Calculations on the molecular orbitals of an isolated $[Zn(4-mxbdt)_2]^{2-}$ complex molecule in **4-Zn·2MeOH**, **4-Zn**, and **4-Zn·H₂O** were carried out based on the atomic coordinates of the Zn complex in each crystal structure obtained by the single-crystal XRD measurements without structural optimization. Energies and distribution of molecular orbitals were shown in Fig. 4-8. For **4-Zn ·2MeOH**, the author adopted the structure refined on X-ray structural analysis with the H atoms in the O–H group of the disordered MeOH-2 and MeOH-3 molecules. The author confirmed that the atomic coordinates were almost the same between the cases with and without the H atoms (The atomic coordinates using the calculations were shown in the Appendix section.).

Calculations of crystal orbitals and absorption spectra were carried out based on the crystal structure obtained by single-crystal XRD measurements. Note that similar to the molecular orbitals calculations, for **4-Zn·2MeOH**, the author adopted the atomic coordinates refined on X-ray structural analysis with the H atoms in the O–H group of the disordered MeOH-2 and MeOH-3 molecules (The atomic coordinates optimized by the calculations were shown in the Appendix section.). For the calculations, totally nine structural models were used: the actual four crystal structures obtained by the XRD measurements (**4-Zn·2MeOH** (minor), **4-Zn·2MeOH** (major), **4-Zn**, and **4-Zn·H₂O**), hypothetical two crystal structures without vapor molecules, obtained by removing absorbed vapor molecules from the crystals **4-Zn·H₂O** or **4-Zn·2MeOH** (**4-Zn·H₂O** without H₂O, **4-Zn·2MeOH** without 2MeOH), and hypothetical three structures consisting of only the absorbed vapor molecules in the crystal (H₂O in **4-Zn·H₂O**, MeOH-1,2 in **4-Zn·2MeOH** (minor), and MeOH-1,3 in **4-Zn·2MeOH** (major)). In these models, the occupancies of the disordered methanol MeOH-2 and MeOH-3 were set to (1.00, 0.00) for **4-Zn·2MeOH** (minor) and MeOH-1,2 in **4-Zn·2MeOH** (minor), and to (0.00, 1.00) for **4-Zn·2MeOH** (major) and MeOH-1,3 in **4-Zn·2MeOH** (major). Structural optimization was applied only H atoms on O atoms of MeOH-2 and MeOH-3 in **4-Zn·2MeOH** because the positions of the H atoms could not be determined by X-ray structural analysis due to positional

disorder of the methanol molecules.

In addition, the number of electrons on each atom was estimated by Mulliken population analysis.[54] The number of transferred electrons between $[Zn(4\text{-mxbdt})_2]^{2-}$ complex and absorbed vapor molecules were calculated from the difference between Mulliken charges calculated from the experimental crystal structure (**4-Zn·2MeOH** (major), **4-Zn·2MeOH** (minor), and **4-Zn·H$_2$O**) and hypothetical crystal structures (**4-Zn·H$_2$O** without H$_2$O, **4-Zn·2MeOH** (minor) without 2MeOH, and **4-Zn·2MeOH** (major) without 2MeOH) or absorbed vapor molecules in the crystal (H$_2$O in **4-Zn·H$_2$O**, MeOH-1,2 in **4-Zn·2MeOH** (minor), and MeOH-1,3 in **4-Zn·2MeOH** (major)), respectively. Also, the number of transferred electrons on each S atoms (S1 ~ S4) was calculated from differences of an average of Mulliken charges for each S atom on four crystallographically equivalent $[Zn(4\text{-mxbdt})_2]^{2-}$ complex molecules in the unit cell. The total number of transferred electrons of $[Zn(4\text{-mxbdt})_2]^{2-}$ complex and absorbed molecules was calculated from total Mulliken charges for all atoms belonging to each molecule.

## 4.3 Structures of $(Ph_4P)_2[Zn(4\text{-mxbdt})_2]$ crystals

Yellow block-like crystals were obtained by the slow evaporation of the crude mixture (Fig. 4-2 (left)). From the X-ray structural analysis, the yellow crystal obtained consisted of two $Ph_4P^+$ cations and one $[Zn(4\text{-mxbdt})_2]^{2-}$ complex, containing two methanol molecules as the crystal solvent. The composition was determined as $(Ph_4P)_2[Zn(4\text{-mxbdt})_2]\cdot2CH_3OH$ (= **4-Zn·2MeOH**) (Fig. 4-2b and Table 4-1). In this crystal, the $[Zn(4\text{-mxbdt})_2]^{2-}$ complex showed tetrahedral coordination without a π-stacking structure because of the presence of bulky $Ph_4P^+$ cations and thus there were no significant intermolecular interactions between the complexes. The spaces in the loosely packed structure were filled with two methanol molecules per formula. These methanol molecules formed [S⋯H–O] H-bonds ($d_{S3\cdots O3} = 3.286(3)$ Å, $d_{S3\cdots O4} = 3.22(1)$

Å, and $d_{S2\cdots O5}$ = 3.264(8) Å; Fig. 4-2c) with S atoms on the $[Zn(4\text{-mxbdt})_2]^{2-}$ complex (S2 and S3 atoms; Fig. 4-2c). In the crystal, one of the methanol molecules was positionally disordered in a ratio of 0.67 (major): 0.33 (minor) (Fig. 4-2b and 4-3). Also, the tetrahedral coordination structure of the zinc complex and remarkably far distance between the Zn atom and O atoms of the vapor molecules (MeOH: 4.11–5.12 Å, $H_2O$: 3.874(3) Å) indicate no coordination of the absorbed molecules to Zn atoms.
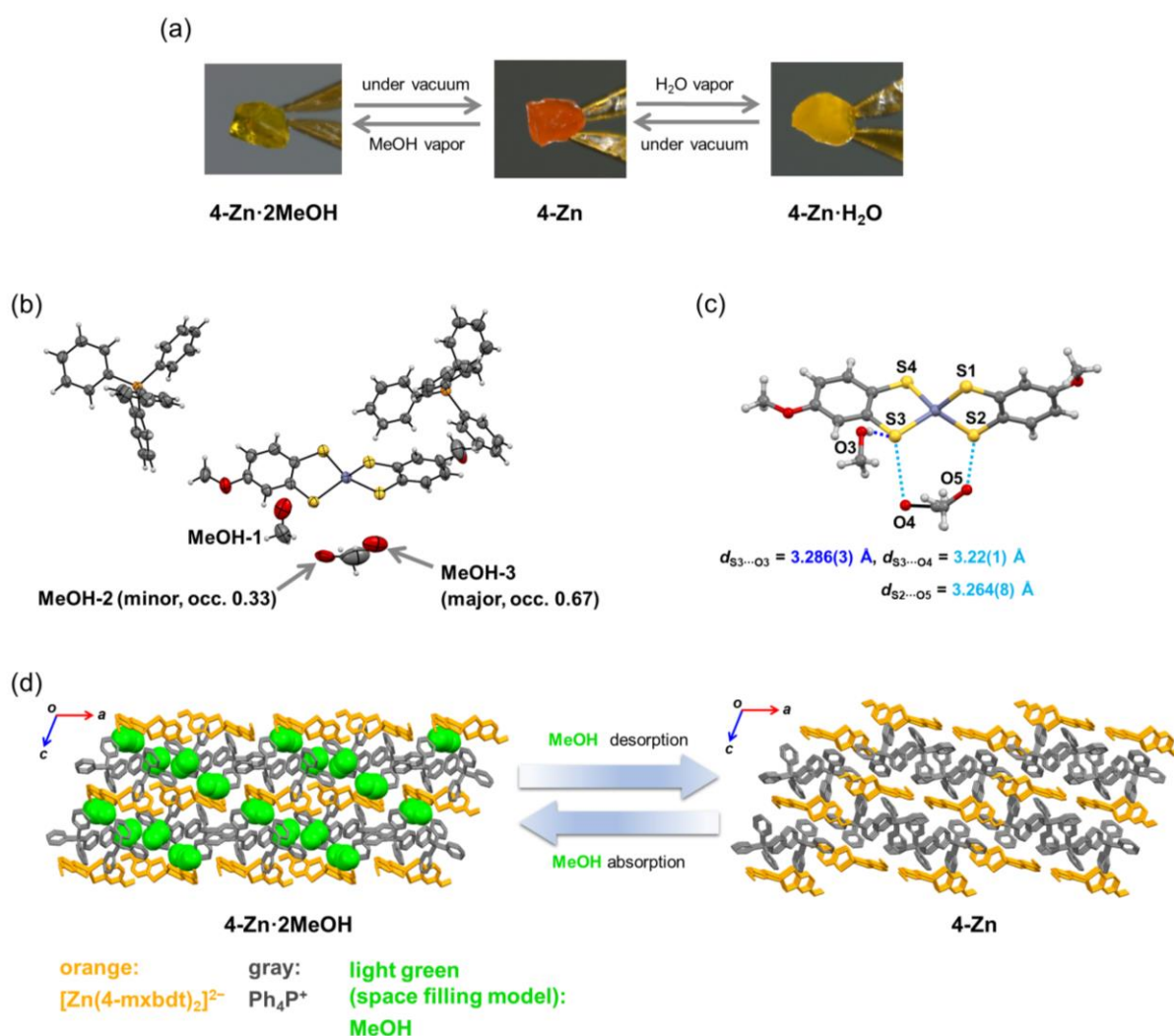


**Fig. 4-2** (a) Color changes of **4-Zn·2MeOH**, **4-Zn**, and **4-Zn·H₂O** single crystals with methanol or water sorption. (b) Crystal structure of **4-Zn·2MeOH** (blue: Zn, yellow: S, orange: P, red: O, grey: C, white: H). (c) H-bonding structure in **4-Zn·2MeOH**. Blue and light blue dashed lines indicate the [S···H–O] H-bonds between the zinc complex and absorbed molecules. (d) Molecular rearrangement of the crystal **4-Zn** during the methanol sorption process.
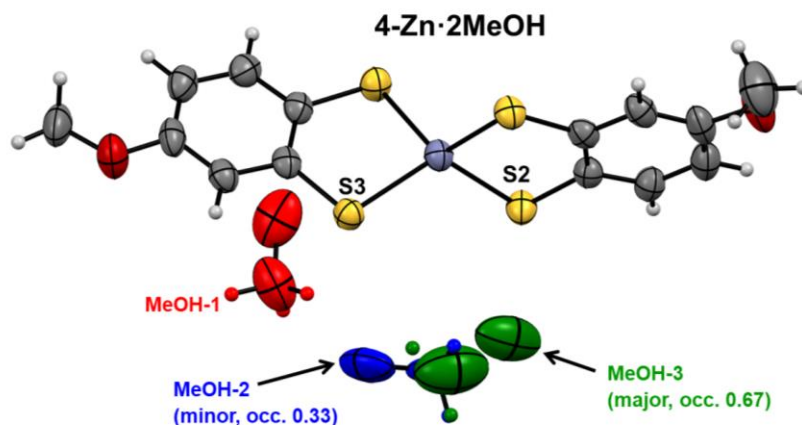
**Fig. 4-3** Positions of methanol molecules in **4-Zn·2MeOH**. (blue: Zn, yellow: S, orange: P, red: O, gray: C, white: H).

**Table 4-1**. Crystallographic parameters for crystals **4-Zn·2MeOH**, **4-Zn**, and **4-Zn·H$_2$O**.

|  | **4-Zn·2MeOH** | **4-Zn** | **4-Zn·H$_2$O** |
|---|---|---|---|
| formula | C$_{64}$H$_{59}$O$_4$P$_2$S$_4$Zn | C$_{62}$H$_{52}$O$_2$P$_2$S$_4$Zn | C$_{62}$H$_{54}$O$_3$P$_2$S$_4$Zn |
| formula weight | 1148.01 | 1084.66 | 1102.67 |
| crystal system | monoclinic | monoclinic | monoclinic |
| space group | $P2_1/c$ | $P2_1/c$ | $P2_1/c$ |
| $a$ (Å) | 22.5655(28) | 22.2168(8) | 22.7885(6) |
| $b$ (Å) | 12.3629(15) | 11.6456(3) | 11.5844(3) |
| $c$ (Å) | 22.0108(29) | 21.9665(6) | 22.2706(5) |
| $\alpha$ (deg.) | 90 | 90 | 90 |
| $\beta$ (deg.) | 111.7447(15) | 110.865(4) | 112.678(3) |
| $\gamma$ (deg.) | 90 | 90 | 90 |
| $V$ (Å$^3$) | 5703.6(12) | 5310.6(3) | 5424.7(3) |
| $Z$ | 4 | 4 | 4 |
| $T$ (K) | 200 | 200 | 200 |
| $D_{calc}$ (g·cm$^{-3}$) | 1.337 | 1.357 | 1.350 |
| $\lambda$ (Å) | 0.71073 | 0.71073 | 0.71073 |
| $R_{int}$ | 0.0462 | 0.0303 | 0.0263 |
| $R_1$ ($I>2.00\sigma(I)$) | 0.0530 | 0.0791 | 0.0460 |
| $wR_2$ (All reflections) | 0.1512 | 0.2367 | 0.1376 |
| GOF | 1.092 | 1.173 | 1.126 |
| CCDC | 2016470 | 2016471 | 2016472 |

Interestingly, drying the crystals overnight under vacuum induced the color change from yellow to orange, maintaining its high crystallinity (Fig. 4-2a (center)). Single-crystal X-ray structural analysis of this orange crystal revealed that two methanol molecules per formula were completely desorbed from the yellow crystal (**4-Zn·2MeOH**), and significant rearrangement of $[Zn(4\text{-mxbdt})_2]^{2-}$ complexes and $Ph_4P^+$ cations occurred to fill the space occupied by the methanol molecules (crystal **4-Zn**; Fig. 4-2d, 4-4, and 4-6). The author confirmed from the X-ray structural analysis that the orange crystal **4-Zn** returned to **4-Zn·2MeOH** and maintained its crystallinity upon exposure to methanol vapor. In addition, reversible structural and color changes (orange to yellow) of the crystal **4-Zn** were observed by the sorption of water vapor in the atmosphere, similar to methanol sorption (Fig. 4-2a (right), 4-5). In this crystal, unlike the methanol vapor sorption, there was one equivalent of a water molecule to the $[Zn(4\text{-mxbdt})_2]^{2-}$ complex (crystal **4-Zn·H$_2$O**; Fig. 4-5a). The water molecule formed two [S···H–O] H-bonds with the S atoms on the $[Zn(4\text{-mxbdt})_2]^{2-}$ complex ($d_{S2\cdots O3} = 3.303(3)$ Å and $d_{S3\cdots O3} = 3.315(3)$ Å; Fig. 4-5b). Furthermore, due to the different numbers and sizes of the absorbed molecules compared to the methanol sorption, no significant changes in the molecular structure and arrangement were observed in **4-Zn·H$_2$O** (Fig. 4-5 and 4-6).

**4-Zn**
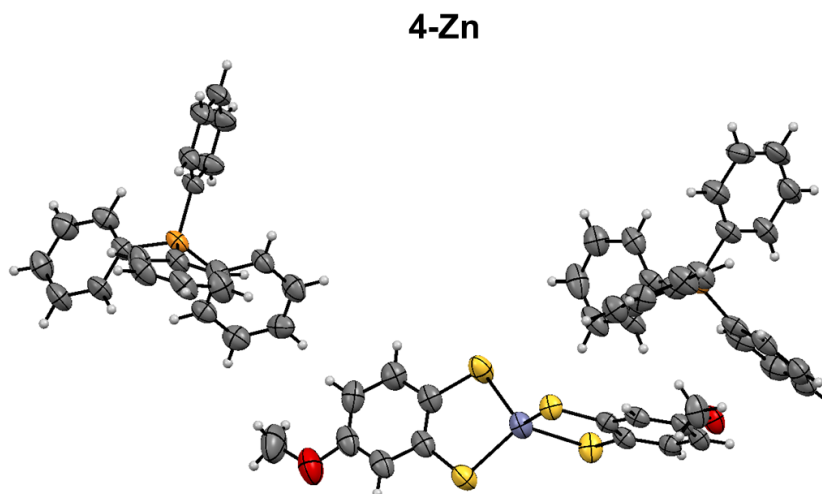


**Fig. 4-4** ORTEP drawing of the crystal **4-Zn**. (blue: Zn, yellow: S, orange: P, red: O, gray: C, white: H).
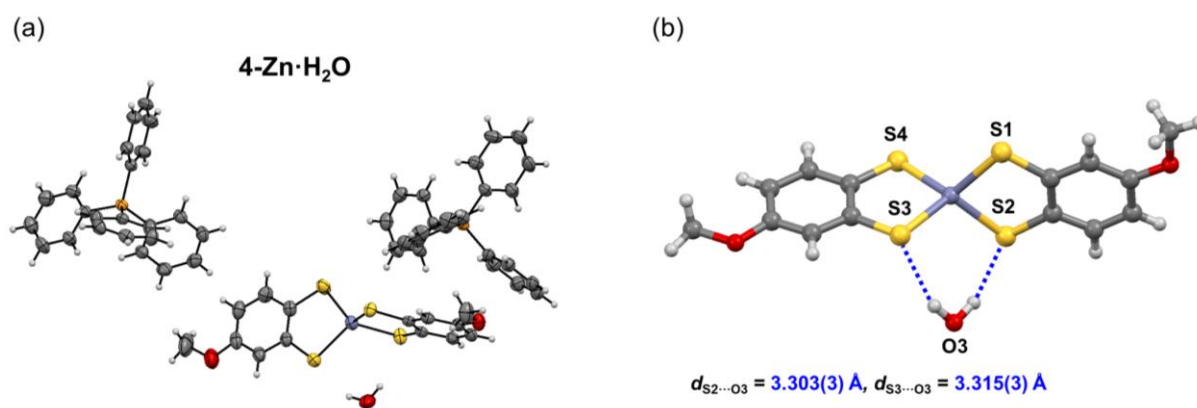


**Fig. 4-5** (a) ORTEP drawing of the crystal **4-Zn**. (blue: Zn, yellow: S, orange: P, red: O, gray: C, white: H). (b) H-bonding structure in **4-Zn·H₂O**. Blue and light blue dashed lines indicate the [S⋯H–O] H-bonds between the zinc complex and absorbed molecules.
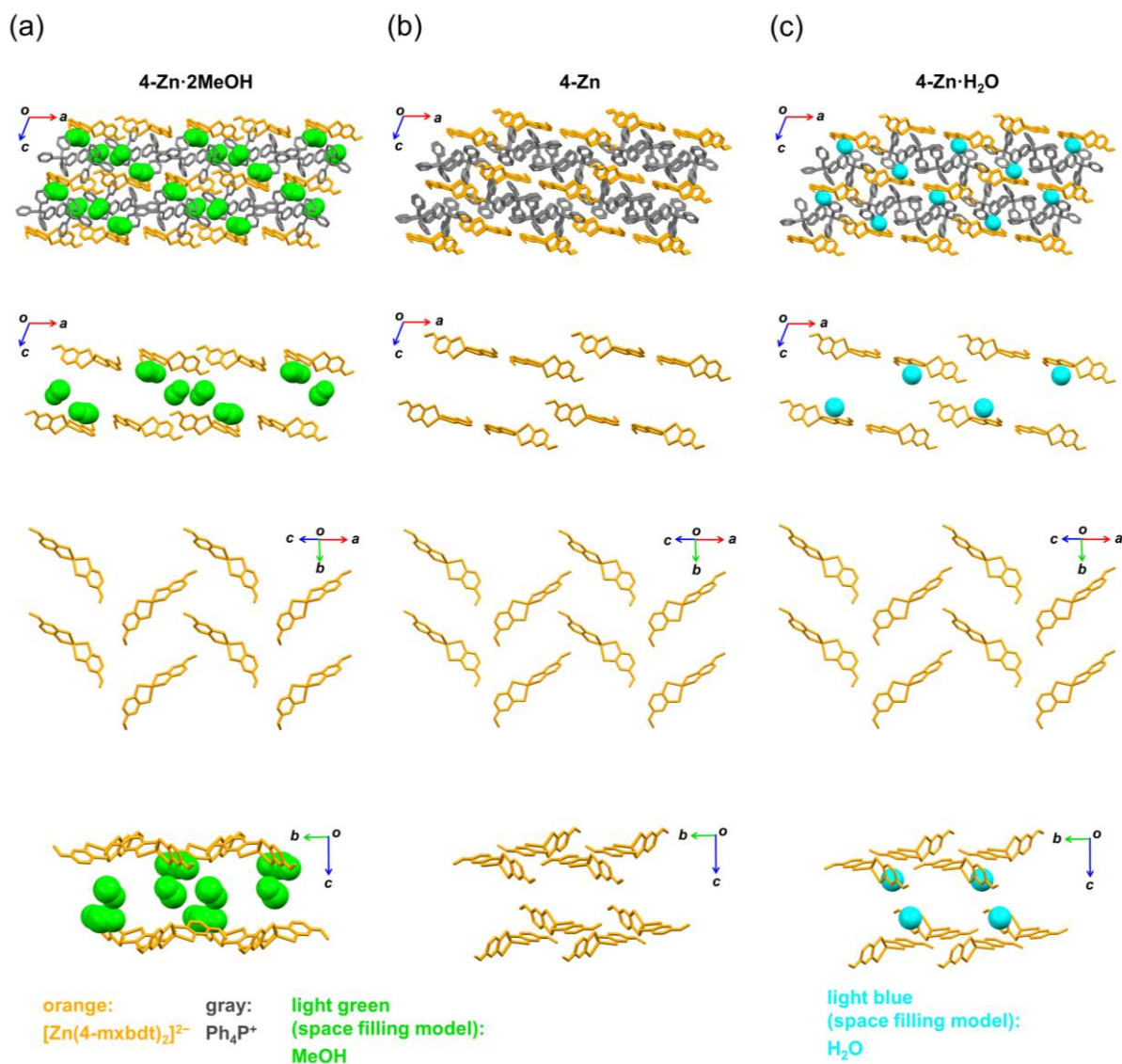
**Fig. 4-6** Molecular arrangements of (a) **4-Zn·2MeOH**, (b) **4-Zn**, and (c) **4-Zn·H₂O**. The molecular arrangement of zinc complexes and $Ph_4P^+$ cations in **4-Zn·H₂O** hardly changed from those in **4-Zn**. Hydrogen atoms were omitted for clarity.

## 4.4 UV-vis and photoluminescence spectra in solid state

As mentioned above, drying the crystals overnight under vacuum induced the color change from yellow to orange, and the orange crystal returned to yellow crystal upon exposure to methanol vapor. In addition, reversible color change (orange to yellow) of the crystal **4-Zn** was observed by the sorption of water vapor in the atmosphere. So, in order to quantitatively evaluated the color change of each crystal, UV–vis absorption spectra measurements in solid

state was performed (Fig. 4-8a, c). Prior to the optical measurements, which use the powder samples, the vapochromic behaviors with structural changes of the polycrystalline powder samples were confirmed by powder XRD measurements (Fig. 4-7). Visible-light absorption edges of the orange crystal **4-Zn** and yellow crystals, **4-Zn·H₂O** and **4-Zn·2MeOH**, were estimated to be 2.29 eV (541 nm), 2.41 eV (514 nm), and 2.45 eV (506 nm), respectively. A blue shift of the absorption edge (0.12–0.16 eV) upon methanol or water vapor absorption was observed, which is consistent with the visually observed color changes. The author also evaluated the photoluminescence properties of these crystals. Significantly, a blue shift was observed in the photoluminescence spectra (0.10-0.14 eV) for both **4-Zn·H₂O** and **4-Zn·2MeOH** (Fig. 4-8b, d), similar to the UV–vis absorption spectra. The apparent color changed from red to yellowish-orange (Fig. 4-8b). These experimental data demonstrate that crystal **4-Zn** is a novel vapochromic material having both visible-light absorption and photoluminescence changes when exposed to methanol or water sorption with reversible SCSC transformations. Remarkably, this is the first report of metal-dithiolene-based vapochromic materials with SCSC transformations.
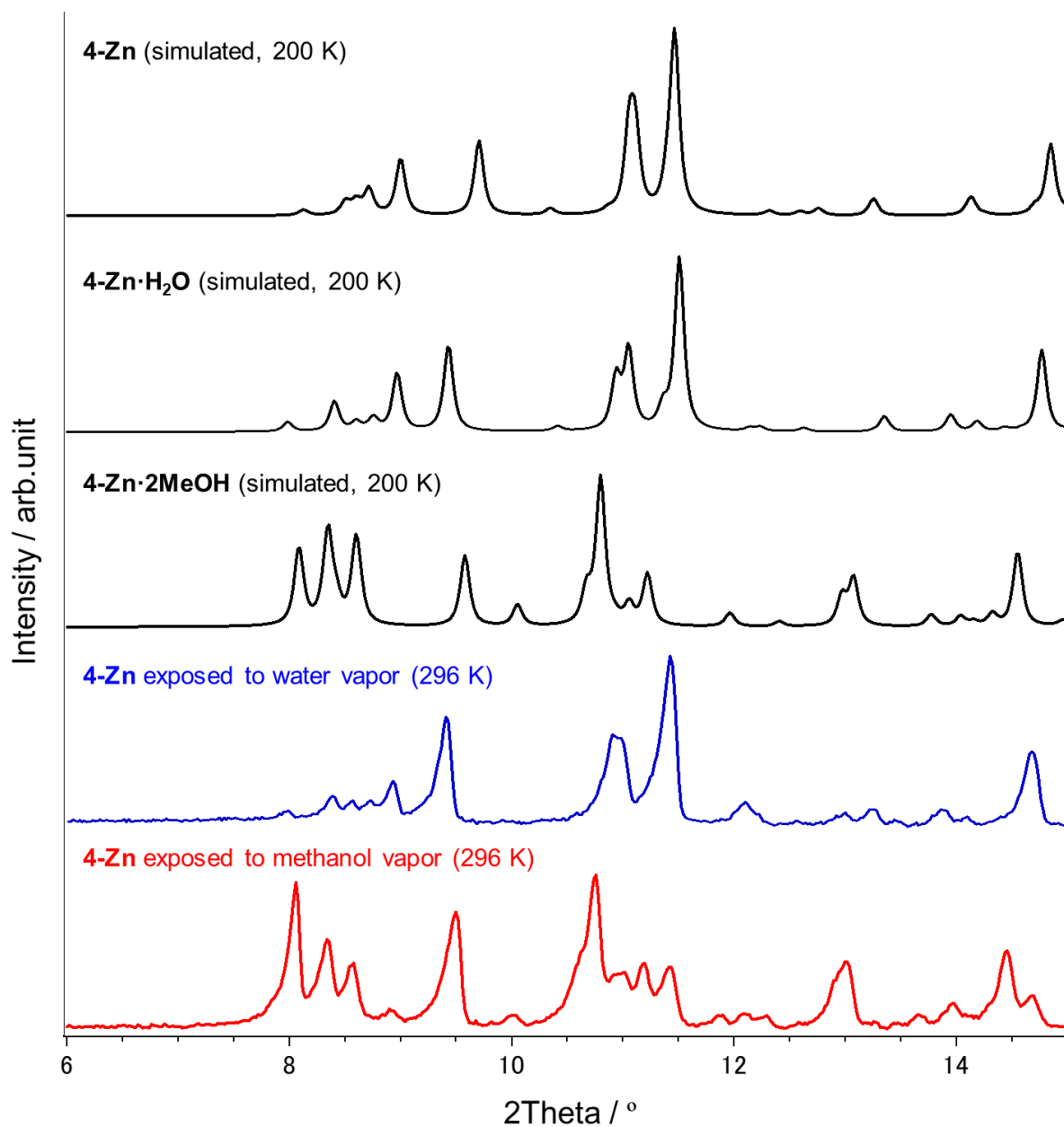
**Fig. 4-7** PXRD patterns of polycrystalline powder of **4-Zn** exposed to water or methanol vapor, and the powder patterns of **4-Zn·2MeOH**, **4-Zn**, and **4-Zn·H₂O** simulated by the structure obtained by single-crystal XRD measurements.
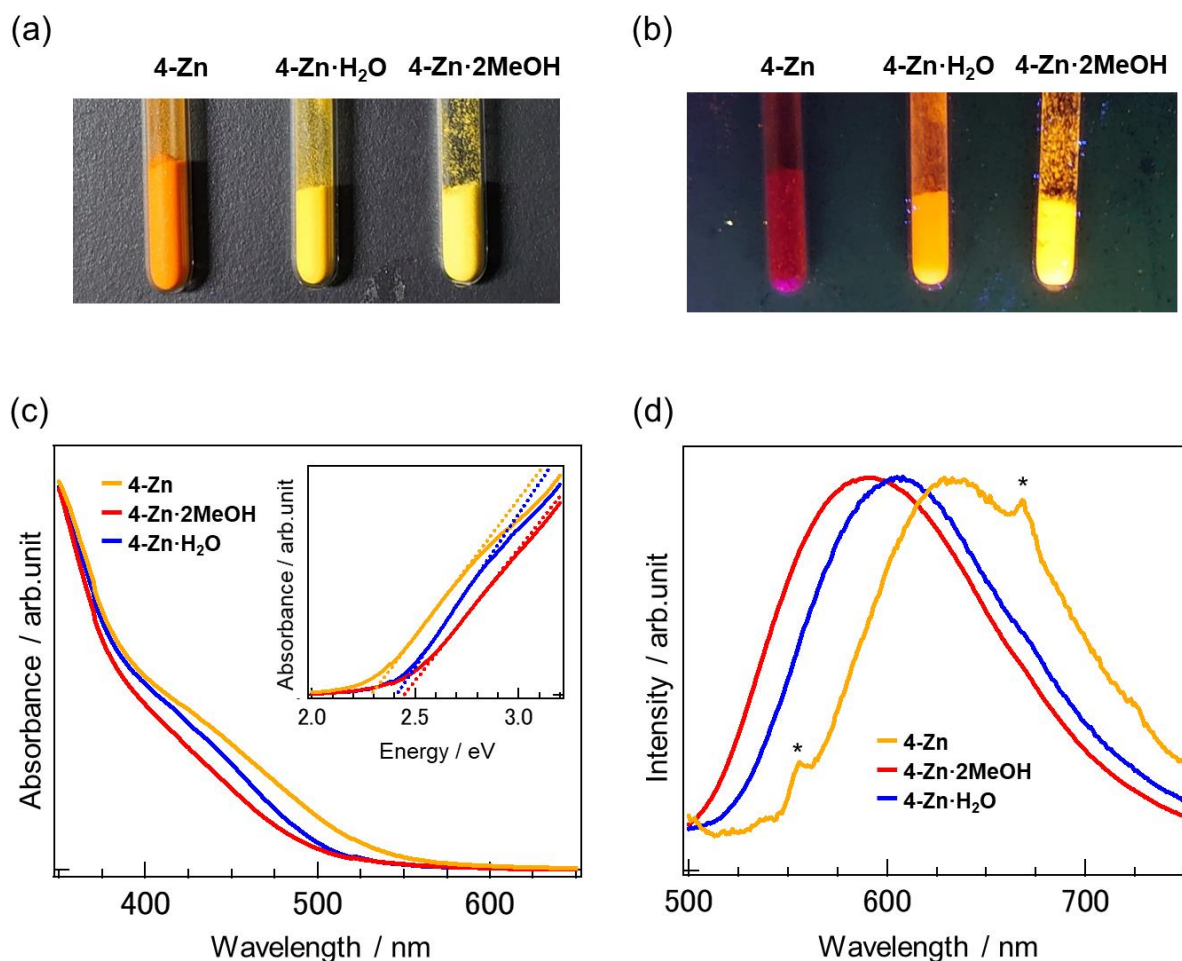
**Fig. 4-8** (a), (b) The photograph of each crystalline material under (a) visible-light and (b) the UV–light (excitation wavelength: 365 nm). (c) The UV–vis absorption spectra and (d) the photoluminescence spectra of each crystal. Asterisks in (d) denote the peaks from the background.

## 4.5 Mechanism of the vapochromism

### 4.5.1 Comparison of crystal structures and DFT calculations based on isolated molecules

In the previous Sections, the author revealed that the crystal **4-Zn** is a novel vapochromic material, and quantitatively evaluated its vapochromic behavior. Then, the author focused on the mechanism of vapochromism in this crystal. Firstly, we compared the molecular and assembled structures (molecular packing structures) of crystal **4-Zn**, **4-Zn·H₂O**, and **4-**

**Zn·2MeOH** in detail. Both **4-Zn·H₂O** and **4-Zn·2MeOH** have [S···H–O] H-bonds between the [Zn(4-mxbdt)₂]²⁻ complex and the absorbed vapor molecules (Fig. 4-2c and 4-5b). On the other hand, significant changes in the molecular structure and arrangement of the [Zn(4-mxbdt)₂]²⁻ complexes and Ph₄P⁺ cations were observed only in the methanol sorption process (between **4-Zn** and **4-Zn·2MeOH**), whereas no such significant changes were observed in the water sorption process (between **4-Zn** and **4-Zn·H₂O**) (Fig. 4-6 and 4-9). Also, considering the no coordination of the absorbed molecules to the zinc atoms, previously reported mechanism[27] induced by the change of the coordination structure of zinc complex should be ruled out. The facts that, for methanol and water vapor sorption, the structural changes are different while the visible-light absorption and photoluminescence are almost the same, suggests that the vapochromism in this crystal is related to H-bond formation rather than the changes in molecular structure and molecular packing.
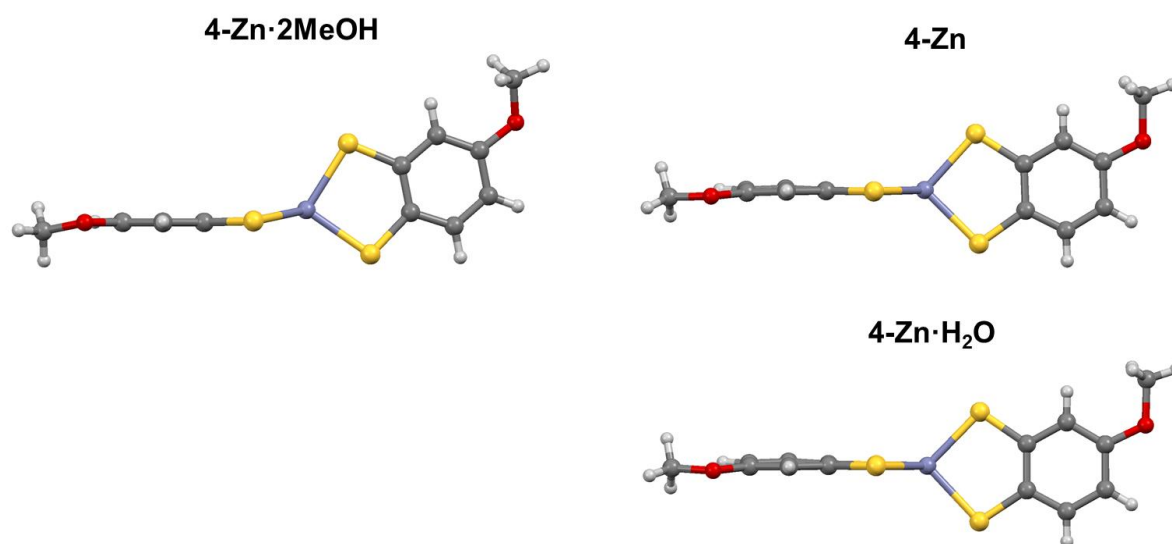


**Fig. 4-9** Changes in molecular structures of [Zn(4-mxbdt)₂]²⁻ complex in **4-Zn·2MeOH**, **4-Zn**, and **4-Zn·H₂O**.

Furthermore, the author calculated the molecular orbitals of an isolated $[Zn(4\text{-mxbdt})_2]^{2-}$ complex in **4-Zn·2MeOH**, **4-Zn**, and **4-Zn·H₂O** based on the atomic coordinates of the zinc complex in each crystal structure obtained by the single-crystal XRD measurements without structural optimization. Energies and distribution of molecular orbitals were shown in Fig. 4-10. As shown in Fig. 4-10b, the distributions of HOMO-1 and HOMO were similar to LUMO and LUMO+1, respectively. As will be mentioned later, the transitions attributed to visible-light absorption correspond mainly to "HOMO−1 to LUMO" and "HOMO to LUMO+1". The transition energies between these orbitals were 2.68–2.70 eV, 2.67–2.71 eV, and 2.65–2.66 eV for **4-Zn**, **4-Zn·H₂O**, and **4-Zn·2MeOH**, respectively (Fig. 4-10a), which indicated a slight red shift, inconsistent with the experimental observations. This result clearly shows that the calculation model of an "isolated" molecule, which has often been employed to discuss the mechanism in previous research, cannot explain the observed blue shift and the mechanism of vapochromism in these crystals.

Therefore, DFT calculations that consider crystalline solid states, taking into account intermolecular interactions, such as H-bonding, are essential to elucidate the mechanism of vapochromism in this crystal. The first-principles calculation software "OpenMX" enabled us to carry out such crystalline solid-state based theoretical calculations in the next section.[47,48,50,51]
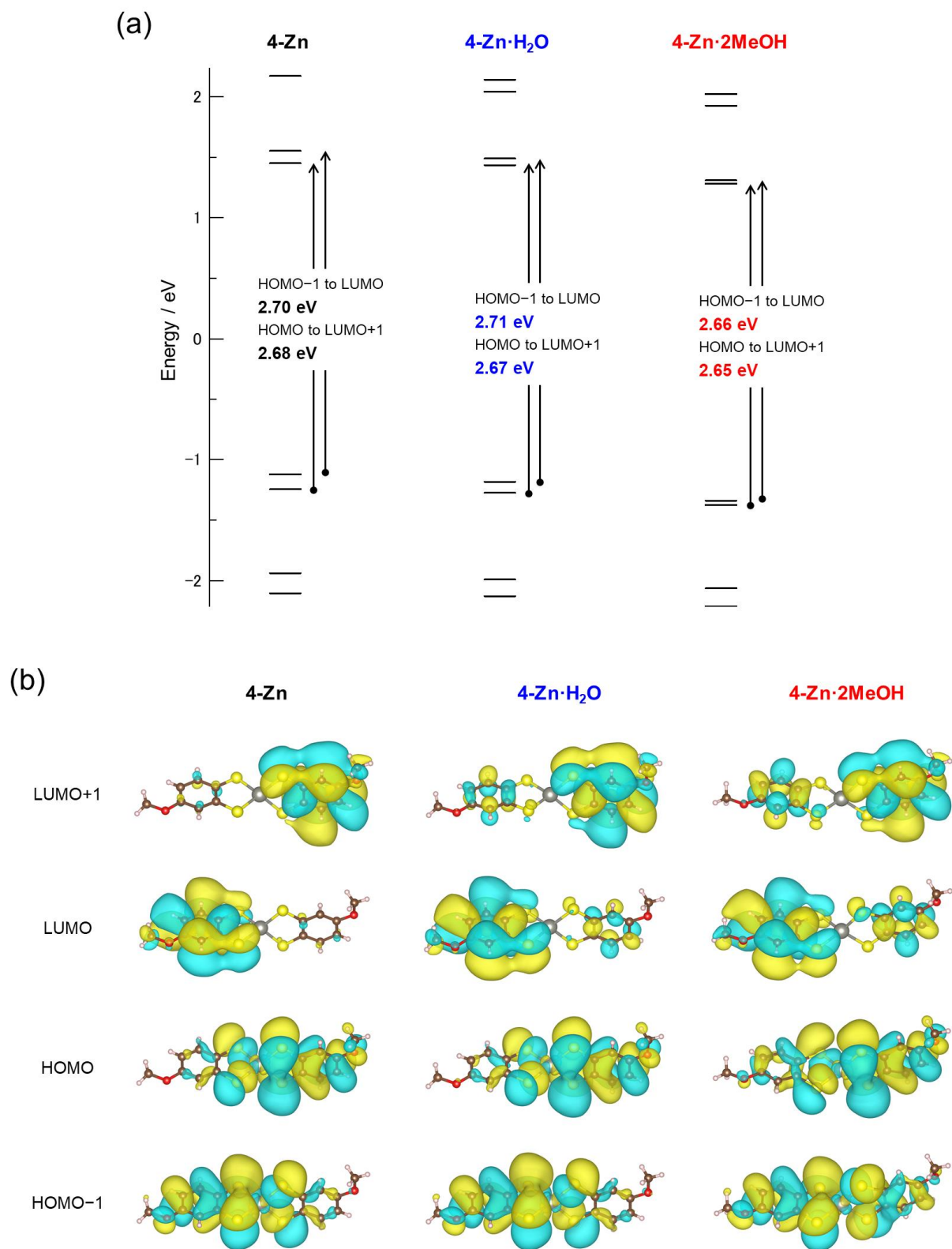
**Fig. 4-10** (a) Energies and (b) distributions of HOMO−1, HOMO, LUMO, and LUMO+1 of an isolated $[Zn(4\text{-mxbdt})_2]^{2-}$ complex molecule in **4-Zn**, **4-Zn·H₂O**, and **4-Zn·2MeOH**.

**4.5.2 Optical absorption simulated by DFT calculations on the crystals**

DFT calculations based on the experimentally observed crystal structures using OpenMX software revealed the mechanism of the vapochromism induced by H-bond formation in these crystals. First, the author confirmed the influence of vapor-sorption-induced changes in the molecular structure and arrangement on the electronic structures in a crystalline solid state (Fig. 4-6 and 4-9). This was done by comparing the calculated absorption spectra based on the real crystal structure "**4-Zn**" and hypothetical crystal structures "**4-Zn·2MeOH** without 2MeOH" and "**4-Zn·H₂O** without H₂O" (Fig. 4-11; see also experimental section). These hypothetical crystal structures were obtained by removing absorbed methanol or water molecules from **4-Zn·2MeOH** or **4-Zn·H₂O**, respectively, while maintaining the molecular structures and arrangements of $Ph_4P^+$ cations and $[Zn(4\text{-mxbdt})_2]^{2-}$ complexes. Here, the intensities of absorption in the crystals were estimated from an average of diagonal terms of the absorption coefficient tensor, $\alpha_{xx}$, $\alpha_{yy}$, and $\alpha_{zz}$. The crystal orbitals related to visible-light absorption in each crystal were determined by comparison of a real part of the optical conductivity ($\propto$ absorption coefficient) resolved for each k point and crystal orbital pair. The unit cells are sufficiently large so that interactions of each crystal orbital among unit cells are small. Thus, calculated absorption spectra can be attributed by just considering transitions between crystal orbitals at Γ point. In this case, the intensity of the absorption spectra is proportional to the magnitude of a real part of the optical conductivity, and we need to consider only the real part of the wave functions.

The crystal orbital pairs for the transitions contributed to visible-light absorption peaks (around 3.0 eV) and optical conductivities in order of magnitude are listed in the tables in the Appendix section. The calculated absorption spectra are shown in Fig. 4-11 (dashed lines). The results clearly show that the absorption edges do not change significantly. Even "**4-Zn·2MeOH** without 2MeOH", in which significant changes in molecular structure and arrangement were observed, showed only a slight red shift (Fig. 4-11a, shown by the red dashed line). However,

the calculated absorption spectra based on the real crystal structures "**4-Zn·2MeOH**" and "**4-Zn·H₂O**" containing absorbed vapor molecules showed blue shifts of approximately 0.14 and 0.08–0.15 eV, respectively (red, pink, and blue solid lines in Fig. 4-11, respectively), which is consistent with the experimental results (0.12 eV and 0.16 eV, Fig. 4-8c). These results indicate that the origin of the vapochromism in this crystal is not structural changes (i.e., changes in molecular structures and molecular packing) but intermolecular interactions via H-bonds between the $[Zn(4\text{-}mxbdt)_2]^{2-}$ complex and the absorbed vapor molecules.
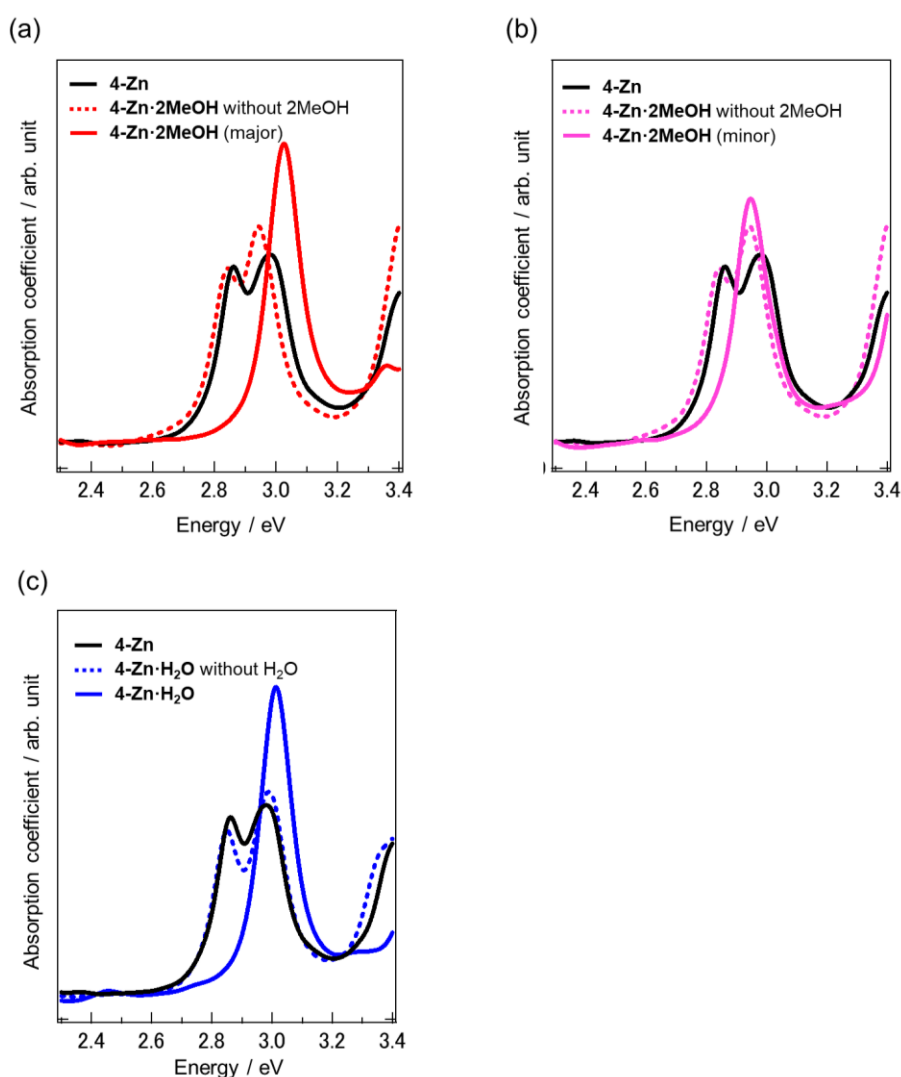


**Fig. 4-11** (a)–(c) The calculated absorption spectra of each model. Black, red, pink, and blue solid lines show the absorption spectra calculated from the real crystal structures of **4-Zn**, **4-Zn·2MeOH** (major), **4-Zn·2MeOH** (minor), and **4-Zn·H₂O**, respectively. The colored dashed lines show absorption spectra calculated from the hypothetical crystal structures.

### 4.5.3 Effect of hydrogen bond on electronic structures

To investigate the influence of H-bond formation on the electronic structure, the author calculated the differential electron-density maps of the crystals in the presence or absence of the vapor molecules (Fig. 4-12, see also "First-principles calculations" in Section 4.2). The differential electron density maps that show the degree of electron transfer caused by the formation of H-bonds were drawn by subtracting the sum of the total electron density of the hypothetical crystal structure ("**4-Zn·H₂O** without $H_2O$", "**4-Zn·2MeOH** (minor) without 2MeOH" or "**4-Zn ·2MeOH** (major) without 2MeOH") and absorbed molecules in the crystals ("$H_2O$ in **4-Zn·H₂O**", "MeOH-1,2 in **4-Zn·2MeOH** (minor)" or "MeOH-1,3 in **4-Zn·2MeOH** (major)") from the total electron density of the actual crystal structure (**4-Zn·H₂O**, **4-Zn·2MeOH** (minor), or **4-Zn·2MeOH** (major)). In both the vapor absorption processes, the electron density near the S atoms on the $[Zn(4\text{-mxbdt})_2]^{2-}$ complex decreased, and that on the absorbed vapor molecules as well as that between the zinc complex and the vapor molecules increased with H-bond formation. This suggests that electron transfer from the $[Zn(4\text{-mxbdt})_2]^{2-}$ complex to the absorbed vapor molecules occurred via the H-bond formation.
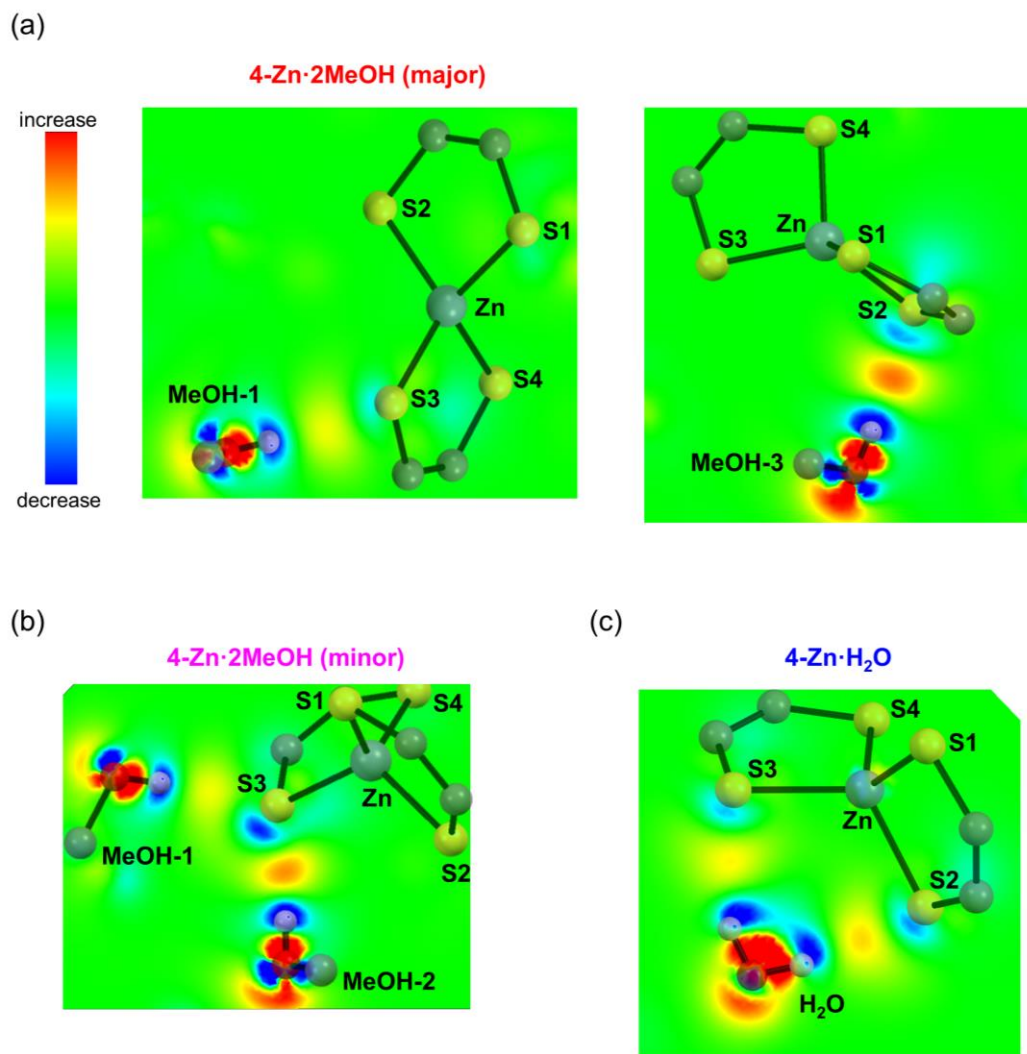
**Fig. 4-12** (a)–(c): Differential electron density map of **4-Zn·2MeOH** (major), **4-Zn·2MeOH** (minor), and **4-Zn·H₂O**. Red/blue region shows increase/decrease of electron density with H-bond formation. Only the selected atoms in the zinc complex are displayed for clarity. The differential electron density maps and crystal orbital distribution were visualized by VESTA.[55]

Moreover, Mulliken population analysis[54] indicated 0.23–0.26 and 0.19 electrons were transferred from the $[Zn(4\text{-mxbdt})_2]^{2-}$ complex to methanol or water molecules, respectively. Note that the number of transferred electrons on the S atoms taking part in the H-bonds was significant (Table 4-2). Therefore, these results indicate that the H-bond formation causes electron transfer.

**Table 4-2** The number of totals transferred electrons of each molecule, and partially transferred electrons on each S atom on the zinc complex in **4-Zn·2MeOH** and **4-Zn·H₂O** calculated by Mulliken population analysis.[54] See also experimental section for details.

| Crystal | Component | The number of transferred electrons (electrons/molecule) | S1 | S2 | S3 | S4 |
|---|---|---|---|---|---|---|
| **4-Zn·H₂O** | $[Zn(4\text{-mxbdt})_2]^{2-}$ | −0.189 | −0.003 | −0.053 | −0.047 | −0.006 |
| | H₂O | 0.205 | – | – | – | – |
| **4-Zn ·2MeOH** (minor) | $[Zn(4\text{-mxbdt})_2]^{2-}$ | −0.234 | −0.004 | −0.011 | −0.093 | −0.007 |
| | MeOH-1 (ordered) | 0.143 | – | – | – | – |
| | MeOH-2 (disordered)* | 0.106 | – | – | – | – |
| **4-Zn·2MeOH** (major) | $[Zn(4\text{-mxbdt})_2]^{2-}$ | −0.262 | −0.008 | −0.063 | −0.050 | −0.003 |
| | MeOH-1 (ordered) | 0.161 | – | – | – | – |
| | MeOH-3 (disordered)* | 0.112 | – | – | – | – |

*The occupancy of disordered methanol molecules (MeOH-2 and MeOH-3) was assumed to be 1.00 in this calculation.

Then, how does the electron transfer through the H-bond formation relate to modulation of the crystal orbital energies, resulting in the blue shift observed in visible-light absorption and emission? To elucidate this mechanism, the author focused on the distribution of the crystal orbitals related to the transition attributable to visible-light absorption (Fig. 4-13, -14, -15, -16, -17). The author identified the transitions involved in absorption in Fig. 4-11 to be α [HOCO−7 to HOCO−4] to γ [LUCO+64 to LUCO+67] and β [HOCO−3 to HOCO] to δ [LUCO+68 to LUCO+71] crystal orbital groups (HOCO: highest occupied crystal orbital, LUCO: lowest

unoccupied crystal orbital, see "First-principles calculations" in Section 4.2 and Table 4-3). Here, due to the existence of the crystallographically equivalent four $[Zn(4\text{-mxbdt})_2]^{2-}$ complexes, four crystal orbitals having almost the same distributions and energy levels degenerated. The author named each four-fold degenerated crystal orbital groups as crystal orbital groups α, β, γ, and δ in order of increasing energy level of **4-Zn**. The energies of each crystal orbital group are estimated from the average of the four crystal orbital energies (Table 4-3). Considering this degeneracy, the transitions listed above are attributed to two kinds of transitions between the same crystal orbital groups: α to γ and β to δ.

**Table 4-3** Energies of crystal orbitals of α (HOCO−7 to HOCO−4), β (HOCO−3 to HOCO), γ (LUCO+64 to LUCO+67), and δ (LUCO+68 to LUCO+71) in each crystal.

| Crystals | **4-Zn** | **4-Zn·H₂O** | **4-Zn·2MeOH** (minor) | **4-Zn·2MeOH** (major) |
|---|---|---|---|---|
| Crystal orbitals | Energy (eV) | Energy (eV) | Energy (eV) | Energy (eV) |
| HOCO−7 | −3.76345937 | −3.96134027 | −4.02732 | −4.09177 |
| HOCO−6 | −3.75930629 | −3.9590735 | −4.02374 | −4.08713 |
| HOCO−5 | −3.75666102 | −3.95557378 | −4.0136 | −4.08271 |
| HOCO−4 | −3.75586814 | −3.95506278 | −4.0135 | −4.08233 |
| Average (α) | −3.7588237 | −3.95776258 | −4.01954 | −4.08598 |
| HOCO−3 | −3.57027136 | −3.76997006 | −3.92155 | −3.93133 |
| HOCO−2 | −3.56592376 | −3.76777623 | −3.9197 | −3.92969 |
| HOCO−1 | −3.55466646 | −3.7583355 | −3.91729 | −3.92087 |
| HOCO | −3.5523635 | −3.75665251 | −3.91653 | −3.92019 |
| Average (β) | −3.56080627 | −3.76318358 | −3.91877 | −3.92552 |
| LUCO+64 | −0.91431822 | −0.95650044 | −1.08336 | −1.07434 |
| LUCO+65 | −0.91118945 | −0.95491357 | −1.07044 | −1.06703 |
| LUCO+66 | −0.90750922 | −0.95330274 | −1.07027 | −1.06262 |
| LUCO+67 | −0.90178345 | −0.95053919 | −1.06986 | −1.05126 |
| Average (γ) | −0.90870008 | −0.95381398 | −1.07348 | −1.06381 |
| LUCO+68 | −0.63176918 | −0.81003675 | −1.00706 | −0.94296 |
| LUCO+69 | −0.59571851 | −0.78422894 | −0.99679 | −0.93528 |
| LUCO+70 | −0.5917281 | −0.78017894 | −0.99407 | −0.93391 |
| LUCO+71 | −0.54730391 | −0.74831665 | −0.98378 | −0.92928 |
| Average (δ) | −0.59162993 | −0.78069032 | −0.99542 | −0.93536 |
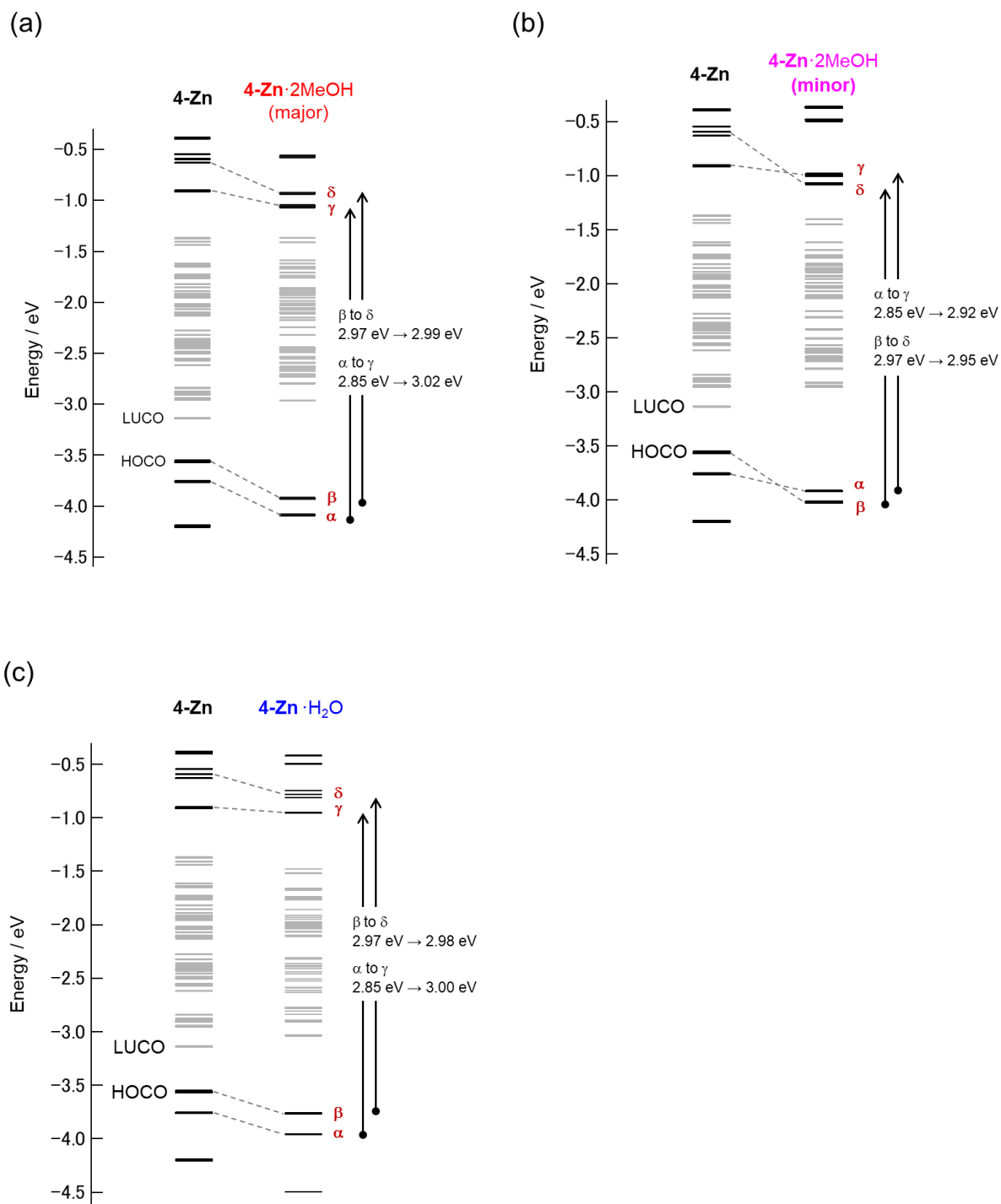
**Fig. 4-13** (a)–(c): Crystal orbital energies of **4-Zn·2MeOH** (major), **4-Zn·2MeOH** (minor), and **4-Zn·H₂O.** Crystal orbitals from −3.2 eV to −1.3 eV (left; gray lines) are mostly on Ph₄P⁺ cation molecules.
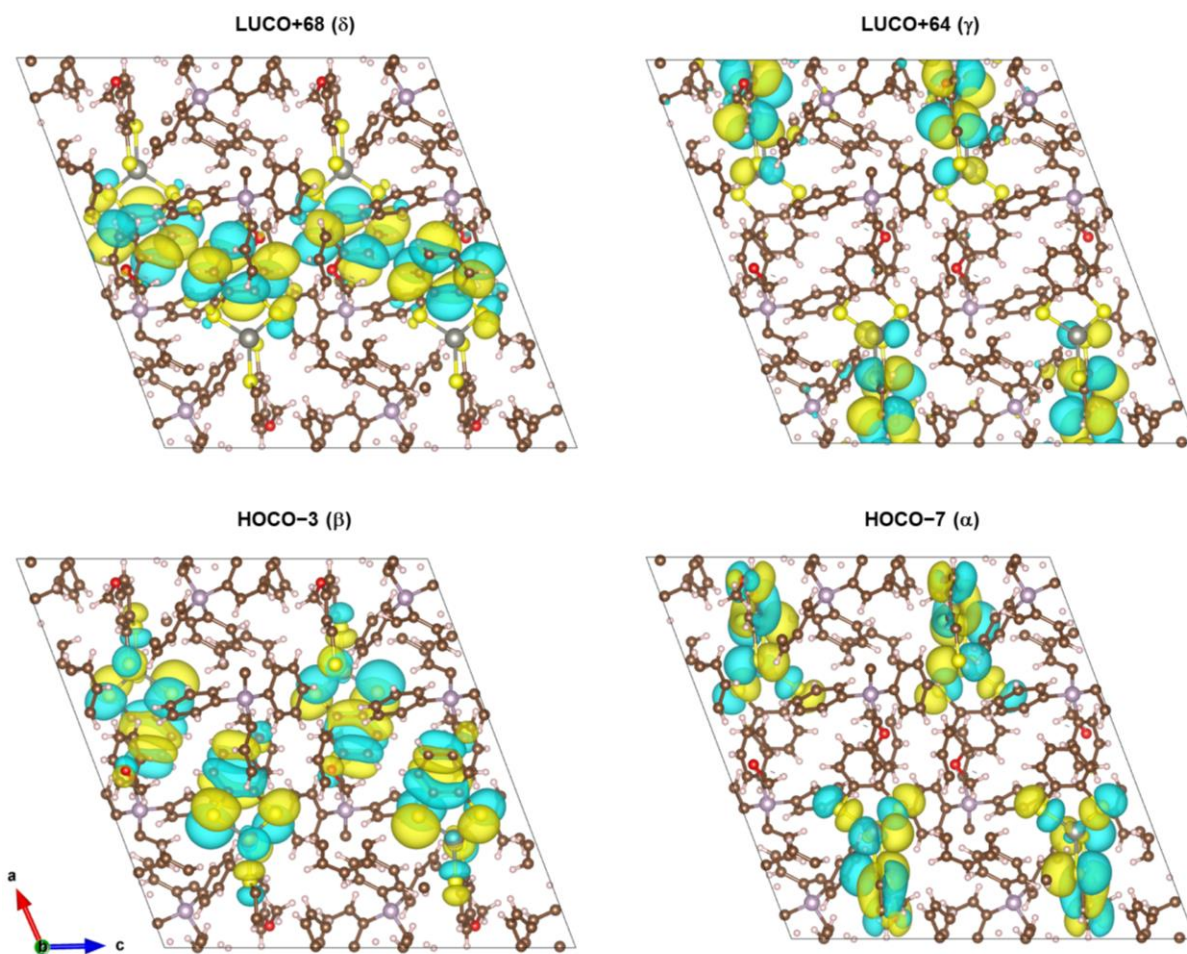
**Fig. 4-14** Distributions of HOCO−7, HOCO−3, LUCO+64, and LUCO+68 in **4-Zn** (α: HOCO−7 to HOCO−4, β: HOCO−3 to HOCO, γ: LUCO+64 to LUCO+67, δ: LUCO+68 to LUCO+71).
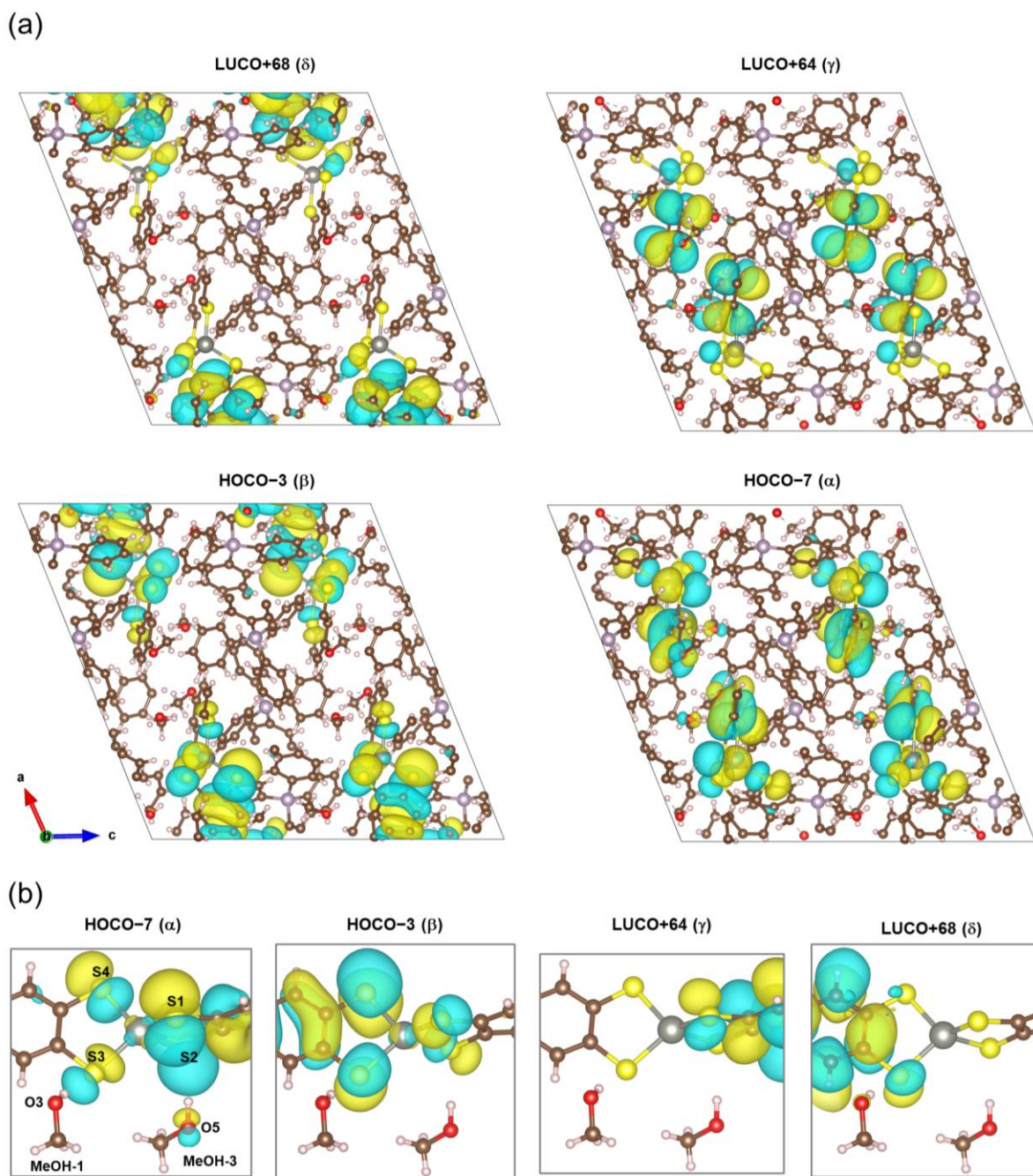
**Fig. 4-15** (a) Distributions of HOCO−7, HOCO−3, LUCO+64, and LUCO+68 in **4-Zn·2MeOH** (major) (α: HOCO−7 to HOCO−4, β: HOCO−3 to HOCO, γ: LUCO+64 to LUCO+67, δ: LUCO+68 to LUCO+71). (b) Interactions between molecular orbitals of [Zn(4-mxbdt)$_2$]$^{2-}$ complex and methanol molecule in the H-bonding part.
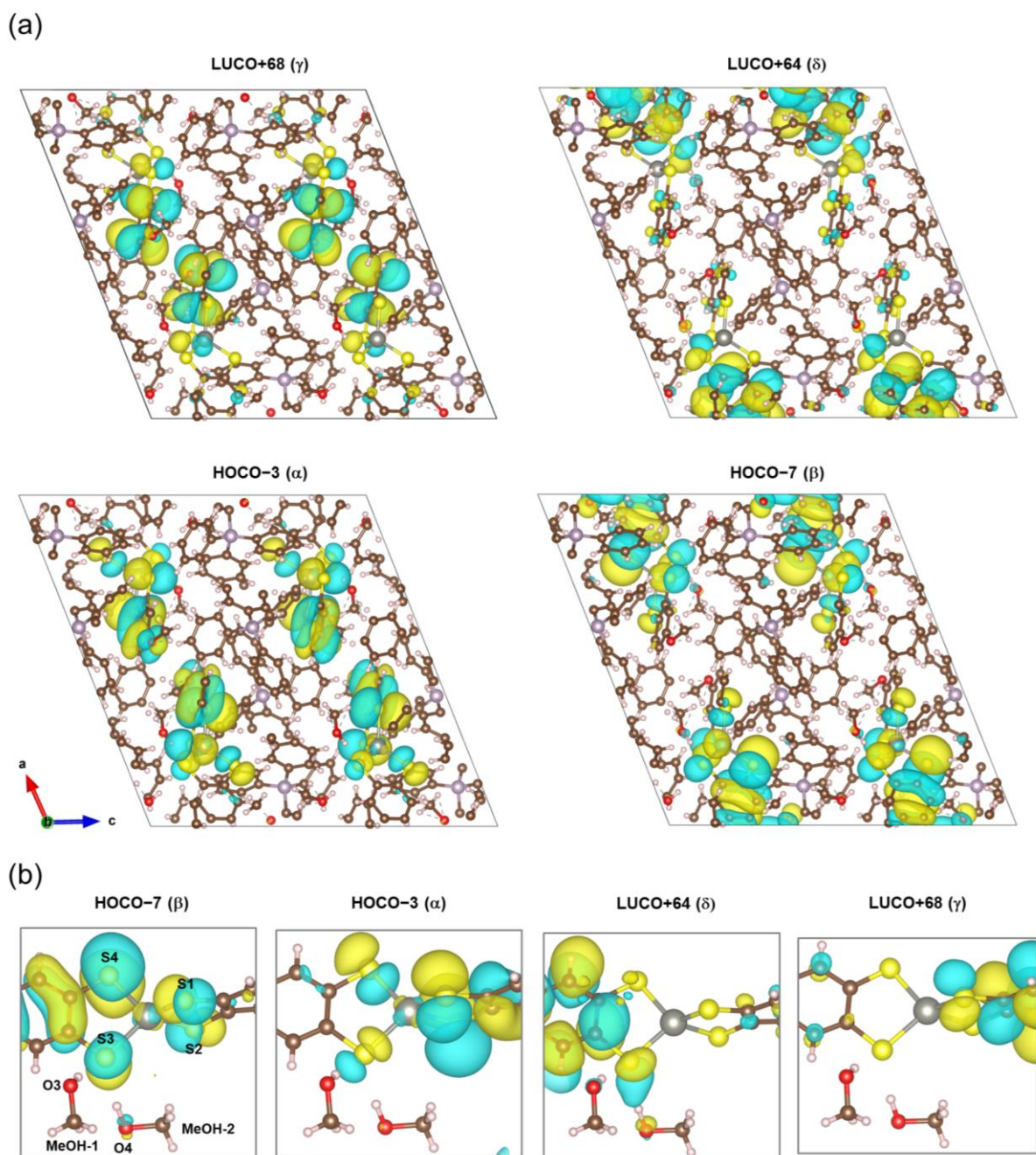
**Fig. 4-16** (a) Distributions of HOCO−7, HOCO−3, LUCO+64, and LUCO+68 in **4-Zn·2MeOH** (minor) (β: HOCO−7 to HOCO−4, α: HOCO−3 to HOCO, δ: LUCO+64 to LUCO+67, γ: LUCO+68 to LUCO+71). (b) Interactions between molecular orbitals of [Zn(4-mxbdt)₂]²⁻ complex and methanol molecule in the H-bonding part.
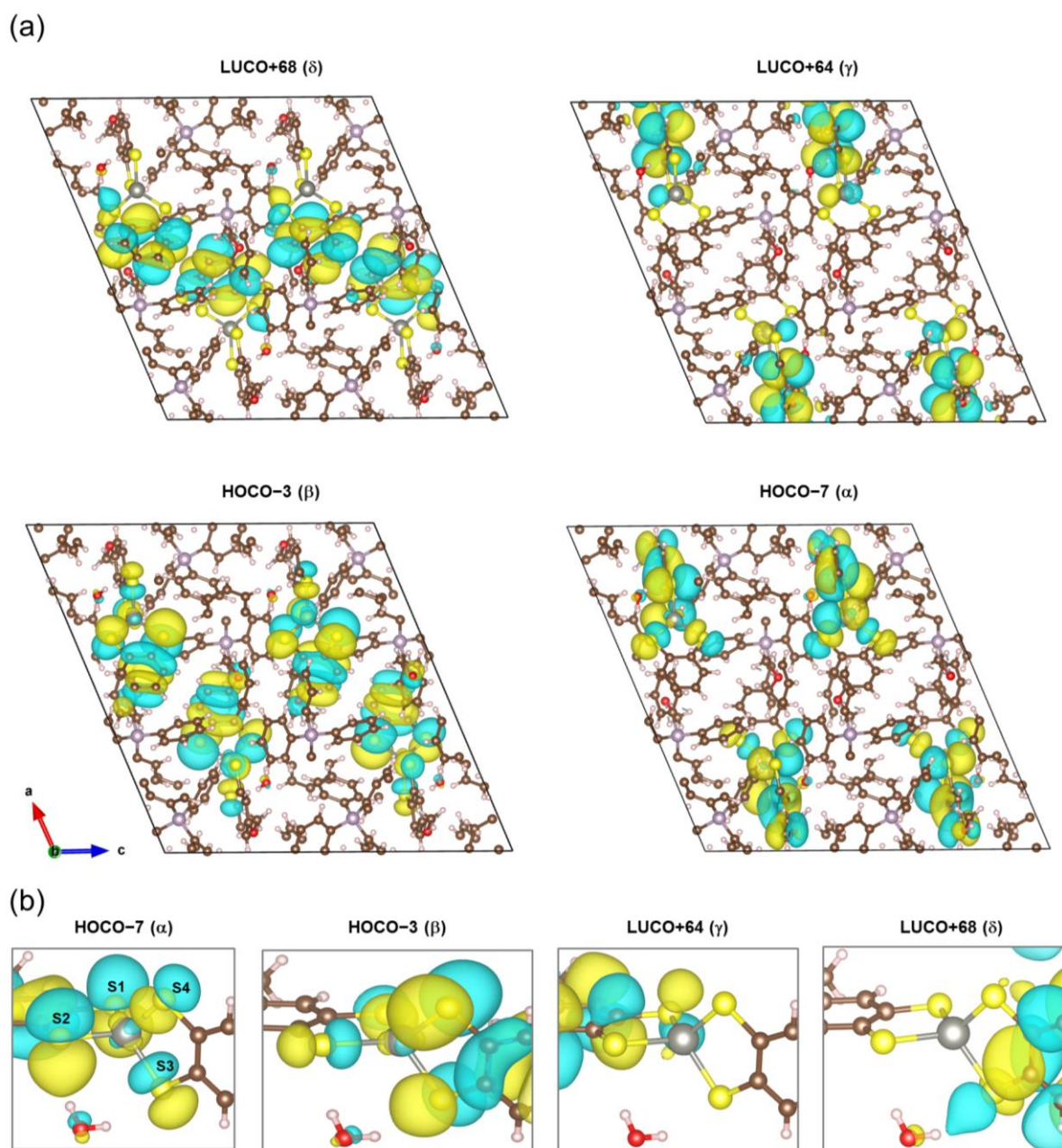
**Fig. 4-17** (a) Distributions of HOCO−7, HOCO−3, LUCO+64, and LUCO+68 in **4-Zn·H₂O** (α: HOCO−7 to HOCO−4, β: HOCO−3 to HOCO, γ: LUCO+64 to LUCO+67, δ: LUCO+68 to LUCO+71). (b) Interaction between molecular orbitals of [Zn(4-mxbdt)$_2$]$^{2-}$ complex and water molecule in the H-bonding part.

Judged from the orbital shapes, the $\alpha$ to $\gamma$ and $\beta$ to $\delta$ transitions are not attributed to intermolecular charge-transfer absorption between the zinc complex and the absorbed vapor molecules. In all the crystals, these crystal orbitals were mainly distributed on the [Zn(4-mxbdt)$_2$]$^{2-}$ complex, especially on the S atoms. Note that these isolated crystal orbitals on the zinc complex and absorbed vapor molecules also demonstrated that the vapochromic behavior is not related to the modulation of assembled structures nor intermolecular interactions between the zinc complexes. In addition, the asymmetric structure of the [Zn(4-mxbdt)$_2$]$^{2-}$ complex derived from the ligand structure and the conformation of methoxy groups make the orbital shape asymmetric (Fig. 4-13, 4-15b, 4-16b, and 4-17b). In **4-Zn·2MeOH** (major), energy gaps for both $\alpha$ to $\gamma$ and $\beta$ to $\delta$ transitions increased ($\alpha$ to $\gamma$: 2.85 eV to 3.02 eV, $\beta$ to $\delta$: 2.97 eV to 2.99 eV), where the $\alpha$ and $\beta$ orbitals were more stabilized than $\gamma$ and $\delta$ (Fig. 4-13 and Table 4-3). This is because of the fact that the occupied orbital groups ($\alpha$ and $\beta$) have a large weight on the H-bonding S atoms, on which the largest changes in the number of electrons were estimated by Mulliken population analysis, compared with the unoccupied orbital groups ($\gamma$ and $\delta$) (Fig. 4-13, 4-15b, and 4-17b and Table. 4-2).

Here, the phase of the wave function in the H-bonding part was the same, and the shape of the crystal orbital on the S atom was deformed toward the H atom (Fig. 4-15b, 4-16b, and 4-17b). These show that the orbitals of the absorbed vapor molecule and the [Zn(4-mxbdt)$_2$]$^{2-}$ complex were hybridized to form bonding orbitals; the crystal orbitals are derived from the hybridization of the frontier orbitals (HOMO−1, HOMO, LUMO, and LUMO+1) of the [Zn(4-mxbdt)$_2$]$^{2-}$ complex with the LUMO of the absorbed vapor molecules at higher energies (Fig. 4-18). Here, focusing on the distribution of HOMO and LUMO of the isolated methanol molecules (Fig. 4-18b), the HOMO forms $\pi$-bonding like interaction, whereas LUMO forms $\sigma$-bonding like interaction with surrounding orbitals. Because the shapes around [S···H−O]-type H-bonds were $\sigma$-type bonds in the crystals (Fig. 4-15b, 4-16b, and 4-17b), $\alpha$, $\beta$, $\gamma$, and $\delta$ correspond to the bonding orbitals between HOMO ($\alpha$ and $\beta$) or LUMO ($\gamma$ and $\delta$) of the [Zn(4-

mxbdt)$_2$]$^{2-}$ complex and LUMO of the absorbed vapor molecules, where the hybridization stabilizes the orbital energies of the [Zn(4-mxbdt)$_2$]$^{2-}$ complex. This hybridization leads to the above-mentioned electron transfer to stabilize both the $\alpha/\beta$ and $\gamma/\delta$ orbitals, which is consistent with the electron transfer indicated by Mulliken population analyses and the calculated differential electron density maps. However, $\alpha$ and $\beta$, which have larger weight on the S atoms, are more stabilized than $\gamma$ and $\delta$ because of the stronger orbital hybridization and the decrease in electron density resulting from electron transfer. In addition, the local electrostatic potentials caused by the [O$^{\delta-}$–H$^{\delta+}$] part of the absorbed vapor molecules, that is, the crystal field of the absorbed molecules, should cause further differences in the degree of orbital stabilization. Therefore, the author concluded that electron transfer through orbital hybridization as well as the crystal field of the absorbed vapor molecules by H-bond formation is the origin of the blue shift of visible-light absorption; such a vapochromism mechanism based on electron transfer through H-bond formation has never been demonstrated before.
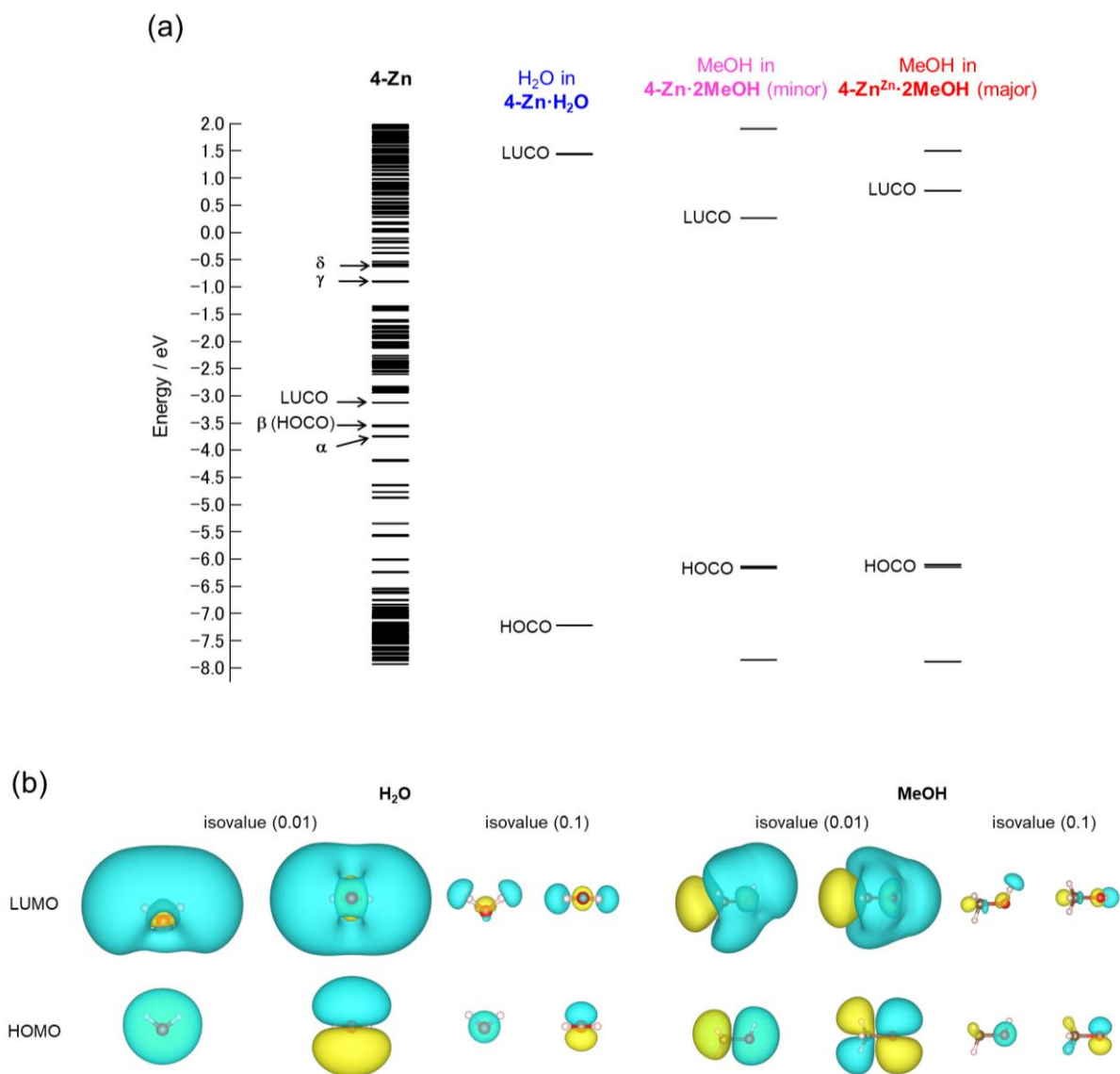
**Fig. 4-18** (a) Energies of the frontier orbitals of the $[Zn(4\text{-mxbdt})_2]^{2-}$ complexes and the vapor molecules in each crystal. (b) Distributions of the frontier orbitals of the vapor molecules (methanol: MeOH-1 in **4-Zn·2MeOH**, water: $H_2O$ in **4-Zn·H₂O**).

A similar blue shift and stabilization of crystal orbital energies in **4-Zn·H₂O** ($\alpha$ to $\gamma$: 2.85 eV → 3.00 eV, $\beta$ to $\delta$: 2.97 eV → 2.98 eV) further supports the validity of this mechanism (Fig. 4-13c). The demonstrated mechanism was also applied to vapochromism in **4-Zn·2MeOH** (minor). The transition of $\beta$ to $\delta$ showed a red shift (2.97 eV to 2.95 eV) and from $\alpha$ to $\gamma$ a blue shift (2.85 eV to 2.92 eV). As a result, the transition with the lowest energy showed a blue shift

in the visible-light absorption (2.85 eV to 2.92 eV, Fig. 4-13b). Considering the orbital shapes in detail, the author found that the energies of β and δ in **4-Zn·2MeOH** (minor) were exchanged with those of α and γ, respectively (Fig. 4-16). This reversal in **4-Zn·2MeOH** (minor) can be understood as a result that the β/δ orbitals having a large weight on the S3 atom are largely stabilized more than α/γ by the two H-bonds to the S3 atom, while, in the other crystal, only one H-bond to the S3 atom exists and the other one is attached to the S2 atom.

In addition, the above-mentioned discussion was applied to the blue shift in the photoluminescence property. In these crystals, the author expects that a change in the molecular structure of the $[Zn(4\text{-mxbdt})_2]^{2-}$ complex in both the ground and excited states are significantly limited in the solid-state. Furthermore, the structural change does not significantly affect the energies of these states, as suggested by the calculations on the hypothetical crystals (Fig. 4-11). Thus, the author concluded that the blue shift in the photoluminescence property could also be understood based on the same mechanism.

Finally, comparing the O-H bond length of the vapor molecules before and after absorption (H-bond formation), in these crystal structures of **4-Zn·2MeOH** (major), **4-Zn·2MeOH** (minor), and **4-Zn·H₂O** with the proton in H-bonds optimized by the DFT calculations, the OH bond lengths are slightly extended compared with that of isolated vapor molecules optimized by the DFT calculations ($d_{O-H}$ (isolated) = 0.968 or 0.970 Å, $d_{O-H}$ (in crystal) = 0.985–0.990Å). From this result, the switching of optical properties can be described to be coupled with the local dynamics of the H-bonding proton. This indicates that the optical property changes can be related to the acidity, $pK_a$, of the absorbed vapor molecules. However, the relationship has not been revealed due to the differences in compositions and the H-bond manners of the absorbed vapor molecules (methanol and water) in **4-Zn·2MeOH** and **4-Zn·H₂O**. Systematic studies of optical property changes using various protonic vapor molecules (e.g., HCl and acetic acid) will demonstrate the relationship between optical property changes and p$K$a. In addition, transient visible-light absorption and/or photoluminescence property measurements with

irradiation of IR light, which activates the vibrational motion of protons in the O–H···S H-bonds, will directly demonstrate the correlation between the optical properties and the position/dynamics of protons in the H-bonds.

## 4.6 Key factors for realization of the vapochromism with reversible single-crystal-to-single-crystal transformation

Finally, the author discusses the key factors in realizing reversible SCSC transformation and vapochromism with the sorption of methanol or water molecules from the viewpoint of the molecular designs of the $[Zn(4\text{-}mxbdt)_2]^{2-}$ complex. The vapochromism in this crystal was due to the differences in the degree of stabilization of the crystal orbitals (Fig. 4-13). This was caused by the characteristic asymmetric molecular orbital shape on the S atoms originating from the asymmetric structure of the $[Zn(4\text{-}mxbdt)_2]^{2-}$ complex, that is, singly methoxy-group-substituted ligands and the difference in crystallographic conformation of the methoxy groups (Fig. 4-3, -15b, -16b, and 17b). In combination with these features, the proton-accepting abilities of the anionic S atoms on the dithiolene ligand and the unique properties of metal-dithiolene complexes, the "frontier orbitals largely distributed on the S atom" and "narrow HOMO-LUMO gap", realized the new mechanism.[56,57] Moreover, instability of the crystal structure of **4-Zn** and intermolecular spaces led to the reversible SCSC transformations with the absorption of methanol and water molecules. This is due to the tetrahedral coordination structure of the $[Zn(4\text{-}mxbdt)_2]^{2-}$ complex and the bulky spherical $Ph_4P^+$ cation as well as the rigidity of the constituent molecules, resulting in a loosely packed structure. All these features mutually realized the first vapochromic metal-dithiolene-based crystal with SCSC transformation based on the new mechanism of vapochromism induced by electron transfer coupled with H-bond formation.

## 4.7 Conclusion

In conclusion, a novel mechanism of vapochromism based on the intermolecular electron transfer coupled with H-bond formation was realized in the newly obtained zinc dithiolene complex crystal **4-Zn**. The crystal **4-Zn** exhibited vapochromic behavior both in visible-light absorption and photoluminescence properties on exposure to methanol or water sorption with reversible SCSC transformation. The absorbed vapor molecules formed H-bonds with S atoms in the dithiolene skeleton in both cases, whereas only **4-Zn·2MeOH** showed a slight molecular structure change of zinc complex. From the first-principles calculations based on the experimentally observed crystal structures, the structural change of the crystals caused almost no impact on the optical properties, and thus is not the origin of the vapochromic behavior. On the other hand, the H-bond formation induced the electron transfer from the zinc complex to the absorbed vapor molecules, which led to the vapochromism in this crystal. Importantly, this is a new mechanism of vapochromism that is intrinsically different from the previous ones based on molecular or assembled structure changes. According to the finding in this study, molecules in which frontier orbitals are significantly distributed to H-bonding parts can be promising candidates for a new class of vapochromic materials as well as other stimuli-responsive materials.[58]

This study achieved d/π electronic-state modulation coupled with H-bond formation, leading to color and photoluminescence property switching. Therefore, in this chapter, d/π electron–proton coupled functionality is successfully realized with an elucidation of the detailed mechanism by crystallographic and theoretical studies.
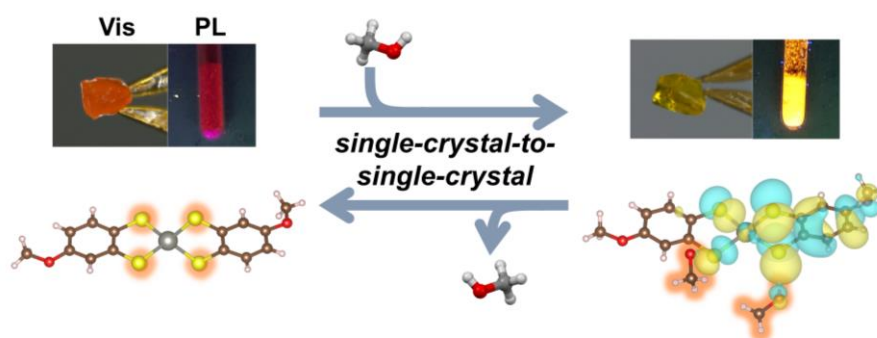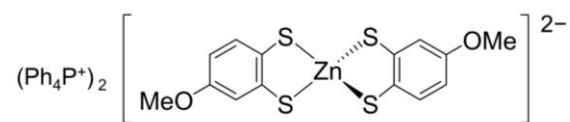
**e⁻ transfer through hydrogen-bonds**

## 4.8 References

1 L. E. Kreno, K. Leong, O. K. Farha, M. Allendorf, R. P. Van Duyne and J. T. Hupp, *Chem. Rev.*, 2012, **112**, 1105.

2 C. Wang, H. Dong, W. Hu, Y. Liu and D. Zhu, *Chem. Rev.*, 2012, **112**, 2208.

3 Z. Hu, B. J. Deibert and J. Li, *Chem. Soc. Rev.*, 2014, **43**, 5815–5840.

4 O. Sato, *Nat. Chem.*, 2016, **8**, 644.

5 S. Uji, H. Shinagawa, T. Terashima, T. Yakabe, Y. Terai, M. Tokumoto, A. Kobayashi, H. Tanaka and H. Kobayashi, *Nature*, 2001, **410**, 908.

6 F. Sawano, I. Terasaki, H. Mori, T. Mori, M. Watanabe, N. Ikeda, Y. Nogami and Y. Noda, *Nature*, 2005, **437**, 522.

7 S. Kimura, H. Suzuki, T. Maejima, H. Mori, J.-I. Yamaura, T. Kakiuchi, H. Sawa and H. Moriyama, *J. Am. Chem. Soc.*, 2006, **128**, 1456.

8 S. Niizeki, F. Yoshikane, K. Kohno, K. Takahashi, H. Mori, Y. Bando, T. Kawamoto and T. Mori, *J. Phys. Soc. Jpn.*, 2008, **77**, 073710.

9 H. Ito, M. Muromoto, S. Kurenuma, S. Ishizaka, N. Kitamura, H. Sato and T. Seki, *Nat. Commun.*, 2013, **4**, 2009.

10 S. Horiuchi, R. Kumai and Y. Tokura, *J. Am. Chem. Soc.*, 2013, **135**, 4492–4500.

11 T. Murata, Y. Morita, K. Fukui, K. Sato, D. Shiomi, T. Takui, M. Maesato, H. Yamochi, G. Saito and K. Nakasuji, *Angew. Chem. Int. Ed.*, 2004, **43**, 6343.

12 T. Murata, Y. Morita, Y. Yakiyama, K. Fukui, H. Yamochi, G. Saito and K. Nakasuji, *J. Am. Chem. Soc.*, 2007, **129**, 10837.

13 S. C. Lee, A. Ueda, H. Kamo, K. Takahashi, M. Uruichi, K. Yamamoto, K. Yakushi, A. Nakao, R. Kumai, K. Kobayashi, H. Nakao, Y. Murakami and H. Mori, *Chem. Commun.*, 2012, **48**, 8673.

14 S. C. Lee, A. Ueda, A. Nakao, R. Kumai, H. Nakao, Y. Murakami and H. Mori, *Chem. Eur. J.*, 2014, **20**, 1909.

15 A. Ueda, S. Yamada, T. Isono, H. Kamo, A. Nakao, R. Kumai, H. Nakao, Y. Murakami, K. Yamamoto, Y. Nishio and H. Mori, *J. Am. Chem. Soc.*, 2014, **136**, 12184.

16 J. Yoshida, A. Ueda, A. Nakao, R. Kumai, H. Nakao, Y. Murakami and H. Mori, *Chem. Commun.*, 2014, **50**, 15557.

17 A. Ueda, *Bull. Chem Soc. Jpn.*, 2017, **90**, 1181.

18 A. Ueda, K. Kishimoto, T. Isono, S. Yamada, H. Kamo, K. Kobayashi, R. Kumai, Y. Murakami, J. Gouchi, Y. Uwatoko, Y. Nishio and H. Mori, *RSC Adv.*, 2019, **9**, 18353.

19 A. Ueda, K. Kishimoto, Y. Sunairi, J. Yoshida, H. Yamakawa, T. Miyamoto, T. Terashige, H. Okamoto and H. Mori, *J. Phys. Soc. Jpn.*, 2019, **88**, 034710.

20 O. S. Wenger, *Chem. Rev.*, 2013, **113**, 3686.

21 P. Kar, M. Yoshida, Y. Shigeta, A. Usui, A. Kobayashi, T. Minamidate, N. Matsunaga and M. Kato, *Angew. Chem. Int. Ed.*, 2017, **56**, 2345.

22 E. Li, K. Jie, M. Liu, X. Sheng, W. Zhu and F. Huang, *Chem. Soc. Rev.*, 2020, **49**, 1517.

23 T. J. Wadas, Q.-M. Wang, Y. Kim, C. Flaschenreim, T. N. Blanton and R. Eisenberg, *J. Am. Chem. Soc.*, 2004, **126**, 16841.

24 A. Kobayashi, H. Hara, S. Noro and M. Kato, *Dalton Trans.*, 2010, **39**, 3400.

25 J. R. Berenguer, E. Lalinde, A. Martín, M. Teresa Moreno, S. Ruiz, S. Sánchez and H. R. Shahsavari, *Chem. Commun.*, 2013, **49**, 5067.

26 S. H. Lim, M. M. Olmstead and A. L. Balch, *Chem. Sci.*, 2013, **4**, 311.

27 I. P. Oliveri, G. Malandrino and S. D. Bella, *Inorg. Chem.*, 2014, **53**, 9771.

28 Z. Chen, D. Wu, X. Han, Y. Nie, J. Yin, G.-A. Yu and S. H. Liu, *RSC Adv.*, 2014, **4**, 63985.

29 P. Rajamalli, P. Gandeepan, M.-J. Huang and C.-H. Cheng, *J. Mater. Chem. C*, 2015, **3**, 3329.

30 Y. Akune, R. Hirosawa, H. Takahashi, M. Shiro and S. Matsumoto, *RSC Adv.*, 2016, **6**, 74506.

31 B. Jiang, J. Zhang, J.-Q. Ma, W. Zheng, L.-J. Chen, B. Sun, C. Li, B.-W. Hu, H. Tan, X. Li and H.-B. Yang, *J. Am. Chem. Soc.*, 2016, **138**, 738.

32 T. Tsukamoto, R. Aoki, R. Sakamoto, R. Toyoda, M. Shimada, Y. Hattori, Y. Kitagawa, E. Nishibori, M. Nakano and H. Nishihara, *Chem. Commun.*, 2017, **53**, 9805.

33 A. Kobayashi, Y. Fukuzawa, S. Noro, T. Nakamura and M. Kato, *Chem. Lett.*, 2009, **38**, 998.

34 B. Li, R.-J. Wei, J. Tao, R.-B. Huang, L.-S. Zheng and Z. Zheng, *J. Am. Chem. Soc.*, 2010, **132**, 1558.

35 R.-J. Wei, J. Tao, R.-B. Huang and L.-S. Zheng, *Inorg. Chem.*, 2011, **50**, 8553.

36 K. Ohno, Y. Kusano, S. Kaizaki, A. Nagasawa and T. Fujihara, *Inorg. Chem.*, 2018, **57**, 14159.

37 E. Takahashi, H. Takaya and T. Naota, *Chem. Eur. J.*, 2010, **16**, 4793.

38 K. Fujii, A. Sakon, A. Sekine and H. Uekusa, *Cryst. Growth Des.*, 2011, **11**, 4305.

39 K. Wang, S. Huang, Y. Zhang, S. Zhao, H. Zhang and Y. Wang, *Chem. Sci.*, 2013, **4**, 3288.

40 J. Zhang, J. Chen, B. Xu, L. Wang, S. Ma, Y. Dong, B. Li, L. Ye and W. Tian, *Chem. Commun.*, 2013, **49**, 3878.

41 S. Yamada, A. Katsuki, Y. Nojiri and Y. Tokugawa, *CrystEngComm*, 2015, **17**, 1416.

42 M. J. Bryant, J. M. Skelton, L. E. Hatcher, C. Stubbs, E. Madrid, A. R. Pallipurath, L. H. Thomas, C. H. Woodall, J. Christensen, S. Fuertes, T. P. Robinson, C. M. Beavers, S. J. Teat, M. R. Warren, F. Pradaux-Caggiano, A. Walsh, F. Marken, D. R. Carbery, S. C. Parker, N. B. McKeown, R. Malpass-Evans, M. Carta and P. R. Raithby, *Nat. Commun.*, 2017, **8**, 1800.

43 I. Hisaki, Y. Suzuki, E. Gomez, Q. Ji, N. Tohnai, T. Nakamura and A. Douhal, *J. Am. Chem. Soc.*, 2019, **141**, 2111.

44 G. Xia, Z. Jiang, S. Shen, K. Liang, Q. Shao, Z. Cong and H. Wang, *Adv. Opt. Mater.*, 2019, **7**, 1801549.

45 A. Ueda and H. Mori, *Mater. Chem. Front.*, 2018, **2**, 566.

46 O. V. Dolomanov, L. J. Bourhis, R. J. Gildea, J. A. K. Howard and H. Puschmann, *J. Appl. Crystallogr.*, 2009, **42**, 339.

47 T. Ozaki, *Phys. Rev. B*, 2003, **67**, 155108.

48 T. Ozaki and H. Kino, *Phys. Rev. B*, 2004, **69**, 195113.

49 OpenMX website, http://www.openmx-square.org/, (accessed May 2020)

50 K. Lejaeghere, G. Bihlmayer, T. Björkman, P. Blaha, S. Blügel, V. Blum, D. Caliste, I. E. Castelli, S. J. Clark, A. Dal Corso, S. de Gironcoli, T. Deutsch, J. K. Dewhurst, I. Di Marco, C. Draxl, M. Dułak, O. Eriksson, J. A. Flores-Livas, K. F. Garrity, L. Genovese, P. Giannozzi, M. Giantomassi, S. Goedecker, X. Gonze, O. Grånäs, E. K. U. Gross, A. Gulans, F. Gygi, D. R. Hamann, P. J. Hasnip, N. A. W. Holzwarth, D. Iuşan, D. B. Jochym, F. Jollet, D. Jones, G. Kresse, K. Koepernik, E. Küçükbenli, Y. O. Kvashnin, I. L. M. Locht, S. Lubeck, M. Marsman, N. Marzari, U. Nitzsche, L. Nordström, T. Ozaki, L. Paulatto, C. J. Pickard, W. Poelmans, M. I. J. Probert, K. Refson, M. Richter, G.-M. Rignanese, S. Saha, M. Scheffler, M. Schlipf, K. Schwarz, S. Sharma, F. Tavazza, P. Thunström, A. Tkatchenko, M. Torrent, D. Vanderbilt, M. J. van Setten, V. Van Speybroeck, J. M. Wills, J. R. Yates, G.-X. Zhang and S. Cottenier, *Science,* 2016, **351**, aad3000.

51 T. Ozaki and H. Kino, *Phys. Rev. B*, 2005, **72**, 045121.

52 J. P. Perdew, K. Burke, M. Ernzerhof, *Phys. Rev. Lett.*, 1996, **77**, 3865.

53 C.-C. Lee, Y.-T. Lee, M. Fukuda, T. Ozaki, *Phys. Rev. B*, 2018, **98**, 115115.

54 R. S. Mulliken, *J. Chem. Phys.*, 1955, **23**, 1833.

55 K. Momma and F. Izumi, *J. Appl. Crystallogr.*, 2011, **44**, 1272.

56 N. Robertson and L. Cronin, *Coord. Chem. Rev*, 2002, **227**, 93.

57 R. Kato, *Chem. Rev.*, 2004, **104**, 5319.

58 S. Yokomori, S. Dekura, T. Fujino, M. Kawamura, T. Ozaki, and H. Mori, *J. Mater. Chem. C,* 2020, **8***,* 14939.

# Chapter 5

# General Conclusion

In this dissertation, the author synthesized the single crystals based on H-bonding metal dithiolene complexes in the aim for development of d/π-electron–proton-coupled functionalities (section 1.4.3): (1) gold and (2) nickel catecholedithiolene complexes and (3) zinc methoxybenzenedithiolene complex. From the detailed crystal and molecular structural analyses, including determination of the position of hydrogen atoms in the H-bonds, the author revealed the intermolecular interactions between the constituent molecules and the electronic structure. Also, the electronic functionalities of the crystals were investigated. By combining these results and DFT calculations based on the crystal structures, the author discussed and revealed the structure-property relationships. Here, the author summarises the obtained results and findings discussed in the preceding chapters in this dissertation into the following paragraphs.

In Chapter 2, as the first step of the development of the d/π electron–proton coupled functionalities, the author synthesized a gold catecholdithiolene complex [Au(catdt)$_2$]$^-$ with four hydroxy groups (Fig. 5-1a). As a result, the first 3D H-bonded frameworks composed of the metal dithiolene complex were demonstrated based on the formation of [O–H$\cdots$O] H-bonds with hydroxy groups and crystal solvent molecules (Fig. 5-1b left and middle). The key for the construction of the 3D frameworks (observed in **3-Au·0.5H$_2$O** and **3-Au·Et$_2$O**) are (1) connecting the planar and rigid [Au(catdt)$_2$]$^-$ complexes with 3D intermolecular H-bonds (Fig. 5-1c) and (2) introducing large Ph$_4$P$^+$ cations into the channels of the frameworks. Interestingly, the assembled structures are significantly influenced by the crystal solvent (especially, the molecular size and shape, and H-bonding abilities), which leads to variations in the assembled structure of the [Au(catdt)$_2$]$^-$ complexes (Fig. 5-1b): a densely-packed 3D framework (**3-**

**Au·0.5H₂O**), a loosely-packed 3D framework (**3-Au·Et₂O**), and a 2D sheet structure (**3-Au·2THF**). The variety of the characteristic framework realized in these crystals, and insight into the role of the crystal solvent on the H-bonding structure are important for developing electronic functionalities related closely to the molecular arrangements.
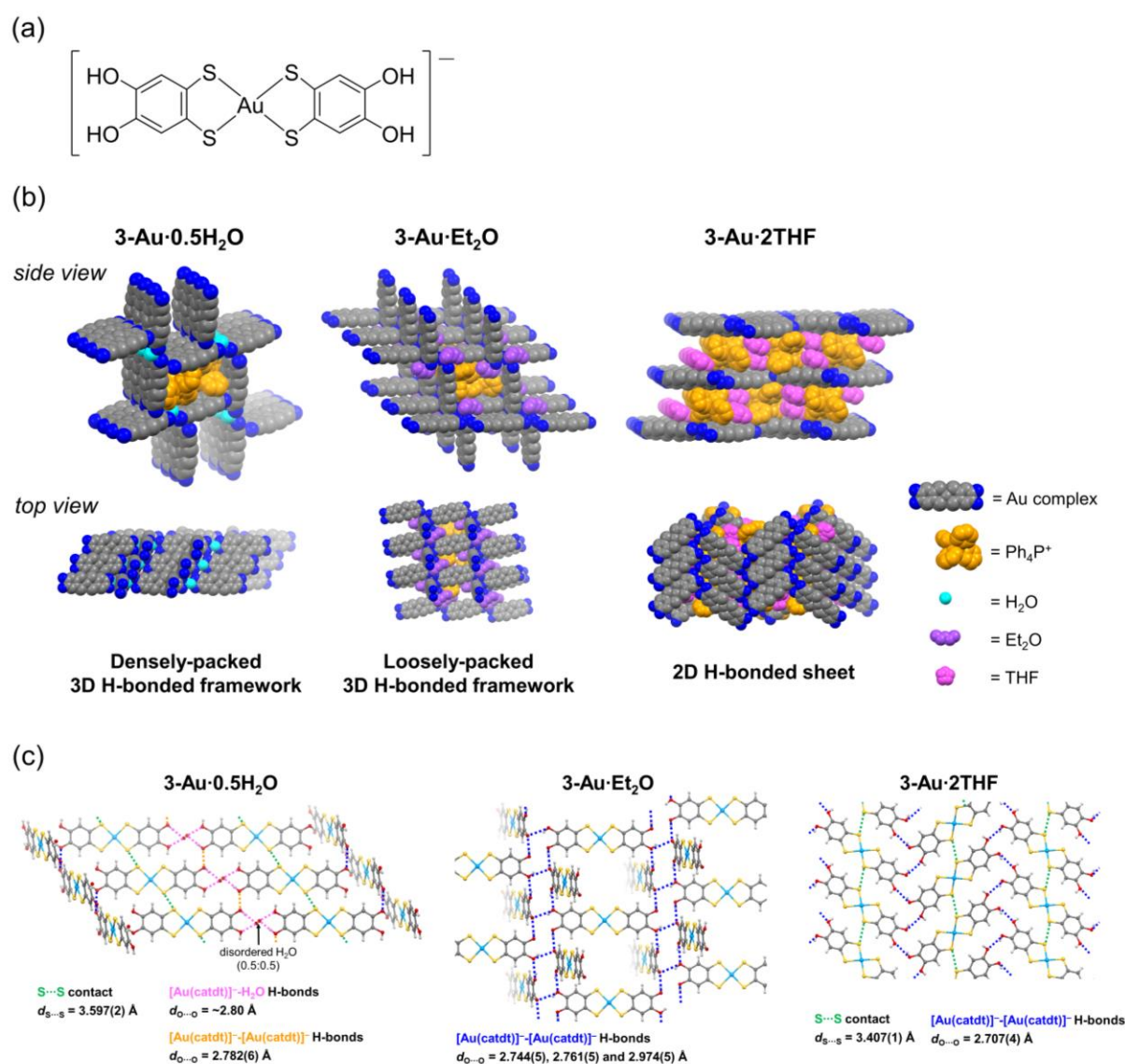


**Fig. 5-1** (a) Chemical structure of the gold catecholdithiolene complex, [Au(catdt)₂]. (b) Assembled structures of **3-Au·0.5H₂O**, **3-Au·0.5H₂O**, and **3-Au·0.5H₂O**. The formula of the crystals are (Ph₄P)[Au(catdt)₂]·0.5H₂O, (Ph₄P)[Au(catdt)₂]·Et₂O·n(solv), and (Ph₄P)[Au(catdt)₂]·2THF, respectively. (c) The H-bonding manner and intermolecular interactions between the gold complexes in each crystal.

In Chapter 3, in order to introduce electronic functionalities based on electron spins into the H-bonded frameworks, the author exchanged the central metal of the catecholdithilene complex from gold to nickel. As a result, the author realized magnetic property changes of the crystals from paramagnetic to non-magnetic based on deprotonation-coupled oxidation via proton-coupled electron transfer (PCET) in solution processes. In the synthesized four crystals, the nickel complexes constructed various assembled structures (3D framework and 2D sheet) based on intermolecular H-bonds similar to the crystals consisting of the gold catecholdithiolene complex. Importantly, in **3-Ni-3H·0.5THF** and **3-Ni-3H·0.5H$_2$O**, the formation of anionic [O–H⋯O]$^-$ H-bonds ($d_{O⋯O}$ = ~2.59 Å) having a potential of proton transfer between the O atoms with external-stimuli is revealed. Furthermore, the molecular structures and ESR measurements indicate that the electronic states of nickel complexes in the crystals except for **3-Ni-4H·DMSO** are changed from open-shell to closed-shell with deprotonation-coupled oxidation: the d/π electronic functionality changed based on PCET in solution processes. In addition, the DFT calculations based on the periodic structures suggest that the d/π electronic states in each crystal are significantly different derived from the deprotonation. Therefore, in this chapter, the author realized magnetic property changes and d/π electronic state modulation caused by multiple PCET in solution processes in new metal-dithiolene-based crystals with anionic [O–H⋯O]$^-$ H-bonds.
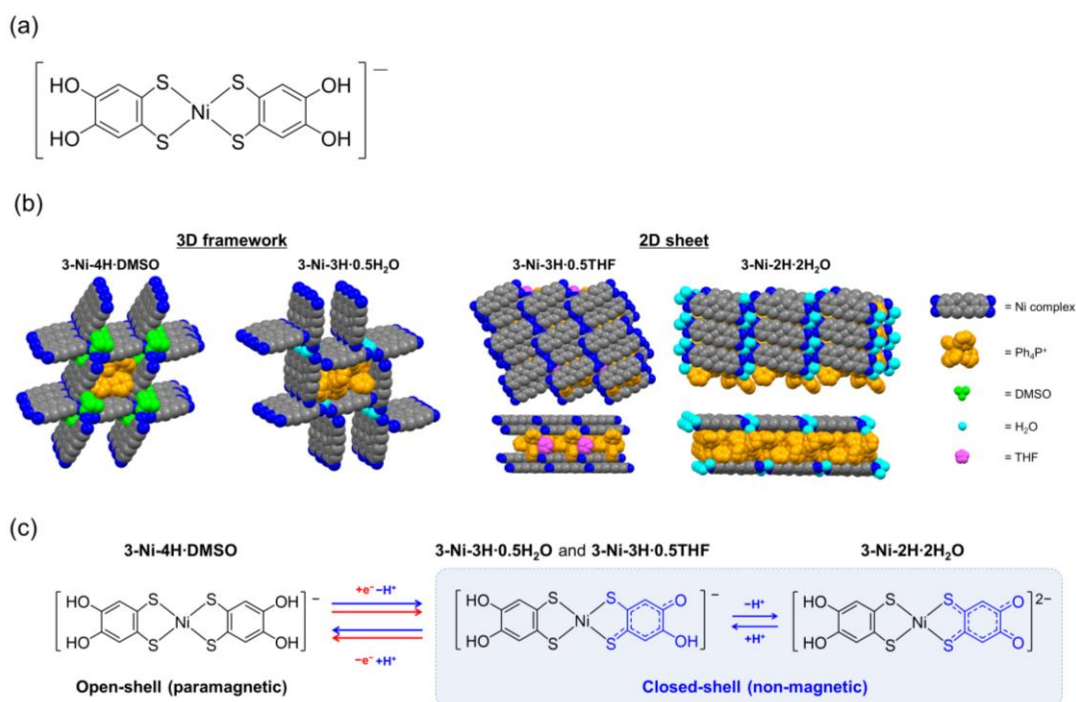
**Fig. 5-2** (a) Chemical structure of the nickel catecholdithiolene complex, [Ni(catdt)₂]. (b) Assembled structures of **3-Ni-4H·DMSO**, **3-Ni-3H·0.5H₂O**, **3-Ni-3H·0.5THF**, and **3-Ni-2H·2H₂O**. The formula of the crystals are (Ph₄P)[Ni-H₄(catdt)₂]·DMSO, (Ph₄P)[Ni-H₃(catdt)₂]·0.5H₂O, (Ph₄P)[Ni-H₃(catdt)₂]·0.5THF, and (Ph₄P)₂[Ni-H₂(catdt)₂]·2H₂O, respectively. (c) Electronic states and PCET scheme of the nickel complexes in each crystal.

In Chapter 4, on developments of new materials using zinc methoxybenzenedithiolene complex to realize novel electron–proton coupled functionalities, a novel mechanism of vapochromism based on the intermolecular electron transfer coupled with H-bond formation was realized in the newly obtained zinc dithiolene complex crystal, **4-Zn**. The crystal **4-Zn** exhibited vapochromic behavior both in visible-light absorption and photoluminescence properties on exposure to methanol or water sorption with reversible SCSC transformation. The absorbed vapor molecules formed H-bonds with S atoms of the zinc complex, whereas only **4-Zn·2MeOH** showed a slight molecular structure change of the zinc complex. Notably, the DFT calculations based on the periodic crystal structures reveal the structural change caused almost no impact on the optical properties; on the other hand, the H-bond formation induced the electron transfer from the zinc complex to the absorbed vapor molecules, which led to the

vapochromism in this crystal. Importantly, this is a new mechanism of vapochromism intrinsically caused by H-bonding formation. Therefore, the author successfully realized d/π electronic-state modulation coupled with H-bond formation, leading to color and photoluminescence property switching.
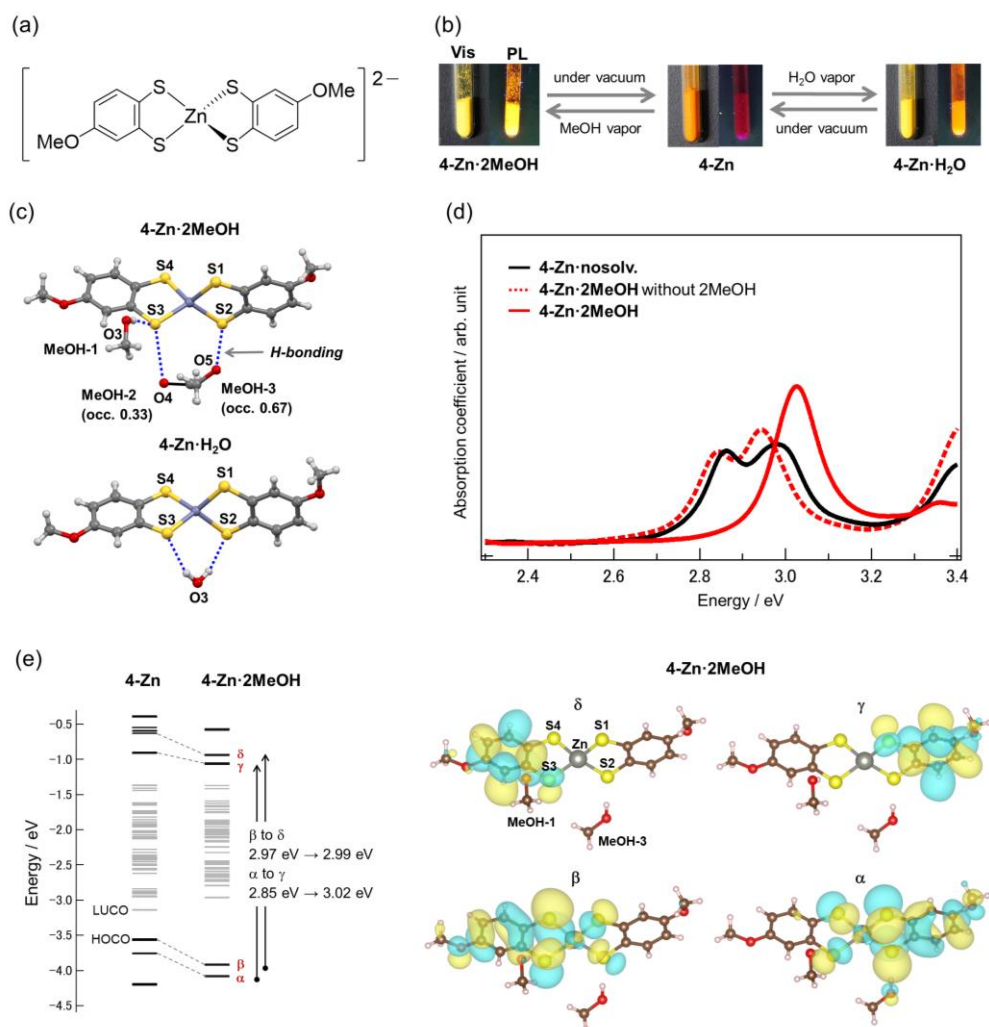


**Fig. 5-3** (a) Chemical structure of the zinc methoxybenzenedithiolene complex, [Zn(4-mxbdt)$_2$]. (b) Vapochromic behavior between **4-Zn**, **4-Zn·2MeOH**, and **4-Zn·H$_2$O**. The formula of the crystals are (Ph$_4$P)$_2$[Zn(4-mxbdt)$_2$], (Ph$_4$P)$_2$[Zn(4-mxbdt)$_2$]·2MeOH, and (Ph$_4$P)$_2$[Zn(4-mxbdt)$_2$]·H$_2$O, respectively. (c) H-bonds between the zinc complexes and absorbed vapor molecules in **4-Zn·2MeOH**, and **4-Zn·H$_2$O**. (d) The calculated absorption spectra of **4-Zn**, **4-Zn·2MeOH** and the hypothetical "**4-Zn·2MeOH** without 2MeOH" based on the experimentally observed crystal structures. (e) (left) Crystal orbital energies of **4-Zn** and **4-Zn·2MeOH**, and (right) corresponding crystal orbitals in **4-Zn·2MeOH**.

As described above, the author demonstrated the potential of the metal catecholdithiolene complexes for constructing various assembled structures with intermolecular [O–H···O] H-bonds. This is a crucial advantage to synthesize the H-bonded molecular crystals consisting of this complex. Also, the magnetic properties of the nickel complex crystals were changed with deprotonation-coupled oxidation through PCET in solution processes. Therefore, the author achieved the modulation of d/π electronic functionalities of crystalline solids induced by PCET in the solution processes, where anionic [O–H···O] H-bonds between the complexes (d/π-conjugated molecules) were formed in the crystals. These findings provide that these complexes should be the basis for the playground to realize new electron–proton coupled functionalities, such as switching the d/π electronic functionalities by proton dynamics in solid states. On the other hand, in Chapter 4, the author demonstrated color and photoluminescence property switching originated from d/π electronic state modulation with H-bonding formation: new electron–proton coupled phenomena related to d/π electrons and H-bonding protons.

Overall, the author successfully archives to realize novel d/π electron–proton coupled functionalities by combining metal dithiolene complexes and H-bonding protons, and provides important insights into molecular/material designs for exploring novel electron–proton coupled functionalities using metal dithiolene complexes in this dissertation. The findings obtained in the dissertation should lead to pioneering novel electron–proton coupled phenomena and functionalities using electrostatic effect and dynamics of H-bonding protons.

# Appendix

**Table S3-1** The crystallographic data for the crystals of the crystals consisting of neutral non-deprotonated nickel complex, [Ni-H$_4$(catdt)$_2$].

| crystals | S1-2-Ni-4H | S2-3-Ni-4H |
|---|---|---|
| formula | C$_{114}$H$_{102}$Br$_4$N$_2$NiO$_8$P$_4$S$_4$ | C$_{42}$H$_{31}$Ni$_{1.5}$O$_6$PS$_6$ |
| formula weight | 2258.44 | 952.13 |
| crystal system | triclinic | triclinic |
| space group | $P\bar{1}$ | $P\bar{1}$ |
| $a$ (Å) | 9.4401(18) | 10.770(5) |
| $b$ (Å) | 14.660(3) | 13.090(6) |
| $c$ (Å) | 21.242(4) | 15.722(7) |
| $\alpha$ (deg) | 92.947(3) | 71.015(14) |
| $\beta$ (deg) | 83.678(7) | 84.98(2) |
| $\gamma$ (deg) | 77.178(6) | 87.58(2) |
| $V$ (Å$^3$) | 77.841(6) | 2087.6(17) |
| $Z$ | 1 | 2 |
| $T$ (K) | 293 | 293 |
| $D_{calc}$ (g· cm$^{-3}$) | 1.341 | 1.515 |
| $\lambda$ (Å) | 0.71073 | 0.71073 |
| $R_{int}$ | 0.0259 | 0.0880 |
| $R_1$ ($I>2.00\sigma(I)$) | 0.0641 | 0.1176 |
| $wR_2$ (All reflections) | 0.2082 | 0.3965 |
| GOF | 1.060 | 1.013 |

The chemical formulas of **S1-2-Ni-4H** and **S2-3-Ni-4H** are (Ph$_4$PBr)$_2$[Ni-H$_4$(catdt)]·DMF (DMF: *N,N*-dimethylformamide) and (Ph$_4$P)$_2$[Ni-H$_3$(catdt)$_2$]$_2$[Ni-4H(catdt)$_2$], respectively.

Recrystallization conditions:

Liquid-liquid diffusion method of DMF and Et$_2$O using **2-Ni** for **S1-2-Ni-4H** (under atmosphere) and of acetone/acetic acid/hexane solution using the green powder in Chapter 3 for **S2-3-Ni-4H** (under argon)
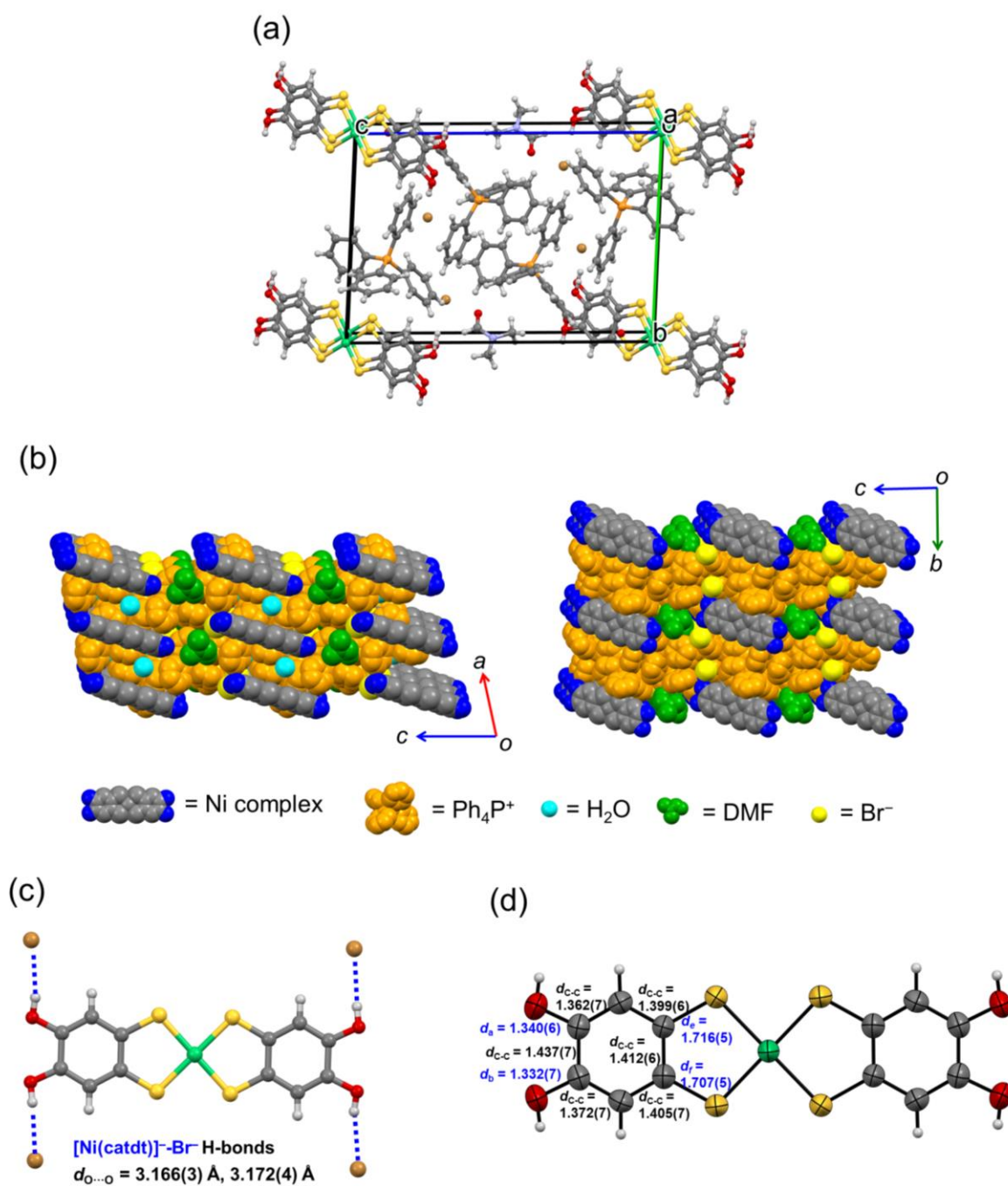
**Fig. S3-1** Structure of the neutral nickel complex crystal **S1-2-Ni-4H**. (a) Unit cell and (b) overview of the assembled structure from viewing along *a* and *b* axis. Light green = Ni, blown = Br, yellow = S, orange = P, blue = N, gray = C, red = O, white = H. (c) H-bonding manner around the nickel complex. (d) Molecular structure and bond lengths of the nickel complex.
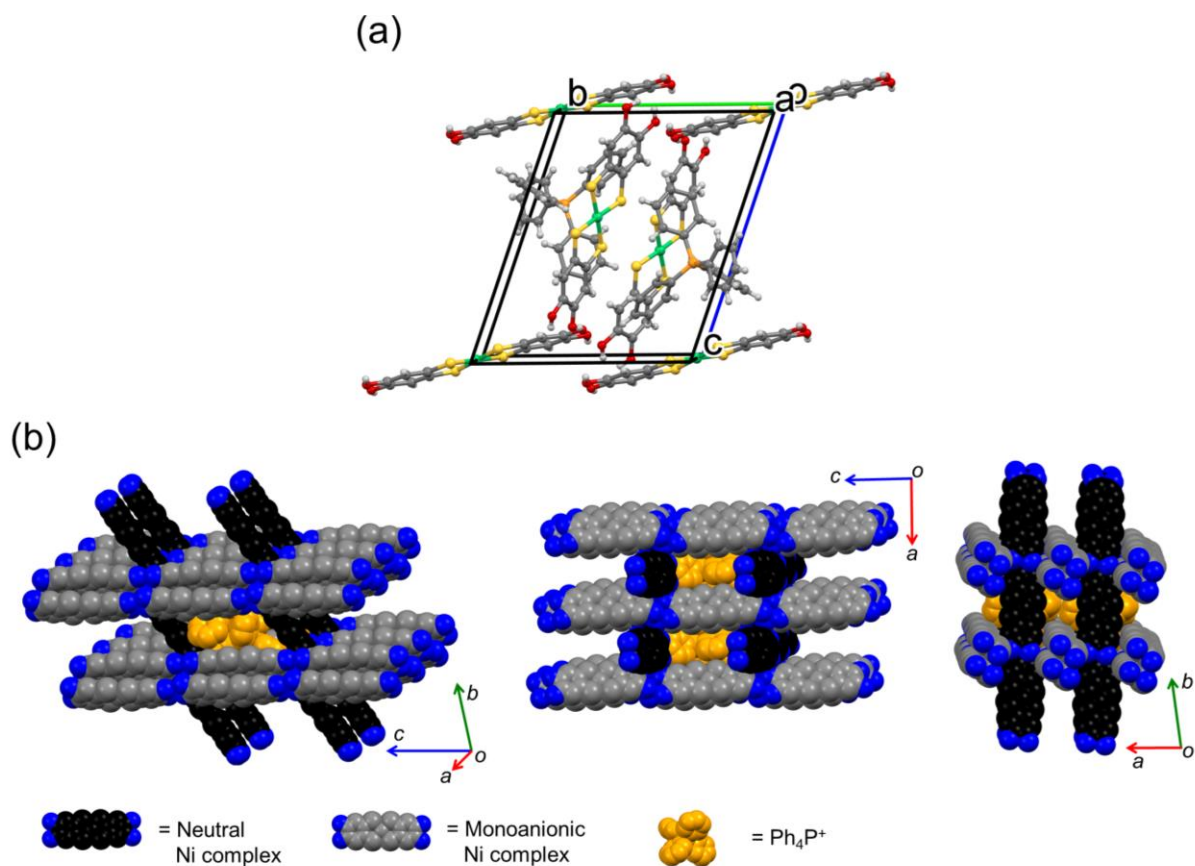
**Fig. S3-2** Structure of the neutral nickel complex crystal **S1-2-Ni-4H**. (a) Unit cell and (b) overview of the 3D framework structure from viewing along *a* and *b* axis. Light green = Ni, yellow = S, orange = P, gray = C, red = O, white = H. Black molecules show neutral non-deprotonated nickel complex and gray molecules indicate monoanionic one-deprotonated nickel complex.
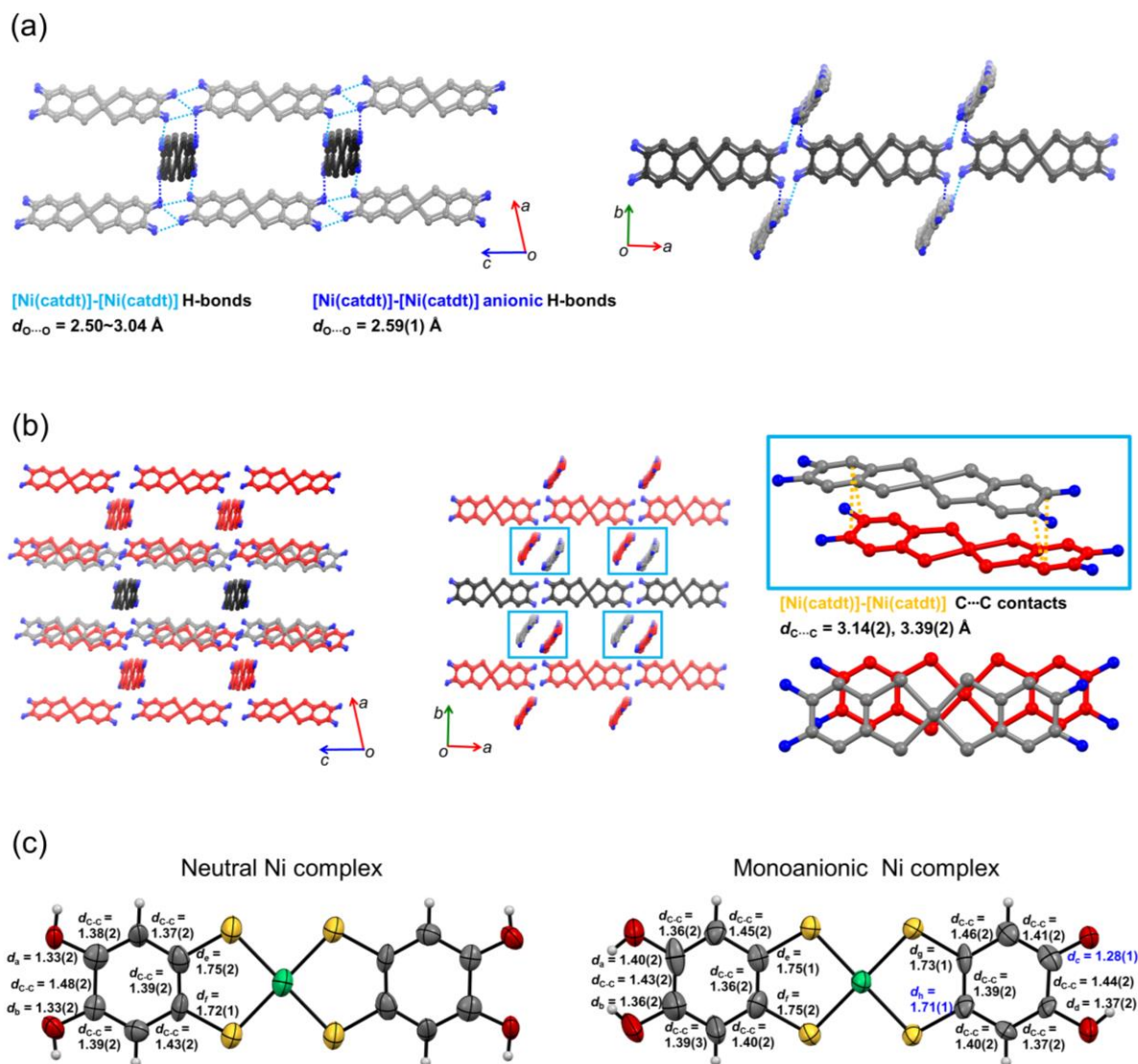
**Fig. S3-3** (a) 2D H-bonded framework structure based on the nickel complexes. There is anionic [O–H···O]$^-$ H-bonds between the deprotonated hydroxy group and the non-deprotonated hydroxy group of the nickel complexes. (b) Stacking manner of the 2D H-bonded frameworks and C···C contacts ($\pi$-$\pi$ interaction) between the nickel complexes belonging to different 2D H-bonded framework. The red molecules show the nickel complexes belonging to neighboring 2D H-boned frameworks. (c) Molecular structures and bond lengths of the nickel complexes. Neutral nickel complex is half-molecules crystallographically independent, and monoanionic nickel complex is one-molecule crystallographically independent.

**Table S4-1** The results of Mulliken population analysis of [Zn(4-mxbdt)₂]²⁻ complex and vapor molecules in **4-Zn·2MeOH (minor)**. Here, Mulliken charges for each atom in neutral state are as follows: Zn = 20, S = 6, O = 6, C = 4, and H = 1.

| Crystal | 4-Zn·2MeOH (minor) | 4-Zn·2MeOH (minor) without 2MeOH | |
|---|---|---|---|
| | [Zn(4-mxbdt)₂]²⁻ | [Zn(4-mxbdt)₂]²⁻ | Difference |
| Zn1 | 19.68553738 | 19.68913075 | −0.003593368 |
| Zn1 | 19.68553733 | 19.68887914 | −0.003341803 |
| Zn1 | 19.6855373 | 19.6891308 | −0.003593497 |
| Zn1 | 19.68553726 | 19.68887911 | −0.003341847 |
| S1 | 6.509375276 | 6.513286775 | −0.003911499 |
| S1 | 6.509375275 | 6.513023147 | −0.003647872 |
| S1 | 6.509375329 | 6.513286755 | −0.003911426 |
| S1 | 6.509375306 | 6.513023168 | −0.003647862 |
| S2 | 6.522154644 | 6.532714725 | −0.010560081 |
| S2 | 6.52215451 | 6.532621143 | −0.010466633 |
| S2 | 6.522154861 | 6.532714887 | −0.010560026 |
| S2 | 6.522154506 | 6.532621153 | −0.010466647 |
| S3 | 6.433217809 | 6.526347263 | −0.093129454 |
| S3 | 6.433217695 | 6.526333597 | −0.093115902 |
| S3 | 6.433217592 | 6.526347212 | −0.09312962 |
| S3 | 6.433217863 | 6.526333746 | −0.093115883 |
| S4 | 6.514067918 | 6.521208849 | −0.007140931 |
| S4 | 6.514067829 | 6.521199831 | −0.007132002 |
| S4 | 6.514067923 | 6.521208821 | −0.007140898 |
| S4 | 6.514067793 | 6.521199782 | −0.007131989 |
| O1 | 6.446548809 | 6.448016786 | −0.001467977 |
| O1 | 6.446549036 | 6.44801 | −0.001460964 |
| O1 | 6.446548816 | 6.448016772 | −0.001467956 |
| O1 | 6.446549037 | 6.448009991 | −0.001460954 |
| O2 | 6.451636727 | 6.451547432 | 8.9295E-05 |
| O2 | 6.451636591 | 6.45159612 | 4.0471E-05 |
| O2 | 6.451636686 | 6.451547401 | 8.9285E-05 |
| O2 | 6.451636684 | 6.451595997 | 4.0687E-05 |
| C1 | 3.839479773 | 3.841588641 | −0.002108868 |
| C1 | 3.839479919 | 3.842092144 | −0.002612225 |
| C1 | 3.839479487 | 3.841588467 | −0.00210898 |
| C1 | 3.839479925 | 3.842092175 | −0.00261225 |

| | | | |
|---|---|---|---|
| C2 | 3.978290903 | 3.980240381 | −0.001949478 |
| C2 | 3.97829132 | 3.97997944 | −0.00168812 |
| C2 | 3.97829101 | 3.980240539 | −0.001949529 |
| C2 | 3.97829129 | 3.979979358 | −0.001688068 |
| H2 | 1.088195783 | 1.092702582 | −0.004506799 |
| H2 | 1.088196015 | 1.09269534 | −0.004499325 |
| H2 | 1.088195799 | 1.092702595 | −0.004506796 |
| H2 | 1.088196001 | 1.092695388 | −0.004499387 |
| C3 | 3.771393633 | 3.773463534 | −0.002069901 |
| C3 | 3.77139285 | 3.773150629 | −0.001757779 |
| C3 | 3.771393482 | 3.773463473 | −0.002069991 |
| C3 | 3.771392875 | 3.773150643 | −0.001757768 |
| C4 | 3.97477655 | 3.984823782 | −0.010047232 |
| C4 | 3.974775852 | 3.985597108 | −0.010821256 |
| C4 | 3.974776602 | 3.984823669 | −0.010047067 |
| C4 | 3.974775903 | 3.985597108 | −0.010821205 |
| H4 | 1.071164617 | 1.059938736 | 0.011225881 |
| H4 | 1.071165082 | 1.059739265 | 0.011425817 |
| H4 | 1.071164638 | 1.059938744 | 0.011225894 |
| H4 | 1.071165032 | 1.059739303 | 0.011425729 |
| C5 | 3.924674265 | 3.925644744 | −0.000970479 |
| C5 | 3.924674491 | 3.92613997 | −0.001465479 |
| C5 | 3.92467452 | 3.925645013 | −0.000970493 |
| C5 | 3.924674613 | 3.926139877 | −0.001465264 |
| H5 | 1.067992012 | 1.068348355 | −0.000356343 |
| H5 | 1.06799184 | 1.068131261 | −0.000139421 |
| H5 | 1.067991643 | 1.068348087 | −0.000356444 |
| H5 | 1.067991787 | 1.068131306 | −0.000139519 |
| C6 | 3.853767872 | 3.858344285 | −0.004576413 |
| C6 | 3.853768108 | 3.858210591 | −0.004442483 |
| C6 | 3.85376805 | 3.858344312 | −0.004576262 |
| C6 | 3.853768059 | 3.858210603 | −0.004442544 |
| C7 | 3.828375227 | 3.862091302 | −0.033716075 |
| C7 | 3.828375333 | 3.862078509 | −0.033703176 |
| C7 | 3.828375485 | 3.862091533 | −0.033716048 |
| C7 | 3.828374888 | 3.862078012 | −0.033703124 |
| C8 | 3.917103812 | 3.938935999 | −0.021832187 |
| C8 | 3.917103531 | 3.938833008 | −0.021729477 |

| | | | |
|------|------------------|------------------|------------------|
| C8 | 3.917103591 | 3.938935801 | −0.02183221 |
| C8 | 3.917103964 | 3.938833811 | −0.021729847 |
| H8 | 1.080140904 | 1.076515537 | 0.003625367 |
| H8 | 1.080141349 | 1.076584627 | 0.003556722 |
| H8 | 1.080141512 | 1.076516193 | 0.003625319 |
| H8 | 1.080141252 | 1.076584664 | 0.003556588 |
| C9 | 3.747284314 | 3.753864793 | −0.006580479 |
| C9 | 3.747284761 | 3.75383584 | −0.006551079 |
| C9 | 3.747283577 | 3.753863929 | −0.006580352 |
| C9 | 3.747284039 | 3.753835845 | −0.006551806 |
| C10 | 4.001905014 | 4.012154382 | −0.010249368 |
| C10 | 4.001905044 | 4.012224356 | −0.010319312 |
| C10 | 4.001905216 | 4.012154607 | −0.010249391 |
| C10 | 4.001905313 | 4.012223949 | −0.010318636 |
| H10 | 1.073473955 | 1.080195608 | −0.006721653 |
| H10 | 1.073473773 | 1.08020853 | −0.006734757 |
| H10 | 1.073473933 | 1.080195653 | −0.00672172 |
| H10 | 1.073473619 | 1.080208068 | −0.006734449 |
| C11 | 3.919895379 | 3.931332064 | −0.011436685 |
| C11 | 3.919895277 | 3.931260956 | −0.011365679 |
| C11 | 3.919895514 | 3.931331935 | −0.011436421 |
| C11 | 3.919895593 | 3.93126149 | −0.011365897 |
| H11 | 1.056633341 | 1.052297578 | 0.004335763 |
| H11 | 1.056633443 | 1.052279114 | 0.004354329 |
| H11 | 1.056633315 | 1.052297623 | 0.004335692 |
| H11 | 1.056633412 | 1.052279123 | 0.004354289 |
| C12 | 3.852664465 | 3.860436448 | −0.007771983 |
| C12 | 3.852664284 | 3.860463076 | −0.007798792 |
| C12 | 3.852664354 | 3.860436467 | −0.007772113 |
| C12 | 3.852664314 | 3.860463109 | −0.007798795 |
| C13 | 3.72961643 | 3.738955125 | −0.009338695 |
| C13 | 3.729616232 | 3.738926514 | −0.009310282 |
| C13 | 3.729615892 | 3.738954611 | −0.009338719 |
| C13 | 3.729616203 | 3.738926584 | −0.009310381 |
| H13A | 1.022272329 | 1.020967657 | 0.001304672 |
| H13A | 1.022272691 | 1.020950556 | 0.001322135 |
| H13A | 1.022272299 | 1.020967633 | 0.001304666 |
| H13A | 1.022272752 | 1.020950524 | 0.001322228 |

| | | | |
|---|---|---|---|
| H13B | 1.019070215 | 1.018021573 | 0.001048642 |
| H13B | 1.019070615 | 1.018056266 | 0.001014349 |
| H13B | 1.019070861 | 1.018022172 | 0.001048689 |
| H13B | 1.0190706 | 1.018056211 | 0.001014389 |
| H13C | 0.984716611 | 0.977971384 | 0.006745227 |
| H13C | 0.984715983 | 0.978019361 | 0.006696622 |
| H13C | 0.984716505 | 0.977971334 | 0.006745171 |
| H13C | 0.984715972 | 0.978019383 | 0.006696589 |
| C14 | 3.744276018 | 3.758512059 | −0.014236041 |
| C14 | 3.744275874 | 3.759204984 | −0.01492911 |
| C14 | 3.744276606 | 3.758512695 | −0.014236089 |
| C14 | 3.744276655 | 3.759204582 | −0.014927927 |
| H14A | 1.008153344 | 1.010354146 | −0.002200802 |
| H14A | 1.008153391 | 1.010597926 | −0.002444535 |
| H14A | 1.008152794 | 1.010353605 | −0.002200811 |
| H14A | 1.008153249 | 1.010598002 | −0.002444753 |
| H14B | 1.021724606 | 1.028734368 | −0.007009762 |
| H14B | 1.021724992 | 1.027412887 | −0.005687895 |
| H14B | 1.021724768 | 1.028734479 | −0.007009711 |
| H14B | 1.021724762 | 1.02741302 | −0.005688258 |
| H14C | 0.985128418 | 0.97030733 | 0.014821088 |
| H14C | 0.985127917 | 0.97052932 | 0.014598597 |
| H14C | 0.985128233 | 0.970307156 | 0.014821077 |
| H14C | 0.985127748 | 0.970529504 | 0.014598244 |
| Crystal | **4-Zn·2MeOH (minor)** | MeOH in **4-Zn·2MeOH (minor)** | |
| | MeOH-1 | MeOH-1 | Difference |
| O3 | 6.602273169 | 6.621176692 | −0.018903523 |
| O3 | 6.602273322 | 6.621183676 | −0.018910354 |
| O3 | 6.602273163 | 6.621178428 | −0.018905265 |
| O3 | 6.602273028 | 6.621183645 | −0.018910617 |
| H3 | 0.770678062 | 0.660520213 | 0.110157849 |
| H3 | 0.770677866 | 0.660513822 | 0.110164044 |
| H3 | 0.770678079 | 0.660518833 | 0.110159246 |
| H3 | 0.770678174 | 0.660513352 | 0.110164822 |
| C63 | 3.713456326 | 3.776465546 | −0.06300922 |
| C63 | 3.713456503 | 3.776467348 | −0.063010845 |
| C63 | 3.713456336 | 3.77646533 | −0.063008994 |
| C63 | 3.713456508 | 3.776463731 | −0.063007223 |

| | | | |
|------|--------------|--------------|--------------|
| H63A | 1.015835102 | 0.975149471 | 0.040685631 |
| H63A | 1.015835435 | 0.975142873 | 0.040692562 |
| H63A | 1.015835115 | 0.975149255 | 0.04068586 |
| H63A | 1.015835135 | 0.975141825 | 0.04069331 |
| H63B | 0.991151858 | 0.964558384 | 0.026593474 |
| H63B | 0.991151562 | 0.964564506 | 0.026587056 |
| H63B | 0.991151826 | 0.964558534 | 0.026593292 |
| H63B | 0.991151572 | 0.964563944 | 0.026587628 |
| H63C | 1.013810063 | 1.00312756 | 0.010682503 |
| H63C | 1.013809989 | 1.003125706 | 0.010684283 |
| H63C | 1.013810075 | 1.00312749 | 0.010682585 |
| H63C | 1.013810177 | 1.003131447 | 0.01067873 |
| | MeOH-2 | MeOH-2 | Difference |
| O4 | 6.530319638 | 6.545956973 | −0.015637335 |
| O4 | 6.530319796 | 6.545959442 | −0.015639646 |
| O4 | 6.530319464 | 6.545957062 | −0.015637598 |
| O4 | 6.530319033 | 6.545959464 | −0.015640431 |
| H4A | 0.8682202 | 0.736628634 | 0.131591566 |
| H4A | 0.868219766 | 0.736624853 | 0.131594913 |
| H4A | 0.868219939 | 0.736628463 | 0.131591476 |
| H4A | 0.868220484 | 0.736624849 | 0.131595635 |
| C65A | 3.710764837 | 3.787279585 | −0.076514748 |
| C65A | 3.710764937 | 3.787279603 | −0.076514666 |
| C65A | 3.710765794 | 3.787279869 | −0.076514075 |
| C65A | 3.710765367 | 3.787279519 | −0.076514152 |
| H65A | 1.025560173 | 0.988939601 | 0.036620572 |
| H65A | 1.025560392 | 0.988937097 | 0.036623295 |
| H65A | 1.025560299 | 0.988939696 | 0.036620603 |
| H65A | 1.025560278 | 0.988937146 | 0.036623132 |
| H65B | 1.018076917 | 0.983543661 | 0.034533256 |
| H65B | 1.018076824 | 0.983552947 | 0.034523877 |
| H65B | 1.018076655 | 0.983543759 | 0.034532896 |
| H65B | 1.018076698 | 0.983552975 | 0.034523723 |
| H65C | 0.988725746 | 0.956653677 | 0.032072069 |
| H65C | 0.988725712 | 0.956648113 | 0.032077599 |
| H65C | 0.988725378 | 0.956653282 | 0.032072096 |
| H65C | 0.988725678 | 0.956648115 | 0.032077563 |

**Table S4-2** The results of Mulliken population analysis of [Zn(4-mxbdt)$_2$]$^{2-}$ complex and vapor molecules in **4-Zn·2MeOH (major)**. Here, Mulliken charges for each atom in neutral state are as follows: Zn = 20, S = 6, O = 6, C = 4, and H = 1.

| Crystal | 4-Zn·2MeOH (major) | 4-Zn·2MeOH (major) without 2MeOH | |
|---|---|---|---|
| | [Zn(4-mxbdt)$_2$]$^{2-}$ | [Zn(4-mxbdt)$_2$]$^{2-}$ | Difference |
| Zn1 | 19.68216665 | 19.68913075 | −0.006964105 |
| Zn1 | 19.68216743 | 19.68887914 | −0.006711702 |
| Zn1 | 19.68216727 | 19.6891308 | −0.006963529 |
| Zn1 | 19.68216725 | 19.68887911 | −0.006711861 |
| S1 | 6.505559352 | 6.513286775 | −0.007727423 |
| S1 | 6.50556001 | 6.513023147 | −0.007463137 |
| S1 | 6.505559895 | 6.513286755 | −0.00772686 |
| S1 | 6.505559897 | 6.513023168 | −0.007463271 |
| S2 | 6.469401987 | 6.532714725 | −0.063312738 |
| S2 | 6.469406312 | 6.532621143 | −0.063214831 |
| S2 | 6.469405856 | 6.532714887 | −0.063309031 |
| S2 | 6.469405739 | 6.532621153 | −0.063215414 |
| S3 | 6.476255219 | 6.526347263 | −0.050092044 |
| S3 | 6.476256235 | 6.526333597 | −0.050077362 |
| S3 | 6.476255969 | 6.526347212 | −0.050091243 |
| S3 | 6.476256316 | 6.526333746 | −0.05007743 |
| S4 | 6.518213909 | 6.521208849 | −0.00299494 |
| S4 | 6.518213838 | 6.521199831 | −0.002985993 |
| S4 | 6.518213935 | 6.521208821 | −0.002994886 |
| S4 | 6.518213743 | 6.521199782 | −0.002986039 |
| O1 | 6.443044951 | 6.448016786 | −0.004971835 |
| O1 | 6.443045137 | 6.448010000 | −0.004964863 |
| O1 | 6.44304496 | 6.448016772 | −0.004971812 |
| O1 | 6.443045184 | 6.448009991 | −0.004964807 |
| O2 | 6.452320053 | 6.451547432 | 0.000772621 |
| O2 | 6.452320043 | 6.45159612 | 0.000723923 |
| O2 | 6.452320138 | 6.451547401 | 0.000772737 |
| O2 | 6.452320058 | 6.451595997 | 0.000724061 |
| C1 | 3.840889493 | 3.841588641 | −0.000699148 |
| C1 | 3.840890063 | 3.842092144 | −0.001202081 |
| C1 | 3.840889569 | 3.841588467 | −0.000698898 |

| | | | |
|---|---|---|---|
| C1 | 3.840889949 | 3.842092175 | −0.001202226 |
| C2 | 3.977452841 | 3.980240381 | −0.00278754 |
| C2 | 3.977453476 | 3.979979440 | −0.002525964 |
| C2 | 3.977453082 | 3.980240539 | −0.002787457 |
| C2 | 3.977453424 | 3.979979358 | −0.002525934 |
| H2 | 1.090762771 | 1.092702582 | −0.001939811 |
| H2 | 1.090763225 | 1.09269534 | −0.001932115 |
| H2 | 1.090762931 | 1.092702595 | −0.001939664 |
| H2 | 1.090763144 | 1.092695388 | −0.001932244 |
| C3 | 3.766044622 | 3.773463534 | −0.007418912 |
| C3 | 3.766044354 | 3.773150629 | −0.007106275 |
| C3 | 3.766044986 | 3.773463473 | −0.007418487 |
| C3 | 3.766044413 | 3.773150643 | −0.00710623 |
| C4 | 3.969946757 | 3.984823782 | −0.014877025 |
| C4 | 3.969946 | 3.985597108 | −0.015651108 |
| C4 | 3.969946896 | 3.984823669 | −0.014876773 |
| C4 | 3.969946185 | 3.985597108 | −0.015650923 |
| H4 | 1.062494663 | 1.059938736 | 0.002555927 |
| H4 | 1.062495096 | 1.059739265 | 0.002755831 |
| H4 | 1.062494756 | 1.059938744 | 0.002556012 |
| H4 | 1.062495241 | 1.059739303 | 0.002755938 |
| C5 | 3.922852138 | 3.925644744 | −0.002792606 |
| C5 | 3.922852663 | 3.92613997 | −0.003287307 |
| C5 | 3.922852572 | 3.925645013 | −0.002792441 |
| C5 | 3.922852631 | 3.926139877 | −0.003287246 |
| H5 | 1.066366436 | 1.068348355 | −0.001981919 |
| H5 | 1.066366474 | 1.068131261 | −0.001764787 |
| H5 | 1.066366346 | 1.068348087 | −0.001981741 |
| H5 | 1.066366468 | 1.068131306 | −0.001764838 |
| C6 | 3.831253723 | 3.858344285 | −0.027090562 |
| C6 | 3.831255502 | 3.858210591 | −0.026955089 |
| C6 | 3.831255184 | 3.858344312 | −0.027089128 |
| C6 | 3.831255246 | 3.858210603 | −0.026955357 |
| C7 | 3.838290509 | 3.862091302 | −0.023800793 |
| C7 | 3.838290538 | 3.862078509 | −0.023787971 |
| C7 | 3.838290641 | 3.862091533 | −0.023800892 |
| C7 | 3.838290259 | 3.862078012 | −0.023787753 |
| C8 | 3.920082959 | 3.938935999 | −0.01885304 |

| C8 | 3.92008275 | 3.938833008 | −0.018750258 |
| C8 | 3.920082871 | 3.938935801 | −0.01885293 |
| C8 | 3.920083104 | 3.938833811 | −0.018750707 |
| H8 | 1.083454443 | 1.076515537 | 0.006938906 |
| H8 | 1.083454936 | 1.076584627 | 0.006870309 |
| H8 | 1.083455128 | 1.076516193 | 0.006938935 |
| H8 | 1.083454869 | 1.076584664 | 0.006870205 |
| C9 | 3.749273371 | 3.753864793 | −0.004591422 |
| C9 | 3.749273759 | 3.75383584 | −0.004562081 |
| C9 | 3.749272595 | 3.753863929 | −0.004591334 |
| C9 | 3.749273124 | 3.753835845 | −0.004562721 |
| C10 | 4.005059645 | 4.012154382 | −0.007094737 |
| C10 | 4.005059823 | 4.012224356 | −0.007164533 |
| C10 | 4.005059747 | 4.012154607 | −0.00709486 |
| C10 | 4.005060106 | 4.012223949 | 0.007163843 |
| H10 | 1.075539311 | 1.080195608 | 0.004656297 |
| H10 | 1.075539239 | 1.08020853 | 0.004669291 |
| H10 | 1.075539462 | 1.080195653 | 0.004656191 |
| H10 | 1.075538992 | 1.080208068 | 0.004669076 |
| C11 | 3.921071606 | 3.931332064 | 0.010260458 |
| C11 | 3.921071318 | 3.931260956 | 0.010189638 |
| C11 | 3.921071353 | 3.931331935 | 0.010260582 |
| C11 | 3.921071639 | 3.93126149 | 0.010189851 |
| H11 | 1.058041332 | 1.052297578 | 0.005743754 |
| H11 | 1.058041508 | 1.052279114 | 0.005762394 |
| H11 | 1.058041482 | 1.052297623 | 0.005743859 |
| H11 | 1.05804146 | 1.052279123 | 0.005762337 |
| C12 | 3.853763592 | 3.860436448 | −0.006672856 |
| C12 | 3.853763521 | 3.860463076 | −0.006699555 |
| C12 | 3.853763663 | 3.860436467 | −0.006672804 |
| C12 | 3.85376342 | 3.860463109 | −0.006699689 |
| C13 | 3.729425207 | 3.738955125 | −0.009529918 |
| C13 | 3.729425207 | 3.738926514 | −0.009501307 |
| C13 | 3.729424744 | 3.738954611 | −0.009529867 |
| C13 | 3.72942512 | 3.738926584 | −0.009501464 |
| H13A | 1.021411825 | 1.020967657 | 0.000444168 |
| H13A | 1.021412274 | 1.020950556 | 0.000461718 |
| H13A | 1.021411782 | 1.020967633 | 0.000444149 |

| | | | |
|---|---|---|---|
| H13A | 1.021412272 | 1.020950524 | 0.000461748 |
| H13B | 1.023934267 | 1.018021573 | 0.005912694 |
| H13B | 1.023934847 | 1.018056266 | 0.005878581 |
| H13B | 1.023935136 | 1.018022172 | 0.005912964 |
| H13B | 1.023934838 | 1.018056211 | 0.005878627 |
| H13C | 0.981058934 | 0.977971384 | 0.00308755 |
| H13C | 0.981058595 | 0.978019361 | 0.003039234 |
| H13C | 0.981059096 | 0.977971334 | 0.003087762 |
| H13C | 0.981058564 | 0.978019383 | 0.003039181 |
| C14 | 3.744717157 | 3.758512059 | −0.013794902 |
| C14 | 3.744716955 | 3.759204984 | −0.014488029 |
| C14 | 3.744717645 | 3.758512695 | −0.01379505 |
| C14 | 3.744717841 | 3.759204582 | −0.014486741 |
| H14A | 1.00785272 | 1.010354146 | −0.002501426 |
| H14A | 1.007852734 | 1.010597926 | −0.002745192 |
| H14A | 1.007852219 | 1.010353605 | −0.002501386 |
| H14A | 1.00785261 | 1.010598002 | −0.002745392 |
| H14B | 1.022380892 | 1.028734368 | −0.006353476 |
| H14B | 1.022381364 | 1.027412887 | −0.005031523 |
| H14B | 1.022381103 | 1.028734479 | −0.006353376 |
| H14B | 1.02238108 | 1.02741302 | −0.00503194 |
| H14C | 0.986433951 | 0.97030733 | 0.016126621 |
| H14C | 0.986433469 | 0.97052932 | 0.015904149 |
| H14C | 0.986433732 | 0.970307156 | 0.016126576 |
| H14C | 0.986433285 | 0.970529504 | 0.015903781 |

| Crystal | 4-Zn·2MeOH (major) | MeOH in 4-Zn·2MeOH (major) | |
|---|---|---|---|
| | MeOH-1 | MeOH-1 | Difference |
| O3 | 6.602609432 | 6.62267698 | −0.020067548 |
| O3 | 6.60260959 | 6.622683903 | −0.020074313 |
| O3 | 6.602609445 | 6.622678665 | −0.02006922 |
| O3 | 6.602609315 | 6.62268386 | −0.020074545 |
| H3 | 0.771091244 | 0.656161968 | 0.114929276 |
| H3 | 0.771091026 | 0.656155648 | 0.114935378 |
| H3 | 0.771091261 | 0.656160677 | 0.114930584 |
| H3 | 0.771091294 | 0.656155188 | 0.114936106 |
| C63 | 3.714730594 | 3.777139478 | −0.062408884 |
| C63 | 3.714730788 | 3.777141202 | −0.062410414 |
| C63 | 3.71473064 | 3.777139251 | −0.062408611 |

| | | | |
|---|---|---|---|
| C63 | 3.714730746 | 3.777137649 | −0.062406903 |
| H63A | 1.014813216 | 0.973740328 | 0.041072888 |
| H63A | 1.014813543 | 0.973733667 | 0.041079876 |
| H63A | 1.014813184 | 0.973740093 | 0.041073091 |
| H63A | 1.014813187 | 0.973732585 | 0.041080602 |
| H63B | 0.991391344 | 0.965505660 | 0.025885684 |
| H63B | 0.991391031 | 0.965511739 | 0.025879292 |
| H63B | 0.991391366 | 0.965505747 | 0.025885619 |
| H63B | 0.991391111 | 0.965511158 | 0.025879953 |
| H63C | 1.017190488 | 1.004843646 | 0.012346842 |
| H63C | 1.017190387 | 1.004841917 | 0.01234847 |
| H63C | 1.017190437 | 1.004843627 | 0.01234681 |
| H63C | 1.017190504 | 1.004847633 | 0.012342871 |
| | MeOH-3 | MeOH-3 | Difference |
| O5 | 6.527360032 | 6.544926663 | −0.017566631 |
| O5 | 6.527345555 | 6.544911991 | −0.017566436 |
| O5 | 6.527358547 | 6.544924538 | −0.017565991 |
| O5 | 6.52735781 | 6.544927794 | −0.017569984 |
| H5A | 0.874450342 | 0.734422083 | 0.140028259 |
| H5A | 0.874473404 | 0.734437337 | 0.140036067 |
| H5A | 0.874452865 | 0.73442465 | 0.140028215 |
| H5A | 0.874454658 | 0.734420198 | 0.14003446 |
| C65B | 3.728446369 | 3.793681380 | −0.065235011 |
| C65B | 3.728446043 | 3.793677455 | −0.065231412 |
| C65B | 3.728446314 | 3.793680898 | −0.065234584 |
| C65B | 3.728445285 | 3.793680166 | −0.065234881 |
| H65D | 0.994414447 | 0.95527323 | 0.039141217 |
| H65D | 0.994415529 | 0.955272323 | 0.039143206 |
| H65D | 0.99441493 | 0.955273214 | 0.039141716 |
| H65D | 0.994414627 | 0.955272782 | 0.039141845 |
| H65E | 1.023324584 | 0.987149203 | 0.036175381 |
| H65E | 1.023324738 | 0.987138115 | 0.036186623 |
| H65E | 1.023324028 | 0.987149087 | 0.036174941 |
| H65E | 1.023324011 | 0.98713756 | 0.036186451 |
| H65F | 1.01290286 | 0.984479381 | 0.028423479 |
| H65F | 1.012905356 | 0.984494706 | 0.02841065 |
| H65F | 1.012903348 | 0.984479551 | 0.028423797 |
| H65F | 1.012904226 | 0.984493426 | 0.0284108 |

**Table S4-3** The results of Mulliken population analysis of [Zn(4-mxbdt)$_2$]$^{2-}$ complex and vapor molecules in **4-Zn·H$_2$O**. Here, Mulliken charges for each atom in neutral state are as follows: Zn = 20, S = 6, O = 6, C = 4, and H = 1.

| Crystal | 4-Zn·H$_2$O | 4-Zn·H$_2$O without H$_2$O | |
| --- | --- | --- | --- |
| | [Zn(4-mxbdt)$_2$]$^{2-}$ | [Zn(4-mxbdt)$_2$]$^{2-}$ | Difference |
| Zn1 | 19.69261456 | 19.70000716 | −0.007392606 |
| Zn1 | 19.69261454 | 19.70000973 | −0.007395197 |
| Zn1 | 19.69261692 | 19.70000713 | −0.007390208 |
| Zn1 | 19.6926169 | 19.7000097 | −0.007392799 |
| S1 | 6.517221222 | 6.520103659 | −0.002882437 |
| S1 | 6.517221253 | 6.520153571 | −0.002932318 |
| S1 | 6.517271141 | 6.520103687 | −0.002832546 |
| S1 | 6.517271238 | 6.520153669 | −0.002882431 |
| S2 | 6.485295353 | 6.537784411 | −0.052489058 |
| S2 | 6.485295258 | 6.537763616 | −0.052468358 |
| S2 | 6.485273166 | 6.537784317 | −0.052511151 |
| S2 | 6.485273136 | 6.537763615 | −0.052490479 |
| S3 | 6.480131539 | 6.526811038 | −0.046679499 |
| S3 | 6.480131645 | 6.526732317 | −0.046600672 |
| S3 | 6.480046617 | 6.526811101 | −0.046764484 |
| S3 | 6.48004643 | 6.526732114 | −0.046685684 |
| S4 | 6.549923731 | 6.555898083 | −0.005974352 |
| S4 | 6.549923669 | 6.555844204 | −0.005920535 |
| S4 | 6.549869957 | 6.555898023 | −0.006028066 |
| S4 | 6.549869868 | 6.555844116 | −0.005974248 |
| O1 | 6.448365804 | 6.449245916 | −0.000880112 |
| O1 | 6.448365905 | 6.449394674 | −0.001028769 |
| O1 | 6.448515282 | 6.449246015 | −0.000730733 |
| O1 | 6.448515368 | 6.449394757 | −0.000879389 |
| O2 | 6.448948016 | 6.449137139 | −0.000189123 |
| O2 | 6.448948106 | 6.449051925 | −0.000103819 |
| O2 | 6.448862427 | 6.44913723 | −0.000274803 |
| O2 | 6.448862553 | 6.449052054 | −0.000189501 |
| C1 | 3.840814461 | 3.844057162 | −0.003242701 |

| | | | |
|---|---|---|---|
| C1 | 3.840814816 | 3.843960570 | −0.003145754 |
| C1 | 3.84071746 | 3.844057520 | −0.00334006 |
| C1 | 3.840717752 | 3.843960866 | −0.003243114 |
| C2 | 3.994563239 | 3.997888080 | −0.003324841 |
| C2 | 3.994563654 | 3.997871622 | −0.003307968 |
| C2 | 3.994545259 | 3.997888495 | −0.003343236 |
| C2 | 3.99454544 | 3.997871807 | −0.003326367 |
| H2 | 1.072391461 | 1.075439711 | −0.00304825 |
| H2 | 1.072391245 | 1.075505287 | −0.003114042 |
| H2 | 1.07245391 | 1.075439485 | −0.002985575 |
| H2 | 1.072453819 | 1.075505191 | −0.003051372 |
| C3 | 3.760865642 | 3.765559020 | −0.004693378 |
| C3 | 3.760864879 | 3.765382816 | −0.004517937 |
| C3 | 3.760688626 | 3.765558267 | −0.004869641 |
| C3 | 3.760688024 | 3.765382215 | −0.004694191 |
| C4 | 3.97266042 | 3.976278957 | −0.003618537 |
| C4 | 3.972660375 | 3.976301512 | −0.003641137 |
| C4 | 3.972682222 | 3.976278921 | −0.003596699 |
| C4 | 3.972681486 | 3.976300798 | −0.003619312 |
| H4 | 1.081987124 | 1.084814587 | −0.002827463 |
| H4 | 1.081987655 | 1.084815151 | −0.002827496 |
| H4 | 1.08198748 | 1.084815116 | −0.002827636 |
| H4 | 1.081987751 | 1.084815412 | −0.002827661 |
| C5 | 3.958841797 | 3.961629587 | −0.00278779 |
| C5 | 3.958841427 | 3.961673336 | −0.002831909 |
| C5 | 3.958884988 | 3.961629224 | −0.002744236 |
| C5 | 3.958885437 | 3.961673783 | −0.002788346 |
| H5 | 1.042977198 | 1.044977298 | −0.0020001 |
| H5 | 1.042977151 | 1.044920148 | −0.001942997 |
| H5 | 1.042920261 | 1.044977249 | −0.002056988 |
| H5 | 1.042920212 | 1.044920093 | −0.001999881 |
| C6 | 3.844567993 | 3.854649473 | −0.01008148 |
| C6 | 3.844568124 | 3.854638457 | −0.010070333 |
| C6 | 3.844563051 | 3.854649583 | −0.010086532 |
| C6 | 3.844563184 | 3.854638558 | −0.010075374 |
| C7 | 3.870014892 | 3.872586887 | −0.002571995 |
| C7 | 3.870014667 | 3.872563175 | −0.002548508 |
| C7 | 3.86999045 | 3.872586653 | −0.002596203 |

| | | | |
|------|--------------|--------------|---------------|
| C7   | 3.869990678  | 3.872563394  | −0.002572716  |
| C8   | 3.95614155   | 3.957257589  | −0.001116039  |
| C8   | 3.956141886  | 3.957285214  | −0.001143328  |
| C8   | 3.956169114  | 3.957257928  | −0.001088814  |
| C8   | 3.956168755  | 3.957284857  | −0.001116102  |
| H8   | 1.026338817  | 1.028033276  | −0.001694459  |
| H8   | 1.026338816  | 1.028020856  | −0.00168204   |
| H8   | 1.026326705  | 1.028033269  | −0.001706564  |
| H8   | 1.026326708  | 1.028020859  | −0.001694151  |
| C9   | 4.041928274  | 4.045361590  | −0.003433316  |
| C9   | 4.041928293  | 4.045351653  | −0.00342336   |
| C9   | 4.04191825   | 4.045361606  | −0.003443356  |
| C9   | 4.041917948  | 4.045351352  | −0.003433404  |
| C10  | 1.047733199  | 1.049894406  | −0.002161207  |
| C10  | 1.047733022  | 1.049903016  | −0.002169994  |
| C10  | 1.047741843  | 1.049894234  | −0.002152391  |
| C10  | 1.047742105  | 1.049903283  | −0.002161178  |
| H10  | 3.763743022  | 3.765649406  | −0.001906384  |
| H10  | 3.76374303   | 3.765710062  | −0.001967032  |
| H10  | 3.763804324  | 3.765649402  | −0.001845078  |
| H10  | 3.763804355  | 3.765710087  | −0.001905732  |
| C11  | 3.941212502  | 3.943902271  | −0.002689769  |
| C11  | 3.941212571  | 3.943869452  | −0.002656881  |
| C11  | 3.941179002  | 3.943902353  | −0.002723351  |
| C11  | 3.941179517  | 3.943869962  | −0.002690445  |
| H11  | 1.060991383  | 1.061370489  | −0.000379106  |
| H11  | 1.060991662  | 1.061399932  | −0.00040827   |
| H11  | 1.061021290  | 1.061370768  | −0.000349478  |
| H11  | 1.061021189  | 1.061399832  | −0.000378643  |
| C12  | 3.853006691  | 3.863229065  | −0.010222374  |
| C12  | 3.853006273  | 3.863259925  | −0.010253652  |
| C12  | 3.853040281  | 3.863228658  | −0.010188377  |
| C12  | 3.853040193  | 3.863259827  | −0.010219634  |
| C13  | 3.770089033  | 3.776198360  | −0.006109327  |
| C13  | 3.770088974  | 3.776292699  | −0.006203725  |
| C13  | 3.770182500  | 3.776198293  | −0.006015793  |
| C13  | 3.770182257  | 3.776292466  | −0.006110209  |
| H13A | 1.005050418  | 1.007655179  | −0.002604761  |

| | | | |
|---|---|---|---|
| H13A | 1.005050566 | 1.007646153 | −0.002595587 |
| H13A | 1.005041479 | 1.007655325 | −0.002613846 |
| H13A | 1.005041896 | 1.007646565 | −0.002604669 |
| H13B | 1.004485900 | 1.005144816 | −0.000658916 |
| H13B | 1.004485594 | 1.005136929 | −0.000651335 |
| H13B | 1.004477842 | 1.005144510 | −0.000666668 |
| H13B | 1.004477592 | 1.005136679 | −0.000659087 |
| H13C | 0.970130273 | 0.969586298 | 0.000543975 |
| H13C | 0.970130489 | 0.969592633 | 0.000537856 |
| H13C | 0.970135529 | 0.969586523 | 0.000549006 |
| H13C | 0.970135589 | 0.969592687 | 0.000542902 |
| C14 | 3.787807140 | 3.788348750 | −0.00054161 |
| C14 | 3.787807309 | 3.788386134 | −0.000578825 |
| C14 | 3.787844555 | 3.788348911 | −0.000504356 |
| C14 | 3.787844205 | 3.788385794 | −0.000541589 |
| H14A | 0.988711104 | 0.988695704 | 1.54E-05 |
| H14A | 0.988711141 | 0.988667981 | 4.316E-05 |
| H14A | 0.988683514 | 0.988695746 | −1.2232E-05 |
| H14A | 0.98868349 | 0.988667949 | 1.5541E-05 |
| H14B | 0.992028638 | 0.994021477 | −0.001992839 |
| H14B | 0.992028614 | 0.994071468 | −0.002042854 |
| H14B | 0.992078469 | 0.994021451 | −0.001942982 |
| H14B | 0.99207864 | 0.994071639 | -0.001992999 |
| H14C | 0.960809403 | 0.960576594 | 0.000232809 |
| H14C | 0.960809200 | 0.960526577 | 0.000282623 |
| H14C | 0.960759221 | 0.960576396 | 0.000182825 |
| H14C | 0.960759396 | 0.960526747 | 0.000232649 |
| Crystal | **4-Zn·H₂O** | H₂O in **4-Zn·H₂O** | |
| | H₂O | H₂O | Difference |
| O3 | 6.684782278 | 6.711115053 | −0.026332775 |
| O3 | 6.684782209 | 6.711045831 | −0.026263622 |
| O3 | 6.684715938 | 6.711114968 | −0.02639903 |
| O3 | 6.684715845 | 6.711045740 | −0.026329895 |
| H1 | 0.768767070 | 0.639402917 | 0.129364153 |
| H1 | 0.768766776 | 0.639535079 | 0.129231697 |
| H1 | 0.768884065 | 0.639402856 | 0.129481209 |
| H1 | 0.768883751 | 0.639535017 | 0.129348734 |
| H3 | 0.751191464 | 0.649482030 | 0.101709434 |

| | | | |
|---|---|---|---|
| H3 | 0.751191809 | 0.649419090 | 0.101772719 |
| H3 | 0.751148416 | 0.649482176 | 0.10166624 |
| H3 | 0.751148759 | 0.649419243 | 0.101729516 |

**Table S4-4** Optical conductivities of transitions between crystal orbitals attributed to visible-light absorption in **4-Zn** at 2.86 eV and 2.98 eV.

| Occupied orbital | Unoccupied orbital | Optical conductivity (a. u.) | Energy difference (eV) |
|---|---|---|---|
| 725 (HOCO−7) | 798 (LUCO+65) | 226.28125 | 2.852 |
| 727 (HOCO−5) | 800 (LUCO+67) | 225.92794 | 2.855 |
| 728 (HOCO−4) | 799 (LUCO+66) | 225.09436 | 2.848 |
| 726 (HOCO−6) | 797 (LUCO+64) | 213.73490 | 2.845 |
| 732 (HOCO) | 802 (LUCO+69) | 44.13738 | 2.957 |
| 730 (HOCO−2) | 803 (LUCO+70) | 34.11675 | 2.974 |
| 732 (HOCO) | 801 (LUCO+68) | 25.84606 | 2.921 |
| 731 (HOCO−1) | 804 (LUCO+71) | 21.84523 | 3.007 |
| 731 (HOCO−1) | 803 (LUCO+70) | 11.18381 | 2.963 |
| 730 (HOCO−2) | 803 (LUCO+70) | 205.16868 | 2.974 |
| 732 (HOCO) | 802 (LUCO+69) | 166.19948 | 2.957 |
| 731 (HOCO−2) | 804 (LUCO+71) | 163.56431 | 3.007 |
| 729 (HOCO−3) | 801 (LUCO+68) | 114.40408 | 2.939 |
| 731 (HOCO−2) | 803 (LUCO+70) | 51.01095 | 2.963 |
| 729 (HOCO−3) | 802 (LUCO+69) | 49.41313 | 2.975 |
| 730 (HOCO−2) | 804 (LUCO+71) | 29.79251 | 3.019 |
| 727 (HOCO−5) | 800 (LUCO+67) | 28.66196 | 2.855 |
| 725 (HOCO−7) | 798 (LUCO+65) | 28.18978 | 2.852 |
| 728 (HOCO−4) | 799 (LUCO+66) | 27.22174 | 2.848 |
| 726 (HOCO−6) | 797 (LUCO+64) | 25.67065 | 2.845 |
| 732 (HOCO) | 801 (LUCO+68) | 25.43513 | 2.921 |

**Table S4-5** Optical conductivities of transitions between crystal orbitals attributed to visible-light absorption in **4-Zn·H₂O** at 3.01 eV.

| Occupied orbital | Unoccupied orbital | Optical conductivity (a. u.) | Energy difference (eV) |
|---|---|---|---|

| | | | |
|---|---|---|---|
| 744 (HOCO−4) | 816 (LUCO+67) | 258.80978 | 3.005 |
| 742 (HOCO−6) | 814 (LUCO+65) | 258.66819 | 3.004 |
| 741 (HOCO−7) | 813 (LUCO+64) | 257.89262 | 3.005 |
| 743 (HOCO−5) | 815 (LUCO+66) | 250.66973 | 3.002 |
| 747 (HOCO−1) | 820 (LUCO+71) | 203.93718 | 3.010 |
| 746 (HOCO−2) | 818 (LUCO+69) | 145.42868 | 2.984 |
| 748 (HOCO) | 819 (LUCO+70) | 126.10082 | 2.976 |
| 745 (HOCO−3) | 817 (LUCO+68) | 89.49873 | 2.960 |
| 745 (HOCO−3) | 819 (LUCO+70) | 37.76301 | 2.990 |
| 746 (HOCO−2) | 820 (LUCO+71) | 36.37202 | 3.019 |
| 747 (HOCO−1) | 818 (LUCO+69) | 29.41311 | 2.974 |
| 748 (HOCO) | 817 (LUCO+68) | 20.02089 | 2.947 |

**Table S4-6** Optical conductivities of transitions between crystal orbitals attributed to visible-light absorption in **4-Zn·2MeOH (minor)** at 2.95 eV.

| Occupied orbital | Unoccupied orbital | Optical conductivity (a. u.) | Energy difference (eV) |
|---|---|---|---|
| 787 (HOCO−1) | 860 (LUCO+71) | 188.25389 | 2.934 |
| 784 (HOCO−4) | 856 (LUCO+67) | 182.12966 | 2.944 |
| 783 (HOCO−5) | 855 (LUCO+66) | 168.92545 | 2.943 |
| 788 (HOCO) | 859 (LUCO+70) | 157.51822 | 2.922 |
| 786 (HOCO−2) | 858 (LUCO+69) | 145.88360 | 2.923 |
| 781 (HOCO−7) | 853 (LUCO+64) | 139.76743 | 2.944 |
| 785 (HOCO−3) | 857 (LUCO+68) | 126.78361 | 2.914 |
| 782 (HOCO−6) | 854 (LUCO+65) | 126.42786 | 2.953 |
| 786 (HOCO−2) | 860 (LUCO+71) | 20.95589 | 2.936 |
| 785 (HOCO−3) | 859 (LUCO+70) | 17.72998 | 2.927 |
| 787 (HOCO−1) | 858 (LUCO+69) | 16.58588 | 2.921 |
| 788 (HOCO) | 857 (LUCO+68) | 12.83607 | 2.909 |
| 782 (HOCO−6) | 856 (LUCO+67) | 12.56533 | 2.954 |
| 781 (HOCO−7) | 857 (LUCO+68) | 11.89809 | 3.020 |
| 782 (HOCO−6) | 858 (LUCO+69) | 11.45663 | 3.027 |
| 781 (HOCO−7) | 855 (LUCO+66) | 10.65922 | 2.957 |
| 781 (HOCO−7) | 855 (LUCO+66) | 10.65922 | 2.957 |

**Table S4-7** Optical conductivities of transitions between crystal orbitals attributed to visible-light absorption in **4-Zn·2MeOH (major)** at 3.03 eV.

| Occupied orbital | Unoccupied orbital | Optical conductivity (a.u.) | Energy difference (eV) |
|---|---|---|---|
| 783 (HOCO−5) | 856 (LUCO+67) | 236.26513 | 3.031 |
| 784 (HOCO−4) | 855 (LUCO+66) | 229.17454 | 3.020 |
| 781 (HOCO−7) | 853 (LUCO+64) | 224.44498 | 3.017 |
| 782 (HOCO−6) | 854 (LUCO+65) | 224.34837 | 3.020 |
| 786 (HOCO−2) | 860 (LUCO+71) | 133.77633 | 3.000 |
| 787 (HOCO−1) | 859 (LUCO+70) | 121.68839 | 2.987 |
| 788 (HOCO) | 858 (LUCO+69) | 113.67270 | 2.985 |
| 785 (HOCO−3) | 857 (LUCO+68) | 110.85168 | 2.988 |
| 782 (HOCO−6) | 856 (LUCO+67) | 41.39571 | 3.036 |
| 781 (HOCO−7) | 855 (LUCO+66) | 40.26094 | 3.029 |
| 783 (HOCO−5) | 854 (LUCO+65) | 38.37522 | 3.016 |
| 784 (HOCO−4) | 853 (LUCO+64) | 34.57263 | 3.008 |
| 786 (HOCO−2) | 859 (LUCO+70) | 17.64467 | 2.996 |
| 785 (HOCO−3) | 858 (LUCO+69) | 17.35995 | 2.996 |

**Table S4-8** Atom coordinations used for the DFT calculations of **4-Zn·2MeOH (minor)** and **4-Zn·2MeOH (major)**.

| 4-Zn ·2MeOH (minor) | x | y | z | 4-Zn ·2MeOH (major) | x | y | z |
|---|---|---|---|---|---|---|---|
| Zn | 10.92371 | 1.96782 | 15.36148 | Zn | 10.92371 | 1.96782 | 15.36148 |
| Zn | -0.58787 | 8.14932 | 15.3067 | Zn | -0.58787 | 8.14932 | 15.30669 |
| Zn | 3.48852 | 10.39518 | 5.083978 | Zn | 3.48852 | 10.39518 | 5.08397 |
| Zn | 15.00009 | 4.21368 | 5.138763 | Zn | 15.00009 | 4.21368 | 5.13876 |
| S | 10.52723 | 12.14207 | 16.06603 | S | 10.52723 | 12.14207 | 16.06603 |
| S | -0.19139 | 5.96057 | 14.60214 | S | -0.19139 | 5.96057 | 14.60214 |
| S | 3.885 | 0.22093 | 4.37942 | S | 3.885 | 0.22093 | 4.37942 |
| S | 14.60362 | 6.40243 | 5.84331 | S | 14.60362 | 6.40243 | 5.84331 |
| S | 8.8302 | 2.12508 | 14.35516 | S | 8.8302 | 2.12508 | 14.35516 |
| S | 1.50564 | 8.30658 | 16.31302 | S | 1.50564 | 8.30658 | 16.31302 |
| S | 5.58203 | 10.23792 | 6.09029 | S | 5.58203 | 10.23792 | 6.09029 |
| S | 12.90659 | 4.05642 | 4.13243 | S | 12.90659 | 4.05642 | 4.13243 |
| S | 11.59127 | 3.58675 | 16.91064 | S | 11.59127 | 3.58675 | 16.91064 |
| S | -1.25543 | 9.76825 | 13.75754 | S | -1.25543 | 9.76825 | 13.75754 |
| S | 2.82095 | 8.77625 | 3.53481 | S | 2.82095 | 8.77625 | 3.53481 |
| S | 15.66766 | 2.59475 | 6.68791 | S | 15.66766 | 2.59475 | 6.68791 |
| S | 12.76919 | 2.35812 | 14.02006 | S | 12.76919 | 2.35812 | 14.02006 |
| S | -2.43334 | 8.53962 | 16.64812 | S | -2.43334 | 8.53962 | 16.64812 |
| S | 1.64304 | 10.00488 | 6.42539 | S | 1.64304 | 10.00488 | 6.42539 |
| S | 16.84557 | 3.82338 | 3.79733 | S | 16.84557 | 3.82338 | 3.79733 |
| O | 6.74252 | 8.93721 | 14.66859 | O | 6.74252 | 8.93721 | 14.66859 |
| O | 3.59333 | 2.75571 | 15.99959 | O | 3.59333 | 2.75571 | 15.99959 |
| O | 7.66971 | 3.42579 | 5.77686 | O | 7.66971 | 3.42579 | 5.77686 |
| O | 10.8189 | 9.60729 | 4.44586 | O | 10.8189 | 9.60729 | 4.44586 |
| O | -6.51767 | 5.86995 | 17.50785 | O | -6.51767 | 5.86995 | 17.50785 |
| O | 16.85351 | 12.05145 | 13.16033 | O | 16.85351 | 12.05145 | 13.16033 |
| O | 20.9299 | 6.49305 | 2.9376 | O | 20.9299 | 6.49305 | 2.9376 |
| O | -2.44128 | 0.31155 | 7.28512 | O | -2.44128 | 0.31155 | 7.28512 |
| C | 9.02973 | 11.8215 | 15.2061 | C | 9.02973 | 11.8215 | 15.2061 |
| C | 1.30611 | 5.64 | 15.46208 | C | 1.30611 | 5.64 | 15.46208 |

| | | | | | | | |
|---|---|---|---|---|---|---|---|
| C | 5.38249 | 0.5415 | 5.23935 | C | 5.38249 | 0.5415 | 5.23935 |
| C | 13.10612 | 6.723 | 4.98337 | C | 13.10612 | 6.723 | 4.98337 |
| C | 8.50292 | 10.51473 | 15.26192 | C | 8.50292 | 10.51473 | 15.26192 |
| C | 1.83292 | 4.33323 | 15.40626 | C | 1.83292 | 4.33323 | 15.40626 |
| C | 5.9093 | 1.84827 | 5.18354 | C | 5.9093 | 1.84827 | 5.18354 |
| C | 12.57931 | 8.02977 | 5.03919 | C | 12.57931 | 8.02977 | 5.03919 |
| H | 8.96374 | 9.849 | 15.75856 | H | 8.96374 | 9.849 | 15.75856 |
| H | 1.3721 | 3.6675 | 14.90962 | H | 1.3721 | 3.6675 | 14.90962 |
| H | 5.44849 | 2.514 | 4.68689 | H | 5.44849 | 2.514 | 4.68689 |
| H | 13.04012 | 8.6955 | 5.53583 | H | 13.04012 | 8.6955 | 5.53583 |
| C | 7.32763 | 10.18093 | 14.60746 | C | 7.32763 | 10.18093 | 14.60746 |
| C | 3.00821 | 3.99943 | 16.06072 | C | 3.00821 | 3.99943 | 16.06072 |
| C | 7.0846 | 2.18207 | 5.83799 | C | 7.0846 | 2.18207 | 5.83799 |
| C | 11.40402 | 8.36357 | 4.38473 | C | 11.40402 | 8.36357 | 4.38473 |
| C | 6.66722 | 11.12175 | 13.84505 | C | 6.66722 | 11.12175 | 13.84505 |
| C | 3.66862 | 4.94025 | 16.82313 | C | 3.66862 | 4.94025 | 16.82313 |
| C | 7.74501 | 1.24125 | 6.6004 | C | 7.74501 | 1.24125 | 6.6004 |
| C | 10.74361 | 7.42275 | 3.62232 | C | 10.74361 | 7.42275 | 3.62232 |
| H | 5.87852 | 10.88886 | 13.36922 | H | 5.87852 | 10.88886 | 13.36922 |
| H | 4.45732 | 4.70736 | 17.29896 | H | 4.45732 | 4.70736 | 17.29896 |
| H | 8.53371 | 1.47414 | 7.07623 | H | 8.53371 | 1.47414 | 7.07623 |
| H | 9.95491 | 7.65564 | 3.14649 | H | 9.95491 | 7.65564 | 3.14649 |
| C | 7.17125 | 0.04574 | 13.78412 | C | 7.17125 | 0.04574 | 13.78412 |
| C | 3.16459 | 6.22724 | 16.88406 | C | 3.16459 | 6.22724 | 16.88406 |
| C | 7.24098 | 12.31726 | 6.66133 | C | 7.24098 | 12.31726 | 6.66133 |
| C | 11.24763 | 6.13576 | 3.56139 | C | 11.24763 | 6.13576 | 3.56139 |
| H | 6.71293 | 0.69052 | 13.25808 | H | 6.71293 | 0.69052 | 13.25808 |
| H | 3.62291 | 6.87202 | 17.4101 | H | 3.62291 | 6.87202 | 17.4101 |
| H | 7.6993 | 11.67248 | 7.18737 | H | 7.6993 | 11.67248 | 7.18737 |
| H | 10.78931 | 5.49098 | 3.03535 | H | 10.78931 | 5.49098 | 3.03535 |
| C | 8.32987 | 0.43518 | 14.46679 | C | 8.32987 | 0.43518 | 14.46679 |
| C | 2.00597 | 6.61668 | 16.20138 | C | 2.00597 | 6.61668 | 16.20138 |
| C | 6.08235 | 11.92782 | 5.97866 | C | 6.08235 | 11.92782 | 5.97866 |
| C | 12.40626 | 5.74632 | 4.24407 | C | 12.40626 | 5.74632 | 4.24407 |
| C | 13.21318 | 3.94256 | 16.28889 | C | 13.21318 | 3.94256 | 16.28889 |
| C | -2.87734 | 10.12406 | 14.37929 | C | -2.87734 | 10.12406 | 14.37929 |
| C | 1.19904 | 8.42044 | 4.15656 | C | 1.19904 | 8.42044 | 4.15656 |
| C | 17.28957 | 2.23894 | 6.06617 | C | 17.28957 | 2.23894 | 6.06617 |

| | | | | | | | |
|---|---|---|---|---|---|---|---|
| C | 14.0482 | 4.74863 | 17.06275 | C | 14.0482 | 4.74863 | 17.06275 |
| C | -3.71235 | 10.93013 | 13.60542 | C | -3.71235 | 10.93013 | 13.60542 |
| C | 0.36403 | 7.61437 | 3.3827 | C | 0.36403 | 7.61437 | 3.3827 |
| C | 18.12458 | 1.43287 | 6.84003 | C | 18.12458 | 1.43287 | 6.84003 |
| H | 13.72702 | 5.09254 | 17.88811 | H | 13.72702 | 5.09254 | 17.88811 |
| H | -3.39118 | 11.27404 | 12.78006 | H | -3.39118 | 11.27404 | 12.78006 |
| H | 0.68521 | 7.27046 | 2.55734 | H | 0.68521 | 7.27046 | 2.55734 |
| H | 17.8034 | 1.08896 | 7.66539 | H | 17.8034 | 1.08896 | 7.66539 |
| C | 15.33296 | 5.0577 | 16.65609 | C | 15.33296 | 5.0577 | 16.65609 |
| C | -4.99712 | 11.2392 | 14.01208 | C | -4.99712 | 11.2392 | 14.01208 |
| C | -0.92073 | 7.3053 | 3.78936 | C | -0.92073 | 7.3053 | 3.78936 |
| C | 19.40935 | 1.1238 | 6.43337 | C | 19.40935 | 1.1238 | 6.43337 |
| C | 15.83231 | 4.55947 | 15.47005 | C | 15.83231 | 4.55947 | 15.47005 |
| C | -5.49646 | 10.74097 | 15.19813 | C | -5.49646 | 10.74097 | 15.19813 |
| C | -1.42008 | 7.80353 | 4.9754 | C | -1.42008 | 7.80353 | 4.9754 |
| C | 19.90869 | 1.62203 | 5.24732 | C | 19.90869 | 1.62203 | 5.24732 |
| H | -5.84502 | 4.75626 | 15.19477 | H | -5.84502 | 4.75626 | 15.19477 |
| H | 16.18086 | 10.93776 | 15.4734 | H | 16.18086 | 10.93776 | 15.4734 |
| H | 20.25725 | 7.60674 | 5.25068 | H | 20.25725 | 7.60674 | 5.25068 |
| H | -1.76863 | 1.42524 | 4.97205 | H | -1.76863 | 1.42524 | 4.97205 |
| C | 15.00668 | 3.76701 | 14.6919 | C | 15.00668 | 3.76701 | 14.6919 |
| C | -4.67084 | 9.94851 | 15.97628 | C | -4.67084 | 9.94851 | 15.97628 |
| C | -0.59445 | 8.59599 | 5.75355 | C | -0.59445 | 8.59599 | 5.75355 |
| C | 19.08306 | 2.41449 | 4.46917 | C | 19.08306 | 2.41449 | 4.46917 |
| H | 15.34092 | 3.43926 | 13.86547 | H | 15.34092 | 3.43926 | 13.86547 |
| H | -5.00507 | 9.62076 | 16.8027 | H | -5.00507 | 9.62076 | 16.8027 |
| H | -0.92869 | 8.92374 | 6.57998 | H | -0.92869 | 8.92374 | 6.57998 |
| H | 19.4173 | 2.74224 | 3.64275 | H | 19.4173 | 2.74224 | 3.64275 |
| C | 13.6991 | 3.42579 | 15.06748 | C | 13.6991 | 3.42579 | 15.06748 |
| C | -3.36326 | 9.60729 | 15.6007 | C | -3.36326 | 9.60729 | 15.6007 |
| C | 0.71313 | 8.93721 | 5.37797 | C | 0.71313 | 8.93721 | 5.37797 |
| C | 17.77549 | 2.75571 | 4.84475 | C | 17.77549 | 2.75571 | 4.84475 |
| C | 7.07176 | 8.11507 | 15.72051 | C | 7.07176 | 8.11507 | 15.72051 |
| C | 3.26408 | 1.93357 | 14.94767 | C | 3.26408 | 1.93357 | 14.94767 |
| C | 7.34047 | 4.24793 | 4.72494 | C | 7.34047 | 4.24793 | 4.72494 |
| C | 11.14815 | 10.42943 | 5.49778 | C | 11.14815 | 10.42943 | 5.49778 |
| H | 7.05113 | 8.62848 | 16.55595 | H | 7.05113 | 8.62848 | 16.55595 |
| H | 3.28472 | 2.44698 | 14.11223 | H | 3.28472 | 2.44698 | 14.11223 |

| H | 7.3611 | 3.73452 | 3.8895 | H | 7.3611 | 3.73452 | 3.8895 |
|---|---|---|---|---|---|---|---|
| H | 11.12751 | 9.91602 | 6.33322 | H | 11.12751 | 9.91602 | 6.33322 |
| H | 7.97181 | 7.75242 | 15.5834 | H | 7.97181 | 7.75242 | 15.5834 |
| H | 2.36403 | 1.57092 | 15.08478 | H | 2.36403 | 1.57092 | 15.08478 |
| H | 6.44042 | 4.61058 | 4.86205 | H | 6.44042 | 4.61058 | 4.86205 |
| H | 12.0482 | 10.79208 | 5.36067 | H | 12.0482 | 10.79208 | 5.36067 |
| H | 6.4276 | 7.37862 | 15.77477 | H | 6.4276 | 7.37862 | 15.77477 |
| H | 3.90824 | 1.19712 | 14.89341 | H | 3.90824 | 1.19712 | 14.89341 |
| H | 7.98463 | 4.98438 | 4.67068 | H | 7.98463 | 4.98438 | 4.67068 |
| H | 10.50399 | 11.16588 | 5.55204 | H | 10.50399 | 11.16588 | 5.55204 |
| C | -5.28462 | 6.41145 | 17.0147 | C | -5.28462 | 6.41145 | 17.0147 |
| C | 15.62046 | 0.22995 | 13.65347 | C | 15.62046 | 0.22995 | 13.65347 |
| C | 19.69684 | 5.95155 | 3.43075 | C | 19.69684 | 5.95155 | 3.43075 |
| C | -1.20823 | 12.13305 | 6.79198 | C | -1.20823 | 12.13305 | 6.79198 |
| H | -5.46224 | 6.95947 | 16.22183 | H | -5.46224 | 6.95947 | 16.22183 |
| H | 15.79808 | 0.77797 | 14.44635 | H | 15.79808 | 0.77797 | 14.44635 |
| H | 19.87447 | 5.40353 | 4.22362 | H | 19.87447 | 5.40353 | 4.22362 |
| H | -1.38585 | 11.58503 | 5.9991 | H | -1.38585 | 11.58503 | 5.9991 |
| H | -4.67839 | 5.67935 | 16.77682 | H | -4.67839 | 5.67935 | 16.77682 |
| H | 15.01423 | 11.86085 | 13.89135 | H | 15.01423 | 11.86085 | 13.89135 |
| H | 19.09062 | 6.68365 | 3.66863 | H | 19.09062 | 6.68365 | 3.66863 |
| H | -0.602 | 0.50215 | 6.5541 | H | -0.602 | 0.50215 | 6.5541 |
| H | -4.87057 | 6.96603 | 17.70883 | H | -4.87057 | 6.96603 | 17.70883 |
| H | 15.20642 | 0.78453 | 12.95935 | H | 15.20642 | 0.78453 | 12.95935 |
| H | 19.2828 | 5.39697 | 2.73662 | H | 19.2828 | 5.39697 | 2.73662 |
| H | -0.79419 | 11.57847 | 7.4861 | H | -0.79419 | 11.57847 | 7.4861 |
| P | 9.34367 | 8.70504 | 10.72078 | P | 9.34367 | 8.70504 | 10.72078 |
| P | 0.99218 | 2.52354 | 19.9474 | P | 0.99218 | 2.52354 | 19.9474 |
| P | 5.06856 | 3.65796 | 9.72467 | P | 5.06856 | 3.65796 | 9.72467 |
| P | 13.42005 | 9.83946 | 0.49805 | P | 13.42005 | 9.83946 | 0.49805 |
| C | 9.66765 | 7.51423 | 12.02131 | C | 9.66765 | 7.51423 | 12.02131 |
| C | 0.6682 | 1.33273 | 18.64686 | C | 0.6682 | 1.33273 | 18.64686 |
| C | 4.74458 | 4.84877 | 8.42414 | C | 4.74458 | 4.84877 | 8.42414 |
| C | 13.74403 | 11.03027 | 1.79859 | C | 13.74403 | 11.03027 | 1.79859 |
| C | 10.31087 | 7.86781 | 13.19692 | C | 10.31087 | 7.86781 | 13.19692 |
| C | 0.02498 | 1.68631 | 17.47125 | C | 0.02498 | 1.68631 | 17.47125 |
| C | 4.10136 | 4.49519 | 7.24853 | C | 4.10136 | 4.49519 | 7.24853 |
| C | 14.38725 | 10.67669 | 2.9742 | C | 14.38725 | 10.67669 | 2.9742 |

| | | | | | | | |
|---|---|---|---|---|---|---|---|
| H | 10.59262 | 8.76371 | 13.33951 | H | 10.59262 | 8.76371 | 13.33951 |
| H | -0.25678 | 2.58221 | 17.32866 | H | -0.25678 | 2.58221 | 17.32866 |
| H | 3.81961 | 3.59929 | 7.10594 | H | 3.81961 | 3.59929 | 7.10594 |
| H | 14.669 | 9.78079 | 3.11679 | H | 14.669 | 9.78079 | 3.11679 |
| C | 10.53847 | 6.89979 | 14.16195 | C | 10.53847 | 6.89979 | 14.16195 |
| C | -0.20263 | 0.71829 | 16.50623 | C | -0.20263 | 0.71829 | 16.50623 |
| C | 3.87376 | 5.46321 | 6.2835 | C | 3.87376 | 5.46321 | 6.2835 |
| C | 14.61485 | 11.64471 | 3.93922 | C | 14.61485 | 11.64471 | 3.93922 |
| H | 10.98898 | 7.13298 | 14.96511 | H | 10.98898 | 7.13298 | 14.96511 |
| H | -0.65314 | 0.95148 | 15.70307 | H | -0.65314 | 0.95148 | 15.70307 |
| H | 3.42325 | 5.23002 | 5.48034 | H | 3.42325 | 5.23002 | 5.48034 |
| H | 15.06536 | 11.41152 | 4.74238 | H | 15.06536 | 11.41152 | 4.74238 |
| C | 10.11672 | 5.59797 | 13.96731 | C | 10.11672 | 5.59797 | 13.96731 |
| C | 0.21912 | 11.77947 | 16.70087 | C | 0.21912 | 11.77947 | 16.70087 |
| C | 4.29551 | 6.76503 | 6.47814 | C | 4.29551 | 6.76503 | 6.47814 |
| C | 14.19311 | 0.58353 | 3.74458 | C | 14.19311 | 0.58353 | 3.74458 |
| H | 10.27449 | 4.94321 | 14.63682 | H | 10.27449 | 4.94321 | 14.63682 |
| H | 0.06135 | 11.12471 | 16.03136 | H | 0.06135 | 11.12471 | 16.03136 |
| H | 4.13774 | 7.41979 | 5.80863 | H | 4.13774 | 7.41979 | 5.80863 |
| H | 14.35088 | 1.23829 | 4.41409 | H | 14.35088 | 1.23829 | 4.41409 |
| C | 9.46727 | 5.25057 | 12.80335 | C | 9.46727 | 5.25057 | 12.80335 |
| C | 0.86857 | 11.43207 | 17.86483 | C | 0.86857 | 11.43207 | 17.86483 |
| C | 4.94495 | 7.11243 | 7.6421 | C | 4.94495 | 7.11243 | 7.6421 |
| C | 13.54366 | 0.93093 | 2.58062 | C | 13.54366 | 0.93093 | 2.58062 |
| H | 9.17338 | 4.35708 | 12.6736 | H | 9.17338 | 4.35708 | 12.6736 |
| H | 1.16246 | 10.53858 | 17.99457 | H | 1.16246 | 10.53858 | 17.99457 |
| H | 5.23885 | 8.00592 | 7.77185 | H | 5.23885 | 8.00592 | 7.77185 |
| H | 13.24977 | 1.82442 | 2.45088 | H | 13.24977 | 1.82442 | 2.45088 |
| C | 9.24258 | 6.19634 | 11.82708 | C | 9.24258 | 6.19634 | 11.82708 |
| C | 1.09327 | 0.01484 | 18.8411 | C | 1.09327 | 0.01484 | 18.8411 |
| C | 5.16965 | 6.16666 | 8.61837 | C | 5.16965 | 6.16666 | 8.61837 |
| C | 13.31896 | 12.34816 | 1.60435 | C | 13.31896 | 12.34816 | 1.60435 |
| H | 8.7994 | 5.95351 | 11.02261 | H | 8.7994 | 5.95351 | 11.02261 |
| H | 1.53644 | 12.13501 | 19.64556 | H | 1.53644 | 12.13501 | 19.64556 |
| H | 5.61283 | 6.40949 | 9.42284 | H | 5.61283 | 6.40949 | 9.42284 |
| H | 12.87579 | 0.22799 | 0.79989 | H | 12.87579 | 0.22799 | 0.79989 |
| C | 7.64547 | 9.26607 | 10.76821 | C | 7.64547 | 9.26607 | 10.76821 |
| C | 2.69038 | 3.08457 | 19.89997 | C | 2.69038 | 3.08457 | 19.89997 |

| | | | | | | | |
|---|---|---|---|---|---|---|---|
| C | 6.76676 | 3.09693 | 9.67724 | C | 6.76676 | 3.09693 | 9.67724 |
| C | 11.72185 | 9.27843 | 0.54548 | C | 11.72185 | 9.27843 | 0.54548 |
| C | 6.6486 | 8.53171 | 11.39507 | C | 6.6486 | 8.53171 | 11.39507 |
| C | 3.68724 | 2.35021 | 19.27311 | C | 3.68724 | 2.35021 | 19.27311 |
| C | 7.76363 | 3.83129 | 9.05038 | C | 7.76363 | 3.83129 | 9.05038 |
| C | 10.72499 | 10.01279 | 1.17234 | C | 10.72499 | 10.01279 | 1.17234 |
| H | 6.87225 | 7.75608 | 11.89682 | H | 6.87225 | 7.75608 | 11.89682 |
| H | 3.46359 | 1.57458 | 18.77136 | H | 3.46359 | 1.57458 | 18.77136 |
| H | 7.53998 | 4.60692 | 8.54863 | H | 7.53998 | 4.60692 | 8.54863 |
| H | 10.94863 | 10.78842 | 1.67409 | H | 10.94863 | 10.78842 | 1.67409 |
| C | 5.33299 | 8.92979 | 11.28773 | C | 5.33299 | 8.92979 | 11.28773 |
| C | 5.00285 | 2.74829 | 19.38045 | C | 5.00285 | 2.74829 | 19.38045 |
| C | 9.07924 | 3.43321 | 9.15772 | C | 9.07924 | 3.43321 | 9.15772 |
| C | 9.40937 | 9.61471 | 1.065 | C | 9.40937 | 9.61471 | 1.065 |
| H | 4.65052 | 8.44163 | 11.73395 | H | 4.65052 | 8.44163 | 11.73395 |
| H | 5.68532 | 2.26013 | 18.93422 | H | 5.68532 | 2.26013 | 18.93422 |
| H | 9.7617 | 3.92137 | 8.7115 | H | 9.7617 | 3.92137 | 8.7115 |
| H | 8.72691 | 10.10287 | 1.51123 | H | 8.72691 | 10.10287 | 1.51123 |
| C | 5.00772 | 10.04123 | 10.52859 | C | 5.00772 | 10.04123 | 10.52859 |
| C | 5.32813 | 3.85973 | 20.13959 | C | 5.32813 | 3.85973 | 20.13959 |
| C | 9.40451 | 2.32177 | 9.91686 | C | 9.40451 | 2.32177 | 9.91686 |
| C | 9.0841 | 8.50327 | 0.30586 | C | 9.0841 | 8.50327 | 0.30586 |
| H | 4.09815 | 10.29891 | 10.43429 | H | 4.09815 | 10.29891 | 10.43429 |
| H | 6.23769 | 4.11741 | 20.23388 | H | 6.23769 | 4.11741 | 20.23388 |
| H | 10.31408 | 2.06409 | 10.01116 | H | 10.31408 | 2.06409 | 10.01116 |
| H | 8.17454 | 8.24559 | 0.21157 | H | 8.17454 | 8.24559 | 0.21157 |
| C | 5.99756 | 10.77806 | 9.90746 | C | 5.99756 | 10.77806 | 9.90746 |
| C | 12.49105 | 4.59656 | 0.31527 | C | 12.49105 | 4.59656 | 0.31527 |
| C | 8.41467 | 1.58494 | 10.53799 | C | 8.41467 | 1.58494 | 10.53799 |
| C | 1.92118 | 7.76644 | 20.13018 | C | 1.92118 | 7.76644 | 20.13018 |
| H | 5.76916 | 11.5405 | 9.38921 | H | 5.76916 | 11.5405 | 9.38921 |
| H | 12.71945 | 5.359 | 0.83352 | H | 12.71945 | 5.359 | 0.83352 |
| H | 8.64306 | 0.8225 | 11.05625 | H | 8.64306 | 0.8225 | 11.05625 |
| H | 1.69278 | 7.004 | 19.61193 | H | 1.69278 | 7.004 | 19.61193 |
| C | 7.31492 | 10.40346 | 10.04097 | C | 7.31492 | 10.40346 | 10.04097 |
| C | 11.17369 | 4.22196 | 0.18176 | C | 11.17369 | 4.22196 | 0.18176 |
| C | 7.09731 | 1.95954 | 10.40449 | C | 7.09731 | 1.95954 | 10.40449 |
| C | 3.23854 | 8.14104 | 20.26369 | C | 3.23854 | 8.14104 | 20.26369 |

| | | | | | | | |
|---|---|---|---|---|---|---|---|
| H | 7.99914 | 10.92393 | 9.63606 | H | 7.99914 | 10.92393 | 9.63606 |
| H | 10.48947 | 4.74243 | 0.58666 | H | 10.48947 | 4.74243 | 0.58666 |
| H | 6.41309 | 1.43907 | 10.80939 | H | 6.41309 | 1.43907 | 10.80939 |
| H | 3.92276 | 7.62057 | 19.85879 | H | 3.92276 | 7.62057 | 19.85879 |
| C | 9.60337 | 7.87029 | 9.15445 | C | 9.60337 | 7.87029 | 9.15445 |
| C | 8.88524 | 1.68879 | 1.06827 | C | 8.88524 | 1.68879 | 1.06827 |
| C | 4.80885 | 4.49271 | 11.291 | C | 4.80885 | 4.49271 | 11.291 |
| C | 5.52699 | 10.67421 | 19.37718 | C | 5.52699 | 10.67421 | 19.37718 |
| C | 8.64775 | 7.92716 | 8.15058 | C | 8.64775 | 7.92716 | 8.15058 |
| C | 9.84087 | 1.74566 | 2.07215 | C | 9.84087 | 1.74566 | 2.07215 |
| C | 5.76448 | 4.43584 | 12.29487 | C | 5.76448 | 4.43584 | 12.29487 |
| C | 4.57136 | 10.61734 | 18.3733 | C | 4.57136 | 10.61734 | 18.3733 |
| H | 7.86191 | 8.44827 | 8.26491 | H | 7.86191 | 8.44827 | 8.26491 |
| H | 10.6267 | 2.26677 | 1.95782 | H | 10.6267 | 2.26677 | 1.95782 |
| H | 6.55032 | 3.91473 | 12.18054 | H | 6.55032 | 3.91473 | 12.18054 |
| H | 3.78552 | 10.09623 | 18.48763 | H | 3.78552 | 10.09623 | 18.48763 |
| C | 8.84996 | 7.21752 | 6.98478 | C | 8.84996 | 7.21752 | 6.98478 |
| C | 9.63865 | 1.03602 | 3.23795 | C | 9.63865 | 1.03602 | 3.23795 |
| C | 5.56227 | 5.14548 | 13.46067 | C | 5.56227 | 5.14548 | 13.46067 |
| C | 4.77357 | 11.32698 | 17.2075 | C | 4.77357 | 11.32698 | 17.2075 |
| H | 8.19452 | 7.2486 | 6.29773 | H | 8.19452 | 7.2486 | 6.29773 |
| H | 10.2941 | 1.0671 | 3.92499 | H | 10.2941 | 1.0671 | 3.92499 |
| H | 6.21771 | 5.1144 | 14.14772 | H | 6.21771 | 5.1144 | 14.14772 |
| H | 4.11813 | 11.2959 | 16.52046 | H | 4.11813 | 11.2959 | 16.52046 |
| C | 9.98347 | 6.46956 | 6.80465 | C | 9.98347 | 6.46956 | 6.80465 |
| C | 8.50515 | 0.28806 | 3.41807 | C | 8.50515 | 0.28806 | 3.41807 |
| C | 4.42876 | 5.89344 | 13.6408 | C | 4.42876 | 5.89344 | 13.6408 |
| C | 5.90708 | 12.07494 | 17.02738 | C | 5.90708 | 12.07494 | 17.02738 |
| H | 10.09997 | 5.97172 | 6.00383 | H | 10.09997 | 5.97172 | 6.00383 |
| H | 8.38865 | 12.15322 | 4.2189 | H | 8.38865 | 12.15322 | 4.2189 |
| H | 4.31226 | 6.39128 | 14.44162 | H | 4.31226 | 6.39128 | 14.44162 |
| H | 6.02358 | 0.20978 | 16.22655 | H | 6.02358 | 0.20978 | 16.22655 |
| C | 10.95301 | 6.43618 | 7.77929 | C | 10.95301 | 6.43618 | 7.77929 |
| C | 7.5356 | 0.25468 | 2.44344 | C | 7.5356 | 0.25468 | 2.44344 |
| C | 3.45921 | 5.92682 | 12.66616 | C | 3.45921 | 5.92682 | 12.66616 |
| C | 6.87663 | 12.10832 | 18.00201 | C | 6.87663 | 12.10832 | 18.00201 |
| H | 11.75034 | 5.94004 | 7.63789 | H | 11.75034 | 5.94004 | 7.63789 |
| H | 6.73827 | 12.12154 | 2.58484 | H | 6.73827 | 12.12154 | 2.58484 |

| | | | | | | | |
|---|---|---|---|---|---|---|---|
| H | 2.66189 | 6.42296 | 12.80756 | H | 2.66189 | 6.42296 | 12.80756 |
| H | 7.67396 | 0.24146 | 17.86061 | H | 7.67396 | 0.24146 | 17.86061 |
| C | 10.77072 | 7.12232 | 8.96022 | C | 10.77072 | 7.12232 | 8.96022 |
| C | 7.7179 | 0.94082 | 1.26251 | C | 7.7179 | 0.94082 | 1.26251 |
| C | 3.64151 | 5.24068 | 11.48523 | C | 3.64151 | 5.24068 | 11.48523 |
| C | 6.69433 | 11.42218 | 19.18294 | C | 6.69433 | 11.42218 | 19.18294 |
| H | 11.4339 | 7.08666 | 9.63972 | H | 11.4339 | 7.08666 | 9.63972 |
| H | 7.05471 | 0.90516 | 0.583 | H | 7.05471 | 0.90516 | 0.583 |
| H | 2.97832 | 5.27634 | 10.80573 | H | 2.97832 | 5.27634 | 10.80573 |
| H | 7.35752 | 11.45784 | 19.86245 | H | 7.35752 | 11.45784 | 19.86245 |
| C | 10.40558 | 10.15002 | 10.87412 | C | 10.40558 | 10.15002 | 10.87412 |
| C | -0.06974 | 3.96852 | 19.79406 | C | -0.06974 | 3.96852 | 19.79406 |
| C | 4.00665 | 2.21298 | 9.57133 | C | 4.00665 | 2.21298 | 9.57133 |
| C | 14.48197 | 8.39448 | 0.65139 | C | 14.48197 | 8.39448 | 0.65139 |
| C | 11.40583 | 10.41583 | 9.94508 | C | 11.40583 | 10.41583 | 9.94508 |
| C | 7.08278 | 4.23433 | 0.27765 | C | 7.08278 | 4.23433 | 0.27765 |
| C | 3.0064 | 1.94717 | 10.50037 | C | 3.0064 | 1.94717 | 10.50037 |
| C | 7.32945 | 8.12867 | 20.1678 | C | 7.32945 | 8.12867 | 20.1678 |
| H | 11.53759 | 9.83991 | 9.20127 | H | 11.53759 | 9.83991 | 9.20127 |
| H | 6.95102 | 3.65841 | 1.02145 | H | 6.95102 | 3.65841 | 1.02145 |
| H | 2.87464 | 2.52309 | 11.24418 | H | 2.87464 | 2.52309 | 11.24418 |
| H | 7.46121 | 8.70459 | 19.424 | H | 7.46121 | 8.70459 | 19.424 |
| C | 12.21245 | 11.53839 | 10.1207 | C | 12.21245 | 11.53839 | 10.1207 |
| C | 6.27616 | 5.35689 | 0.10202 | C | 6.27616 | 5.35689 | 0.10202 |
| C | 2.19978 | 0.82461 | 10.32475 | C | 2.19978 | 0.82461 | 10.32475 |
| C | 8.13606 | 7.00611 | 20.34343 | C | 8.13606 | 7.00611 | 20.34343 |
| H | 12.89554 | 11.73212 | 9.48951 | H | 12.89554 | 11.73212 | 9.48951 |
| H | 5.59307 | 5.55062 | 0.73321 | H | 5.59307 | 5.55062 | 0.73321 |
| H | 1.51669 | 0.63088 | 10.95594 | H | 1.51669 | 0.63088 | 10.95594 |
| H | 8.81915 | 6.81238 | 19.71224 | H | 8.81915 | 6.81238 | 19.71224 |
| C | 12.02553 | 0.00865 | 11.20513 | C | 12.02553 | 0.00865 | 11.20513 |
| C | -1.68969 | 6.19015 | 19.46305 | C | -1.68969 | 6.19015 | 19.46305 |
| C | 2.38669 | 12.35435 | 9.24032 | C | 2.38669 | 12.35435 | 9.24032 |
| C | 16.10192 | 6.17285 | 0.9824 | C | 16.10192 | 6.17285 | 0.9824 |
| H | 12.59067 | 0.76286 | 11.32782 | H | 12.59067 | 0.76286 | 11.32782 |
| H | -2.25483 | 6.94436 | 19.34035 | H | -2.25483 | 6.94436 | 19.34035 |
| H | 1.82156 | 11.60014 | 9.11763 | H | 1.82156 | 11.60014 | 9.11763 |
| H | 16.66706 | 5.41864 | 1.1051 | H | 16.66706 | 5.41864 | 1.1051 |

| | | | | | | | |
|---|---|---|---|---|---|---|---|
| C | 11.0116 | 12.10832 | 12.117 | C | 11.0116 | 12.10832 | 12.117 |
| C | -0.67575 | 5.92682 | 18.55118 | C | -0.67575 | 5.92682 | 18.55118 |
| C | 3.40063 | 0.25468 | 8.32845 | C | 3.40063 | 0.25468 | 8.32845 |
| C | 15.08798 | 6.43618 | 1.89427 | C | 15.08798 | 6.43618 | 1.89427 |
| H | 10.87699 | 0.32633 | 12.85667 | H | 10.87699 | 0.32633 | 12.85667 |
| H | -0.54115 | 6.50783 | 17.8115 | H | -0.54115 | 6.50783 | 17.8115 |
| H | 3.53523 | 12.03667 | 7.58878 | H | 3.53523 | 12.03667 | 7.58878 |
| H | 14.95338 | 5.85517 | 2.63395 | H | 14.95338 | 5.85517 | 2.63395 |
| C | 10.2006 | 11.00802 | 11.9518 | C | 10.2006 | 11.00802 | 11.9518 |
| C | 0.13525 | 4.82652 | 18.71638 | C | 0.13525 | 4.82652 | 18.71638 |
| C | 4.21163 | 1.35498 | 8.49365 | C | 4.21163 | 1.35498 | 8.49365 |
| C | 14.27698 | 7.53648 | 1.72907 | C | 14.27698 | 7.53648 | 1.72907 |
| H | 9.50248 | 10.83428 | 12.57211 | H | 9.50248 | 10.83428 | 12.57211 |
| H | 0.83336 | 4.65278 | 18.09606 | H | 0.83336 | 4.65278 | 18.09606 |
| H | 4.90975 | 1.52872 | 7.87334 | H | 4.90975 | 1.52872 | 7.87334 |
| H | 13.57887 | 7.71022 | 2.34939 | H | 13.57887 | 7.71022 | 2.34939 |
| P | 15.22094 | 7.53525 | 11.58603 | P | 15.22094 | 7.53525 | 11.58603 |
| P | -4.8851 | 1.35375 | 19.08215 | P | -4.8851 | 1.35375 | 19.08215 |
| P | -0.80871 | 4.82775 | 8.85942 | P | -0.80871 | 4.82775 | 8.85942 |
| P | 19.29733 | 11.00925 | 1.3633 | P | 19.29733 | 11.00925 | 1.3633 |
| C | 14.44067 | 8.24859 | 13.03745 | C | 14.44067 | 8.24859 | 13.03745 |
| C | -4.10483 | 2.06709 | 17.63073 | C | -4.10483 | 2.06709 | 17.63073 |
| C | -0.02844 | 4.11441 | 7.408 | C | -0.02844 | 4.11441 | 7.408 |
| C | 18.51706 | 10.29591 | 2.81473 | C | 18.51706 | 10.29591 | 2.81473 |
| C | 14.51698 | 7.56986 | 14.24721 | C | 14.51698 | 7.56986 | 14.24721 |
| C | -4.18114 | 1.38836 | 16.42097 | C | -4.18114 | 1.38836 | 16.42097 |
| C | -0.10475 | 4.79314 | 6.19824 | C | -0.10475 | 4.79314 | 6.19824 |
| C | 18.59337 | 10.97464 | 4.02448 | C | 18.59337 | 10.97464 | 4.02448 |
| H | 14.99783 | 6.75262 | 14.30417 | H | 14.99783 | 6.75262 | 14.30417 |
| H | -4.66198 | 0.57112 | 16.36401 | H | -4.66198 | 0.57112 | 16.36401 |
| H | -0.5856 | 5.61038 | 6.14128 | H | -0.5856 | 5.61038 | 6.14128 |
| H | 19.07421 | 11.79188 | 4.08144 | H | 19.07421 | 11.79188 | 4.08144 |
| C | 13.89285 | 8.0854 | 15.36762 | C | 13.89285 | 8.0854 | 15.36762 |
| C | -3.557 | 1.9039 | 15.30056 | C | -3.557 | 1.9039 | 15.30056 |
| C | 0.51938 | 4.2776 | 5.07783 | C | 0.51938 | 4.2776 | 5.07783 |
| C | 17.96923 | 10.4591 | 5.14489 | C | 17.96923 | 10.4591 | 5.14489 |
| H | 13.95057 | 7.62422 | 16.19642 | H | 13.95057 | 7.62422 | 16.19642 |
| H | -3.61472 | 1.44273 | 14.47176 | H | -3.61472 | 1.44273 | 14.47176 |

| | | | | | | | |
|---|---|---|---|---|---|---|---|
| H | 0.46166 | 4.73877 | 4.24903 | H | 0.46166 | 4.73877 | 4.24903 |
| H | 18.02695 | 10.92028 | 5.97369 | H | 18.02695 | 10.92028 | 5.97369 |
| C | 13.18454 | 9.27101 | 15.28441 | C | 13.18454 | 9.27101 | 15.28441 |
| C | -2.8487 | 3.08951 | 15.38377 | C | -2.8487 | 3.08951 | 15.38377 |
| C | 1.22769 | 3.09199 | 5.16104 | C | 1.22769 | 3.09199 | 5.16104 |
| C | 17.26093 | 9.27349 | 5.06168 | C | 17.26093 | 9.27349 | 5.06168 |
| H | 12.74724 | 9.61578 | 16.05399 | H | 12.74724 | 9.61578 | 16.05399 |
| H | -2.4114 | 3.43428 | 14.61418 | H | -2.4114 | 3.43428 | 14.61418 |
| H | 1.66499 | 2.74722 | 4.39146 | H | 1.66499 | 2.74722 | 4.39146 |
| H | 16.82362 | 8.92872 | 5.83127 | H | 16.82362 | 8.92872 | 5.83127 |
| C | 13.11099 | 9.94974 | 14.09264 | C | 13.11099 | 9.94974 | 14.09264 |
| C | -2.77514 | 3.76824 | 16.57554 | C | -2.77514 | 3.76824 | 16.57554 |
| C | 1.30124 | 2.41326 | 6.35281 | C | 1.30124 | 2.41326 | 6.35281 |
| C | 17.18737 | 8.59476 | 3.86991 | C | 17.18737 | 8.59476 | 3.86991 |
| H | 12.6309 | 10.76781 | 14.04437 | H | 12.6309 | 10.76781 | 14.04437 |
| H | -2.29505 | 4.58631 | 16.62381 | H | -2.29505 | 4.58631 | 16.62381 |
| H | 1.78133 | 1.59519 | 6.40108 | H | 1.78133 | 1.59519 | 6.40108 |
| H | 16.70728 | 7.77669 | 3.82164 | H | 16.70728 | 7.77669 | 3.82164 |
| C | 13.73555 | 9.44657 | 12.95587 | C | 13.73555 | 9.44657 | 12.95587 |
| C | -3.39971 | 3.26507 | 17.7123 | C | -3.39971 | 3.26507 | 17.7123 |
| C | 0.67668 | 2.91643 | 7.48958 | C | 0.67668 | 2.91643 | 7.48958 |
| C | 17.81194 | 9.09793 | 2.73315 | C | 17.81194 | 9.09793 | 2.73315 |
| H | 13.68141 | 9.91626 | 12.13174 | H | 13.68141 | 9.91626 | 12.13174 |
| H | -3.34557 | 3.73476 | 18.53644 | H | -3.34557 | 3.73476 | 18.53644 |
| H | 0.73082 | 2.44674 | 8.31371 | H | 0.73082 | 2.44674 | 8.31371 |
| H | 17.7578 | 8.62824 | 1.90901 | H | 17.7578 | 8.62824 | 1.90901 |
| C | 14.1966 | 6.23466 | 10.89538 | C | 14.1966 | 6.23466 | 10.89538 |
| C | -3.86075 | 0.05316 | 19.77279 | C | -3.86075 | 0.05316 | 19.77279 |
| C | 0.21563 | 6.12834 | 9.55007 | C | 0.21563 | 6.12834 | 9.55007 |
| C | 18.27298 | 12.30984 | 0.67266 | C | 18.27298 | 12.30984 | 0.67266 |
| C | 13.24406 | 5.59797 | 11.68212 | C | 13.24406 | 5.59797 | 11.68212 |
| C | -2.90822 | 11.77947 | 18.98605 | C | -2.90822 | 11.77947 | 18.98605 |
| C | 1.16816 | 6.76503 | 8.76333 | C | 1.16816 | 6.76503 | 8.76333 |
| C | 17.32045 | 0.58353 | 1.4594 | C | 17.32045 | 0.58353 | 1.4594 |
| H | 13.06232 | 5.91415 | 12.55919 | H | 13.06232 | 5.91415 | 12.55919 |
| H | -2.72648 | 12.09565 | 18.10899 | H | -2.72648 | 12.09565 | 18.10899 |
| H | 1.34991 | 6.44885 | 7.88626 | H | 1.34991 | 6.44885 | 7.88626 |
| H | 17.13871 | 0.26735 | 2.33647 | H | 17.13871 | 0.26735 | 2.33647 |

| | | | | | | | |
|---|---|---|---|---|---|---|---|
| C | 12.56082 | 4.50137 | 11.18407 | C | 12.56082 | 4.50137 | 11.18407 |
| C | -2.22498 | 10.68287 | 19.48411 | C | -2.22498 | 10.68287 | 19.48411 |
| C | 1.8514 | 7.86163 | 9.26138 | C | 1.8514 | 7.86163 | 9.26138 |
| C | 16.63721 | 1.68013 | 0.96135 | C | 16.63721 | 1.68013 | 0.96135 |
| H | 11.91471 | 4.06125 | 11.72379 | H | 11.91471 | 4.06125 | 11.72379 |
| H | -1.57886 | 10.24275 | 18.94439 | H | -1.57886 | 10.24275 | 18.94439 |
| H | 2.49752 | 8.30175 | 8.72166 | H | 2.49752 | 8.30175 | 8.72166 |
| H | 15.99109 | 2.12025 | 1.50106 | H | 15.99109 | 2.12025 | 1.50106 |
| C | 12.81435 | 4.04641 | 9.91052 | C | 12.81435 | 4.04641 | 9.91052 |
| C | 5.67426 | 10.22791 | 0.3122 | C | 5.67426 | 10.22791 | 0.3122 |
| C | 1.59788 | 8.31659 | 10.53493 | C | 1.59788 | 8.31659 | 10.53493 |
| C | 8.73797 | 2.13509 | 20.13325 | C | 8.73797 | 2.13509 | 20.13325 |
| H | 12.33858 | 3.29582 | 9.57538 | H | 12.33858 | 3.29582 | 9.57538 |
| H | 6.15003 | 9.47732 | 0.64734 | H | 6.15003 | 9.47732 | 0.64734 |
| H | 2.07365 | 9.06718 | 10.87007 | H | 2.07365 | 9.06718 | 10.87007 |
| H | 8.26219 | 2.88568 | 19.79811 | H | 8.26219 | 2.88568 | 19.79811 |
| C | 13.75599 | 4.67321 | 9.11376 | C | 13.75599 | 4.67321 | 9.11376 |
| C | 4.73263 | 10.85471 | 1.10896 | C | 4.73263 | 10.85471 | 1.10896 |
| C | 0.65624 | 7.68979 | 11.33169 | C | 0.65624 | 7.68979 | 11.33169 |
| C | 9.6796 | 1.50829 | 19.33649 | C | 9.6796 | 1.50829 | 19.33649 |
| H | 13.92136 | 4.35678 | 8.23328 | H | 13.92136 | 4.35678 | 8.23328 |
| H | 4.56726 | 10.53828 | 1.98944 | H | 4.56726 | 10.53828 | 1.98944 |
| H | 0.49087 | 8.00622 | 12.21217 | H | 0.49087 | 8.00622 | 12.21217 |
| H | 9.84497 | 1.82472 | 18.45601 | H | 9.84497 | 1.82472 | 18.45601 |
| C | 14.45576 | 5.76116 | 9.60261 | C | 14.45576 | 5.76116 | 9.60261 |
| C | 4.03286 | 11.94266 | 0.62011 | C | 4.03286 | 11.94266 | 0.62011 |
| C | -0.04353 | 6.60184 | 10.84284 | C | -0.04353 | 6.60184 | 10.84284 |
| C | 10.37937 | 0.42034 | 19.82534 | C | 10.37937 | 0.42034 | 19.82534 |
| H | 15.11111 | 6.1864 | 9.06267 | H | 15.11111 | 6.1864 | 9.06267 |
| H | 3.37751 | 0.0049 | 1.16005 | H | 3.37751 | 0.0049 | 1.16005 |
| H | -0.69888 | 6.1766 | 11.38278 | H | -0.69888 | 6.1766 | 11.38278 |
| H | 11.03472 | 12.3581 | 19.2854 | H | 11.03472 | 12.3581 | 19.2854 |
| C | 15.48775 | 8.83089 | 10.35726 | C | 15.48775 | 8.83089 | 10.35726 |
| C | -5.15191 | 2.64939 | 20.31092 | C | -5.15191 | 2.64939 | 20.31092 |
| C | -1.07553 | 3.53211 | 10.08819 | C | -1.07553 | 3.53211 | 10.08819 |
| C | 19.56414 | 9.71361 | 0.13453 | C | 19.56414 | 9.71361 | 0.13453 |
| C | 14.68011 | 8.9471 | 9.22785 | C | 14.68011 | 8.9471 | 9.22785 |
| C | 3.8085 | 2.7656 | 0.99488 | C | 3.8085 | 2.7656 | 0.99488 |

| | | | | | | | |
|---|---|---|---|---|---|---|---|
| C | -0.26789 | 3.4159 | 11.2176 | C | -0.26789 | 3.4159 | 11.2176 |
| C | 10.60373 | 9.5974 | 19.45057 | C | 10.60373 | 9.5974 | 19.45057 |
| H | 13.979 | 8.32355 | 9.0768 | H | 13.979 | 8.32355 | 9.0768 |
| H | 4.50961 | 2.14205 | 1.14593 | H | 4.50961 | 2.14205 | 1.14593 |
| H | 0.43322 | 4.03945 | 11.36865 | H | 0.43322 | 4.03945 | 11.36865 |
| H | 9.90262 | 10.22095 | 19.29952 | H | 9.90262 | 10.22095 | 19.29952 |
| C | 14.90377 | 9.972 | 8.32743 | C | 14.90377 | 9.972 | 8.32743 |
| C | 3.58484 | 3.7905 | 1.89529 | C | 3.58484 | 3.7905 | 1.89529 |
| C | -0.49154 | 2.391 | 12.11802 | C | -0.49154 | 2.391 | 12.11802 |
| C | 10.82739 | 8.5725 | 18.55016 | C | 10.82739 | 8.5725 | 18.55016 |
| H | 14.35074 | 10.05469 | 7.55921 | H | 14.35074 | 10.05469 | 7.55921 |
| H | 4.13787 | 3.87319 | 2.66351 | H | 4.13787 | 3.87319 | 2.66351 |
| H | 0.06149 | 2.30831 | 12.88624 | H | 0.06149 | 2.30831 | 12.88624 |
| H | 10.27435 | 8.48981 | 17.78194 | H | 10.27435 | 8.48981 | 17.78194 |
| C | 15.91602 | 10.86955 | 8.53516 | C | 15.91602 | 10.86955 | 8.53516 |
| C | 2.57259 | 4.68805 | 1.68757 | C | 2.57259 | 4.68805 | 1.68757 |
| C | -1.50379 | 1.49345 | 11.91029 | C | -1.50379 | 1.49345 | 11.91029 |
| C | 11.83963 | 7.67495 | 18.75788 | C | 11.83963 | 7.67495 | 18.75788 |
| H | 16.06449 | 11.56968 | 7.91055 | H | 16.06449 | 11.56968 | 7.91055 |
| H | 2.42412 | 5.38818 | 2.31218 | H | 2.42412 | 5.38818 | 2.31218 |
| H | -1.65226 | 0.79332 | 12.5349 | H | -1.65226 | 0.79332 | 12.5349 |
| H | 11.98811 | 6.97482 | 18.13327 | H | 11.98811 | 6.97482 | 18.13327 |
| C | 16.71548 | 10.75952 | 9.64207 | C | 16.71548 | 10.75952 | 9.64207 |
| C | 1.77314 | 4.57802 | 0.58065 | C | 1.77314 | 4.57802 | 0.58065 |
| C | -2.30325 | 1.60348 | 10.80338 | C | -2.30325 | 1.60348 | 10.80338 |
| C | 12.63909 | 7.78498 | 19.8648 | C | 12.63909 | 7.78498 | 19.8648 |
| H | 17.41103 | 11.39045 | 9.78744 | H | 17.41103 | 11.39045 | 9.78744 |
| H | 1.07759 | 5.20895 | 0.43528 | H | 1.07759 | 5.20895 | 0.43528 |
| H | -2.9988 | 0.97255 | 10.65801 | H | -2.9988 | 0.97255 | 10.65801 |
| H | 13.33464 | 7.15405 | 20.01017 | H | 13.33464 | 7.15405 | 20.01017 |
| C | 16.51213 | 9.72597 | 10.55721 | C | 16.51213 | 9.72597 | 10.55721 |
| C | -6.17628 | 3.54447 | 20.11096 | C | -6.17628 | 3.54447 | 20.11096 |
| C | -2.0999 | 2.63703 | 9.88824 | C | -2.0999 | 2.63703 | 9.88824 |
| C | 20.58851 | 8.81853 | 0.33449 | C | 20.58851 | 8.81853 | 0.33449 |
| H | 17.0792 | 9.64063 | 11.31472 | H | 17.0792 | 9.64063 | 11.31472 |
| H | -6.74336 | 3.45913 | 19.35346 | H | -6.74336 | 3.45913 | 19.35346 |
| H | -2.66697 | 2.72237 | 9.13073 | H | -2.66697 | 2.72237 | 9.13073 |
| H | 21.15559 | 8.90387 | 1.09199 | H | 21.15559 | 8.90387 | 1.09199 |

| | | | | | | | |
|---|---|---|---|---|---|---|---|
| C | 16.78712 | 6.81201 | 12.0898 | C | 16.78712 | 6.81201 | 12.0898 |
| C | -6.45128 | 0.63051 | 18.57837 | C | -6.45128 | 0.63051 | 18.57837 |
| C | -2.37489 | 5.55099 | 8.35565 | C | -2.37489 | 5.55099 | 8.35565 |
| C | 20.86351 | 11.73249 | 1.86708 | C | 20.86351 | 11.73249 | 1.86708 |
| C | 17.19292 | 5.60662 | 11.52203 | C | 17.19292 | 5.60662 | 11.52203 |
| C | -6.85707 | 11.78812 | 19.14614 | C | -6.85707 | 11.78812 | 19.14614 |
| C | -2.78069 | 6.75638 | 8.92342 | C | -2.78069 | 6.75638 | 8.92342 |
| C | 21.2693 | 0.57488 | 1.29931 | C | 21.2693 | 0.57488 | 1.29931 |
| H | 16.64071 | 5.1693 | 10.88454 | H | 16.64071 | 5.1693 | 10.88454 |
| H | -6.30487 | 11.3508 | 19.78363 | H | -6.30487 | 11.3508 | 19.78363 |
| H | -2.22849 | 7.1937 | 9.56091 | H | -2.22849 | 7.1937 | 9.56091 |
| H | 20.7171 | 1.0122 | 0.66182 | H | 20.7171 | 1.0122 | 0.66182 |
| C | -4.16134 | 5.05029 | 11.89066 | C | -4.16134 | 5.05029 | 11.89066 |
| C | 14.49719 | 11.23179 | 18.77751 | C | 14.49719 | 11.23179 | 18.77751 |
| C | 18.57357 | 7.31271 | 8.55479 | C | 18.57357 | 7.31271 | 8.55479 |
| C | -0.08496 | 1.13121 | 1.66794 | C | -0.08496 | 1.13121 | 1.66794 |
| H | -3.88374 | 4.22493 | 11.50968 | H | -3.88374 | 4.22493 | 11.50968 |
| H | 14.21958 | 10.40643 | 19.15849 | H | 14.21958 | 10.40643 | 19.15849 |
| H | 18.29597 | 8.13807 | 8.93577 | H | 18.29597 | 8.13807 | 8.93577 |
| H | 0.19265 | 1.95657 | 1.28696 | H | 0.19265 | 1.95657 | 1.28696 |
| C | -3.3544 | 5.68945 | 12.81132 | C | -3.3544 | 5.68945 | 12.81132 |
| C | 13.69025 | 11.87095 | 17.85685 | C | 13.69025 | 11.87095 | 17.85685 |
| C | 17.76663 | 6.67355 | 7.63413 | C | 17.76663 | 6.67355 | 7.63413 |
| C | 0.72198 | 0.49205 | 2.5886 | C | 0.72198 | 0.49205 | 2.5886 |
| H | -2.5152 | 5.31238 | 13.04896 | H | -2.5152 | 5.31238 | 13.04896 |
| H | 12.85104 | 11.49388 | 17.61921 | H | 12.85104 | 11.49388 | 17.61921 |
| H | 16.92743 | 7.05062 | 7.39649 | H | 16.92743 | 7.05062 | 7.39649 |
| H | 1.56119 | 0.86912 | 2.82624 | H | 1.56119 | 0.86912 | 2.82624 |
| C | -3.76502 | 6.87383 | 13.38666 | C | -3.76502 | 6.87383 | 13.38666 |
| C | 14.10086 | 0.69233 | 17.28152 | C | 14.10086 | 0.69233 | 17.28152 |
| C | 18.17725 | 5.48917 | 7.05879 | C | 18.17725 | 5.48917 | 7.05879 |
| C | 0.31136 | 11.67067 | 3.16393 | C | 0.31136 | 11.67067 | 3.16393 |
| H | -3.21423 | 7.3029 | 14.03126 | H | -3.21423 | 7.3029 | 14.03126 |
| H | 13.55008 | 1.1214 | 16.63691 | H | 13.55008 | 1.1214 | 16.63691 |
| H | 17.62646 | 5.0601 | 6.41419 | H | 17.62646 | 5.0601 | 6.41419 |
| H | 0.86215 | 11.2416 | 3.80854 | H | 0.86215 | 11.2416 | 3.80854 |
| C | -4.97444 | 7.44005 | 13.02886 | C | -4.97444 | 7.44005 | 13.02886 |
| C | 15.31029 | 1.25855 | 17.63931 | C | 15.31029 | 1.25855 | 17.63931 |

| Atom | X | Y | Z | Atom | X | Y | Z |
|---|---|---|---|---|---|---|---|
| C | 19.38667 | 4.92295 | 7.41659 | C | 19.38667 | 4.92295 | 7.41659 |
| C | -0.89806 | 11.10445 | 2.80614 | C | -0.89806 | 11.10445 | 2.80614 |
| H | -5.25407 | 8.25731 | 13.42522 | H | -5.25407 | 8.25731 | 13.42522 |
| H | 15.58991 | 2.07581 | 17.24296 | H | 15.58991 | 2.07581 | 17.24296 |
| H | 19.6663 | 4.10569 | 7.02023 | H | 19.6663 | 4.10569 | 7.02023 |
| H | -1.17769 | 10.28719 | 3.20249 | H | -1.17769 | 10.28719 | 3.20249 |
| O | 16.97203 | 2.94239 | 9.68399 | O | 16.97203 | 2.94239 | 9.68399 |
| O | 1.51659 | 9.12389 | 0.53874 | O | 1.51659 | 9.12389 | 0.53874 |
| O | -2.5598 | 9.42061 | 10.76146 | O | -2.5598 | 9.42061 | 10.76146 |
| O | 12.89564 | 3.23911 | 19.90671 | O | 12.89564 | 3.23911 | 19.90671 |
| H | 16.70887 | 2.86343 | 8.89011 | H | 16.70887 | 2.86343 | 8.89011 |
| H | 1.77974 | 9.04493 | 1.33261 | H | 1.77974 | 9.04493 | 1.33261 |
| H | -2.29665 | 9.49957 | 11.55534 | H | -2.29665 | 9.49957 | 11.55534 |
| H | 12.63249 | 3.31807 | 19.11284 | H | 12.63249 | 3.31807 | 19.11284 |
| C | 16.15966 | 2.17465 | 10.52327 | C | 16.15966 | 2.17465 | 10.52327 |
| C | -5.82381 | 8.35615 | 20.1449 | C | -5.82381 | 8.35615 | 20.1449 |
| C | -1.74743 | 10.18835 | 9.92218 | C | -1.74743 | 10.18835 | 9.92218 |
| C | 20.23604 | 4.00685 | 0.30055 | C | 20.23604 | 4.00685 | 0.30055 |
| H | 15.57534 | 2.76578 | 11.04269 | H | 15.57534 | 2.76578 | 11.04269 |
| H | -5.23949 | 8.94728 | 19.62549 | H | -5.23949 | 8.94728 | 19.62549 |
| H | -1.16311 | 9.59722 | 9.40276 | H | -1.16311 | 9.59722 | 9.40276 |
| H | 19.65172 | 3.41572 | 0.81996 | H | 19.65172 | 3.41572 | 0.81996 |
| H | 16.72063 | 1.65168 | 11.13287 | H | 16.72063 | 1.65168 | 11.13287 |
| H | -6.38479 | 7.83318 | 19.5353 | H | -6.38479 | 7.83318 | 19.5353 |
| H | -2.3084 | 10.71132 | 9.31258 | H | -2.3084 | 10.71132 | 9.31258 |
| H | 20.79702 | 4.52982 | 0.91015 | H | 20.79702 | 4.52982 | 0.91015 |
| H | 15.61175 | 1.56799 | 9.98196 | H | 15.61175 | 1.56799 | 9.98196 |
| H | 2.87686 | 7.74949 | 0.24077 | H | 2.87686 | 7.74949 | 0.24077 |
| H | -1.19952 | 10.79501 | 10.46349 | H | -1.19952 | 10.79501 | 10.46349 |
| H | 11.53536 | 4.61351 | 20.20468 | H | 11.53536 | 4.61351 | 20.20468 |
| O | 1.15205 | 11.85983 | 13.21594 | O | 2.8693 | 9.44286 | 13.55533 |
| O | 9.1838 | 5.67833 | 17.45224 | O | 7.46654 | 3.26136 | 17.11284 |
| O | 13.26018 | 0.50317 | 7.22951 | O | 11.54293 | 2.92014 | 6.89012 |
| O | 5.22843 | 6.68467 | 2.99321 | O | 6.94568 | 9.10164 | 3.33261 |
| H | 0.34813 | 11.33801 | 13.44823 | H | 2.44078 | 9.05852 | 14.3603 |
| H | 9.98771 | 5.15651 | 17.21994 | H | 7.89508 | 2.877 | 16.30785 |
| H | 14.0641 | 1.02499 | 6.99722 | H | 11.97145 | 3.30449 | 6.08515 |
| H | 4.42452 | 7.20649 | 3.22551 | H | 6.51716 | 9.48599 | 4.13757 |

| | | | | | | | |
|---|---|---|---|---|---|---|---|
| C | 2.27904 | 11.03521 | 13.52467 | C | 2.51002 | 10.83617 | 13.52262 |
| C | 8.0568 | 4.85371 | 17.14351 | C | 7.82582 | 4.65467 | 17.14555 |
| C | 12.13319 | 1.32779 | 6.92078 | C | 11.90221 | 1.52683 | 6.92283 |
| C | 6.35543 | 7.50929 | 3.30194 | C | 6.58641 | 7.70833 | 3.2999 |
| H | 2.15811 | 10.1513 | 13.11905 | H | 3.11452 | 11.31489 | 12.91893 |
| H | 8.17773 | 3.9698 | 17.54913 | H | 7.22133 | 5.13339 | 17.74925 |
| H | 12.25412 | 2.2117 | 7.3264 | H | 11.29771 | 1.04811 | 7.52652 |
| H | 6.2345 | 8.3932 | 2.89632 | H | 7.1909 | 7.22961 | 2.6962 |
| H | 2.35965 | 10.9406 | 14.4966 | H | 2.58132 | 11.2133 | 14.42443 |
| H | 7.97619 | 4.7591 | 16.17157 | H | 7.75452 | 5.0318 | 16.24375 |
| H | 12.05257 | 1.4224 | 5.94885 | H | 11.83091 | 1.1497 | 6.02102 |
| H | 6.43604 | 7.6039 | 4.27388 | H | 6.6577 | 7.3312 | 4.2017 |
| H | 3.09351 | 11.44886 | 13.16836 | H | 1.58799 | 10.92742 | 13.20263 |
| H | 7.24233 | 5.26736 | 17.49981 | H | 8.74786 | 4.74592 | 17.46555 |
| H | 11.31872 | 0.91414 | 7.27709 | H | 12.82424 | 1.43558 | 7.24282 |
| H | 7.1699 | 7.09564 | 2.94564 | H | 5.66437 | 7.61708 | 2.9799 |

# List of publication

**[Related to this dissertation]**

1. <u>So Yokomori</u>, Akira Ueda, Toshiki Higashino, Reiji Kumai, Youichi Murakami, and Hatsumi Mori "Construction of Three-dimensional Anionic Molecular Frameworks Based on Hydrogen-bonded Metal Dithiolene Complexes and the Crystal Solvent Effect" *CrystEngComm*, **2019**, *21*, 2940-2948.

2. <u>So Yokomori</u>, Shun Dekura, Tomoko Fujino, Mitsuaki Kawamura, Taisuke Ozaki, and Hatsumi Mori "Vapochromism Induced by Intermolecular Electron Transfer Coupled with Hydrogen-bond Formation in Zinc Dithiolene Complex" *J. Mater. Chem. C,* **2020**, *8,* 14939-14947.

**[Not related to this dissertation]**

1. Dongwei Zhang, <u>So Yokomori</u>, Ryohei Kameyama, Changbin Zhao, Akira Ueda, Lei Zhang, Reiji Kumai, Youichi Murakami, Hong Meng, and Hatsumi Mori, "Effect of Alkyl Chain Length on Charge Transport Property of Anthracene Based Organic Semiconductors" *ACS Appl. Mater. Interfaces*, **2021**, *13*, 1, 989–998.

# Acknowledgements

**Chiba, January 2021**

横森 創